

Proteomics-based Investigation of Substrates for the *Leishmania mexicana* Deubiquitinase DUB2.

Sergios Antoniou (BSc Honours)

Doctor of Philosophy

University of York

Biology

November 2023

Abstract

Leishmaniasis is a neglected tropical vector-borne disease and is caused by the protozoan parasite *Leishmania*. *Leishmania* has a complex digenetic life cycle, and the cellular differentiation that occurs during differentiation is orchestrated in part by the ubiquitin-proteasome pathway, including the ubiquitin-cleaving deubiquitinase (DUB) cysteine peptidases. The parasite expresses 20 DUBs, and four of them are essential for the viability of the insect-stage promastigote form of the parasite. Inducible gene deletion also identifies DUB2 as being important in establishing infection in mice, therefore reflecting a potential drug target. However, the function of DUB2 is not clear. Thus, we aimed to identify the substrates of DUB2 using two approaches. Firstly, using affinity-based ubiquitinated peptide enrichment (ubiquitinomics), 113 proteins were identified that had an increased ubiquitin level upon inducible deletion of DUB2. Secondly, proximity dependent biotinylation (interactomics) revealed 73 proteins that were significantly enriched and therefore in close proximity to DUB2. Gene ontology enrichment analysis categorised these proteins in various biological processes, with transporting and translation top for the ubiquitinomics and interactomics datasets, respectively. DUB2 appears therefore to have a pleiotropic function. Overlapping hits, including UBC2 and SUMO, have been classified as promising DUB2 substrates, and validation is in progress. In the same study, we also conducted a drug screening campaign in collaboration with Novartis (Fast lab), in which 50,000 compounds were tested against the recombinantly expressed *LmDUB2*. From this initial screen, 438 compounds inhibited *Leishmania mexicana* DUB2 proteolytic activity, with a followed-up dose response experiment categorizing 86 of these compounds as high/moderate inhibitors ($IC_{50} < 10 \mu M$). Subsequently, in further collaboration with Novartis, we are actively investigating an additional screening strategy involving chemically related compounds. This effort is aimed at expanding the pool of potential selective and promising compounds against and *LmDUB2*.

Table of Contents

Proteomics-based Investigation of Substrates for the <i>Leishmania mexicana</i> Deubiquitinase DUB2.	1
Abstract	2
Table of Contents	3
List of Tables	8
List of Figures	9
List of Accompanying Material	10
Acknowledgments	11
Author's Declaration	13
1 Introduction	14
1.1 <i>Leishmania</i> and Leishmaniasis	14
1.1.1 Epidemiology and Pathophysiology	14
1.1.2 Life Cycle of <i>Leishmania</i>	15
1.1.3 Cellular Morphology	18
1.1.4 Current Treatments	20
1.1.5 Gene Expression and Regulation	21
1.1.6 Genetic Approaches Applicable in <i>Leishmania</i>	22
1.2 Ubiquitination in Non-Trypanosomatids	24
1.2.1 The Ubiquitin Code	24
1.2.2 Role of Ubiquitin	26
1.2.3 E1 Ubiquitin-Activating Enzymes	28
1.2.4 E2 Ubiquitin-Conjugating Enzymes	29
1.2.5 E3 Ubiquitin Ligases	30
1.2.6 Deubiquitinating Enzymes	31
1.2.7 Proteasome	33
1.2.8 Ubiquitin-Like Molecules	34
1.3 Ubiquitination in <i>Leishmania</i>	35
1.3.1 Ubiquitin and UBLs in <i>Leishmania</i>	35
1.3.2 Ubiquitination and Deubiquitination Components in <i>Leishmania</i>	36
1.3.3 UPS and the <i>Leishmania</i> Life Cycle	36
1.3.4 DUBs and Trypanosomatids	36
1.3.5 DUBs in <i>Toxoplasma gondii</i> and <i>Plasmodium falciparum</i>	37
1.4 Aims	39
2 Materials and Methods	40

2.1 Molecular biology techniques	40
2.1.1 Polymerase Chain Reaction (PCR).....	40
2.1.2 Agarose Gel Electrophoresis.....	41
2.1.3 Site Directed Mutagenesis.....	41
2.1.4 DNA Sequencing.....	42
2.1.5 Ethanol Precipitation.....	42
2.1.6 DNA Extraction.....	42
2.1.7 <i>E. coli</i> Transformation, Culture and Storage	42
2.1.8 DNA Extraction from <i>E. coli</i>	43
2.2. Biochemical techniques	43
2.2.1 SDS-PAGE Gel and Coomassie Blue Staining	43
2.2.2 Western Blotting	43
2.2.3 Stain-Free Imaging	43
2.2.4 Activity-Based Protein Profiling	44
2.2.5 Competitive ABPP for DUB Inhibitors using Cy5UbPA.....	44
2.2.6 Quantification of Protein Concentration	44
2.3 Protein Expression and Purification	44
2.3.1 Generation and Validation of DUB2 Expressing Plasmids	44
2.3.2 Transfection of Insect Cells with Bacmids (P0 Virus Stock)	45
2.3.3 Production of P1 and P2 Virus Stock.....	45
2.3.4 Nickel Affinity Purification	45
2.3.5 His-Tag Cleavage	46
2.3.6 Size-Exclusion Chromatography	46
2.3.7 Buffer Exchange of Recombinant DUB2.....	46
2.3.8 Native-PAGE Gel.....	46
2.3.9 SEC-MALS.....	46
2.3.10 Intact Mass Protein Characterisation using Mass Spectrometry	46
2.3.11 Ubiquitin Rhodamine 110 Kinetic Assay	47
2.3.12 Ubiquitin Rhodamine 110 Endpoint Assay (Drug Screen)	47
2.4 <i>L. mexicana</i> and HeLa cell cultures	47
2.4.1 Promastigote Cell Culture.....	47
2.4.2 Promastigote to Amastigote Differentiation.....	48
2.4.3 Cell Counting.....	48
2.4.4 Growth Curve.....	48
2.4.5 HeLa Cell Culture.....	48

2.4.6 Storage of HeLa Cells.....	49
2.5 Genetic Modification of <i>Leishmania</i>	49
2.5.1 Endogenous Tagging	49
2.5.2 Transfection	49
2.5.3 Cloning of Cells.....	50
2.5.4 DiCre T7 Cas9 Cell Line and Rapamycin-Induced Knockout.....	50
2.5.5 AlamarBlue Viability Assay.....	51
2.5.6 Immunofluorescence	51
2.6 XL-miniTurboID.....	52
2.6.1 BioLock Treatment	52
2.6.2 Biotin Labelling and Crosslinking	52
2.6.3 Lysis, Streptavidin Pull-Down and On-Bead Protein Digestion	52
2.6.4 Peptide Desalting	53
2.6.5 Liquid Chromatography with Tandem Mass Spectrometry (LC-MS/MS)	53
2.6.6 Data Analysis of MS Data.....	53
2.6.7 Bioinformatics	54
2.6.8 Co-Immunoprecipitation	54
2.7 Ubiquitinomics	55
2.7.1 Harvesting, Lysis and Protein Digestion	55
2.7.2 K- ϵ -GG Remnant Immunoaffinity Purification.....	56
2.7.3 timsTOF MS Data Acquisition	56
2.7.4 timsTOF MS Data Analysis	56
3 Investigation of Proximal Proteins of DUB2 using XL-miniTurboID	58
3.1 Introduction	58
3.1.1 Proximity Dependent Biotinylation.....	58
3.1.2 Proximity Dependent Biotinylation Enzymes	59
3.1.3 Proximity Dependent Biotinylation in Kinetoplastids	60
3.1.4 Aims	60
3.2 Results	62
3.2.1 Generation and Validation of MiniTurbo-Tagged Cell Lines	62
3.2.2 Optimization of MiniTurbo Workflow Using BioLock	64
3.2.4 Comparison of DUB2 Interactomes Generated via XL-BioID using miniTurbo and Immunoprecipitation	75
3.2.5 Investigation of DUB2-Interacting Proteins Relationship via Co-Immunoprecipitation	75
3.2.6 DUB2 Localization	79
3.3 Discussion	81

4 Investigation of Total Ubiquitinomics and Proteomics Changes in <i>L. mexicana</i> Promastigotes in Response to DUB2 Depletion	86
4.1 Introduction	86
4.1.1 Identification of DUB Substrates	86
4.1.2 DUB Substrates and Ubiquitinomics in Parasitology	87
4.1.3 Aims	87
4.2 Results	88
4.2.1 Optimization Steps of the Ubiquitinomics Workflow in <i>L. mexicana</i> Promastigotes	88
4.2.1.1 Buffers and Loading Input	88
4.2.1.2 Mass-spectrometer, Acquisition Mode and MG132 Proteasome Inhibitor	89
4.2.2 Generation of DUB2-HA ^{FLOX^{+/+}} <i>Leishmania</i> Promastigote Cell Line	91
4.2.3 Identification of Changes in the Total Ubiquitinome of <i>Leishmania</i> Promastigotes upon Inducible Deletion of DUB2	94
4.2.4 Identification of Changes in the Total Proteome of <i>Leishmania</i> Promastigotes upon DUB2 Knockout.....	104
4.2.5 Overlapping Proteins Across Datasets of Interest.....	115
4.3 Discussion	117
4.3.1 Ubiquitinomics Workflow Optimization.....	117
4.3.2 Advantages of DUB2 ^{FLOX^{+/+}} Promastigote Cell Line.....	120
4.3.3 Insights into the Most Promising Substrates of DUB2.....	120
4.3.4 Insights into the Overlapping Proteins across Datasets	122
5 Biochemical Assays against <i>Leishmania</i> DUBs and Small Molecule Inhibitor Discovery against DUB2	126
5.1 Introduction	126
5.1.1 Activity-Based Probes.....	126
5.1.2 Applications of ABPs.....	127
5.1.3 Cleavable Ubiquitin-Based Substrate.....	128
5.1.4 Aims	128
5.2 Results	130
5.2.1 Competitive Activity Based Protein Profiling for <i>Leishmania</i> DUBs	130
5.2.2 Expression and Characterisation of <i>LmDUB2</i> Recombinant Protein.....	134
5.2.3 High-Throughput Drug Screening Against DUB2.....	136
5.2.3.1 Experimental Workflow	136
5.2.3.2 Optimization	137
5.2.3.3 Primary HT Drug Screen against DUB2	139
5.2.3.4 Dose-Response Screens	140
5.3 Discussion	143

5.3.1 Development of a Robust Competitive-ABPP in <i>L. mexicana</i>	143
5.3.2 Pyrithione and its Derivatives as Inhibitors of <i>Leishmania</i> DUB16	143
5.3.3 <i>LmDUB2</i> – a catalytic active monomeric DUB.....	143
5.3.4 Identification of Promising DUB2 Inhibitors.....	145
6 General Discussion	148
6.1 DUB2 has a Pleiotropic Function in <i>L. mexicana</i> Promastigotes.....	148
6.2 DUB2 - an anti-Leishmanial Drug Target.....	151
6.3 Impact and Future Perspectives	152
Abbreviations	153
References	157

List of Tables

Table 1: PCR Ingredients and Concentration. Ingredients and final concentrations of PCR reactions used along with either Q5 DNA Polymerase or Ultra Mix Red.	40
Table 2: PCR conditions. Standardized conditions used for Q5 DNA Polymerase and Ultra Mix Red-based PCRS.....	41
Table 3: Proximal interacting proteins of DUB2.	71
Table 4: Significantly upregulated ubiquitinated peptides in DUB2 depleted samples.	100
Table 5: Significantly downregulated proteins in response to deletion of DUB2 derived from the DIA dataset.	108
Table 6: Significantly downregulated proteins in response to DUB2 depletion derived from the DDA dataset..	113
Table 7: Overlapping significantly downregulated hits in response to DUB2 depletion between DDA and DIA datasets.	115
Table 8: Top 3 inhibitors for <i>LmDUB2</i> and <i>TcDUB2</i>	141

List of Figures

Figure 1: Life cycle of <i>Leishmania</i> .	17
Figure 2: The organelles of <i>Leishmania</i> .	19
Figure 3: Ubiquitination and deubiquitination.	25
Figure 4: Generation and validation of DUB2 and CLK1 tagged with miniTurbo cell lines.	63
Figure 5: Optimization of XL-BioID using miniTurbo workflow using BioLock.	67
Figure 6: Impact of BioLock in the metabolism and growth of the <i>Leishmania</i> promastigotes.	69
Figure 7: Investigation of the proximal interactome of DUB2.	71
Figure 8: Proximal interactome of DUB2.	74
Figure 9: Investigation of the overlapping proteins between the two DUB2 interactomes derived from XL-BioID using miniTurbo and immunoprecipitation (Damianou <i>et al.</i> , 2020).	75
Figure 10: Use of co-IP to explore the interacting relationship between selected proteins and DUB2.	78
Figure 11: Localization of DUB2.	80
Figure 12: Optimization steps for the ubiquitinomics workflow in <i>L. mexicana</i> promastigotes.	89
Figure 13: Continuation of the optimizations for the ubiquitinomics workflow.	90
Figure 14: Generation of T7Cas9 DUB2-HA ^{Flox^{+/+}} <i>L. mexicana</i> promastigote cell line.	93
Figure 15: Insights into the ubiquitinomics data in response to the DUB2 KO.	95
Figure 16: Exploration and imputation of missing values.	97
Figure 17: Exploration of the significantly different ubiquitinated peptides between DUB2-depleted and wild-type samples.	99
Figure 18: DIA-dependent proteomics data in response to deletion of DUB2.	105
Figure 19: Insights into the significantly different proteins identified via DIA-MS/MS.	107
Figure 20: Insights into the DDA proteomics data in response to deletion of DUB2.	111
Figure 21: Changes in the total proteome upon DUB2 knockout (DIA-datasets)	113
Figure 22: Overlapping proteins across all the generated datasets.	116
Figure 23: Development of competitive ABPP.	131
Figure 24: Investigation of possible <i>L. mexicana</i> DUB inhibitors.	133
Figure 25: Biochemical characterisation of recombinant <i>LmDUB2</i> protein.	136
Figure 26: Optimization of High-Throughput Drug Screen conditions against <i>LmDUB2</i> .	139
Figure 27: Primary and secondary HT drug screens.	141

List of Accompanying Material

Supplemental .xlsx files containing:

S1: List of primers and plasmids

S2: MS data from miniTurbo experiment

S3: MS data from ubiquitinomics and proteomics in response to DUB2 depletion

Acknowledgments

A four-year of PhD has come to an end!! This beautiful era was full of research, fun challenges, troubleshooting, reading and more reading, self-reflection, tears (just some), conferences, meetings, writing and of course an unexpected pandemic! Despite these, I could have not chosen a better way of exploring and developing my research skills, and for exploring and discovering so many aspects of myself!

Nonetheless, first and most importantly, I would like to express my sincere gratitude to my primary supervisor, Jeremy Mottram, who he always provided his insightful advice and guidance, for challenging my results when necessary, as well as developing my communication skills (e.g. use of correct arguments) and feeding my curiosity, while encouraging me to explore a diversity of techniques. The list of the opportunities he had provided me with is endless, and I will be forever thankful for that! Of course, I extend my appreciation to my second supervisor, Anthony Wilkinson, whose exceptional biochemical and structural understanding contributed to getting a step ahead with various assays. Additionally, his positivity and kindness was always present in our meetings (even during mass-spec discussions about DIA and DDA), making the environment friendly and comfortable for my stressed presence. I would also like to thank my third and final supervisor Chris MacDonald for sharing his experience with the ubiquitin system and fluorescence microscopy.

Special thanks to our collaborators from Novartis Institute for Biomedical Research (NIBR), and especially Dominick Casalena and Douglas Auld for introducing me to the fascinating world of high-throughput drug screening during my 3-week placement at NIBR in Cambridge, and for their overall immense contribution to the success of our project. This irreplaceable experience it would not have been accomplished without the internally-distributed funding provided by the University of York (UoY), which I am very thankful for. In addition, I would like to express my gratitude to Steven Cobb's lab and in particular Hirunika Perera for placing trust in me to explore the DUB selectivity of their compounds. I would like to express my appreciation to Paul Kaye's lab, for providing me with the HeLa cell stabilates and several other antibodies.

Furthermore, I am particularly grateful to so many individuals from the University of York Technology Facilities and York Structural Biology Laboratories. Specifically, I would like to acknowledge Jared Cartwright, Rebecca Reece and Mick Miller for teaching me all the secrets of protein production, Andrew Leech for his assistance in SEC-MALLS, Jamie Blaza and Sam Hart for guiding me through my CryoEM adventures, Manal Alzahrani for her support in CryoEM data analysis, Juliet Borgia, Lena Blagova, Jim Brannigan and Marek Brzozowski for assisting me with my crystallographic attempts, and Chris Taylor for all his MS-related technical support. I am forever grateful to the best of the best Adam Dowle for his outstanding contribution to all my MS-related studies, for acquiring and analysing all the raw MS data, and for patiently explaining to me every single aspect of MS.

The success of this endeavour is owed in large part to the Mottram lab – I would not have achieved as much if these guys were not around to happily teach me the essentials, patiently answer my questions (including the very, very, VERY nonsensical) and make me feel so welcome! These people and their willingness to supporting me not only in research but in any aspect of my life are rare, and I will nurture them and the memories we generated together for as long as my brain allows me to (and yes – they were one of the main reasons why I was keep showing up in the lab – so a 'thank you' feels really little).

From the Mottram's group, I would like to give special thanks to Vincent Geoghegan for taking me under his wings and helping me tremendously throughout this journey, for cheering me up, sharing his love for science, as well as for happily introducing me to the field of proteomics. I would also like to acknowledge Nathaniel Jones for his constructive criticism and invaluable discussions throughout my project, for always being willing to share his novel ideas and for sending me so many useful papers that I have elegantly missed. I could not be more grateful for having Charlotte Hughes in the team, who is ninja-level organisation skills, along with her support in the lab, administration and mental-health, were invaluable to me (and of course for all the endless anime-discussions)! I am also deeply grateful to Romina Nievas for teaching me how to perform the ABPP assay, for all the fun and insightful discussions during the long-CAT3 hours and of course for hosting me for almost a month when I needed a space to stay! Heartfelt thanks to Rachel Neish for keep reminding how important the work-life balance is and for pointing out all the mistakes I was doing in the lab, Nicola Baker for making me realise how important it is to be independent in research (and in life in general), and Juliana Brambilla Carnielli Trindade (the First) for teaching me (apart from portuguese) how to use the fluorescence microscopy and how to test compounds against the parasite! I further extend my appreciation to the following for their support in the laboratory and for contributing to a positive work environment in H block: Eden Ramalho de Araujo Ferreira, Rebecca Burge, Ewan Parry, Edward Muscutt (my PhD partner in crime), James Smith, James Fox, Marie-Christine Labarthe-Last, Natalia Teles, Katrien Van Bocxlaer, Ciara Loughrey, Giulia Bandini, Helen Ashwin, Mathieu Cayla, Joana Correia Faria, Elisa Nightingale, Jodie Dixon, Lianne Lansink, Nidhi Dey and Shoumit Dey.

I would also like to express my sincere gratitude to Andreas Damianou for being always available to reply to any DUB- and ubiquitinomics-related questions, for listening to my presentation before my first conference, for all the inspiring discussions and of course for boosting my confidence when needed! Special thanks to Marjan Van Der Woude and Jamie Blaza for being an exceptional thesis advisor panel, for encouraging me to participate in activities outside the lab and for reminding me to keep realistic goals. In this section, I would also like to express my thankfulness to Naj Brown – firstly for being my only human-bubble during the pandemic time, as well as supporting me mentally throughout the difficult times of the PhD. Naj was always there to listen, and as the amazing person she is, our discussions about books, films, rugby, theatre, food, BAKING, and life, I was able to escape endless mental-breakdowns!

Last but not least, I wish to acknowledge the unwavering support of my friends during this challenging yet rewarding journey. Most importantly, I would like to highlight the contribution of my family over these four years. Mom, Dad, Sis, Granny, and Nikos thank you for always believing in me, showering me with endless love, and for always being there to ensure my well-being and provide a safe space when needed!

Author's Declaration

I declare that this thesis is a presentation of original work and I am the sole author (unless stated otherwise). This work has not previously been presented for an award at this, or any other, university.

All sources are acknowledged as References.

Sergios Antoniou

1 Introduction

1.1 *Leishmania* and Leishmaniasis

1.1.1 Epidemiology and Pathophysiology

Leishmaniasis is a spectrum of zoonotic diseases that stem from intracellular, obligate, protozoan parasites belonging to the *Leishmania* genus. Transmission occurs among mammalian hosts through the bites of *Leishmania*-infected female sandflies, specifically from the *Phlebotomus* genus (Old World) and the *Lutzomyia* genus (New world). While there are over than 50 distinct *Leishmania* species, only 20 have been identified as being the causative agents of leishmaniasis (das Chagas *et al.*, 2022). This genetic diversity within the pathogenic *Leishmania* parasite is one of the underlying reasons behind the varying spectrum of diseases that leishmaniasis manifests as. Overall, these manifestations of leishmaniasis are classified in five types: visceral leishmaniasis (VL), mucocutaneous leishmaniasis (MCL) and cutaneous leishmaniasis (CL) which are the most common forms of the disease, and diffuse cutaneous leishmaniasis (DCL) and post-kala-azar dermal leishmaniasis (PKDL) which are rarer. Each form of leishmaniasis has different symptoms and thus, their severity varies. For instance, CL is characterized by a range of symptoms including punctuate self-healing lesions at the site of the sandfly bite (localised CL [LCL]) or by multiple non-ulcerative nodules (diffuse CL [DCL]) that categorizes CL with the lowest mortality rate. Conversely, on the other side of the mortality spectrum is VL. VL is characterized by disseminated visceral (liver and spleen specifically) infection that could be lethal, if untreated (Sasidharan *et al.*, 2021; Gupta *et al.*, 2022).

Among all parasitic diseases, leishmaniasis ranks second only to malaria in terms of mortality. When considering disability-adjusted life years (DALYs), it stands as the third most prevalent cause of morbidity, following malaria and schistosomiasis (Hotez *et al.*, 2023). In 2021, among the 200 countries and territories providing data to the World Health Organization, leishmaniasis was prevalent in 99 countries and territories. This indicated that over a billion people were at risk of contracting the disease, with an estimation of ~1 million cases to occur annually. In 2021, the worldwide tally of CL and VL cases reported to the WHO surpasses 220,000 and 11,000, respectively. For CL, the Syrian Arab Republic accounted for the largest proportion of CL-infected patients, approximately 35%, followed by Afghanistan with around 18%, and Pakistan with 8%. Regarding VL, the countries with the highest reported cases were Sudan, comprising approximately 29%, succeeded by Kenya at about 15% and Brazil at 13% (WHO, 2023). Collectively, leishmaniasis is endemic in Asia, Africa and Latin America.

The reasons of the endemic state of leishmaniasis is in the already mentioned countries and territories are various. For instance, tropical and subtropical conditions contribute to the optimal growth of the sandfly vector, which in response promotes the spread of the zoonotic disease. In addition, poverty is another factor contributing in epidemiology of the disease. The inadequate housing and unsatisfactory domestic sanitation, such as a lack of waste disposal or exposed sewage systems, could potentially amplify the proliferation of sandflies, providing them with more breeding and resting locations, while also facilitating their proximity to humans (Alvar *et al.*, 2006). Due to the epidemiology of leishmaniasis being closely linked to socioeconomic conditions, the disease is classified among the twenty neglected tropical diseases (NTDs; Molyneux, 2012). Furthermore, several significant factors elevate the risk of leishmaniasis transmission: malnutrition and co-infection with HIV, environmental alterations and population movement. The first two factors compromise the immune system, thereby heightening susceptibility to leishmaniasis (Alvar *et al.*, 2008). Meanwhile, the latter two factors contribute to the broader distribution of sandflies, amplifying the global significance of leishmaniasis (Sutherst, 2004).

1.1.2 Life Cycle of *Leishmania*

Leishmania parasites have a complex dimorphic life cycle with two predominant developmental forms: the promastigote form that is found inside the sandfly vector and the amastigote form that is present in the mammalian host (Fig. 1). In morphological terms, promastigotes exhibit an elongated ovoid cell body with a long, motile flagellum, while amastigotes display a relatively compact, rounded cell body and a short, non-motile flagellum (Omondi *et al.*, 2022). Despite the observable differences in morphology between the two stages of the parasite, there are also notable variations in their metabolic activity and growth characteristics. For example, *Leishmania* amastigotes undergo a strict metabolic response, which includes reducing lipid production and increasing fatty acid β -oxidation. This metabolic shift helps protect the parasite from various stresses, such as nutrient scarcity, encountered within the mammalian host (Saunders *et al.*, 2021). Consequently, lesion-derived amastigotes exhibit a significantly slower growth rate, with a doubling time of 12 days, compared to the highly metabolically active promastigotes, which have a much quicker doubling time of 18 hours (Kloehn *et al.*, 2015; Sunter *et al.*, 2017).

Nonetheless, focusing first on the life-cycle of the *Leishmania* parasite at the sandfly promastigote stage, there are six different promastigote forms, which are found in the following sequence after the sandfly receives its first *Leishmania*-infected blood meal: procyclic, nectomonad, leptomonad, haptomonad, retroleptomonad and metacyclic promastigotes (Omondi *et al.*, 2022). The infection of the female sandfly begins with the insect biting the skin of an infected mammal that induces a haemorrhagic pool. The sandfly then ingests the *Leishmania*-infected blood (~3200 amastigotes per 1.6 μ l blood meal) and digests it at its abdominal midgut (Rogers *et al.*, 2002). Sequentially, a chitin-containing peritrophic matrix (PM) is formed from secretions of the midgut epithelium, which encloses the blood meal, and causes the amastigote cells to cluster together (Rogers *et al.*, 2002; Sunter *et al.*, 2017). By that point several factors, including temperature and the pH, trigger the differentiation of the amastigotes to the highly replicative procyclic promastigotes. Procyclic promastigotes have a short flagellum relative to their cell body and their motility is relatively weak. After 72 hours post-differentiation, procyclic promastigotes transform to nectomonad promastigotes that are characterised by negligible cell-division and strong motility. The initiating factor for cells to undergo differentiation at this life stage could be attributed to the presence of saliva, depletion of hemin within the ingested blood, or a potential interplay of both factors (Charlab *et al.*, 1995). Eventually, the PM disintegrates at its anterior site, allowing the parasites to enter the midgut lumen of the sandfly. This process, along with the capacity of nectomonad promastigotes to attach to the microvilli of the midgut using their flagellum and surface-exposed lipophosphoglycans (LPG), work in conjunction to hinder the removal of the parasites from the sandfly through defecation (Pimenta *et al.*, 1997).

Sequentially, at 96 hours post-infection, nectomonad promastigotes migrate at the cardia, stomodeal valve and the thoracic midgut of the sandfly, where they differentiate to leptomonad promastigotes. The leptomonad promastigote acquire the same size as the procyclic, however they have longer flagellum compared to their cell body (Sunter *et al.*, 2017). The parasites at this form undergo highly proliferation via binary fission and they can differentiate to either haptomonad or metacyclic form. Focusing first on the haptomonad stage of the parasite, it has a leaf-like shape and adheres to the cuticular lining of the stomodeal valve of the sandfly using an extended tip of their flagellum. This attachment damages the stomodeal valve, impacting its functionality, and simultaneously promotes the backflow of parasites from the midgut (Schlein *et al.*, 1992; Volf *et al.*, 2004). Like the metacyclic promastigotes, they are highly motile parasites with the shortest length compared to the rest of the promastigotes. They do not undergo cell-division. However, they can swim freely inside the midgut of

the sandfly. This phenomenon is attributed to the alteration of their surface-exposed LPGs, where longer phosphoglycan repeats are introduced, and the masking of their midgut adhering side-chain galactose residues through the addition of terminal arabinose (McConville *et al.*, 1992).

Eventually, at a follow-up blood meal, the infected female sandfly injects the infectious metacyclic promastigotes into the mammalian host, which establishes a new infection and the *Leishmania* life-cycle starts all over again. However, apart from the parasites itself, the insect injects saliva that prevents blood clotting and the promastigote secretory gel (PSG). PSG is produced by the leptomonad promastigotes within the anterior midgut of the sandfly. PSG is composed of proteophosphoglycans and it is responsible for several crucial functions. Firstly, it obstructs the anterior midgut of the sandfly, thereby hindering the blood-feeding process. This leads to more attempts at blood-feeding by the sandfly, resulting in an increased likelihood of parasite transmission (Rogers *et al.*, 2002; Rogers *et al.*, 2007). Secondly, PSG promotes the regurgitation of a greater number of parasites per sandfly bite. This action synergistically complements the haptomonad attachment function previously mentioned (Rogers *et al.*, 2004). Lastly, PSG significantly enhances the severity of leishmaniasis diseases. It achieves this by triggering the recruitment of macrophages (ultimate target of *Leishmania*) to the lesion site, through the activation of the wound healing process (Giraud *et al.*, 2018). At this point, it is noteworthy that the consumption of additional uninfected blood by a *Leishmania*-infected sandfly induces the *in vivo* de-differentiation of metacyclic promastigotes into retroleptomonad promastigotes. These recently discovered retroleptomonad promastigotes share phenotypical similarities with the leptomonad form, while also displaying a high replicative capacity within the midgut. Intriguingly, these retroleptomonad promastigotes undergo re-differentiation into metacyclic promastigotes. Consequently, their significantly proliferative behaviour contributes to an increased count of infectious parasites within the sandfly prior the subsequent transmission occurrence (Serafim *et al.*, 2018).

Focusing next at the interaction between the mammalian host and the *Leishmania* parasite, the sandfly bite triggers the accumulation of firstly neutrophils and secondly of macrophages at the bite site of the host skin. Sequentially, the metacyclic *Leishmania* promastigotes, which were released via regurgitation from the vector to the host, interact and adhere to the recruited neutrophils and macrophages, but also to various types of host cells, including Langerhans cells and fibroblasts (Peters *et al.*, 2008). The high motility of metacyclic promastigotes allows migration of the cells through the collagen matrix, enhancing the possibility of encountering the desired host cells located either at the bite site or near to it (Petropolis *et al.*, 2014). Interestingly, infected neutrophils act as the “Trojan horse” ensuring that the parasites will reach their primary target, the macrophages (Laskay *et al.*, 2003). Delivery of the parasites to the macrophages is achieved via the ingestion of the *Leishmania*-infected apoptotic neutrophils by the macrophage (Laskay *et al.*, 2008).

Nevertheless, direct encounter of the parasite with a macrophage involves binding of the parasite at different surface receptors of the macrophage. For instance, the surface-expressed zinc-metalloprotease gp63 plays a role in opsonisation of the parasite. This results in the adherence of the parasite to complement macrophage receptors CR1 and CR3 (Bogdan, 2020). Once the parasite adheres to the surface of the macrophage, the macrophage forms pseudopods and phagocytose the parasite. The engulfed parasite becomes enclosed within a vacuole called the parasitophorous vacuole (PV), all the while keeping up its flagellar movement. This flagellar movement damages the plasma membrane of the macrophages, leading to the triggering of lysosomal exocytosis. Consequently, the PV eventually merges with the phagolysosome of the host cell (Forestier *et al.*, 2011). The change in the pH due to the acid environment of the phagolysosome combined with the change of the temperature triggers the differentiation of the metacyclic promastigotes to non-motile amastigotes

(Barak *et al.*, 2005). Amastigotes proliferate within the vacuole, which ruptures following successive rounds of cell division. This results in the liberation of the newly reproduced amastigotes within the infected tissue. This enables amastigotes to extend the infection by invading additional macrophages, or to transmit the infection to new hosts through ingestion by an uninfected female sandfly during its blood meal (Teixeira *et al.*, 2013; Sasidharan *et al.*, 2020). It is noteworthy that there are two types of PV: the multi-occupancy PV and the small single-occupancy PV. The former PV encloses multiple amastigotes, such as the case in *L. mexicana*, while the latter PV contains a single amastigote, such as in the case of *L. major* (Real *et al.*, 2010).

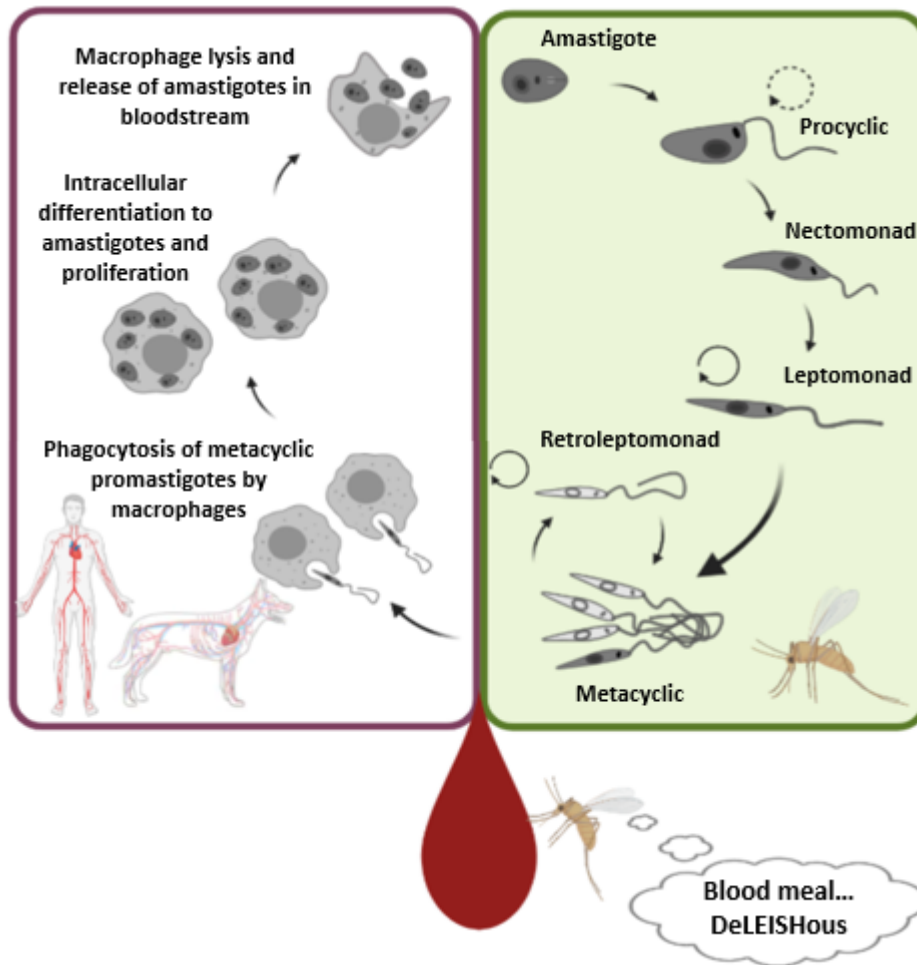


Figure 1: Life cycle of *Leishmania*. Starting from the blood-meal received by a *Leishmania*-infected sandfly, *Leishmania* metacyclic promastigotes are injected in the host (e.g. dog, human), phagocytosed by the host immune cells (e.g. macrophages), differentiate into amastigotes, proliferate and establish infection (purple box). Subsequent blood-meal by a naïve sandfly from an infected host leads to the ingestion of *Leishmania*, and therefore to the infection of the sandfly. Inside the sandfly, amastigotes differentiate to the following promastigote forms: procyclic, nectomonad, leptomonad, metacyclic, and retroleptomonad.

1.1.3 Cellular Morphology

Overall, *Leishmania* cells possess several organelles that commonly observed in other eukaryotic cells. For instance, it contains a nucleus, a single mitochondrion, endoplasmic reticulum, Golgi apparatus, and various components of the endocytic pathway, as illustrated in Fig. 2 (Besteiro *et al.*, 2009). Nonetheless, *Leishmania* genus belongs in the order of kinetoplastida, an evolutionary early-divergent unicellular class of eukaryotes that possesses a unique structure known as the kinetoplast (Camacho *et al.*, 2019). The kinetoplast is a specialized section of the mitochondria housing the most intricate and unique mitochondrial DNA found in nature (Rudzinska *et al.*, 1964). The kinetoplast DNA (kDNA) is comprised of a singular interconnected network of circular DNA molecules, representing the 30% of the cellular DNA. This network consists of approximately 25 to 50 larger circular DNA molecules called maxicircles, along with a much larger number, ranging from 5,000 to 10,000 of smaller circular DNA molecules known as minicircles (Yilmaz *et al.*, 2022). The maxicircles, typically ranging in size from 20 to 40 kb, have the role of expressing mitochondrial-associated proteins, including those participating in the respiratory chain, and they also involve in the encoding of rRNAs. Meanwhile, minicircles vary in size from 0.5 to 10 kb and are responsible for encoding guide RNAs, which are involved in the editing of maxicircle-derived transcripts (Cavalcanti *et al.*, 2018). Kinetoplast is localized at the anterior site of the parasite, in between the nucleus and the flagellum of the parasite.

The *Leishmania* promastigote flagellum emerges from the flagellar pocket and bears a resemblance to other eukaryotic flagella, featuring a flagellum axoneme composed of the typical arrangement of 9 + 2 outer doublet and central pair microtubules (Landfear, 2022). A unique characteristic of the kinetoplastid flagellum is the existence of a paracrystalline structure known as the paraflagellar rod (PFR). This PFR extends along the axoneme, running parallel from just beyond the flagellar pocket to the farthest tip, and plays a significant role in the motion of the parasite (Maga *et al.*, 1999). However, during the transformation of the promastigotes into amastigotes, a remarkable change occurs in the flagellum. It becomes extremely short, almost to the point of not extending beyond the flagellar pocket (Hoare *et al.*, 1966). The arrangement of the axoneme shifts to 9 + 0 configuration, due to the loss of the central pair of microtubules, and the PFR is also eliminated (Wheeler *et al.*, 2015). Consequently, these changes result in restricted movement of the amastigote flagellum. Additionally, the flagellum becomes associated with the parasitophorous vacuole membrane of the host cell and acquires a sensory function (Wheeler *et al.*, 2015). Nevertheless, the arrangement of the flagellum, kinetoplast, and nucleus serves as a helpful indicator for determining the life stage of *Leishmania* parasite (Hoare *et al.*, 1966).

Another fascinating feature of the *Leishmania* cell is the flagellar pocket. It is a small invagination of the outer membrane of the cell, serving as a site through which the flagellum extends from the interior of the cell. In *Leishmania*, the flagellar pocket is divided into two distinct regions: the bulbous lumen and the flagellar pocket neck. The flagellar pocket neck is where the flagellum firmly attaches to the cell body. This attachment is facilitated by a complex called the flagellum attachment zone (FAZ), which comprises various cytoskeletal proteins (Wheeler *et al.*, 2016; Corrales *et al.*, 2021). Notably, the flagellar pocket is also the site where the new flagellum emerges, alongside the old one. Subsequently, this flagellar pocket splits into two separate pockets, each associated with its own flagellum (requiring a functional FAZ2; Halliday *et al.*, 2020). Beyond its role as an anchor for the flagellum, the flagellar pocket also serves as a site for cellular processes like endo- and exocytosis. This makes it crucial interface through which the parasite interacts with its host environment (Wheeler *et al.*, 2016). Interestingly, the *Leishmania* amastigote flagellar pocket maintains the same two-part structure, but it undergoes significant restructuring due to changes in the localization of FAZ proteins. This restructuring results in a narrowing of the gap between the flagellum and the flagellar pocket

neck membrane (Wheeler *et al.*, 2016). This adaptation may contribute to protecting the parasite from the harsh environment within the parasitophorous vacuole of the macrophage, which is acidic and rich in proteases (Sunter *et al.*, 2017).

Glycosomes are another distinct subcellular structure in *Leishmania*. Glycosomes are microbody organelles characterized by a protein-rich matrix enclosed by a single membrane (Jamdhade *et al.*, 2015). Their name comes from their role in housing nine enzymes crucial for the glycolysis pathway (Opperdoes *et al.*, 1977). However, glycosomes also play a significant role in other essential energy-producing processes like the fatty acid β -oxidation pathway. The compartmentalization of these pathways ensures the survival of the parasite in anaerobic conditions, such as during infection in host macrophages (Opperdoes *et al.*, 1993). What is intriguing is that glycosomes exhibit peroxisome-like targeting mechanisms, even though peroxisomes themselves are absent in these cells. This led to the classification of glycosomes as specialized peroxisomes (Haanstra *et al.*, 2016). Notably, the number of glycosomes varies between promastigotes and amastigotes, with an average of around 20 in the former and 10 in the latter (Cull *et al.*, 2014).

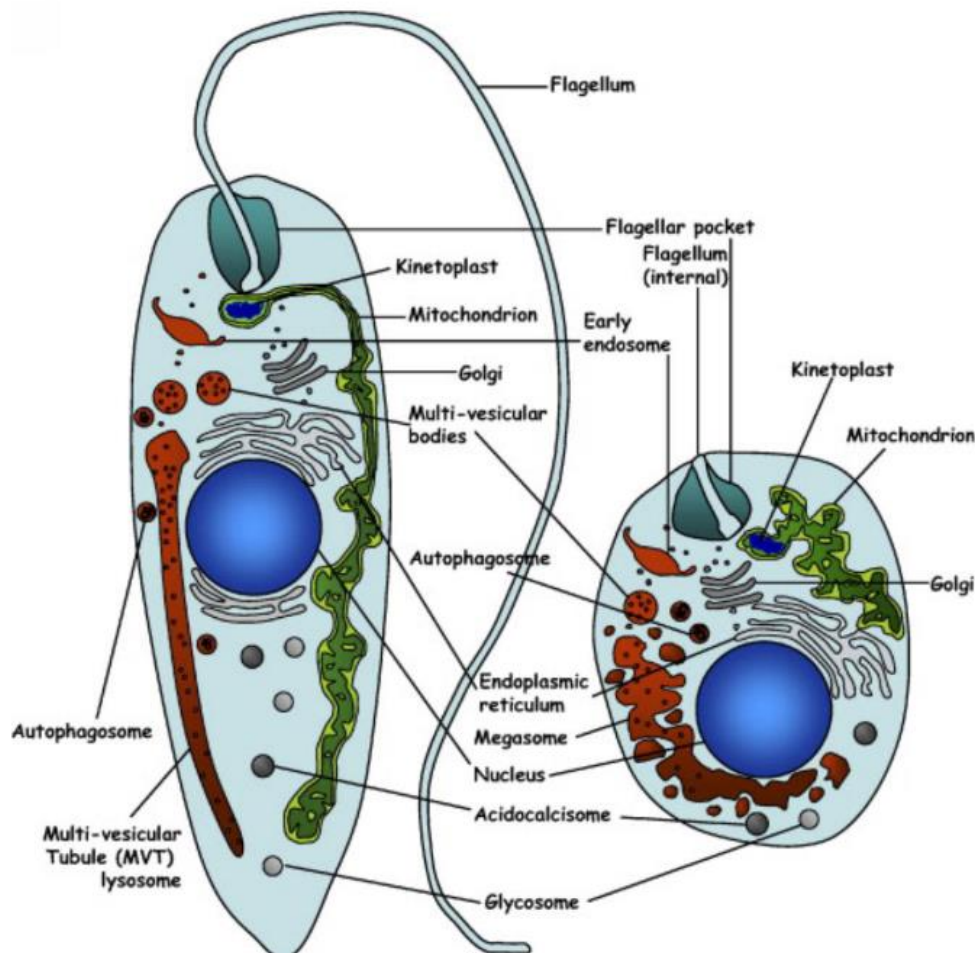


Figure 2: The organelles of *Leishmania*. Organellar composition of *Leishmania* promastigote (left) and amastigote (right). Reproduced image from Besteiro *et al.* (2007).

1.1.4 Current Treatments

Over the past few decades, there has been a development of a wide range of medicines to treat leishmaniasis. However, many of these medications are characterised by their high toxicity, resistance issues, prohibitively high costs, lengthy treatment durations, or impractical methods of administration, rendering them unsuitable for effective treatment. One of the first leishmaniasis treatments was the pentavalent antimonial monotherapy, including meglumine antimoniate (Glucantime®) and sodium stibogluconate (Pentostam®; Brahmachari, 1940). Antimonials function by converting prodrugs from Sb (V) to the more potent Sb (III) form of antimony, and subsequently, they interfere with thiol metabolic pathways. Furthermore, there are reports suggesting that sodium antimony gluconate stimulates the production of reactive oxygen species (ROS) and the synthesis of nitric oxide, both of which play a role in killing the parasites (Kumari *et al.*, 2022). However, in the Indian subcontinent, the potency of pentavalent antimonials has been observed to diminish since the late 1990s. This decrease is attributed to the environmental selection of *L. donovani* strains (causes VL) that have an increased gene copy number of *MRPA*, which expresses an ATP-binding transporter involved in sequestering Sb (III) into intracellular vesicles (Perry *et al.*, 2015; Dumetz *et al.*, 2018). In addition to the emergence of antimony resistance, pentavalent antimonials come with further drawbacks. These include lengthy treatment regimens lasting at least 20 to 28 days, involving daily and often painful intramuscular injections or intravenous infusions. Furthermore, their use can lead to adverse side effects such as nausea, vomiting, pancreatitis, as well as cardiac and hepatic toxicity (Moore *et al.*, 2010).

Another available treatment is the use of the repurposed macrolide polyene antifungal Amphotericin B (AmB; Dutcher, 1968). The mechanism of action of this drug against *Leishmania* involves binding to ergosterol molecules present on the membrane of the parasite, causing membrane depolarization and an influx of ions that leads to oxidative stress (Ponte-Sucre *et al.*, 2017). Currently, AmB stands as the most potent treatment for VL in India. However, similar to antimonials, it has its drawbacks. Firstly, AmB has been associated with adverse effects such as anemia, hypokalemia, hypomagnesemia, and renal toxicity. It can also cause less severe effects like fever, chills, nausea, vomiting, and headaches. Secondly, the cost of AmB can be prohibitive, making it financially inaccessible to poorer patients (Kumari *et al.*, 2022). Thirdly, resistance to AmB has been observed in clinical isolates of *L. donovani*, with increased expression of the multidrug resistance gene *MDR1*, leading to a higher efflux rate of amphotericin B from the parasite (Purkait *et al.*, 2012). Nonetheless, efforts to reduce the toxicity of the drug have been successful by shifting from a sodium deoxycholate-based formulation to a lipid-based one. For example, liposomal amphotericin B (AmBisome), which contains di-stearoyl phosphatidylglycerol, phosphatidylcholine, cholesterol, and AmB in a unilamellar liposome formulation, has been reported to reduce toxicity significantly (Adler-Moore *et al.*, 1993). It successfully treats 95% of VL cases in India with just a single infusion, however expensive cold-chain storage is required. This can pose a significant challenge in developing countries that do not have the required infrastructure and resources (Sundar *et al.*, 2010).

Next, miltefosine stands out as the sole orally administered medication for treating leishmaniasis, originally designed as an anticancer drug (Sundar *et al.*, 2000). Its mechanism of action against the parasite can be categorised into two main aspects. Firstly, it directly combats the *Leishmania* parasite by interacting with the miltefosine transporter, disrupting its membrane metabolism and composition. Secondly, it modulates the signalling of T-helper cell type 1 to enhance the clearance of the intracellular parasite by macrophages (Palić *et al.*, 2022). Despite its widespread use, resistance to miltefosine can develop. This resistance may arise due to the absence of the Miltefosine Sensitivity Locus or through mutations in the miltefosine transporter, as observed in clinical and cultured

Leishmania, respectively (Laffitte *et al.*, 2016; Carnielli *et al.*, 2019). Additionally, administering miltefosine to pregnant women has been associated with teratogenic effects. Other side effects of the drug include gastrointestinal disturbances and hepatorenal toxicity (Soni *et al.*, 2022).

Two additional treatments for leishmaniasis are paromomycin and pentamidine (Sundar *et al.*, 2007; Wiwanitkit, 2012). Paromomycin works by inhibiting the protein biosynthesis of the parasite, while pentamidine targets the mitochondrial topoisomerase II and also inhibits transcription (Fernández *et al.*, 2011; Coser *et al.*, 2020). However, paromomycin can be toxic to the kidneys and the hearing system, while pentamidine may induce gastrointestinal disorders, and diabetes mellitus (Soni *et al.*, 2022). While these treatments can be used individually, they are also administered in combination. For example, paromomycin can be given with miltefosine or pentavalent antimonials to treat VL in India and East Africa, respectively (Burza *et al.*, 2018). The primary reason for using combination therapies is to reduce the development of drug-resistant *Leishmania* strains. Therefore, organizations like the Drugs for Neglected Diseases initiative (DNDi) are dedicated to improve these combination therapies and to develop new treatments (Bhattacharya *et al.*, 2020). For instance, gold-derived complexes were found to have anti-leishmanial activity against *L. infantum* and *L. braziliensis* amastigotes, while new targetable proteins, including the *Leishmania* proteasome, were successfully explored as ideal therapeutic targets (Wyllie *et al.*, 2019; Tunes *et al.*, 2020). Furthermore, there is a lack of availability of prophylactic vaccines against leishmaniasis due to the intracellular nature of the infection and the complex interaction between *Leishmania* and the host (Soni *et al.*, 2022). Despite this statement, a number of promising vaccines have recently entered the clinical trials, including the live attenuated *LmCen*^{-/-} vaccine and the ChAD63-KH adenovirus-based vaccine (Osman *et al.*, 2017; Zhang *et al.*, 2020). Nonetheless, regardless the progress made on these promising drugs and vaccines, the results are yet to be finalized. Therefore, this underscores the urgent need for a more comprehensive understanding of *Leishmania* cell biology.

1.1.5 Gene Expression and Regulation

As previously mentioned, there are various species of *Leishmania*, each having a unique genetic structure and signature corresponding to its number of chromosomes and sets of genes (Rogers *et al.*, 2011). For instance, *L. mexicana* has 34 chromosomes and potentially 9,169 protein coding genes, of which 90% were identified as transcripts in both axenic promastigotes and axenic amastigotes (Fiebig *et al.*, 2015). As the rest of trypanosomatids, the *Leishmania* genes are organised into polycistronic transcription units (PCU; Bartholomeu *et al.*, 2021). Most of the genes have intron-less open reading frames and are placed in head-to-tail fashion. The order of the genes per PCU is partially evolutionary conserved in other kinetoplastids, however the arrangement of these genes is independent of their mRNA expression levels as well as the functions of their encoded proteins (Clayton, 2019). Nevertheless, transcription of protein encoding genes is conducted by RNA polymerase II in a bidirectional manner. It initiates transcription at the divergent strand switch regions situated between two polycistronic transcription units that are orientated away from each other (Martínez-Calvillo *et al.*, 2003). The transcription initiation regions are DNA sites that lack open reading frames, have open chromatin with rich GT sequences and have a unique combination of acetylated histones and bromodomain factors (Thomas *et al.*, 2009; Chandra *et al.*, 2017; Jones *et al.*, 2022; Russel *et al.*, 2022). Concerning transcription termination, specific DNA regions come into play that mark the conclusion of a PCU. These regions include the convergence strand switch region situated between two PCUs and regions upstream of either tRNA-encoding genes or genes transcribed by Pol-I (Marchetti *et al.*, 1998; Siegel *et al.*, 2009). Once the polycistronic pre-mRNA is transcribed, a series of co-transcriptional

processes occur, including cleavage, polyadenylation, and trans-splicing, leading to the formation of mature mRNAs (Santi & Murta, 2022).

Typically, the expression levels of individual protein coding genes are controlled by the 3' untranslated region (UTR), which serves as a target for RNA binding proteins. These proteins can influence gene expression by stabilizing, sequestering, or degrading the RNA (De Pablos *et al.*, 2019). Moreover, regulation can also occur at the protein level, involving mechanisms such as translation control, post-translation modifications, and protein degradation (De Pablos, Ferreira & Walrad, 2016; Karamysheva *et al.*, 2020). For instance, when the alpha-subunit of eukaryotic initiation factor 2 undergoes phosphorylation, it results in the reduction in the overall mRNA translation. This event acts as a trigger for the differentiation of the promastigote to amastigote form (Cloutier *et al.*, 2012). In addition to post-transcriptional regulation, it is important to note that the *Leishmania* genome exhibits high plasticity (Santi & Murta, 2022). For instance, the parasite undergoes mosaic aneuploidy, which means it acquires an abnormal number of chromosomes compared to other strains of the same species. Consequently, the gene copy number of certain genes also changes, contributing to variations in gene dosage within the cell. This serves as a significant adaptive mechanism for the parasite under stressful conditions (Restrepo *et al.*, 2019). Similarly, other stress-adaptive mechanisms that influence gene copy numbers entail the addition or removal of genes in tandem, or the generation of linear or circular extrachromosomal gene copies (Rogers *et al.*, 2011).

1.1.6 Genetic Approaches Applicable in *Leishmania*

As previously mentioned in section 1.1.5, the *Leishmania* genome displays remarkable plasticity, presenting significant obstacles in genetically modifying essential genes. Furthermore, the absence of functional RNA interference in many *Leishmania* species, including *L. mexicana*, along with the digenetic life cycle of the parasite, introduces additional complexities when attempting genetic interventions. This complexity extends not only to the execution of genetic approaches but also to comprehending the essential role of a gene throughout the entire life cycle of the parasite (Duncan, Jones & Mottram, 2017; Jones *et al.*, 2018). Nevertheless, throughout the years several genetic modification approaches have been developed in *Leishmania*. However, the most widely used one is the clustered regularly interspaced short palindromic repeats (CRISPR) CRISPR-associated gene 9 (Cas9) system.

Briefly, the CRISPR-Cas9 system consists of two crucial components: the Cas9 nuclease and a guide RNA (gRNA). Cas9 is an RNA-dependent DNA endonuclease, while gRNA is an RNA molecule comprising scaffold RNA components for binding to Cas9 and a complementary RNA sequence called the protospacer, responsible for guiding Cas9 to the desired genomic target. To induce a double-stranded break, the DNA target site must be located downstream of the protospacer-adjacent motif (PAM), which consists of the triple nucleotide NGG (Gostimskaya, 2022). *Leishmania* can repair double stranded breaks using two methods: homologous recombination and micro-homology mediated end joining (MMEJ; Passos-Silva *et al.*, 2010; Lafitte *et al.*, 2016). Although, various studies have utilized either systems for genetic modification in *Leishmania* using CRISPR-Cas9 since 2015, the most effective tool, as developed by Beneke *et al.* (2017), uses the innate homologous recombination mechanism of the parasite (Zhang & Matlashewski, 2015; Sollelis *et al.*, 2015; Zhang, Lypaczewski & Matlashewski, 2017). The way of using HR in this approach is by introducing PCR-generated repair cassette with homologous arms and gRNA (cDNA) in *L. mexicana* or *L. major* cell lines expressing Cas9 and T7 RNA polymerase from the tubulin locus. The T7 RNA polymerase is responsible to transcribe the gRNA from DNA into a functional RNA molecule. Cells carrying the successful genetic modification

can be selected via antibiotics. This approach can be used either for knocking out or endogenously tagging *Leishmania* genes (Beneke *et al.*, 2017).

Alternatively, a modified CRISPR-Cas9 approach, known as CRISPR/Cas9 cytosine base editor (CBE), has been recently introduced in *Leishmania* as a way to perform precision editing. Briefly, CBE is a cytidine deaminase domain fused to an impaired form of Cas9 (Cas9 nickase), in which the former converts cytidine to uridine via deamination, while the latter targets CBE to a precise target. To prevent base excision repair, which will reverse the cytidine-to-uridine conversion, two monomers of uracil glycosylase inhibitor domains were tethered on the protein. In addition, to improve the CBE editing rates, a *L. major* Rad51-derived single-stranded DNA-binding domain was also inserted. All these modifications led to the formation of the hyBE4max CBE that was successfully expressed within four *Leishmania* species, and facilitated the conversion of arginine, tryptophan, or glutamine codons into STOP codons. The CRISPR/Cas9 CBE approach does not require neither the use of donor DNA for achieving precise editing nor the use of antibiotics for selecting successfully edited cells, while the editing efficiency of this approach reaches 100%. Thereby, this approach is ideal for studying loss-of-function in *Leishmania* (Engstler & Beneke, 2023).

Nonetheless, the use of CRISPR-Cas9 system is revolutionary in the field of *Leishmania* in terms of practicality and efficiency. Furthermore, the use of CRISPR-Cas9 as a knockout tool could be informative in terms of characterizing the essentiality of a *Leishmania* gene. For instance, the knockout of essential gene will prevent the recovery of mutants upon transfection, suggesting that the investigated gene is essential for the parasite. However, this observation is inconclusive due to the possibility of a technical failure (Damianou *et al.*, 2020). A way to counteract this limitation is through the generation of a facilitated mutant. This involves transfection of the cell line prior the deletion of chromosomal gene copies with a plasmid carrying an episomal copy of the gene (=transgene). If the cell line survives the CRISPR-Cas9 KO, while retaining the plasmid over time, it means that the investigated gene is essential. This is known as an unforced plasmid shuffle. An alternative way involves a process known as forced plasmid shuffle, where negative selection pressure is applied to encourage cells to lose the transgene (Dacher *et al.*, 2014; Jones *et al.*, 2018). In this method, the transgene is expressed alongside a thymidine kinase (TK) suicide cassette, rendering cells sensitive to ganciclovir (GCV). When GSV is present, TK produces a toxic metabolite called GCV triphosphate, which inhibits DNA synthesis. This serves as a negative selection pressure on the plasmid. However, if cells lacking the endogenous gene rely on the plasmid for their survival, even with the fitness cost it incurs, it indicates that the gene is essential (Murta *et al.*, 2009).

The primary limitation of the CRISPR-Cas9 system developed by Beneke *et al.* (2017) is its lack of inducibility. Consequently, it is not possible to observe the cellular impact of knocking out an essential gene in a time-dependent manner before the death of the cell. To facilitate such experiments, an alternative genetic modification approach exists, known as the inducible di-Cre recombinase system. This method incorporates two crucial components: the Cre recombinase enzyme and genes flanked by locus of crossover of bacteriophage P1 (loxP) sites, with the former facilitating the excision of the latter. To render this system inducible, the Cre enzyme was split and fused into two inactive fragments, each coupled with a FK506-binding protein (FKBP12) and the binding domain of the FKBP12-rapamycin associated protein (FRB). In the presence of rapamycin, these two inactive fragments of Cre dimerizes (forming DiCre), thereby creating a functional Cre recombinase capable of excising loxP-flanked genes (Duncan, Jones & Mottram, 2017). In *L. mexicana*, the initial strategy entailed replacing one allele of the target gene with the DiCre sequence, and the second allele with a loxP-flanked (floxed) copy of the gene (Duncan *et al.*, 2016). Subsequently, to ensure sufficient Cre recombinase expression, the DiCre sequence was placed under the ribosomal locus, while the second allele of the target gene was

replaced with a hygromycin resistance cassette (Damianou *et al.*, 2020). Overall, this approach enables the characterization of genes, whether they are essential or not, in an inducible manner, while also permitting the study of how the cell responds to the depletion of the investigated gene. More recently, the CRISPR-Cas9 system and the diCre system have been combined, with the former being employed to replace both wild-type alleles with floxed versions in a cell line expressing, Cas9 nuclease, T7 RNA polymerase, and rapamycin-induced DiCre recombinase (Yagoubat *et al.*, 2020; Damasceno *et al.*, 2020).

1.2 Ubiquitination in Non-Trypanosomatids

1.2.1 The Ubiquitin Code

Ubiquitin, a protein with a molecular weight of 8.6 kDa, is composed of 76 amino acid residues organised into a compact β -grasp structural fold. This canonical ubiquitin fold is formed through the assembly of a 5-stranded β -sheet, a short 3_{10} helix and a 3.5-turn α -helix (Vijay-Kumar *et al.*, 1987; Dikic, Wakatsuki & Walters, 2009). Initially, ubiquitin is expressed as an inactive precursor by cytosolic ribosomes. It exists in various forms, including monoubiquitin, polyubiquitin (consisting of two or more ubiquitin molecules), or fused with other proteins. Remarkably, it exhibits a strong preference for fusion with eS31 and eL40 ribosomal proteins (Martín-Villanueva *et al.*, 2021). The maturation of ubiquitin involves the release and activation of its C-terminal glycine residue. Upon activation, ubiquitin gains the ability to be covalently and reversibly attached to target proteins, a process commonly referred to as ubiquitination (Hochstrasser, 2000).

Ubiquitination is just one among hundreds of diverse post-translational modifications (PTMs), akin to phosphorylation and acetylation (Ramazi & Zahiri, 2021). It possesses remarkable functional flexibility, characterised by a multitude of intricate layers (Mevisse & Komander, 2017). Initially, ubiquitin primarily forms an isopeptide bond with the ϵ -amino group of a lysine residue in the target protein, a process known as canonical ubiquitination (Busch, 1984). However, non-lysine ubiquitination, often considered atypical, also exists. Ubiquitin can attach to proteins at their N-terminal amino group through a peptide bond, as well as to specific amino acid residues such as serine, threonine and tyrosine (supported by *in vitro* evidence) via an oxyester bond. Additionally, ubiquitin can form a thioester bond with cysteine amino acid residues. Remarkably, ubiquitin is not limited to modifying proteins alone; it can also conjugate to various non-protein substrates. These include ADP-ribose, bacterial lipopolysaccharide, and cellular sugars (Kelsall, 2022; Squair & Virdee, 2022; Ikeda, 2023). Notably, ubiquitin, being a protein itself, can also undergo ubiquitination. Currently, there are thirteen known ubiquitination sites in ubiquitin. Among these, the seven lysine residues (K6, K11, K27, K29, K33, K48 and K63) and the N-terminal methionine (M1) are well-characterised, while the four threonine residues (T12, T14, T22 and T55) and serine (S28) were recently identified McCrory *et al.*, 2021; Rodriguez Carvajal *et al.*, 2021). The diversity of ubiquitination sites within ubiquitin, coupled with its ability to function as a single molecule (monoubiquitination) or as part of polyubiquitin chains with varying lengths and architectures, significantly enhances the complexity of this PTM (Ohtake & Tsuchiya, 2017). Furthermore, ubiquitin itself can undergo additional PTMs, such as acetylation and phosphorylation, and can be conjugated to other ubiquitin-like molecules, such as NEDD8 and SUMO (Lacoursiere, Hadi & Shaw, 2022). Together, these intricate ubiquitin patterns constitute the “ubiquitin code”, which is recognised and interpreted by proteins containing ubiquitin-binding domains.

Regarding the mechanism of ubiquitin conjugation, three universally conserved types of enzymes that function sequentially are involved: E1 ubiquitin-activating enzymes, E2 ubiquitin-conjugating enzymes

and E3 ubiquitin ligases. Briefly, E1 enzyme activates ubiquitin via an ATP-dependent process involving addition of an adenylyl group to the C-terminus of ubiquitin. This adenylation step enables the formation of a thioester bond between the active site of E1 and ubiquitin. Sequentially, ubiquitin is transferred via trans-thioesterification on the cysteine residue at the active site of E2. Eventually, ubiquitin will be conjugated to the target substrate either through or facilitated by the E3 ligase (Dikic & Schulman, 2023). As it was mentioned previously, the ubiquitin chain might vary in length. This is predominantly determined by the E2 and E3 activity, however in some rare cases an E4 accessory factor supports this lengthening process (Koege *et al.*, 1999). Ubiquitination is reversible, and cleavage of ubiquitin moieties from its target is achieved via the class of proteases known as deubiquitinases (DUB; Fig. 3).

Nevertheless, the ubiquitin system is evolutionary conserved across eukaryotes, however elements of this system were tracked beforehand of eukaryogenesis, in at least three different archaeal groups (Grau-Bové Sebé-Pedros & Ruiz-Trillo, 2015). On the other hand, prokaryotes do not contain the complete ubiquitin toolkit. For instance, some of the bacteria contain E1 and E2 enzymes, which instead of participating in protein labelling, they are involved in molybdopterin and thiamin biosynthesis (Taylor *et al.*, 1998; Leimkühler, Wuebbens & Rajagopalan, 2001). Furthermore, obligate intracellular bacteria, such as *Legionella pneumophila* and pathogenic *Escherichia coli* (*E. coli*), possess genes that code for E3 ligases and DUB enzymes. These genes function as virulence factors, allowing these bacteria to manipulate the ubiquitin system of the host (Vozandychova *et al.*, 2021). Moreover, ubiquitin-like related proteins are also present in prokaryotes. The small sulphur-carrier protein Moad and ThiS, which are involved in molybdopterin and thiamin biosynthesis, have the characteristic β -grasp fold as ubiquitin. Conversely, the *Mycobacterium tuberculosis* protein Pup does not share any sequence or structural homology with ubiquitin, however it is involved in targeting proteins for proteasomal degradation via pupylation. Interestingly, all three ubiquitin-like related proteins share the same GlyGly (DiGly) motif at their C-terminal sequence with ubiquitin (Wang *et al.*, 2001; Rudolph *et al.*, 2001; Pearce *et al.*, 2008). Collectively, it is understood that different elements of the ubiquitin system can be found in various domains of life. However, the entire system is exclusively present in archaea and eukaryotes.

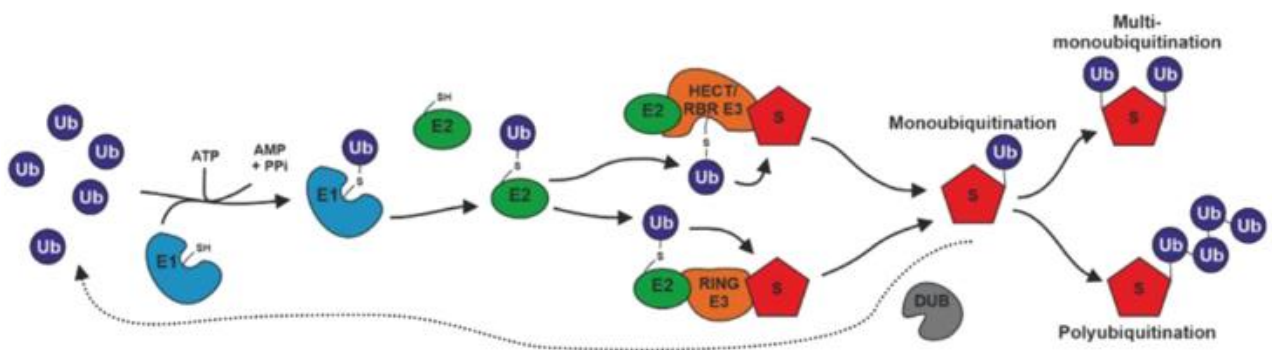


Figure 3: Ubiquitination and deubiquitination. E1 activates ubiquitin through adenylation of its C-terminus, using ATP. Ubiquitin is attached at the active site cysteine of E1 via thioester bond, while free AMP and inorganic pyrophosphate (PPi) are released. Subsequently, ubiquitin is transferred to the E2 active site via trans-thioesterification. Then, E3 ligases facilitate either the direct (ubiquitin is not transferred to the active site cysteine of the E3 RING ligase) or indirect (ubiquitin is transferred to the active site cysteine of the E3 HECT/RBR ligase) conjugation of ubiquitin to the targeted substrate via isopeptide bond. The covalent attachment of a single ubiquitin is known as monoubiquitination, while conjugation of multiple ubiquitin molecules, either onto the monoubiquitin or at different sites on the substrate, are known as polyubiquitination and multi-monoubiquitination, respectively.

Cleavage of ubiquitin molecules is performed by DUBs. Reproduced image from Burge, Mottram & Wilkinson (2022).

1.2.2 Role of Ubiquitin

Ubiquitination is a PTM involved in a plethora of cellular processes, and this is attributed to the diversity and multi-dimensionality of the ubiquitin code. Focusing first on monoubiquitination, which has been shown to be important for the degradation of proteins with a size smaller than 150 amino acids that contain low structural disorder (Braten *et al.*, 2016). Specifically, monoubiquitination-dependent proteasomal degradation is associated with proteins involved in the carbohydrate transport and oxidative stress response pathway, but also with translation and proteasomal degradation (Braten *et al.*, 2016; Jung *et al.*, 2017). Furthermore, monoubiquitination can function as a subcellular localization signal. For instance, it triggers the endocytosis of the receptor tyrosine kinases from the plasma membrane, and facilitates the secretion of the cancer stem cell marker CD133 into extracellular vesicles (Haglund *et al.*, 2003; Yang *et al.*, 2018). Additionally, the conjugation of a single ubiquitin facilitates protein-protein interactions (Magits & Sablina, 2022). For instance, monoubiquitination of the insulin receptor substrate (IRS-2) allows interaction with the ubiquitin-binding protein EPSIN-1. As a result, cell proliferation induced by the insulin-like growth factor 1 (IGF-1) is stimulated (Fukushima *et al.*, 2015). On the other hand, monoubiquitination can also block the interaction of two proteins. An illustrative case is that of RAS-related protein B, of which its monoubiquitination prevents its binding to the effector exocyst complex component EXO84. Consequently, this inhibition prevents the initiation of autophagy (Simicek *et al.*, 2013).

Complexity in the ubiquitin code is added when two or more ubiquitin molecules are bound on a protein substrate. An example of this category is multi-monoubiquitination, of which single ubiquitin moieties are attached to unoccupied lysine residues on the substrate protein (Sewduth, Baietti & Sablina, 2020). Multi-monoubiquitination, just like monoubiquitination, could act as an alternative degradation signal. For example, the anaphase-promoting complex targets Cyclin B1 for proteasomal degradation through multi-monoubiquitination, which subsequently triggers the mitotic exit of the cell (Dimova *et al.*, 2012). Multi-monoubiquitination has also a degradation-independent biological role. A noteworthy example is the multi-monoubiquitination of the heat shock protein 70 (HSP70), a process mediated by the E3 ubiquitin ligase parkin. In this context, multi-monoubiquitination prevents the proteasomal degradation of HSP70, suggesting a potential mechanism for rescuing its functionality as a chaperone (Moore *et al.*, 2008). In addition, multi-monoubiquitination plays a crucial role in regulating changes in cell morphology and motility in mammalian cells. This regulation occurs by modulating the interaction between the VASP protein and actin, in which multi-monoubiquitination of the former diminishes the polymerization of the latter (McCormick *et al.*, 2023).

As mentioned previously, ubiquitin has multiple sites of ubiquitination. Thereby, polyubiquitination chains, depending on which ubiquitination site are developed, acquire linkage-specific function (Tracz & Bialek, 2021). For instance, Lys48-linked chains, which are the most abundant polyubiquitination type in most of cells, act as a signal that targets proteins for proteasomal degradation (Akimov *et al.*, 2018). This type of polyubiquitin chain has a primary contribution in the overall regulation of protein homeostasis, including the removal of mislocalized, misfolded or prematurely folded proteins from the cell (Song, Herrmann & Becker, 2021). One of the many specific examples highlighting the importance of the K48-linked polyubiquitination is in the regulation of the protein levels of the centrosomal OLA1 through proteasomal degradation, which is required for the proper maturation of the centrosome during the G2 phase of the cell (Fang *et al.*, 2023). The second most understood

polyubiquitin chain is the one with Lys63 linkages, which is involved in various cellular processes, including membrane trafficking and DNA repair (Hu *et al.*, 2023; Qin *et al.*, 2023). In regards of the biological significance of the rest linkages, K6-linked polyubiquitination chains are involved predominantly in mitophagy and the DNA damage response, while K11-linked polyubiquitin chains are associated with the cell cycle and responses to biotic and abiotic stressors (Tracz & Bialek, 2021). Furthermore, K27-, K29- and K33-linked polyubiquitination chains play a major role in innate immunity, intracellular signalling pathways and protein trafficking respectively (Yuan *et al.*, 2014; Chen *et al.*, 2023; Jiang *et al.*, 2023). Finally, M1-linked polyubiquitination chains are involved in NF- κ B signalling under stress-induced inflammation (Aalto *et al.*, 2022).

Nevertheless, all these polyubiquitination chains are composed of ubiquitins that are attached to each other using the same ubiquitination site. Therefore, the structure of such chains is characterised as homogenous. Conversely, polyubiquitination chains containing a mixture of ubiquitin linkages are classified as heterotypic, and their architecture can be mixed or branched. Interestingly, the biological significance of heterotypic chains is less understood. Nonetheless, a study conducted in 2016 has revealed that the K48-K63 branched chains act as a signal stabilizer that promotes NF- κ B signaling. Specifically, the heterotypic polyubiquitination prevented the deubiquitination of the initially K63-linked polyubiquitinated TRAF6 protein, which in response enhanced NF- κ B activity. Thus, it was further concluded that heterotypic polyubiquitination provides an additional level of protein regulation (Ohtake *et al.*, 2016). Another example of a studied heterotypic polyubiquitin chain is the K11-K48. K11-K48 polyubiquitination serves as an efficient proteasomal degradation signal against aggregation-prone proteins and dislocated protein-substrates of the endoplasmic reticulum-associated degradation system. In particular, K11-K48 chains bind with higher affinity to proteasomes and p97/VCP, making them a priority signal for efficient coupling and degradation (Leto *et al.*, 2019).

Apart from being ubiquitinated, ubiquitin can be subjected to other PTMs. For instance, acetylation, which is the covalent attachment of acetyl group on the basic amino acid residues lysine and arginine, was observed on both free and substrate-conjugated ubiquitin molecules. Interestingly, acetylated ubiquitin molecules are unable to form elongated polyubiquitin chains, such as in the case of the histone protein H2B, suggesting that acetylation might act as a protein stabilization mechanism that regulates polyubiquitin-linked proteasomal degradation (Ohtake *et al.*, 2015). Phosphorylation is another PTM that targets ubiquitin, in which it attaches a phosphoryl group predominantly on serine, threonine and/or tyrosine amino acid residues. Phosphorylation of the ubiquitin serine 65 by the PINK1 kinase is one of the few well-characterised phospho-ubiquitin events. It takes place when the inner mitochondrial membrane is depolarized due to a damage of the mitochondrion and it is involved in the activation of the E3 ligase Parkin. As a result, the activated Parkin ubiquitinates various outer membrane mitochondrial proteins, which subsequently triggers mitophagy (Lambourne *et al.*, 2023)

As previously mentioned, ubiquitination is also observed in sugars and lipids and this is known as atypical ubiquitination. The first evidence of non-protein ubiquitination was identified on the lipid A moiety of the lipopolysaccharides of the Gram-negative bacterium *Salmonella enterica* serovar Typhimurium (*S. Typhimurium*) during infection of mammalian cells. This non-canonical ubiquitination event was performed by the E3 ubiquitin ligase ring finger protein 213 of the host cell, as a triggering mechanism to eliminate the intracellular pathogen via autophagy (Otten *et al.*, 2021). Furthermore, it has been discovered that conjugation of ubiquitin also occurs in the phospholipids of yeast and mammalian cells, with a preference for phosphatidylethanolamine (PE) located in endosomes and the vacuole of yeast. Interestingly, ubiquitination of PE is mediated by enzymes of the canonical ubiquitin system, such as the Tul1 ubiquitin E3 ligase complex. This ubiquitination event is speculated to contribute into the formation of intraluminal vesicles through the recruitment of the ESCRT complex.

Similarly, ubiquitinated-PE has also been observed in baculoviruses under insect-cell infection, and it is hypothesised that this modification might contribute in the egress of the virus through ESCRT complex (Sakamaki *et al.*, 2022). Finally, elegant *in vitro* experiments introduced atypical ubiquitination in sugars. Specifically, it has been shown that the mammalian E3 ligase HOIL-1, which is part of the LUBAC complex, monoubiquitinates glycogen and α 1:4-linked maltoheptaose at the C6 hydroxyl moiety of their glucose residues. However, two other components of the LUBAC complex predominantly bind to unbranched glucosaccharides. As a result, it is speculated that the LUBAC complex is recruited solely at these unbranched glucosaccharides inside the cell, and through monoubiquitination it ensures that these glucosaccharides will be removed. This prevents the formation of polyglucosan that is toxic for vital organs (Kelsall *et al.*, 2022). Collectively, non-canonical ubiquitination is important as a defence mechanism against intracellular bacteria and sugar-derived toxins, and also is required for intracellular vehicle trafficking.

1.2.3 E1 Ubiquitin-Activating Enzymes

Overall, there are eight E1 ubiquitin-activating enzymes in the human proteome, of which according to their structural and biochemical properties are subdivided in two classes: canonical and non-canonical (Barghout & Schimmer, 2021). Focusing first on the eukaryotic canonical E1 enzymes, one of their multiple types of domains is the adenylation domain (AD). The AD is pseudosymmetric, possessing an active and inactive domain, of which the former is responsible for recognising and adenylating ubiquitin and ubiquitin-like molecules (collectively are called UBLs) and the latter maintains structural stability (Lv *et al.*, 2017). Another domain of E1s is the catalytic cysteine domain (CCD), which as the adenylation domain, is sub-divided into the first and second CCD. Together, the CCDs are involved in the formation of thioester bond between the UBLs and the E1 enzyme (Lv *et al.*, 2017). Furthermore, the ubiquitin-fold domain is also conserved in E1s, and it interacts with the cognate E2s for transferring the UBL via transthiolation (Lv *et al.*, 2017). In the case of non-canonical E1s, one of the most striking differences is the presence of other domains, such as in the case of UBA4 that possesses a C-terminal rhodanese homology domain. This domain is important for transferring sulfur to its UBL substrate known as URM1 (Jüdes *et al.*, 2016).

Focusing solely on the enzymatic activity of canonical E1s, they activate UBL molecules in a multistep and ATP-dependent procedure. The first step involves the adenylation of a free UBL molecule at its C-terminus (UBL~AMP) in the presence of ATP and Mg^{2+} . Sequentially, the adenylated UBL is attached to the active AD of the E1, while a PP_i is released. Then, a nucleophilic interdomain reaction takes place, where the catalytic cysteine of the CCD attacks the adenylated UBL. As a result, the AMP is released, and the UBL binds at the CCD of the E1 via thioester bond. In the meantime, a second free UBL undergoes adenylation and is non-covalently attached at the active AD of the same E1 enzyme (Haas & Rose, 1982). This leads to the formation of a double-UBL-loaded E1 enzyme, which favours the enzyme energetically and/or conformationally and accelerates the transfer of the UBL to the E2-conjugating enzyme (Cappadocia & Lima, 2018). Transfer of the UBL from E1 to E2 is achieved via transthiolation reaction, while the ubiquitin-fold domain of E1 plays a crucial role in maintaining the interaction between these two proteins until the reaction is completed. Finally, the now single UBL~AMP-bound E1 is available to repeat the same cycle of thioesterification, adenylation and transthiolation (Schulman & Harper, 2009).

As previously mentioned, the ubiquitination system is involved in a plethora of biological processes, ranging from regulating the cell cycle to contributing in inflammation and immune responses. Several diseases have been associated with the dysregulation of this PTM, including various forms of cancer

and neurodegeneration. Thus, different components of the ubiquitin system have been utilized as drug targets (Barghout & Schimmer, 2021). Focusing on the E1 enzymes, there are two ideal sites that have been targeted for therapeutic discoveries. The first one is their specialised nucleotide-binding pocket in the active AD, which selectively binds to the UBL~AMP. Various small-molecule E1 inhibitors have been developed throughout the years, with the adenosine sulfamate E1 inhibitors that mimicking the UBL~AMP intermediate to stand out (Brownell *et al.*, 2010). Alternatively, the catalytic cysteine of the CCD has been also explored as a drug targeting site. For instance, PYR-41 and PYZD-4409 are two inhibitors utilizing this mechanism of action, selectively against the most well studied E1, the UBA1 (Yang *et al.*, 2007; Xu *et al.*, 2010). However, none of these compounds have entered clinical trials. This could be attributed to the fact that E1 enzymes are the initiating component of ubiquitination, thus targeting such enzymes will provoke inhibitions of various cellular functions. The only E1 inhibitor that has entered the clinical trials is pevonedistat. Pevonedistat targets the E1 enzyme NAE, which is involved in neddylation. Overall, neddylation participates in a smaller number of biological functions, therefore it makes NAE ideal for therapeutic targeting (Soucy *et al.*, 2009). Despite targeting E1 enzymes for inhibition, E1 activity enhancers are also under investigation. For instance, auranofin was found to improve the overall performance of UBA1, promoting ubiquitination and degradation of misfolded ER proteins, and thereby opening the horizons for developing specialized drugs of various neurodegenerative disorders (Yan *et al.*, 2023).

1.2.4 E2 Ubiquitin-Conjugating Enzymes

Overall, there are 40 E2-ubiquitin conjugating enzymes in humans. Members of the E2 family share a highly conserved 150-200 amino acid ubiquitin-conjugating catalytic (UBC) fold, which act as a binding site for E1s, E3s and the activated ubiquitin/UBL (van Wijk & Timmers, 2010). Within the UBC domain, there is an active site cysteine and about 10 residues upstream of this cysteine, there is an HPN-motif. The former is involved in two crucial reactions: firstly, in the transfer of activated ubiquitin/UBL from the E1 to E2 via transthioesterification and secondly, in the transfer of ubiquitin to either on E3 ligase or targeted substrate via aminolysis (Huang *et al.*, 1999; Olsen & Lima, 2013). On the other hand, the asparagine from the HPN-motif is responsible for creating the peptide bond between the C-terminal glycine of ubiquitin and a lysine of the targeted substrate, while the histidine and proline residues provide structural support throughout the process (Wu *et al.*, 2003). In many E2 enzymes, there is an additional backside surface of the UBC domain. It is situated opposite the catalytic pocket and it binds to the activated ubiquitin/UBL via non-covalent interactions. This backside surface facilitates the proper positioning of ubiquitin/UBL, exposing the thioester bonding site for undergoing aminolysis (Nguyen *et al.*, 2014). Nevertheless, E2 enzymes containing solely the catalytic UBC core are classified as class I, while those consisting of an additional N- or C-terminal extension, or both, are categorised as class II, III and IV respectively (Lei *et al.*, 2023). These additional extensions provide functional differences across the E2s. For instance, the N-terminal extension in the UBE2E proteins promotes monoubiquitination, while the C-terminal extension of UBE2R1 facilitates the formation of polyubiquitin chains (Kolman, Toth & Gonda, 1992; Schumacher, Wilson, & Day, 2013). Thus, E2 terminal extensions modulate the ubiquitin activity of the interacting E3s, and also provides some selectivity to the enzymes themselves.

As was already mentioned, the smaller number and the lack of specificity of E1 enzymes make them poor therapeutic targets. However, this is not the case of E2 enzymes (Celebi *et al.*, 2020). For instance, Ubc13 has been found to participating in the constitutive activation of the NF- κ B signaling and also, in the ubiquitination of the tumour suppressor gene p53, which causes reduction of its activity. One approach of inhibiting the Ubc13 enzymatic activity is by targeting the active site cysteine.

Interestingly, the chemical compound NSC697923 was found to covalently bind at the catalytic cysteine of Ubc13, and selectively interacting further with a unique Ubc13 binding cleft (Hodge *et al.*, 2015). At this point is worth mentioning that Ubc13, as well as some other E2s, require to form a complex with a catalytic inactive E2, such as Uev1A and MMS2, in order to perform their enzymatic activity. Thus, another appealing therapeutic approach is to disrupt the formation of such complexes. The natural products Leucettamol A and manadosterols A and B have been found to disrupt the Ubc13-Uev1A interaction *in vitro*, however this was never validated *in vivo* (Tsukamoto *et al.*, 2008; Ushiyama *et al.*, 2012). In the case of the CC0651 inhibitor, it interferes with the discharge of the ubiquitin molecule from the cell division cycle 34 protein (CDC34) to the acceptor lysine residue. The compound inhibits the E2 activity allosterically via binding at the cryptic binding pocket of the E2 enzyme, causing subtle changes in the structural conformation of the enzyme (Ceccarelli *et al.*, 2011). Nonetheless, at the moment there are no ongoing clinical trials exploring E2 inhibitors.

1.2.5 E3 Ubiquitin Ligases

The final step of ubiquitination involves transferring of the ubiquitin molecule from the E2 conjugating enzyme to the targeted substrate. This step is achieved in the presence of the class of enzymes known as E3 ligases, which contains more than 600 members. The diversity in this class is critical for providing selectivity and efficiency of substrate ubiquitination. Overall, the E3 ligases are categorised in three broad families; the really interesting new gene (RING) finger family, the homologous to E6AP C terminus (HECT) family and the RING between RING (RBR) family (Zou *et al.*, 2023). Focusing firstly on the largest subgroup of E3 ligases, RING finger E3 ligases are distinguished by their RING or U-box domain, which are structurally similar (Metzger, Hristova & Weissman, 2012). Notably, one of the main differences between the two domains is that the enzymatic activity of the former requires chelation of two zinc ions (Zn^{2+}), while the latter domain does not (Zheng & Shabek, 2017). Nevertheless, RING E3s serve as a scaffold for the concomitant recruitment of the active ubiquitin-conjugated E2 and the specific substrate during ubiquitination. The E2-E3 interaction causes allosteric activation of the E2, which stimulates the ubiquitin release (Branigan, Carlos Penedo & Hay, 2020). In regards of HECT E3s, they all contain the conserved 350 amino-acid long HECT domain, which is located at their C-terminal. Notably, the HECT domain has three main features: the N-terminal N-lobe, the C-terminal C-lobe and the flexible linker connecting the two. The N-lobe is involved in the E2 interaction, while the C-lobe contains an active site cysteine, which acts as an attachment site for ubiquitin that is transferred via transthioesterification from E2. As about the flexible linker, it facilitates the ubiquitin transfer by rearranging the conformation of the N- and C-lobes, thereby bringing the active sites of E2 and E3 into close proximity (Huang *et al.*, 1999; Sluimer & Distel, 2018). Finally, the RBR family of E3s exhibits functional characteristics from both RING and HECT E3 ligases, categorising them as RING/HECT E3 hybrids. Overall, they contain three domains, which are arranged in the given order: RING1 domain, R_{cat} (required-for-catalysis) and BR_{cat} (benign-catalytic). The RING1 domain is involved in E2 interactions, while the R_{cat} domain contains an active site cysteine to which ubiquitin is attached to. The BR_{cat} domain shares structural similarities with the R_{cat} domain, however it lacks the catalytic cysteine residue. As in the case of HECT E3 ligases, RBRs utilize a two-step catalytic mechanism for conjugating ubiquitin to the substrate (Wenzel *et al.*, 2011; Spratt, Walden & Shaw, 2014).

Compared to the E1s and E2s, the E3 ligases possess specific roles within the cells (Sampson *et al.*, 2023). For instance, MDM2 is an E3 ligase that tightly regulates the activity of tumour suppressor p53 through both direct protein-protein interaction and ubiquitination, under non-stress conditions. However, overexpression of MDM2 has been associated with various human malignancies, making it

ideal therapeutic target. Nutlins, which is a class of cis-imidazoline analogs, were found to inhibit the MDM2-p53 interaction via binding at the p53 binding pocket of MDM2 (Vessilev *et al.*, 2004). Interestingly, a nutlin-derivative known as RG7388 has been discovered to disrupt the MDM2-p53 interaction with a superior potency and selectivity (Ding *et al.*, 2013). It has undergone clinical trials for the treatment of neuroblastoma and acute myelogenous leukemia (Yee *et al.*, 2014). Two other examples of E3 ligases with a specific cellular function are the cellular inhibitor of apoptosis proteins (cIAP) 1 and 2. These two proteins act as key regulators of the innate immunity response via contributing to the survival signal derived from the tumour necrosis factor (TNF) surface receptors. However, dysregulation of cIAP1 and cIAP2 has been associated with various cancers, including liver carcinomas and pancreatic cancers, thus they have been persuaded as anticancer drug targets. TL32711, LCL161 and GDC-0152 are some of the many inhibitors that have been under clinical investigation for treating solid tumours via targeting cIAP1 and cIAP2 (Flygare *et al.*, 2012; Benetatos *et al.*, 2014; Bardia *et al.*, 2018).

1.2.6 Deubiquitinating Enzymes

Ubiquitination is associated with myriad cell-based physiological and biological aspects. However, the ubiquitination status established by the ubiquitin-conjugating enzymes (E1, E2 and E3) is tightly regulated and counterbalanced by another class of enzymes, the deubiquitinases (or deubiquitylases; hereafter DUBs; Wilkinson, 1997). In general, the number of identified DUBs in each organism varies. For instance, in humans there are ~100 DUBs but in *Saccharomyces cerevisiae* there are only 20 (Clague, Urbé & Komander, 2019). Furthermore, sequence and domain conservation analysis classified DUBs in seven major evolutionary conserved families: ubiquitin-specific proteases (USP), ubiquitin carboxy-terminal hydrolases (UCHs), ovarian tumour proteases (OTU), Machado-Josephin domain-containing protease (MJDs), motif-interacting with ubiquitin-containing novel DUB family (MINDY), JAB1-MPN-MOV34 Pad1 N-terminal+ (MPN+) domain proteases (JAMMs) and zinc finger with UFM1-specific peptidase domain protein (ZUFSP; Xue *et al.*, 2023). The DUBs are further categorised based on their mechanism of action into two classes: metalloproteases (only JAMMs family) and cysteine proteases (the rest of the families). Focusing on the former class, these DUB metalloproteases possess a catalytic core composed of two histidines and an aspartate/glutamate, which, in association with a water molecule, coordinate a Zn²⁺ ion to carry out their isopeptidase activity (Shrestha *et al.*, 2014). In regards of the latter class, canonical cysteine protease DUBs contain a catalytic triad composed of a cysteine, a histidine and an aspartate/asparagine residues, which coordinates the hydrolysis of the isopeptide bond that links the C-terminus of the ubiquitin with its substrate (Komander & Barford, 2008).

DUBs are crucial for maintaining the ubiquitin homeostasis of the cells. For instance, DUBs are involved in the generation of *de novo* ubiquitin molecules by processing ubiquitin precursors expressed either as polyubiquitin chains (UBB, UBC) or fused with other proteins, such as ribosomal subunits (UBA52, UBA80; Grou *et al.*, 2015). Furthermore, DUBs rescue ubiquitin from degradation at the site of proteasome, allowing its re-use, but they also deubiquitinate various ubiquitinated substrates elsewhere in the cell, contributing in the maintenance of the ubiquitin pool (de Poot, Tian & Finley, 2017). In addition, DUBs function as interpreters and editors of the ubiquitin code, of which their activity is influenced by various factor, including the subcellular localisation, structure of the catalytic domain and presence of additional domains (Caba, Mohammadzadeh & Tong, 2022). For instance, the presence of ubiquitin binding sites S1 and S1' provide ubiquitin linkage specificity to the DUB. Specifically, S1 site interacts with the distal ubiquitin a di-ubiquitin, while S1' site binds to the proximal ubiquitin, placing the scissile bond into the catalytic active site for hydrolysis. However, the S1' site

determines the orientation of the proximal ubiquitin, which subsequently determines the lysine residue that is presented to the catalytic center and thereby, the linkage specificity of the DUB (Sato, 2022). These ubiquitin-binding sites can be present on the catalytic domain of the DUB, as exemplified by the K6-specific USP30 (Sato *et al.*, 2017). Alternatively, they may be found on an ubiquitin-binding domain (UBD) situated within the DUB (i.e. in *cis*), such as the C-terminal ubiquitin interacting motif (UIM) in the case of the K63-specific OTUD1 (Mevisen *et al.*, 2013). Furthermore, another scenario involves the presence of a UBD on an interacting partner (i.e. in *trans*), such as the UIM located on the interacting partner of the K63-specific AMSH, known as signal transducing adaptor molecule (STAM; McCullough *et al.*, 2006). Linkage specificity for polyubiquitin chains is provided by additional ubiquitin sites that accommodate more distal or proximal ubiquitin moieties, such as the S2 site found on the K11 chain specific OTUD2 (Mevisen *et al.*, 2013). All DUBs possess at least one ubiquitin binding site (S1), however DUBs exhibit substrate specificity and no linkage-specificity feature a S1' substrate-binding site instead of a S1' ubiquitin-binding site (Mevisen & Komander, 2017).

Despite the type of ubiquitin linkage, there are additional features of the substrate that interlink substrate specificity and DUB activity, including length and architecture of ubiquitin chains, whether the modifier is ubiquitin or ubiquitin-like molecule, the presence of other PTMs on ubiquitin, and the nature of the substrate itself (Mevisen & Komander, 2017). Furthermore, there are some DUBs that process polyubiquitin chains bound to a substrate, either in a distal to proximal orientation (*exo*-cleavage) or from within the chain (*endo*-cleavage; Ye *et al.*, 2011; Hospenthal, Freund & Komander, 2013). There are also DUBs capable of cleaving intact ubiquitin chains from their substrates, which is known as *en bloc* cleavage. For instance, USP14 and PSMD14 are two DUBs that perform *en bloc* cleavage of polyubiquitin chains, aiming to prevent substrates from proteasomal degradation and rescue functional ubiquitin from substrates committed to proteasomal degradation, respectively (Lu *et al.*, 2015; Lee *et al.*, 2016). Thereby, *en bloc* cleavage has been closely associated with proteasomal degradation, highlighting the correlation between the cellular activity of DUBs and their substrate specificity (Clague, Urbé & Komander, 2019).

As it was previously discussed, ubiquitination is involved in a plethora of biological processes, such as protein homeostasis, DNA repair and immune responses. Unsurprisingly, DUBs also play a major role in these cellular functions, therefore their dysregulation has been associated with many health conditions, such as cancer and neurological disorders (Celebi *et al.*, 2020; Bello *et al.*, 2022). For example, the USP7 overexpression has been associated with neuroblastoma, due to the deubiquitination and thereby the stabilization of the oncoprotein transcription factor MYCN (Tavana *et al.*, 2016). In addition, USP10 overexpression contributes in the pathology of tauopathies, including Alzheimer's disease, by inducing the formation of stress granules that promote Tau aggregation in neurons of brain lesions (Piatnitskaia *et al.*, 2019). Nevertheless, inhibition of such DUBs suppresses their disease-inducing functions, including the destabilization of specific target proteins associated with the pathology of a disease. For instance, FT671 (non-covalent) and FT827 (covalent) were discovered to strongly and selectively inhibit USP7, resulting in the suppression of tumour growth in mice. This inhibition leads to the degradation of the oncoprotein E3 ligase MDM2, subsequently stabilizing the tumour suppressor p53 and promoting tumour cell death *in vivo* (Turnbull *et al.*, 2017). IMP-1710 is another potent and stereoselective small DUB-inhibitor targeting UCHL1, resulting in the suppression of fibrotic phenotypes in idiopathic pulmonary fibrosis cellular models, with minimal cytotoxicity (Panyain *et al.*, 2020). A USP14-specific inhibitor known as VLX1570 reached Phase I in clinical trials as a treatment for relapsed and refractory multiple myeloma. However, the study was discontinued due to high pulmonary toxicity (Rowinsky *et al.*, 2020). Nonetheless, the selective nature of DUBs making these proteins promising targets for future drug development.

Recently, the concept of targeted protein stabilization (TPS) via DUBs has been introduced as a potential therapeutic approaches of diseases, such as cystic fibrosis (CF). These diseases are characterised by proteins that undergo abnormal ubiquitination and subsequent degradation, like the CF transmembrane regulator (CFTR) channels. The idea behind TPS involves the targeted recruitment of a specialised DUB to its aberrantly ubiquitinated substrate. Through deubiquitination, this process will stabilize the protein of interest and rescue its cellular function. So far, there are two currently available approaches. The first approach utilizes engineered DUBs (enDUBs) that perform nanobody-directed deubiquitination. This is achieved by expressing a DUB substrate of interest with a yellow-fluorescence protein (YFP) tag and its respective DUB, as an enDUB whose catalytic unit is fused to a nanobody specific for GFP and YFP, making the enDUB YFP-targeted. This method was applied and validated in a long QT type 1 cardiomyocyte model, using OTUD1 as enDUB and the potassium voltage-gated channel subfamily Q member 1 (KCNQ1) as a substrate. The ubiquitination of KCNQ1 prevents its trafficking to the cell surface (Kanner *et al.*, 2020). In regards of the second approach, it uses a heterobifunctional stabilizer, known as DUBTAC, to bring in close proximity the abnormally ubiquitinated substrate and its DUB by forming a ternary complex. This process leads to the deubiquitination and subsequent stabilization of the substrate. DUBTAC is a small molecule composed of three components: a covalent recruiter that selectively and allosterically binds to the DUB of interest, a small-molecule ligand that specifically targets the substrate, and a linker connecting these molecules together. The length and composition of the linker is critical for the overall functionality of the stabilizer. As a proof of concept, a DUBTAC called NJH-2-057 was developed, consisting of an EN523 OTUB1 recruiter linked to lumacaftor, a drug that binds to the mutant CFTR. When applied to human CF bronchial epithelial cells, this DUBTAC led to improved chloride channel conductance in the mutant CFTR channel due to the stabilization of the CFTR channel protein levels (Henning *et al.*, 2022). Although there is limited information available about the kinetics of the ternary DUB-substrate complex formation in both approaches, it is noteworthy that the DUB-substrate association did not adversely affect the function of either protein. This finding makes both approaches promising therapeutic strategies.

1.2.7 Proteasome

Ubiquitination and 26S proteasome are tightly associated for regulating protein turnover within the cell, with the former targeting undesirable or damaged proteins to the latter, while the latter proteolytically cleaves these proteins into short peptides (Abi Habib *et al.*, 2022). Together, they comprise the ubiquitin-proteasome pathway (UPS), and in this section I am going to focus solely on the proteasome. Firstly, the 26S proteasome is a ~2.5MDa complex comprising 47 subunits in humans, making it the largest known eukaryotic protease (Livneh *et al.*, 2016). Secondly, the 26S subunit is compartmentalized into two particles: the hollow cylindrical 20S core particle (CP) and the 19S regulatory particle (RP) that caps CP at one or both of its ends. CP is made of four stacked heptameric rings, two identical outer α -rings and two identical inner β -rings, which are comprised of seven α and seven β subunits respectively. The central catalytic chamber of the proteasome is formed by the two heptameric β -rings and is localized internally of the complex, preventing uncontrollable degradation of surrounding functional proteins (Groll *et al.*, 1997). Within the catalytic chamber, there are three catalytically active subunits: β 1, β 2 and β 5, which cleave acidic, basic and hydrophobic residues respectively. Thus, the proteasome has been associated with caspase-like, trypsin-like and chymotrypsin-like activities (Dick *et al.*, 1998). Nevertheless, proteins targeted for proteasomal degradation are getting de-ubiquitinated, if ubiquitin/ubiquitin chain is present, and unfolded by RP proteins before are inserted into the catalytic chamber (Ruschak *et al.*, 2010). Ultimately, these mis-

functional proteins are converted into 3 to 30 amino acid long peptides by the proteasome, which are then degraded down to amino acids by cytoplasmic peptidases (Kisselev *et al.*, 1998).

Malfunction of the proteasome has been associated with several cancer, such as multiple myeloma, and age-related and neurodegenerative diseases, including Parkinson's disease and Alzheimer's disease (George & Tepe, 2021). As a result, multiple compounds have been developed throughout the years targeting the proteasome. One of them is Bortezomib (Velcade). Bortezomib is an approved by the US Food and Drug Administration (FDA) proteasomal inhibitor for treating multiple myeloma (MM) and mantle cell lymphoma (Herndon *et al.*, 2013). As a dipeptide boronate inhibitor, Bortezomib targets the side-chain hydroxyl group of the N-terminal threonine located in the β 1 and β 5 active site of the proteasome, thereby inducing various cellular pathways, including an apoptotic response against the carcinogenic cells (Hideshima *et al.*, 2003). However, treatment with Bortezomib has been associated with peripheral neuropathy, probably due to an off-target inhibition of proteases, including serine proteases (Arastu-Kapur *et al.*, 2011). This led to the development of the first irreversible FDA-approved proteasomal inhibitor, Carfilzomib (Kyprolis[®]). Carfilzomib is a tetrapeptide epoxyketone that forms a dual covalent adduct specifically with the side-chain hydroxyl group and the free amine of the N-terminal threonine active site of β 5, making it selective and potent inhibitor of proteasome (Kuhn *et al.*, 2007). It is used for treating relapsed and refractory MM patients, including the ones with bortezomib-resistance (Herndon *et al.*, 2013). Other approved proteasomal-targeting drugs are: Ixazomib (Ninlaro[®]), Marizomib (salinosporamide A), Oprozomib (ONX 0912), and Delanzomib (CEP-18 770; Ambrosio *et al.*, 2023).

1.2.8 Ubiquitin-Like Molecules

Ubiquitin and its cellular functions have been widely studied. However, there are at least 17 ubiquitin like (UBL) molecules in humans that share similar folding structure with ubiquitin that have been reported to be attached on other molecules (type I) or to occur as protein domains, fulfilling protein-protein interaction roles (type II; Schulman & Wade Harper, 2009; Santonico, 2020). Similarly with ubiquitin, covalent attachment of type I UBLs is achieved via their C-terminus, which contains either one or two glycine residues, and the cycle of conjugation-deconjugation of each UBL is performed by specialised E1-E2-E3 and isopeptidase enzymes (Hwang, Lee & Kho, 2022). One UBL that has been well characterised is the small ubiquitin molecule (SUMO). So far, there are five SUMO isoforms, expressed at different mammalian organs, such as SUMO1 in brain. However, for the SUMOylation cycle to kick off, SUMO undergoes a maturation process performed by sentrin isopeptidases (SENPs; Queiroz, Kageyama & Cimarosti, 2023). Nevertheless, SUMO is known for its predominant nuclear role involved in transcription, nuclear transport and DNA repair (Wang & Dasso, 2009). Another UBL molecule is the neuronal precursor cell-expressed developmentally downregulated protein 8 (NEDD8). NEDD8 has the highest identity and similarity to ubiquitin of up-to 55%, and predominantly, it acts as a scaffold protein within the multi-component assembly of E3 ligases referred to as Cullin-Ring-Ligases (Hochstrasser, 2009). Furthermore, NEDD8 is involved in various other processes, including the formation of stress granules, degradation of misfolded aggregation-prone proteins and DNA damage (Meszka, Polanowska & Xirodimas, 2022). Some of other UBLs are the interferon-stimulated gene 15 (ISG15), autophagy-related protein 12 (ATG12), and ATG8, of which ATG8 is the only UBL molecule that is solely attached to a lipid (Lystad & Simonsen, 2019).

1.3 Ubiquitination in *Leishmania*

1.3.1 Ubiquitin and UBLs in *Leishmania*

Ubiquitin is present in all eukaryotes, including *Leishmania*. In particular, the protein sequence of the 76-amino acid long ubiquitin is highly conserved between *Leishmania* and humans, with ubiquitin of *L. major* and *L. mexicana* varying at amino acid 14 (A instead of T) and 52 (E instead of D), while the one from *L. tarentolae* having additional two differences at position 11 (T instead of K) and 47 (D instead of G; Graeff *et al.*, 1993; Fleischmann & Campbell, 1994). Furthermore, as previously mentioned, ubiquitin is expressed as inactive precursor in the form of either monoubiquitin, polyubiquitin or fused to another protein. An early study revealed that *L. donovani* genome contains a gene with a minimum of 44 tandemly arranged ubiquitin coding repeats, which was almost 5 times bigger than the human one (Wiborg *et al.*, 1985; Kirchoff *et al.*, 1988). Furthermore, a recent comprehensive examination of ubiquitin genes, which exhibit a minimum of 80% identity in at least 80% of their length compared to yeast ubiquitin, discovered several noteworthy findings. In the *L. braziliensis* genome, two polyubiquitin genes were identified, of which the one contains 13 and the other one 14 tandem ubiquitin repeats. Additionally, a single ubiquitin gene in *L. braziliensis* was found to be fused with the 60S ribosomal subunit L40 (RPL40). The same study unveiled significant insights into the genome of *L. infantum*. It identified a pair of polyubiquitin genes, featuring 9 and 11 tandem repeats of ubiquitin, respectively. Notably, the latter of these genes was observed to be fused with RPL40. Additionally, a tandem arrangement of 9 ubiquitin repeats was also detected in *L. major* (Martín-Villanueva *et al.*, 2021). In *L. major*, there is also evidence of another ubiquitin gene that is fused to a 52 amino acid-long sequence, encoding for the ribosomal protein S27a (Graeff *et al.*, 1993; TriTrypDB, 2023). Finally, *L. tarentolae* was demonstrated to possess both a polyubiquitin-encoding (*ubiC*) and RPS27a-fused ubiquitin protein genes (*ubiA* and *ubiB*), all of which exhibit expression (Fleischmann & Campbell, 1994). Collectively, it is concluded that there is a considerable heterogeneity across the *Leishmania* genomes in regards of the architecture of ubiquitin genes.

Like other eukaryotes, *Leishmania* expresses various ubiquitin-like modifiers (UBLs) alongside ubiquitin. In *L. major*, the UBLs ATG8 and ATG12 have been identified as participants in the process of autophagy. Specifically, ATG12 become covalently attached to ATG5, facilitated by the activity of the E1-like ATG7 and E2-like ATG10. The resulting ATG5-ATG12 complex plays a crucial role in autophagosome formation by ensuring the attachment of phosphatidylethanolamine to ATG8. Furthermore, this complex is also essential for the proper functioning of the mitochondrion, particularly in terms of oxidative capacity and energy generation, but it is also required for the differentiation process of the parasite (Williams *et al.*, 2012). Similarly, AT8 sustains the survival of *L. donovani* throughout its life-cycle and under stress exposure. Both of these conditions are dependable on autophagy, justifying the necessity of ATG8 (Giri & Shaha, 2019). The ubiquitin fold modifier-1 (UFM1) is also present in *Leishmania*. In particular, UFM-1 was found to be activated in the presence of ATP by the E1-like UBA5 and conjugated to mitochondrial proteins via the E2-like UFC1. Interestingly, ufmylation contributes in β -oxidation of fatty acids and macrophage survival of *L. donovani* amastigotes (Gannavaram *et al.*, 2011; Gannavaram *et al.*, 2012). Furthermore, the small ubiquitin-like modifier (SUMO) is another UBL found in *Leishmania*, expressed as an inactive precursor by a single gene. The SUMO expressing gene is essential for the survival of *L. donovani* promastigotes and it is primarily localized in the nucleus, supporting the known involvement of SUMO in nuclear organization and chromosome segregation. However, nuclear localization and SUMOylation is observed only when it is activated by the sentrin-specific protease (SENP), which cleaves its C-terminus (Bea *et al.*, 2020). Moreover, ubiquitin-related modifier-1 (URM1) and its conjugation pathway do also exist in *Leishmania*. The localization of URM1 near the flagellar pocket, combined with identified

proteins undergo urmylation, suggesting that the URM1 pathway is involved in early endosome-mediated processes (Sharma *et al.*, 2016).

1.3.2 Ubiquitination and Deubiquitination Components in *Leishmania*

The eukaryotic ubiquitination system is composed of ubiquitin-activating (E1), ubiquitin-conjugating (E2) and ubiquitin-ligating (E3) enzymes for performing ubiquitination, and deubiquitinating enzymes (DUBs) for deconjugating ubiquitin. A recent genomic survey of these components in *L. mexicana* revealed that there are 2 E1, 13 E2, 79 E3 and 20 DUBs (Burge *et al.*, 2020; Damianou *et al.*, 2020). Focusing on the DUBs, 2 belong in the C12 family (UCH), 17 in the C19 family (UPS), and 1 in the C65 family (OTU). They are all cysteine peptidases and belong to the cysteine peptidase clan CA due to their similar structure to that of papain. Another study from the same group has also introduced 8 more DUBs, of which 1 belongs to the C78 family (Ufm1-specific protease; UFSP), 1 the C85 family (OTU-like), and 5 the C97 family (PPPDE; Grewal *et al.*, 2019). The first two families belong also to clan CA, while the last one is part of the clan CP, which is known for its papain-like fold (Rawlings *et al.*, 2014). Nevertheless, the last 8 DUBs are predicted to function as UBL – specific proteases (Grewal *et al.*, 2019).

1.3.3 UPS and the *Leishmania* Life Cycle

The *Leishmania* parasite, as it was described in section, undergoes extensive cellular transformations throughout its digenetic life cycle. For instance, whole cell protein profiling demonstrated variations in the expression of more than 1,100 proteins across procyclic promastigotes, metacyclic promastigotes, and intracellular amastigotes (De Pablos *et al.*, 2019). In addition, a separate investigation highlighted the necessity of protein degradation through autophagy for the effective differentiation of the parasite (Cull *et al.*, 2014). The ubiquitination system in association with the proteasome are known to be responsible for orchestrating the protein homeostasis within eukaryotic cells. Thus, to investigate whether UPS contributes to the progression of the life cycle of *L. mexicana*, null mutant promastigotes were created using deletion mutagenesis. Out of the 2 E1, 13 E2, 13 E3 (12 HECT, 1 RBR), and 20 DUBs that underwent double allele knockout, it was found that the E1, UBA1a, the E2s, UBC3, UBC7, UBC12 and UBC13, as well as the DUBs, DUB1, DUB2, DUB12 and DUB16, could not be recovered. This observation suggested that these UPS components are essential for the *Leishmania* promastigote stage. The remaining 37 null mutants, excluding $\Delta ubc5$ and $\Delta dub18$, were each assigned a unique barcode, pooled together and subjected to promastigote-to-amastigote differentiation via three different ways: by infecting either footpads of mice or macrophages, or axenically. Subsequently, their survival was assessed via high-throughput DNA-sequencing based bar-seq. The null mutants $\Delta ubc1/cdc34$, $\Delta ubc2$, $\Delta uev1$, $\Delta hect2$, $\Delta dub4$, $\Delta dub7$ and $\Delta dub13$ exhibited the most pronounced and consistently observed fitness deficits. Thus, it was concluded that these proteins are key players for the *Leishmania* differentiation cycle (Burge *et al.*, 2020; Damianou *et al.*, 2020).

1.3.4 DUBs and Trypanosomatids

Although DUBs play a crucial part in the life cycle of *Leishmania*, they have also been linked to various functions within the trypanosomatids (Burge, Mottram & Wilkinson, 2022; Kumar *et al.*, 2022). Focusing first in *L. infantum*, a study identified an OTU deubiquitinase, called OtuLi (DUB17 in *L. mexicana*), which has K48- and K63-linked polyubiquitin chain specificity. When OtuLi was incubated

with murine peritoneal macrophages, it induced the biogenesis of lipid droplets and the release of pro-inflammatory cytokines TNF α and IL-6. This suggests that OtuLi may have an immunomodulatory role that could aid in establishing a parasitic infection in the host. However, it remains unclear whether OtuLi is secreted, and additional evidence is needed to address this aspect (Azevedo *et al.*, 2017). Furthermore, ubiquitin modifiers of *T. b. brucei*, including the DUBs Tb927.9.5520 and Tb927.9.14470 (DUB9 and DUB6 in *L. mexicana*, respectively), have been identified as contributing factors that render sensitivity against the trypanolytic apolipoprotein-L1, which is present in the human serum. Thus, these proteins might explain why trypanosomes, such as *T. b. brucei*, are non-infectious to humans (Currier *et al.*, 2018).

In addition to the involvement of establishing infection, DUBs also contribute to intracellular protein trafficking via the endosomal system and endocytosis. Interestingly, an RNAi screen revealed that *T. brucei* USP7 and VDU1 (DUB6 and DUB7 in *L. mexicana*, respectively) play a role in the therapeutic sensitivity of *T. brucei* to suramin (Alford *et al.*, 2012). Specifically, they were found to regulate the ubiquitination status and, consequently, the protein stability of the invariant surface glycoprotein 75 (ISG75), which is also known to be involved in the mechanism of action of suramin. However, it is worth noting that the direct deubiquitination of ISG75 by USP7 or VDU1 was not investigated. Nevertheless, the knockdown of both proteins individually disrupted the endocytosis process in bloodstream *T. brucei*, underscoring the importance of these DUBs in intracellular trafficking and endocytosis (Zoltner *et al.*, 2015). Finally, two *L. infantum* DUBs, DUB10 and DUB15, have been linked with translation and ribosome-associated quality control pathways. This conclusion was reached through a study conducted on the RNA helicase DDX3. When DDX3 was knocked out, ribosomes were arrested in elongation. As a result, co-translational ubiquitination, which is responsible of eliminating truncated nascent polypeptides, increased, supporting that ribosomal stalling led to the production of aberrant polypeptides. This, in turn, led to the increased recruitment of ubiquitination components, including E3 ligases and the DUB15, to the ribosomes. Additionally, it resulted in the upregulation of other ubiquitin-related components, including DUB10, highlighting the importance of these proteins in quality control pathways and translation (Padmanabhan *et al.*, 2021).

1.3.5 DUBs in *Toxoplasma gondii* and *Plasmodium falciparum*

Apart from the *Leishmania* and *Trypanosoma* species, insights into parasitic DUBs have also been extracted from other parasites, including *Toxoplasma gondii* and *Plasmodium falciparum*. Focusing first in *T. gondii*, the causing agent of toxoplasmosis, four active DUBs were initially identified using an ubiquitin activity-based protein profiling approach coupled with mass spectrometry. The human orthologue *T. gondii* UCHL3 was one of them, which was found to localize to both the cytoplasm and nucleus of the tachyzoite stage of *T. gondii* and to possess deubiquitinating and deNeddylation activity (Frickel *et al.*, 2007). Dhara and Sinai (2016) predicted that 12 ovarian-tumor domain-containing (OTU) cysteine proteases were present in *T. gondii*, of which TgOTU7, TgOTU8 and TgOTU9 were predicted to possess a distinct protein structure relative to human OTU domain containing proteins. Despite the structural uniqueness of the three TgOTU proteins, the authors focused on the TgOTUD3A protein due to its fluctuating mRNA and protein levels during the endodyogeny process of tachyzoites. The protein is localized predominantly in the cytoplasm, with partial localization to the developing daughter scaffolds during cytokinesis. Recombinant expression of TgOTUD3A further revealed lysine-linkage specificity with descending preference towards K48-, K11- and K63-linked polyubiquitin chains. However, the recombinant TgOTUD3A protein selectively deubiquitinates endogenous K48-linked *Toxoplasma* proteins (Dhara & Sinai, 2016). The same group provided additional functional characterisation of TgOTUD3A, in which knocking out the protein-coding gene provided a fitness advantage to the mutant *T. gondii* tachyzoites over the wild-type cells. This advantageous change was

attributed to the production of 3 to 5 viable daughter cells within the gravid mother, instead of the typical 2, during endodyogeny due to the dysregulation of centrosome duplication. Thus, the two studies combined have associated *TgOTUD3A* with the cell cycle of *T. gondii* (Dhara *et al.*, 2017). Wilde *et al.*, (2023) expanded the predicted number of OTU domain containing proteins in *T. gondii* to 14 and characterised the di-ubiquitin linkage specificity of 11 of these proteins. Specifically, truncated protein constructs containing the OTU catalytic domain were screened against 7 different di-ubiquitin proteins, each possessing specificity for at least one of the following four di-ubiquitin linkages: K6, K11, K48 and K63. Furthermore, *in vivo* characterisation of *TgOTUD6B* and *TgOTUD3B* revealed that the former is essential for the intracellular growth of tachyzoite parasites within host cells, while both localize in the cytoplasm (Wilde *et al.*, 2023). Finally, insights into another OTU domain containing protein, *TgOTU7*, were provided by Xia *et al.* (2024). *TgOTU7* was found to localize solely at the apicoplast membrane of tachyzoite cells throughout the cell cycle, with its protein levels changing at each given stage. Interestingly, *TgOTU7*-knocked out tachyzoites were defecting in establishing plague formation, host cell invasion, and replication, underscoring the essentiality of the protein in the lytic cycle of the parasite. In addition, depletion of *TgOTU7* disrupted apicoplast biogenesis during the cell cycle, highlighting once more the importance the protein within *T. gondii*. *TgOTU7* was further validated as linkage-nonspecific deubiquitinase, linking the ubiquitination system of the *T. gondii* with its cell growth regulation and apicoplast homeostasis (Xia *et al.*, 2024).

In regards to *P. falciparum*, the blood-born parasite responsible for up to 2 million people annual malaria-related deaths, it is predicted to express 29 DUBs. The first-ever characterised DUB in this parasite, *P. falciparum* UCH54 (*PfUCH54*), was found to possess both deubiquitinating and deNeddylating activity (Artavanis-Tsakonas *et al.*, 2006). The dual activity of *PfUCH54* is uncoupled, with its former deubiquitinating activity being essential for the blood stage *P. falciparum*, while the latter activity is dispensable (Karpiyevich *et al.*, 2019). Similarly, *PfUCL3* also exhibits dual activity, however its function is essential for the survival and growth of the parasite (Artavanis-Tsakonas *et al.*, 2010). This makes the *PfUCL3* protein an ideal target for antimalarial drugs, leading to the conduction of three independent compound screens. The first study performed an *in silico* screening using AutoDock Vina, assessing 320,000 compounds against the crystal structure of *PfUCL3*. Interestingly, two compounds, Zinc 17465979 and Zinc 04366855, inhibited the growth of the asexual erythrocytic stages of *P. falciparum* at nano molar concentrations, though selectivity and cytotoxicity against human cells were not assessed (Franco *et al.*, 2013). Conversely, another virtual screen was conducted using the 400 compounds of the Pathogen Box, selective for disease types II and III. It identified MMV676603 and MMV688704 as effective inhibitors of *PfUCL3* at micromolar concentrations *in vitro*. These findings were supported by *in vivo* experiments, demonstrating selective parasite killing at their asexual stage without toxicity to mammalian cells (Bharti *et al.*, 2022). Finally, a covalent fragment library of 1700 members was screened against *PfUCL3*, identifying 7 scaffold proteins that selectively inhibited the recombinant *PfUCL3* activity over its human homologue, although 3 of these compounds were found to be toxic to human cells (Imhoff *et al.*, 2023).

In addition to the extensive characterisation of ubiquitin C-terminal hydrolase DUBs (UCHs) of *P. falciparum*, insights into some ubiquitin-specific peptidases (USPs) have also been gained. For instance, *PfUSP* is a DUB with a K48 linkage diubiquitin specificity and is associated with the ER, contributing to the ER morphology and development. Its function is indispensable for the asexual blood stages of the parasite and has been linked to regulating protein homeostasis and drug-induced stress tolerance against dihydroartemisinin (Arora *et al.*, 2023). Another studied USP DUB is *PfUSP14*, which co-purifies with the 26S proteasome of *P. falciparum*. Despite being a homologue of human USP14, which requires the proteasomal complex for deubiquitinating activity, *PfUSP14* is catalytically active independently, although the presence of the 26S proteasome slightly enhances its activity. Known human USP14-specific inhibitors such as b-AP15 and IUI inhibit the growth of intraerythrocytic

P. falciparum parasites at micromolar concentrations (Wang *et al.*, 2015). UBP1, another well-characterised USP DUB, has been linked to antimalarial drug resistance in African-derived *P. falciparum* clinical isolates against artemisinin-based therapies due to single point polymorphisms (SNPs; Adams *et al.*, 2018; Yan *et al.*, 2020). A recent study has deciphered the mechanism by which UBP1 SNPs provide resistance to these therapies, showing that impaired UBP1 affects the ubiquitination state and localization of the multidrug resistance transporter 1, establishing multidrug resistance (Xu *et al.*, 2024). In summary, DUBs have also been investigated in other non-trypanosomatid parasites such as *T. gondii* and *Plasmodium*, with their functions spanning diverse biological pathways of these organisms.

1.4 Aims

As previously mentioned, Damianou *et al.* (2020) identified four DUBs, including DUB2, as essential for the survival of *L. mexicana* promastigotes. Focusing on DUB2, it was also discovered that it plays a crucial role in establishing infections in the footpads of mice, establishing itself as a key virulence factor of *Leishmania*. Live cell imaging demonstrated that DUB2 is predominantly localized in the nucleus. This finding was further supported by an immunoprecipitation assay, which identified, among others, nuclear protein interactors involved in transcription/ chromatin dynamics, mRNA splicing and mRNA capping. Moreover, recombinantly expressed DUB2 was used to experimentally confirm its deubiquitinating activity. This was achieved through an activity-based probe assay (more details can be found in chapter 3). In addition, it was observed that DUB2 displays a broad linkage specificity, as it cleaves all the di-ubiquitin chains except for Lys27 and Met1. Nevertheless, the essential role of DUB2 for the parasite raised two crucial questions: “Why is DUB2 essential?” or, in other words, “What are the substrates of DUB2”, and “Can *L. mexicana* DUB2 be targeted for therapeutic purpose?” With these questions in mind, the project had the following objectives:

- Expand the analysis of the interacting proteins of DUB2 using biotin proximity labelling.
- Develop a peptide-centric ubiquitinomics workflow using *L. mexicana* promastigotes.
- Identify substrates of DUB2 using total ubiquitinomics and proteomics workflows.
- Identify compounds inhibiting DUB2 activity.

2 Materials and Methods

2.1 Molecular biology techniques

2.1.1 Polymerase Chain Reaction (PCR)

Primers for PCR were designed using either the QIAGEN CLC Main Workbench software, LeishGEdit (<http://www.leishgedit.net/>; Beneke *et al.*, 2017) or manually and synthesized by Sigma-Aldrich. PCRs were performed using either the PCR BIO Ultra Mix Red (BioSystems) or Q5® High-Fidelity DNA Polymerase (NEB), according to the manufacturer's protocols. Ingredients and conditions of both approaches are summarized in **Tables 1 & 2**. Annealing temperature of primers was calculated using the Tm Calculator (NEB; <https://tmcalsculator.neb.com/#!/main>).

Table 1: PCR Ingredients and Concentration. Ingredients and final concentrations of PCR reactions used along with either Q5 DNA Polymerase or Ultra Mix Red.

	Ingredients	Final concentration
Q5 DNA Polymerase	5x Q5 reaction buffer	1x
	10mM dNTPs	200µM
	10µM forward primer	0.5µM
	10µM reverse primer	0.5µM
	Template DNA	<100ng
	Q5 High-fidelity DNA polymerase	0.02U/ µl
	5X Q5 High GC enhancer (optional)	(1x)
	Nuclease-free water	Up to 25µl final vol.
Ultra Mix Red	2x PCR BIO Ultra Mix Red	1x
	10µM forward primer	0.4µM
	10µM reverse primer	0.4µM
	Template DNA	<500ng genomic
	Nuclease-free water	Up to 25µl final vol.

Table 2: PCR conditions. Standardized conditions used for Q5 DNA Polymerase and Ultra Mix Red-based PCRS

	Step	Temperatures	Time
Q5 DNA Polymerase	Initial Denaturation	98°C	30sec
	35-45 cycles	98°C	10sec
		50-72°C	30sec
		72°C	30sec/kb
	Final extension	72°C	2min
	Hold	16 °C	
Ultra Mix Red	Initial Denaturation	95 °C	2min
	35 cycles	95 °C	30sec
		55 °C - 65 °C	30sec
		72 °C	15sec/kb
	Final extension	72 °C	10min
	Hold	16 °C	

2.1.2 Agarose Gel Electrophoresis

Gels were prepared using 1% w/v or 2% w/v agarose in 1 x TAE buffer (40 mM Tris (Invitrogen), 20 mM acetic acid (Thermo Fisher Scientific) and 1 mM EDTA (Thermo Fisher Scientific, pH 8) for DNA products <500 bp or >500 bp respectively. Agarose solution was then heated for 3 min in the microwave. Upon cooling down, 1 x SYBR Safe DNA gel stain (Invitrogen) was added into the gel mixture, which was then poured into a plastic gel mould that contained a comb for producing the wells. 2 µl DNA samples were resuspended with 1 x Purple Gel Loading Dye (NEB) and then loaded onto the solidified gel. 5 µl of 1 kb Plus DNA Ladder (NEB) was used as a DNA marker. Samples were run at 80-100 V for 35-45 min and the gel was then imaged using the UV illumination from ChemiDoc (Bio-Rad).

2.1.3 Site Directed Mutagenesis

Site-directed mutagenesis of plasmids was performed using the Q5® Site- Directed Mutagenesis Kit (NEB). Briefly, primers carrying the mutated site of interest were designed using the NEBaseChanger (<https://nebasechanger.neb.com/>). To generate the site-directed mutated DNA product, an exponential amplification via PCR was performed, using the following reaction setup: 1 x Q5 Hot Start High-Fidelity 2 X Master Mix, 0.5 µM forward primer, 0.5 µM reverse primer, 1-25 ngµl⁻¹ template DNA and nuclease-free water up to 25 µl. The PCR run conditions were: initial denaturation step of 98°C for 30 sec, 25 cycles of 98 °C for 10 sec, 50°C - 72°C for 30 sec and 72°C for 30 sec/kb⁻¹, final extension of 72°C for 2 min and hold at 4°C. To check the presence of the amplified DNA product, agarose gel electrophoresis was conducted as described in section 2.1.2. Sequentially, circularization of the generated plasmid was performed by re-suspending 1 µl PCR product, with 5 µl 2 X KLD reaction buffer, 1 µl 10 X KLD enzyme mix and 3 µl nuclease-free water and then incubating it at RT for 1 h. Plasmids were transformed in NEB® 5-alpha Competent *E. coli* cells (High Efficiency; NEB) and cells were grown as described in section 2.1.7. Plasmids were extracted using the QIAprep Spin Miniprep Kit (Qiagen; section 2.1.8), quantified using NanoDrop and the site-directed mutation was validated via subsequent DNA sequencing (Plasmidsaurus or Eurofins Genomics; section 2.1.4).

2.1.4 DNA Sequencing

For validating the sequence of a DNA fragment from either PCR product or genomic DNA, samples were sent for Sanger Sequencing (Eurofins Genomics). Briefly, samples were prepared by mixing 15 μl of 50-100 $\text{ng}/\mu\text{l}$ of purified DNA with 2 μl of 10 μM primer. Primers were designed using either the QIAGEN CLC Main Workbench software or manually and synthesised by Sigma-Aldrich.

To fully sequence plasmids, samples were analysed via long reads sequencing to high consensus accuracy, which was performed by Plasmidsaurus. 10 μl of 10 $\text{ng } \mu\text{l}^{-1}$ plasmid was sent to the company in PCR strips (StarLab). The DNA concentration was calculated using the Qubit 3 Fluorometer (Thermo Fisher Scientific).

2.1.5 Ethanol Precipitation

PCR products were mixed and precipitated following the ethanol precipitation assay protocol by Thermo Scientific. This was performed to clean-up and concentrate PCR amplicons. Briefly, DNA samples were mixed with 1/10 volume of 3 M sodium acetate, 2.5 volumes of ice-cold 100% ethanol and glycogen to a final concentration of 1 mg mL^{-1} (Thermo Scientific TM). The mixture was then incubated for 60 min at -20°C , centrifuged for 15 min at 10,000 rpm and eventually the supernatant was discarded. The pellet was rinsed with 200 μl of cold 70% ethanol, centrifuged for 3 min at 10,000 rpm, air-dried and resuspended in 10 μl of deionized water. If the material was used for transfections e.g. sgRNA and donor DNA cassettes, then a downstream sterilization step was performed where the products were incubated for 5 min at 95°C .

2.1.6 DNA Extraction

DNA extraction from cells was performed using the DNeasy[®] Blood & Tissue Kit (QIAGEN), according to the manufacturer's protocol. 5×10^6 cells were harvested ($2,000 \times g$, 10 min, RT) and then resuspended in 200 μl 1 x phosphate-buffered saline (PBS). 20 μl of proteinase K and 200 μl of buffer AL were added in the sample and incubated for 10 min at 56°C . Sequentially, 200 μl of 100% ethanol were added in the solution, which solution was then transferred into a DNeasy Mini spin column. Sample was centrifuged at $6,000 \times g$ – as all the following centrifugation steps- for 1 min and the flow through was discarded. Washes with 500 μl buffer AW1 and then with 500 μl buffer AW2, coupled with a centrifugation step of 1 min and 3 min respectively, were performed. DNA was eluted in a new collection tube, by adding 200 μl buffer AE on the DNeasy Mini spin column. NanoDrop[™] 1000 Spectrophotometer (Thermo Fisher Scientific) was utilized for determining DNA purity and concentration.

2.1.7 *E. coli* Transformation, Culture and Storage

Unless otherwise stated, transformations were performed into NEB[®] 5 -alpha Competent *E. coli* (NEB). Briefly, 1-100 ng of plasmid was added in the *E. coli* cells, which were already thawed on ice for 10 min. Then, sample was gently vortexed and incubated on ice for 30 min followed by a 30 sec heat-shocked at 42°C . Sequentially, cells were placed on ice for 2-5 min; mixed with 950 μl of pre-warmed at RT SOC media; incubated for 1 h at 37°C and eventually 100 μl of cells were spread on a Luria Broth (LB) agar containing 100 $\mu\text{g mL}^{-1}$ ampicillin, which was incubated o/n at 37°C . Isolated colonies were selected and grew o/n in a liquid LB containing 100 $\mu\text{g mL}^{-1}$ ampicillin. 600 μl of overnight culture and 400 μl of

50% v/v glycerol (20% v/v final concentration) were mixed and stored at -80 °C into cryovial for a long-term storage.

2.1.8 DNA Extraction from *E. coli*

DNA was extracted from 1-5 mL of *o/n E.coli* cultures in LB medium using the QIAprep Spin Miniprep Kit (QIAGEN) according to the manufacturer's protocol. NanoDrop™ 1000 Spectrophotometer (Thermo Fisher Scientific) was utilized for determining DNA purity and concentration.

2.2. Biochemical techniques

2.2.1 SDS-PAGE Gel and Coomassie Blue Staining

For SDS electrophoresis, samples were mixed with 1 x NuPAGE™ LDS Sample Buffer containing 10 mM dithiothreitol (DTT) as a reducing agent. Samples were heated for 10 min at 70°C and loaded into NuPAGE™ 4-12% Bis-Tris Protein Gels (Invitrogen). Sequentially, samples were run at 150 V for 1-2 h in 1 x NuPAGE™ MOPS SDS Running Buffer (Invitrogen). When gel staining was required, gels were incubated in 10 mL of InstantBlue™ (Expedeon), under gentle shaking, *o/n*, at RT. Imaging was performed using the optimal auto-exposure on the Coomassie Blue Gel application of ChemiDoc (Bio-Rad). To estimate molecular weights, Spectra™ Multicolor Broad Range Protein Ladder (Thermo Fisher Scientific) was used.

2.2.2 Western Blotting

For western blotting, samples were prepared and run as described in section 2.2.1, unless otherwise indicated. All the following incubation and washing steps were performed under gentle shaking at RT. However, instead of performing gel staining, gels were incubated in 10 mL of 20% ethanol for 10 min. Blotting was then performed using PVDF iBlot™ 2 Transfer Stacks (Invitrogen) and the dry blotting system iBlot™ 2 (Thermo Fisher Scientific). Membrane was then blocked with either 5% skim milk in Tris-buffered saline with 0.1% Tween® 20 detergent (TBST; Sigma-Aldrich) or 5% BSA (Sigma -Aldrich) for 1 h. Probing with primary antibodies diluted in either 5 % milk TBST or 5% BSA in TBST at indicated concentrations was performed, followed by a 10 min washing step with TBST that was repeated thrice. Secondary antibodies diluted in 5% milk at indicated dilutions were then added into the blot for 1h and then the blot was washed with TBST three times. In the case of using HRP-conjugated secondary antibodies, Clarity™ Western ECL Substrate (Bio-Rad) was added to the blot for 5 min and then imaged via the chemiluminescent channel of ChemiDoc imaging system (Bio-Rad). Fluorescent and colorimetric channels of ChemiDoc (Bio-Rad) were used for imaging fluorescent secondary antibodies and protein ladders respectively.

2.2.3 Stain-Free Imaging

For stain-free imaging, the entire preparation of samples was identical with section 2.2.1, however samples were loaded into 4–15% Mini-PROTEAN® TGX Stain-Free™ Protein Gels (Bio-Rad). Protein standards, including Precision Plus Protein™ Unstained Protein Standards (Bio-Rad) were loaded as well. Samples were run in 25 mM Tris, 190 mM glycine and 0.1% SDS (TGS; pH 8.3) buffer at 200 V for 40 min. After gel electrophoresis, gel was activated using the following parameters on ChemiDoc MP imaging system: Stain-Free Gel, 45 sec and optimal automatic exposure for application, gel activation

time and image exposure respectively. Sequentially, blotting was performed as described in section 2.2.2 and blot was then imaged using the Stain-Free Blot application of ChemiDoc under optimal automatic exposure. This image was used as total protein loading control and for normalization, which was performed via Image Lab. Blots were then blocked, probed and imaged as indicated in section 2.2.2.

2.2.4 Activity-Based Protein Profiling

Activity-based protein profiling (ABPP) of the *L. mexicana* DUBs was performed following the protocol published by Damianou *et al.* (2020). Briefly, 3×10^7 log-phased *L. mexicana* promastigote cells were harvested and washed with ice-cold TSB buffer thrice ($1,000 \times g$, 10 min, RT). TSB buffer contained 44 mM NaCl, 5 mM KCl, 3 mM NaH_2PO_4 , 118 mM sucrose and 10 mM glucose (pH 7.4). Sequentially, cells were lysed using the following ice-cold lysis buffer: 50 mM Tris-HCl pH 7.4, 120 mM NaCl, 1% NP40 with the following inhibitors being added in the given order; $1 \mu\text{g mL}^{-1}$ pepstatin, 1 x cComplete ULTRA Tablets (Mini, EASYpack Protease Inhibitor Cocktail, Roche), 1 mM DTT, 1 mM PMSF and 0.01 mM E64. Samples were incubated for 15 min at 4°C and then pelleted at $17,000 \times g$ for 15 min. Supernatant was kept and protein concentration was calculated using Bradford Assay (section 2.2.6). Protein samples were diluted at 1 mg mL^{-1} in a final volume of 25 μl using lysis buffer, while kept on ice. Then, 1 μl of 1 μM of Cy5UbPA probe (UbiQ) and 2 μl of 50 mM NaOH were added in the samples and incubated between 5 min and 60 min at RT. Then, samples were prepared and run on SDS-PAGE gel (section 2.2.1), however this was performed at 4°C and with 200 V. Gel was then washed with dH_2O and the Cy5UbPA-labelled DUBs were imaged using the Amersham Typhoon (excitation: 635 nm; filter: Cy5 670BP30; GE Healthcare Life Sciences).

2.2.5 Competitive ABPP for DUB Inhibitors using Cy5UbPA

To investigate whether a chemical compound was inhibiting a *Leishmania* DUB, the ABPP methodology was used (section 2.2.4). However, the diluted protein samples were incubated for 1 h with 30 μM of the tested compound prior the addition of the Cy5UbPA probe, of which was incubated for only 5-10 min. Some of the tested compounds were light-sensitive, therefore the experimental procedure was performed in the dark. Image lab was used to quantify band intensities and Rstudio was used to perform statistical analysis.

2.2.6 Quantification of Protein Concentration

To quantify protein concentration of samples, Bradford or Bicinchoninic acid (BCA) assay was used according to manufacturer's protocol. Compatibility of the lysis buffer reagents determined which assay was used and absorbance readings were recorded at 562 nm and 595 nm for BCA and Bradford assay respectively, using the CLARIOstar^{Plus} Microplate Reader (BMG LabTech).

2.3 Protein Expression and Purification

2.3.1 Generation and Validation of DUB2 Expressing Plasmids

Successful expression of the recombinant proteins DUB2 and its catalytic inactive mutant DUB2^{C302A} was previously achieved by Damianou *et al.* (2020) using the baculovirus expression system following the Bac-to-Bac Baculovirus expression protocol (Invitrogen). The PFastBacNKI-his-3C-DUB2 and

PFastBacNKI-his-3C-DUB2^{C302A} vectors previously generated by Damianou *et al.* (2020) were re-validated via sequencing (section 2.1.4). Subsequently, *DUB2* was transposed into the EMBacY bacmid DNA (baculovirus genome), which bacmid was then purified and used for transfecting and infecting insect cells.

2.3.2 Transfection of Insect Cells with Bacmids (P0 Virus Stock)

The ovarian cells isolated from *Spodoptera frugiperda* (Sf21) cells were used as the insect host. They were grown in SF-900™ II Serum Free Medium (SFM; Thermo Fisher Scientific) and incubated at 27°C on a shaker (68 rpm). Cells were counted using the Trypan Blue Dye Exclusion method combined with the Vi-CELL XR Cell Viability Analyser (Beckman Coulter) and kept diluted at 1×10^6 cells mL⁻¹. For transfecting Sf21 cells with the bacmids, a transfection mixture was prepared containing: 10 µl of isolated bacmid ($\sim 2 \mu\text{g mL}^{-1}$) and 5 µl of lipofectamine® 3000 (Thermo Fisher Scientific) added in 200 µl media. This was incubated for 30 min at RT and then it was topped up with 3 mL of fresh media. Meanwhile, 2 mL of 0.5×10^6 sf21 insect cells mL⁻¹ were seeded in a 6-well dish through a 30 min incubation at 27°C and their medium was then removed. Afterwards, the transfection mixture was added to wells seeded with the sf21 insect cells and incubated o/n at 27°C. Gibco Fetal Bovine Serum (FBS; Thermo Fisher Scientific) was then added in 2% v/v final concentration to minimize the breakdown of the recombinant proteins from the insect peptidases. Cells were incubated for up to 8 days at 27°C, until green fluorescence was observed. The green fluorescence indicated that the first virus stock (P0 virus stock) was produced. P0 virus stock was stored at 4°C.

2.3.3 Production of P1 and P2 Virus Stock

0.5-1 mL of P0 virus stock was added into 25 mL sf21 culture at concentration of 1×10^6 cells mL⁻¹. Cells were harvested usually after 3-4 days, when enough YFP signal was expressed and the growth of the cells slowed down. This virus stock was P1 and the entire amplification procedure was repeated once more, which produced the P2 virus stock. P2 was then used to determine the minimal amount of virus stock needed to infect sufficiently scaled up sf21 cultures for protein production. This is known as virus titer determination.

2.3.4 Nickel Affinity Purification

The overall purification of the DUB2 recombinant protein was performed as follows: nickel affinity purification; His-tag cleavage; nickel affinity purification and size-exclusion chromatography (SEC). Focusing on nickel affinity purification first, scaled-up baculovirus-infected sf21 cells were harvested and stored in pellets at -20°C. Pellets were resuspended in lysis buffer containing 30 mM Tris-HCl pH 8.0, 0.3 M NaCl, 0.03 M imidazole, 5 mM β-mercaptoethanol and a tablet of cOmplete™ ULTRA tablets, Mini, EASYpack Protease Inhibitor Cocktail (Roche) and lysed via sonication. Lysates were then centrifuged at $21,000 \times g$ for 30 min at 4°C and supernatant was loaded onto AKTA Start (GE Life Sciences) at a rate of 5 mL min⁻¹. A 5 mL His-trap crude FF column (GE Life Sciences) was attached onto AKTA and washed with buffer A consisting 30 mM Tris-HCl (pH 8.0), 0.3 M NaCl, 0.03 M imidazole and 5 mM β-mercaptoethanol. Protein purification was achieved via gradient elution using the following buffer B – 30 mM Tris – HCl (pH 8.0), 0.3 M NaCl, 0.5 M imidazole and 5 mM β-mercaptoethanol. Selection and validation of DUB2 containing fractions was achieved via observing the absorbance at 260 nm and performing SDS-PAGE gel combined with Coomassie Blue gel staining (section 2.2.1).

2.3.5 His-Tag Cleavage

Overnight dialysis at 4°C in buffer A mixed with a H3C protease (Protein Production Facility, University of York) and newly expressed DUB2 in 1:50 ratio was performed to cleave the His-tag from DUB2. To accomplish this, SnakeSkin™ of 10K molecular weight cut-off (MWCO) was used. Dialysed samples were then loaded onto AKTA Start (GE Life Sciences) and nickel affinity purification was repeated, with DUB2 being collected in the flow-through due to the lack of His-Tag.

2.3.6 Size-Exclusion Chromatography

Protein samples were concentrated in Amicon® spin columns (30K MWCO; Millipore) and SEC was carried out using the HiLoad 16/600 S75pg column (GE Life Sciences) attached on AKTA Start GE Life Sciences). Equilibration of the column and elution of the DUB2 recombinant protein was achieved using the SEC buffer (25 mM Tris-HCl pH 8.0, 150 mM NaCl and 5 mM β-mercaptoethanol). Selection and validation of DUB2 containing fractions was achieved via observing the absorbance at 260 nm and performing SDS-PAGE gel combined with Coomassie Blue gel staining (section 2.2.1). Fractions containing DUB2 were pooled and concentrated (3-6 mg mL⁻¹); aliquoted in Protein LoBind® tubes (Eppendorf); snap-froze and stored in -80°C.

2.3.7 Buffer Exchange of Recombinant DUB2

Buffer exchange was carried out using the Zeba™ Spin Desalting Columns (7K MWCO) according to the manufacturer's protocol. Briefly, column was equilibrated with the desired buffer (e.g. 1 mM TCEP, 25 mM Tris-HCl pH 8.0 and 150 mM NaCl) by adding 300 µl of buffer on top of the column and centrifuging it at 1,500 x g for 1 min at 4°C. This step was repeated five times and then 130 µl of concentrated protein sample was added into the column. Sample was centrifuged at 1,500 x g for 2 min at 4°C and the buffer exchanged sample was used as desired.

2.3.8 Native-PAGE Gel

Protein samples were mixed in 1 x Novex™ Tris-Glycine Native Sample Buffer and were loaded onto a Novex™ WedgeWell™ 4 to 20%, Tris-Glycine, 1.0 mm, Mini Protein Gel. Then, samples were run for ~1 h at 225 V. 1 X Tris-Glycine native buffer was used as running buffer. Gel staining was carried out using Coomassie Blue as described in section 2.2.1.

2.3.9 SEC-MALS

Size-exclusion chromatography-multi angle laser light scattering (SEC-MALLS) was performed using Superdex S200-2 10/300 GL column (G.E. Healthcare), Wyatt HELEOS-II multi-angle light scattering detector and a Wyatt rEX refractive index detector linked to a Shimadzu HPLC system. 200 µl of protein samples (2 mg mL⁻¹) were loaded onto the column and the 0.2 µm filtered SEC buffer (section 2.3.7) was used as running buffer.

2.3.10 Intact Mass Protein Characterisation using Mass Spectrometry

Protein sample was ten-fold diluted with aqueous 50% (v/v) acetonitrile containing 1% (v/v) formic acid and then it was injected at a rate of 3 µl min⁻¹ into Bruker maXis-HD qTOF mass spectrometer using electrospray ionisation. Maximum entropy deconvolution was used to convert multiply charged

species to average neutral masses and this was carried out using Compass 1.7 software (Bruker Daltonics).

2.3.11 Ubiquitin Rhodamine 110 Kinetic Assay

This assay was carried out to identify the optimal molarities for DUB2 and Ubiquitin Rhodamine 110 (Ub-Rho; Boston Biochem) substrate. Serial dilutions were performed using assay buffer (50 mM Tris pH 8, 50 mM NaCl, 0.002% Tween 20 and 5 mM DTT), with final molarities being twice concentrated (2 x final). Each DUB2 and Ub-Rho dilution was incubated for 10 min at RT and then, 5 μ l of tested dilution of DUB2 and Ub-Rho were dispensed in the same well and mixed in Nunc 384-well plates (Thermo Fisher Scientific). The last two columns were used as control, without DUB2 being added. Plates were centrifuged at 1,000 x g for 1 min and then fluorescence data were collected every 5 min for 1 h using the PheraStar fluorescence plate reader at 485 nm excitation and 535 nm emission wavelengths (Varca *et al.*, 2021). All data were normalized and plotted in Rstudio.

2.3.12 Ubiquitin Rhodamine 110 Endpoint Assay (Drug Screen)

For drug screening, compounds were acoustically transferred on a Greiner medium binding 1536-well plate and then 2.5 μ l of DUB2 solution in assay buffer at a 2 x final concentration was dispensed. In columns 44-48, no compounds were added and in columns 47-48, assay buffer without DUB2 was added instead. The former was the active control and the latter was the negative control. Plates were incubated for 10 min and then 2.5 μ l of Ub-Rho at 2 x final concentration in the assay buffer was added to the plate. Plates were incubated for 70 min at RT and then fluorescence was recorded once, using the PheraStar plate reader at excitation and emission wavelengths at 485 nm and 535 nm, respectively. Helios, a software developed at Novartis to analyse high-throughput screening data (Gubler *et al.*, 2018) was used to analyse the screening data. Data were: a) normalized using the positive and negative controls, b) corrected in regards of systematic plate location-dependent errors and c) fitted in a dose response curve (for compounds tested in various concentrations). To assess the potency of compounds, the data was subjected to a fitting process using a four-parameter sigmoid Hill curve model. The qualified absolute activity concentration (QAC50) was calculated and compounds that did not achieve an acceptable QAC50, their AC50 was reported as the % of activation of DUB2 at their highest tested molarity (Varca *et al.*, 2021).

2.4 *L. mexicana* and HeLa cell cultures

2.4.1 Promastigote Cell Culture

L. mexicana (MNYC/BZ/62/M379) promastigote cell lines were grown at 25°C, in HOMEM medium (modified Eagle's medium; Gibco) supplemented with 10% v/v heat-inactivated fetal bovine serum (FBS; Gibco) and 1% v/v penicillin-streptomycin solution (Sigma-Aldrich). Cells were kept at log-phase, unless otherwise stated. Selection drugs were added at the following concentrations (Beneke *et al.*, 2017): 10 μ g mL⁻¹ blasticidin (InvivoGen), 15 μ g mL⁻¹ G418 (InvivoGen), 50 μ g mL⁻¹ hygromycin (InvivoGen), 50 μ g mL⁻¹ nourseothricin (Jena Bioscience) and 40 μ g mL⁻¹ puromycin (InvivoGen).

For long-term storage, stabilates were prepared by mixing 500 μ l of log-phase promastigote cultures with 500 μ l of 0.2 μ m filtered HOMEM (Gibco) supplemented with 20% v/v FBS and 5% DMSO and then stored at either -80°C or liquid nitrogen. To recover stabilates, cells were defrosted at RT and

added into 10 mL of HOMEM supplemented with 20% v/v FBS and 1% v/v penicillin-streptomycin, at 25°C. Antibiotics were added the following day.

2.4.2 Promastigote to Amastigote Differentiation

Promastigote cell lines were incubated for 3-4 days at stationary phase and then the cells were harvested at 1,000 x g for 10 min. Pelleted cells were resuspended in amastigote medium (pH 5.5) containing Schneider's Drosophila medium (Gibco), 20% FBS (Gibco) and 15 µg mL⁻¹ HEMIN (Sigma). Cells were incubated at 33°C with 5% CO₂ in either 6-well plates or flasks, and kept at or below 1 x 10⁷ cells mL⁻¹.

2.4.3 Cell Counting

Cell density of promastigote cell cultures was determined either via manual or automated counting. The former was performed using haemocytometer, of which cells were 2-4 times diluted with 2% formaldehyde. The latter one was performed using the Beckman Coulter Z1 Particle Counter (> 3 µm diameter), of which cells were diluted either 1000 for not stationary cells or 2000 times for stationary cells in a final volume of 10 mL of filtered Beckman Coulter™ ISOTON™ II Diluent. For amastigote cells, only manual counting was performed followed by de-clustering of 500 µl cells through a needle.

2.4.4 Growth Curve

To determine the growth rate of a cell line, cells were seeded at 1 x 10⁵ cells mL⁻¹ at growing conditions and then counted every 24 h for 5 days. Then, growth curves were plotted and analysed using Rstudio.

2.4.5 HeLa Cell Culture

Stabilates of HeLa (Henrietta Lacks) cervical cancer cells, which were kindly provided by Prof. Paul Kaye's group, were thawed for 1 min in a 37°C water bath. Cells were then transferred in a 15 mL falcon tube. Dulbecco's Modified Eagle Medium (DMEM) supplemented with 10% fetal bovine serum (FBS) and 100 units mL⁻¹ penicillin/streptomycin (Thermo Fisher Scientific) was used as culturing media of HeLa cells. Therefore, 10 mL of pre-warmed at 37 °C media was added drop-by-drop (to avoid osmotic shock) in thawing HeLa cells. Cells were centrifuged at 5,000 rpm for 2 min and cells were resuspended in fresh 10 mL medium. Cells were counted using haemocytometer (section 2.4.3) and 0.7 x 10⁶ cells mL⁻¹ were seeded in a Corning® 25 cm² Rectangular Canted Neck Cell Culture Flask (Corning) containing 10 ml media. Growing cultures were incubated at 37°C, with the flask placed horizontal for cells to adhere and the lid slightly unscrewed.

HeLa cells were growing at ~70% confluent. To split the cells, media was gently removed from the adhered cell culture and gently washed with 5 mL of 1 x PBS. Sequentially, PBS was removed and 1.5 mL of Corning® Cellstripper solution (Corning) was added to detach the adhered cells from the walls of the flask. Cells were then incubated for ~10 min and gently mixed during this time-period. Once all the cells were detached, 9 mL of DMEM was added. Cells were counted using haemocytometer (section 2.4.3) and cells were diluted to reach the optimal seeding density, which is 0.7 x 10⁶ cells mL⁻¹. Final growing volume was always 10 mL and all the already mentioned PBS, Corning Cellstripper solution and DMEM were warmed at 37°C before used.

2.4.6 Storage of HeLa Cells

Filter sterile freezing media containing 10% DMSO and 20% FBS in DMEM, which was stored at 4°C, was used for a long-term storage of 70% confluent HeLa cells. Cells were prepared and counted as described in 2.4.5. Sequentially, 1×10^6 cells were centrifuged for 3 min at 500 rpm; supernatant was removed and pellet was resuspended in the freezing media. Cells were stored at -80°C and then in liquid nitrogen.

2.5 Genetic Modification of *Leishmania*

2.5.1 Endogenous Tagging

For endogenous tagging of *L. mexicana* promastigotes, the CRISPR-Cas9-based approach developed by Beneke *et al.* (2017) was used. This involves the use of the *L. mexicana* promastigote cell line expressing Cas9 and T7RNAP (T7/Cas9). Two sets of primers were designed per GOI through the online resource LeishGEdit (<http://www.leishgedit.net/>; section 2.1.1): the first one for generating the single guide RNA (sgRNA) in the form of double-stranded DNA, and the second one to amplify the DNA repair cassettes that will be used for tagging. The double-stranded sgDNA is transcribed into sgRNA *in vivo* by T7RNAP and is responsible for targeting the Cas9 at the desired site of cleavage where DNA repair cassette will be inserted. The sgDNA is generated through the combination of two primers: the forward primer that contains a T7 promoter, 20 nucleotide-sequence that determines the Cas9 targeting site, and a complementary sequence with the 3' end of the reverse primer, while the reverse primer contains the rest elements required for generating the sgDNA scaffold. The reverse primer is the same for every generated sgDNA (OL6137). As about the set of primers for generating the DNA repair cassette, both primers have a 30-nucleotide long sequence that is homologous with the regions situated upstream and downstream the intended double-stranded break. This addition was meant to aid in homologous recombination.

For generating and amplifying the sgDNA scaffold, the following PCR reaction was used at final volume of 20 μ l: 2 μ M forward primer, 2 μ M reverse OL6137 primer, 0.2 mM dNTPs, 1U Q5[®] DNA Polymerase (NEB), 1 X Q5 reaction buffer (NEB) and diH₂O. Regarding the PCR conditions, the following PCR protocol was employed: 98°C for 30 sec followed by 35 cycles of 98°C for 10 sec, 60°C for 30 sec and 72°C for 15 sec. Finally, after all cycles, there was a terminal extension at 72°C for 10 min. In the case of DNA donor cassette, the following PCR reaction was performed at a final volume of 40 μ l: 2 μ M forward primer, 2 μ M reverse primer, 0.2 mM dNTPs, 1U Q5[®] DNA Polymerase (NEB), 1 X Q5 reaction buffer (NEB), 30 ng of a pPLOTv1 plasmid and diH₂O. The PCR conditions for this PCR reaction were: 94°C for 5 min, 45 cycles of 94°C for 30 s, 65°C for 30 sec and 72°C for 2 min 15s and 72°C for 7 min. PCR amplicons were validated via gel electrophoresis (section); sgRNA and DNA donor cassettes were mixed and then purified and concentrated via glycogen precipitation (section 2.); and transfected in the parental cell line (section 2.5.2). Primers and plasmids used are listed in a supplementary document.

2.5.2 Transfection

PCR-derived amplicons from section 2.5.1 were concentrated and sterilized as described in section 2.1.5. Sequentially, 1×10^6 log-phase cells from the parental promastigote cell line were harvested (1,000 x g, 10 min, RT) and resuspended in 16.4 μ l P3 buffer and 3.6 μ l supplement from the P3 Primary Cell 4D – Nucleofector[™] X Kit S (Lonza). From the same kit there is a 16-well transfection strip, in which 2 μ l of DNA and 20 μ l of resuspended cells were dispensed. Transfection was carried out via

electroporation using the T cell, human, unstim (HE unstimulated FI 115) program of Lonza 4D. Transfected cells were transferred in 25°C pre-warmed HOMEM medium and incubated overnight at 25°C. Antibiotic selection was carried out the following day (section 2.4.1).

2.5.3 Cloning of Cells

For most generated cell lines, cloning was performed to ensure homozygous cell lines were used, to subsequently minimize variation across replicates. One day post-transfection, cells were cloned out in a 96-well plate (Thermo Fisher Scientific) using promastigote medium containing the required antibiotics. Specifically, 200 µl of cell culture containing 10,000 cells were added in A1 well, and then a 2-fold serial dilution was performed firstly across A1-H1 wells and secondly from column 1 to column 12. Highly-diluted cloned cells were then harvested (1,000 x g, 10 min, RT) and tested whether they were possessing homozygous mutation through PCR.

2.5.4 DiCre T7 Cas9 Cell Line and Rapamycin-Induced Knockout

To generate the inducible DiCre DUB2 cell line, the Crispr-Cas9-based endogenous tagging approach was utilized (section 2.5.1) to replace the endogenous *DUB2* gene with a loxP-flanked DUB2 C-terminally HA tagged cassette containing puromycin resistance expressing gene. The DiCre T7/Cas9 promastigote cell line, of which the diCre machinery was integrated into the ribosomal locus, was used as the parental line (Geoghegan *et al.*, 2022). The donor cassette was generated via Gibson assembly using the NEBuilder assembly tool. Briefly, the *L. mexicana DUB2* gene was amplified via PCR using primers designed via NEBuilder, which contained homology arms that bind to the desired site of the plasmid (pGL2938). Specifically, the desired site was at an EcoRI restriction site, downstream of the N-terminal loxP site and upstream of the HA tag, with the *DUB2* stop codon and a linker being excluded and included, respectively. Generated *DUB2* amplicons were validated via gel electrophoresis. Sequentially, the plasmid was linearized using the EcoRI restriction enzyme. This was performed by incubating 1 µg of pGL2938, 1 x NEBuffer EcoRI and nuclease-free water (50 µl reaction) at 37°C, for 15 min. Successful linearization was confirmed via gel electrophoresis, of which linearized DNA was migrating faster on the agarose gel. Sequentially, both *DUB2* amplicons and linearized plasmids were purified via gel extraction followed by glycogen precipitation. For a successful ligation, vector (linearized plasmid) and insertion (*DUB2*) were mixed at 1:1 ratio, with the vector being at 27 femtomole, and they were incubated with 10 µl of Master Mix NEBuilder HiFi DNA assembly buffer and with diH₂O at a final volume of 20 µl for 1 h at 50°C. Sequentially, transformation of chemically competent *E. coli* cells was performed (section 2.1.7), plasmid was extracted (section 2.1.8) and validated via sequencing (Plasmidsaurus; section 2.1.4). Eventually, the loxP-flanked DUB2 C-terminally HA tagged cassette containing puromycin resistance expressing gene was amplified from the plasmid, using primers containing homology arms that recombine at the 5' and 3' UTR of the endogenous *DUB2* and transfected within the parental cell line. Successful gene replacement was achieved via the use of two sgRNAs, which target the 5' and 3' UTR of endogenous *DUB2*, and cloning followed by diagnostic PCR was performed to ensure double allele replacement. To excise the *DUB2* gene from the homozygous mutants, the following procedure was performed: cells derived from a log-phase culture were seeded at 1-5 x 10⁵ cells mL⁻¹ into growing medium; incubated for 2 d in the presence of 300 nM of rapamycin; cells were then re-seeded at desired cell density and incubated for 2-3 d in *fresh* media containing 300 nM rapamycin. If desired, cells were harvested at 1,000 x g for 10 min and prepared accordingly for downstream analyses. All the primers and plasmids used are attached in a supplementary file.

2.5.5 AlamarBlue Viability Assay

AlamarBlue assay (Thermo Fisher Scientific) was performed in order to see whether a tag affected the metabolic activity of the parasite compared to the un-tagged control. 200 μl of tagged promastigote cultures diluted at a cell density of 1×10^6 cells mL^{-1} were added in triplicates in a 96-well plates. Similarly, an un-tagged promastigote culture of the same cell density and a media-only solution were added in triplicates as positive and negative control respectively. 125 $\mu\text{g mL}^{-1}$ of resazurin dissolved in 1 x PBS was added to tested wells and incubated for 8 h at 25°C. Metabolically active cells convert resazurin to resorufin. To detect such activity, fluorescence was recorded at 590 nm using the CLARIOstar^{Plus} Microplate Reader (BMG LabTech). To calculate the percentage difference of fluorescence between tagged and un-tagged cells, the following formula was used, of which FI 590 is the fluorescent intensity at 590 nm emission. Statistical analysis and plotting was performed in Rstudio.

$$\text{Percentage difference between treated and control cells} = \frac{\text{Average FI 590 of test agent dilution}}{\text{Average FI 590 of untreated control}} \times 100$$

For testing how the tag affects the differentiation process of the parasite, axenic amastigote cells were prepared as described in section 2.4.2 at a cell density of 1×10^6 cells mL^{-1} . 200 μl of axenic amastigote cell cultures were added in triplicates in a 96-well plates, along with the controls, and incubated at 33°C. At 0 h, 24 h, 48 h and 72 h post-induction of promastigote-to-amastigote differentiation, 125 $\mu\text{g mL}^{-1}$ of resazurin was added for 8 h at 33°C. Recording of fluorescence and data analysis was performed as in promastigote cells.

Specificity of promising DUB inhibitors against *L. mexicana* promastigote cells were also determined via the AlamarBlue viability assay. 100 μl of 1×10^5 cells mL^{-1} were added in triplicate at a 96-well plate and mixed with a 100 μl diluted inhibitor at 2 x final concentration. DMSO-treated cells from the same cell line were used as negative control and cells treated with miltefosine were used as positive controls. Serial dilutions were performed for all tested compounds, including the controls. Cells were then incubated for 24 h at 25°C, under dark conditions and then 125 $\mu\text{g mL}^{-1}$ of resazurin was added for 4 h. Fluorescence was recorded as described previously and data were analysed and plotted using GraphPad Prism (log [inhibitor] vs normalized response-variable).

2.5.6 Immunofluorescence

Immunofluorescence was performed on cover glass coated with poly-L-Lysine. Cover glass (22x50 mm; VWR; CN: 631-0137) was incubated in 0.01% poly-L-lysine solution (P4707; Sigma-Aldrich) for 1 h, at 37°C. Coated cover glass was then washed twice with dH_2O , dried at RT and sterilized under UV light exposure o/n. Coated cover glass could be store up for a year, under dust-free conditions.

2.5×10^6 promastigotes were washed once with 1 x PBS solution (P4417; Sigma-Aldrich) and pelleted at 1,500 x g, for 10 min, at RT. Cells were resuspended in 200 μl of 1 x PBS and were left to adhere on coated cover glass for 15 min, at RT. Sequentially, the adhered promastigotes were washed twice with 1 x PBS and fixed with 4% w/v formaldehyde/PBS (FA; 28906; Thermo Scientific) for 10 min, at RT. FA was quenched with 250 mM glycine/PBS (G7126; Sigma-Aldrich) for 5 min at RT. Cells were washed twice with 1 X PBS, permeabilised with 0.1 %v/v Triton X-100/PBS (300024N; BDH) for 15 min at RT and blocked with 5% w/v bovine serum albumin(A7030; Sigma-Aldrich)/0.01% w/v saponin(440914Y; BDH)/PBS for 1 h, at RT. Immunostaining of cells was performed by incubating the cells for 1 h with

the primary antibody diluted in the blocking buffer at RT, followed by 3 washes with 0.1% v/v Triton X-100/PBS, for 3 min each. Cells were then incubated with the secondary antibody diluted in blocking solution under dark conditions, for 1 h, at RT, washed twice with 0.1% v/v Triton X-100/PBS for 2 min per time, further washed twice with 1 x PBS for 2 min per wash and finally washed for 1 min with diH₂O. Cells were dried, embedded in ProLong™ Diamond antifade mountant with DAPI o/n, under dark conditions (P36962; Invitrogen™) and covered with an Eprelia Superfrost™Plus Adhesion microscope slide (J1800AMNZ; Fisher Scientific). Cell imaging was performed using Z-stack on the multi-channel inverted Zeiss Axio Observer microscope, which was equipped with an Orca-Flash4.0 V3 Digital CMOS camera (Hamamatsu Photonics). To deconvolve the image Z-stacks, the Microvolution plugin of Fiji was used with 100 iterations.

2.6 XL-miniTurboID

All the following steps apart from the BioLock treatment (section 2.5.1) were performed as described in Geoghegan *et al.* (2022). Briefly, *DUB2* and *CLK1* were endogenously tagged with the miniTurbo biotin ligase at their C- and N- terminus, respectively, using CRISPR-Cas9 endogenous tagging. This was performed in the parental T7/Cas9 promastigote cell line. Double allele tagging was achieved using two different donor constructs containing either BLA or PAC resistance cassettes, which were generated using the pPLOTv1 myc::miniTurboID::myc plasmids pGL2822 and pGL2835, respectively. The generated cell lines were called DUB2::miniTurbo::Myc and Myc::miniTurbo::CLK1. Primers are listed in the supplementary file.

2.6.1 BioLock Treatment

2 µl of BioLock Biotin blocking solution (IBA Lifescience) per mL of HOMEM was added in a log-phase promastigote cell culture for 16 h. Cells were pelleted (1,000 x g, 10 min, RT), washed with filtered 1 x PBS, harvested (1,000 x g, 10 min, RT) and resuspended with fresh HOMEM at a cell density of 5 x 10⁶ cells mL⁻¹.

2.6.2 Biotin Labelling and Crosslinking

For *in vivo* biotin labelling, biotin solution (Sigma-Aldrich) was added in log-phase (BioLock-treated) promastigote cell culture at final concentration of 500 µM for 30 min at 25°C. Samples were gently shaken every 5 min. Cells were then harvested (1,000 x g, 10 min, 4°C) and washed twice with ice-cold 1 x PBS (1,000 x g, 10 min, 4°C). *In vivo* cross-linking was then performed, of which cells were resuspended with 1 mM DSP crosslinker dissolved in pre-warmed at 37°C 1 x PBS and incubated for 10 min at 25°C. Cells were gently shaken every 2 min. To quench cross-linking, Tris-HCl pH 7.5 was added for 5min at a final concentration of 20 mM. Cells were harvested (1,000 x g, 10 min, RT) and stored at -80°C until lysis.

2.6.3 Lysis, Streptavidin Pull-Down and On-Bead Protein Digestion

Pelleted cells were resuspended in 500 µl of ice-cold Radioimmunoprecipitation assay (RIPA) buffer supplemented with 0.1 mM PMSF, 1 µg mL⁻¹ pepstatin A, 1 µM E-64 and 0.4 mM 1-10 phenanthroline. Furthermore, for every 3 mL of RIPA buffer 1 tablet of cOmplete ULTRA Tablets (Mini, EASYpack Protease Inhibitor Cocktail, Roche) was added. Cells were then sonicated using the Bioruptor® Pico sonication device (Diagenode) with 2 sonication cycles 30'' ON/30'' OFF and samples were then

treated with 1 μ l of Benzonase (250 Units, Abcam) for 1 h on ice. Cell extracts were then centrifuged (10,000 x g, 10 min, 4 °C) and the supernatant was retained. Biotinylated material was enriched using 100 μ l of magnetic streptavidin bead suspension (Resyn Bioscience) per sample and this step was performed by end-over-end rotation o/n at 4°C. Beads were then washed in 500 μ l of the following solutions, for 5 min each, on end-over-end rotation at RT: RIPA (4 x washes), 4 M urea in 50 mM triethyl ammonium bicarbonate (TEAB) pH 8.5 (1 x wash), 6 M urea in 50 mM TEAB pH8.5 (1 x wash), 1 M KCl (1 x wash) and 50 mM TEAB pH8.5 (1 x wash). On-bead digestion was then performed by re-suspending beads 200 μ l 50 mM TEAB pH 8.5 containing 10 mM TCEP, 10 mM iodoacetamide, 1 mM CaCl₂, 1M urea and 500 ng trypsin Lys-C (Promega) and incubating them o/n at 37°C under 200 rpm shaking conditions. Supernatant was retained in protein LoBind eppendorf tubes. Beads were washed twice with 50 μ l diH₂O for 5 min at end-over-end rotation at RT and these 100 μ l were mixed with the retained supernatant. Peptides were then acidified with trifluoroacetic acid (TFA) to a final concentration of 0.5% v/v, centrifuged (17,000 x g, 10 min, RT) and the supernatant was kept for peptide desalting.

2.6.4 Peptide Desalting

In-house C18 tips were used to desalt peptide-containing supernatants. C18 desalting tips were equilibrated with 100 μ l of the following solutions in the given order: aqueous 100% v/v acetonitrile (ACN) solution, aqueous 80% v/v ACN 0.1% v/v TFA solution and aqueous 0.1% v/v TFA solution. Then, peptide-containing supernatants were loaded onto the equilibrated C18 tips and the flow-through was re-loaded onto the column. This step was repeated thrice. C18 tips were washed twice with 100 μ l of 0.1% v/v TFA solution and peptides were finally eluted with 30 μ l of aqueous 80% v/v ACN 0.1% v/v TFA solution. The elution step was performed twice and eluates were mixed and dried for MS analysis. All the centrifugation steps in this section were performed at 2,000 rpm for 1-2 min at RT.

2.6.5 Liquid Chromatography with Tandem Mass Spectrometry (LC-MS/MS)

Samples were resuspended in aqueous 0.1% v/v TFA solution and loaded onto an mClass nanoflow UPLC system (Waters) equipped with a PepMap, 2 μ m, 100 Å, C18 EasyNano nanocapillary column (75 mm x 500 mm, Thermo). Peptides were eluted into an Orbitrap Fusion™ Tribrid mass spectrometer over 3 h acquisition and data were acquired using data-dependent acquisition (DDA) mode performed in top speed mode utilizing a fixed 1 s cycle. The most intense precursors with charge states ranging from 2 to 5 were selected.

2.6.6 Data Analysis of MS Data

Peak lists in.raw format were imported into Progenesis QI (Version 2.2., Waters) to allow peak picking and chromatographic alignment. Concatenated MS2 peak list exported in.mgf format and was searched through the Mascot programme (Matrix Science Ltd., version 2.7.0.1) against the TriTrypDB-derived *L. mexicana* subset database, which is composed of 8,250 sequences and 5,180,224 residues. The percolator algorithm was used for peptide identification to 1% FDR and identified peptides were then imported into Progenesis QI, in which they were associated with precursor intensities. Non-conflicting, relative precursor intensities that were normalized based on the total peptide signal per sample were utilized for relative protein quantification. Quantifications were filtered to include only proteins with a minimum of two unique peptides. Sections 2.6.5 and 2.6.6 up to this point were

performed by the MS facility of the University of York. Next, data were transformed in Rstudio and proximal proteins were identified from the statistical package limma at 1% FDR.

2.6.7 Bioinformatics

Gene Ontology (GO) enrichment analysis was performed either manually through literature or via the Gene Ontology Enrichment tool of TriTrypDB at chosen ontology (biological process, cellular component or/and molecular function) at a p-value of 0.05 as a cut-off. To identify possible orthologues of *L. mexicana* proteins, protein-protein BLAST (BLASTp; NCBI) and/or HMMER (MPI Bioinformatics Toolkit) was used at pre-defined conditions and hits were selected at E-value equalled with or less than 0.05. TrypTag (<http://tryptag.org/>) and LeishTag (<http://www.leishtag.org/>) websites were used to predict protein localization (Billington *et al.*, 2023).

2.6.8 Co-Immunoprecipitation

Co-immunoprecipitation (co-IP) was performed to test whether the XL-miniTurboID hits form stable protein complexes with DUB2 (procedure adapted from Jones *et al.*, 2022). In the *L. mexicana* T7/Cas9 promastigote cell line, proteins of interest (POI) were tagged endogenously with a 3xHA tag, positioned either at their N- or C-terminus. The decision on where to place the tag was guided by the presence of N-terminal signal peptides for secretion, as determined using SignalP from TriTrypDB, or indications of mitochondrial targeting, identified with MitoProt from TriTrypDB. Additionally, previously documented tagging sites for these proteins were considered in the selection process. Concomitantly, *DUB2* endogenously 3xMyc-tagged at its C-terminus (DUB::Myc).

The process of generating these cell lines expressing POI::HA or HA::POI and DUB2::Myc was carried out following the procedure outlined in section 2.5.1. In summary, the PCR reagents and conditions used to create DNA donor cassettes and sgRNAs were consistent with those previously described in the same section. Specific primer sequences for each case were provided in the supplementary file. Plasmids pGL2966, pGL2967 and pGL2666 were used to generate DNA donor cassettes for tagging *POI* at its N-terminus, *POI* at its C-terminus and *DUB2* at its C-terminus, respectively. Upon validation of PCR products via gel electrophoresis, the DNA donor cassette and sgRNA of *POI* were mixed with the DNA donor cassette and sgRNA of *DUB2*. Then, glycogen precipitation was performed, followed by transfection. Blasticidine and puromycin antibiotics were used for selecting successful tagging of *POI* and *DUB2*, respectively.

To perform co-IP, 30 mL of mid-log cultures were harvested (1,200 x g, 10 min, RT) and then resuspended and incubated with 10 mL of 1 mM DSP crosslinker dissolved in pre-warmed at 37°C 1 x PBS incubated for 10 min at 25°C. To quench cross-linking, Tris pH 7.5 was added to a final concentration of 20mM and then parasites were washed with 1 x PBS (1,200 x g, 10 min, RT). Cells were then resuspended in 100 µl RIPA buffer supplemented with 1 µl BaseMuncher Endonuclease (250 units) and cOMplete ULTRA Tablet (Mini, EASYpack Protease Inhibitor Cocktail; 1 tablet per 3 mL of RIPA buffer; Roche). To ensure sufficient lysis of the cells, sonication was also performed using the Bioruptor® Pico sonication device (Diagenode) with 2 sonication cycles 30'' ON/30'' OFF. Cell extracts were then centrifuged (10,000 x g, 10 min, 4°C) and 20 µl of the supernatant was extracted and prepared for western-blot analysis (section 2.2.2) as pre-immunoprecipitation sample. The rest of the supernatant was HA-tag immunoprecipitated using 30 µl anti-HA magnetic beads (Pierce) for 2 h at an end-over-end rotation at 4°C. The anti-HA magnetic beads were twice washed with a 1 x PBS buffer supplemented with 50 mM NaH₂PO₄ pH 7.5, 150 mM NaCl and 0.025% Tween. Beads were then

washed thrice in 500 μ l lysis buffer for 5 min at an end-over-end rotation at RT. Proteins were then eluted using 40 μ l of 1 x LDS buffer supplemented 250 mM DTT followed by a 10 min incubation at 70°C. The presence of investigated prey proteins and DUB2 bait protein were investigated via western-blotting for the HA and Myc epitopes respectively.

2.7 Ubiquitinomics

2.7.1 Harvesting, Lysis and Protein Digestion

Promastigotes were grown to a cell density of 4×10^6 cells mL^{-1} and then, 1.5×10^9 cells were pelleted (3,500 rpm, 10 min, RT). In the case of MG-132 (Abcam) treatment, the proteasomal inhibitor was added in the growing culture for 6 h at a final concentration of 20 μ M pre-harvesting. Followed by two washes with 1 x PBS, cells were lysed with 5% w/v SDS buffer (SDS; Thermo Fisher Scientific, 50 mM TAEB buffer; Sigma-Aldrich) and sonicated with a microtip sonicator (Sonics Vibra-Cell) for two rounds of 10 sec, each at an amplitude of 50% and 1 min resting on ice in between. Due to the high viscosity of the lysate, additional sonication was performed using the Bioruptor[®] Pico sonication device (Diagenode) with 2 sonication cycles 30" ON/ 30" OFF, at 4°C. Lysate was centrifuged for 15 min at 10,000 x g and the supernatant was transferred in a new protein LoBind eppendorf tube. Sequentially, protein quantification was performed using the Pierce BCA assay (23225; Thermo Fisher Scientific). Upon protein quantification, equal amounts of total protein were used per sample for the downstream experimental workflow. To reduce the disulphide bonds of proteins, DTT was added at a final concentration of 1 mg mL^{-1} for 1 h, under the stirring conditions of 350 rpm and 55°C using a Thermomixer (BIOER). Lysate was then cooled down to RT using ice, and proteins were then alkylated with 1/10 volume of 100 mM 2-chloroacetic acid (Sigma-Aldrich) for 30 min, under dark and RT conditions. At this point, 10 μ g of protein sample were isolated (pre-trypsinisation sample), resuspended in 1 x LDS buffer (NuPAGE[™]; NP0007; Thermo Fisher Scientific) containing 10 mM DTT (R0861; Thermo Fisher Scientific), denatured at 70°C for 10min and stored at -20°C. To the remained lysate, 1/10 sample volume of 12% phosphoric acid (Sigma-Aldrich) was added and mixed thoroughly. Sequentially, 6.6 x sample volume of 90% methanol (Honeywell)/100 mM TEAB (Sigma-Aldrich) buffer was added to the lysate and a cloudy protein colloid was formed. Immediately, the sample was transferred onto the S-Trap Midi Cartridge (≥ 300 μ g; ProtiFi) and centrifuged for 2 min at 4,000 x g, at RT, where the flow-through was discarded. To desalt the sample, the S-Trap cartridge was further washed 4 times using each time 3 mL of 90% methanol/100 mM TEAB buffer under the same spinning conditions and then transferred into a new 15 mL falcon tube. To digest the proteins into peptides, 500 μ l of trypsin/Lys-C protease mix (Mass Spec Grade; V5071; Promega) resuspended in 50 mM TAEB (pH ~8) at a concentration of 1:50 protease mix: protein sample was added onto the S-Trap cartridge, o/n, at 37°C. The falcon tube was placed vertically to ensure even absorption of the protease mix and the lid of the tube was loosely placed to ensure absorption into the cartridge without creating negative pressure. The following day, three sequential centrifugation steps of 2 min, at 4,000 x g and RT, without discarding the flow-through were performed using: firstly 500 μ l of 50 mM TAEB buffer, secondly 500 μ l of 0.5% v/v TFA in water (Sigma-Aldrich) and thirdly 50% v/v ACN (Thermo Fisher Scientific)/ 0.5% v/v TFA in water. The pH of the eluate was tested to be less than 3 (if not, 50% v/v TFA in water was added). Then, 10 μ g of peptides were isolated and prepared as the pre-trypsinisation sample, and together they were used in stain-free gel imaging (section 2.2.3) to test the successful digestion of proteins to peptides. Furthermore, 100 μ g of peptides per sample were transferred in a 1.5 mL protein LoBind tube, while the rest were transferred in a 2 mL protein LoBind tube. All of the samples were dried using a vacuum concentrator (Speed-Vac), o/n, at 37°C and stored at -80°C. The former samples were used for total proteomics, while the latter samples were further prepared for

total ubiquitinomics. All the MS-related experiments were conducted using filter tips, Protein LoBind® tubes (Eppendorf) and the MS-grade water (Thermo Fisher Scientific).

2.7.2 K-ε -GG Remnant Immunoaffinity Purification

Immunoaffinity purification was conducted according to the PTMScan HS K-ε -GG remnant magnetic immunoaffinity beads protocol (Cell Signalling Technology). Briefly, the lyophilized peptides were centrifuged for 5 min at 2,000 x g, RT and resuspended in 1.5 mL of 1 X HS IAP Bind buffer. The pH of the dissolved peptides was tested to be not lower than 7 (neutralized with 1M Tris base, if necessary) and the tube was gently shaken for 5 min, at RT, using thermomixer (<500 rpm, RT). Solution was cleared by centrifugation for 5 min at 10,000 x g at 4°C and further cooled on ice. Meanwhile, the vial of antibody-bead slurry was spin for 2 sec at 2,000 x g, gently resuspended by pipetting and then 20 µl of bead slurry were placed in 2 mL of protein LoBind eppendorf tube. Ice-cold 1 x PBS was added to the beads and mixed by inverting the tube five times. The tube was then placed on a magnetic wrack for 10 sec and the buffer was carefully removed. This washing step was then repeated for four times in total. The soluble peptides were transferred into the tube containing the antibody beads and incubated for 2 h on an end-over-end rotator, at 4°C. Sequentially, the tube was spin for 2 sec at 2,000 x g, placed on a magnetic wrack for 10 sec and the peptide solution from within was discarded. Beads were resuspended in 1 mL of HS IAP Wash buffer, mixed by inverting the tube five times, centrifuged for 2 sec at 2,000 x g, and the buffer was removed upon placing the tube for 10 sec on a magnetic wrack. This washing step was repeated for another three times and then additional two washes with 1 mL chilled LCMS water were performed following the exact same procedure as for washing the beads with the HS IAP wash buffer. To elute peptides from the antibodies bound beads, 50 µl aqueous 0.15% v/v TFA was added and gently mixed using a thermomixer at <500 rpm, RT. The tube was centrifuged at 2,000 x g for 2 sec and the eluted sample was transferred in a new 1.5 mL protein LoBind eppendorf tube. This step was repeated once more. DiGly peptides were then desalted as described in section 2.6.4.

2.7.3 timsTOF MS Data Acquisition

Lyophilised peptides were resuspended in 10 µl of aqueous 0.1% TFA solution and loaded onto a C18 performance column (15 cm x 150 µm) attached to the HPLC Evosep One instrument (Evosep, Odense, Denmark). Peptides were eluted into a trapped ion mobility spectrometry coupled to a time-of-flight mass spectrometer (TimsTOF HT; Bruker) working on a parallel accumulation–serial fragmentation (PASEF) mode. The 15 sample per day (SPD) and 30 SPD elution methods were used for data-dependent (DDA) and data-independent (DIA) acquisition modes respectively. The former uses a 90 min gradient, while the latter one 48 min gradient.

2.7.4 timsTOF MS Data Analysis

The following approach was used for both proteomics- and ubiquitinomics-based experiments performed in timsTOF mass spectrometer. Peak lists in.raw format were imported into FragPipe and DIA-NN for DDA- and DIA- derived raw data, respectively. All data were searched against the LmxMC9T7 FAST database and trypsin was selected as a protein digestion approach. For variable amino acid modifications, oxidised methionine and GlyGly (GG) derivatisation of lysine (+114 DA) were selected. FDR was set at 1% for both peptide precursor and protein, and for the proteomics datasets, only proteins with at least two unique peptides were kept for downstream analysis. Further

protein/peptide filtering, data processing and statistical analysis in order to identify significantly enriched ubiquitination sites or proteins was performed using limma package integrated in DEP package of Rstudio.

3 Investigation of Proximal Proteins of DUB2 using XL-miniTurboID

3.1 Introduction

Insights into the biological function of a protein are often achieved through the discovery of its interacting partners, known as the protein interactome. Protein interactomes have been extensively studied using affinity purification, in which a specific antibody against the target protein is used to affinity purify the protein along with any other proteins that are bound to it. The co-purified proteins are then identified via mass-spectrometry and this is known as affinity purification mass spectrometry (AP-MS). AP-MS relies on the principle that the protein interactions would be preserved throughout the cell lysis and protein purification. However, this is not always the case due to the loss of the native environment of the interacting proteins post-cell lysis. Consequently, the recovered molecules, such as the low-affinity and transiently interacting proteins, are prone to be lost. Another limitation of AP-MS is the requirement of high-quality antibodies against the baits, which limits diversity. Nevertheless, the use of chemical cross-linkers immediately after cell lysis or directly in cells, has been shown to improve the maintenance of protein interactions in AP-MS. However, it also increases the likelihood of obtaining false positive interactors (Gingras *et al.*, 2007; Subbotin & Chait, 2014).

3.1.1 Proximity Dependent Biotinylation

In the last decade, proximity dependent biotinylation (PDB) has emerged as an alternative approach for profiling protein interactomes (Roux *et al.*, 2012; Rhee *et al.*, 2013). PDB utilizes engineered enzymes that are capable in the presence of their substrates to synthesis highly reactive intermediate chemical adducts that diffuse away and attach covalently to proteins localized in close proximity with them. *In vivo* fusion of these enzymes to a specific target protein (the “bait”), followed by the addition of the substrates of that PDB enzyme leads to the subsequential covalent modification of the endogenously proximal interacting proteins (the “prey”) of the bait. The covalently labelled preys are purified using an affinity matrix, and then identified via MS. The high affinity between preys and matrix, such as the one between biotin and streptavidin (with a dissociation constant, K_d , of approximately 10^{-14} M), ensures that neither the harsh cell lysis nor washing conditions can adversely affect the ultimate identification of the investigated protein interactome. This overcomes the primary limitation of AP-MS (Samavarchi-Tehrani *et al.*, 2020).

Another advantage of PDB is the availability of two classes of enzymes that are currently utilized, providing flexibility to the system in terms of choosing the optimal approach for answering different questions in different organisms. Biotin protein ligases and peroxidases are the two enzymatic classes employed in PDB technique and each of them performs distinct chemical reactions. For instance, the former enzymatic class converts biotin (substrate) into biotinyl-5'-AMP in the presence of ATP, which is then released into the cellular environment around the enzyme forming a reactive biotinyl-5'-AMP cloud. Eventually, these highly reactive molecules react with the primary amine of lysine residues of proximal proteins, resulting in their biotinylation. The peroxidases catalyse redox reactions, such as the redaction of hydrogen peroxide (H_2O_2) via oxidizing aromatic molecules (e.g. biotin-phenol). This results to the formation of active radicals (e.g. phenoxyl radicals), which subsequently covalently label the electron-rich amino acid residues (mainly tyrosine) of nearby proteins. In both approaches, labelled proximal interacting proteins can be purified with streptavidin as an affinity matrix, and then identified via MS (Gentzel *et al.*, 2019; Zhou & Zou, 2020; Xu *et al.*, 2023).

3.1.2 Proximity Dependent Biotinylation Enzymes

Currently, there are three peroxidases and eight available biotin protein ligases, which have been used to map various protein interacting profiles. Briefly, the former group of enzymes consists of horseradish peroxidase (HRP), soybean ascorbate peroxidase (APEX) and its catalytic activity improved version APEX2 (Rhee *et al.*, 2013; Hung *et al.*, 2016; Bar *et al.*, 2018). The main advantage of these enzymes is their capability of performing PDB as short as a minute. This enables the characterisation of dynamic processes, such as the G-protein-coupled receptor signalling (Paek *et al.*, 2017). As discussed previously, protein labelling takes place in the presence of H₂O₂, however H₂O₂ is toxic for the cells. This can lead to membrane disruption, making the use of these enzymes less attractive, especially for whole organism PDB studies.

Nevertheless, biotin protein ligases are predominantly used in the field of PDB for investigating interacting proteins of proteins of interest. The first engineered enzyme used in PDB was the 35 kDa BioID (known as BirA*), which is a mutant (R118G) version of *Escherichia coli*'s (*E.coli*) BirA (Roux *et al.*, 2012). BioID has relatively slow labelling kinetics, requiring 18-24 h for efficient biotinylation, which subsequently prevents the temporal resolution of dynamic processes. Despite this limitation, the slow kinetics of BioID might be beneficial in reducing the background through the increased exposure of the true interactors to biotinylation. Another limitation of BioID is that the enzyme works optimally at 37°C, which can reduce the efficiency of the enzyme in organisms growing under lower or higher temperatures. Later on, in 2016, BioID2 was introduced as an improved second-generation BioID enzyme, derived from *Aquifex aeolicus* (*A. aeolicus*). BioID2 has a molecular weight of 26.6 kDa, which is smaller than BioID, mainly because it lacks the N-terminal DNA-binding domain. This makes the enzyme less likely to affect the localization and function of the bait, but also it reduces the DNA/chromatin associated protein background. Regardless, the labelling kinetics of the enzyme is slow, thus several hours of labelling is required (Kim *et al.*, 2016). Similarly, BASU, an engineered BirA* biotin ligase derived from *Bacillus subtilis*, lacks the N-terminal DNA binding domain. Initially, it was suggested that BASU exhibited up to a 1000-fold increase in labelling kinetics compared to BioID (Ramanathan *et al.*, 2018). However, a follow-up study revealed that its kinetics are more similar to BioID and BioID2 (Branon *et al.*, 2018).

On the other hand, TurboID and miniTurbo, which were created by directed evolution of the *E. coli* biotin ligase BirA-R118S, outperformed BioID, BioID2 and BASU with up to 23-fold higher enzymatic activity. This reduces the incubation time at less than 10 minutes and also, it permits the use of lower biotin concentration (<500 nM). Interestingly, between the two enzymes, TurboID is more active, making it ideal for experiments requiring maximized biotinylation yield, sensitivity and recovery. Nonetheless, this heightened enzymatic activity results in the utilization of even the limited amounts of biotin present in both the growing media and cells, which subsequently leads to promiscuous biotinylation. This is less profound in the less active miniTurbo, making this enzyme a better candidate for time specific experiments, where restricted background biotinylation is required. In addition, miniTurbo (28 kDa) is smaller than TurboID (35 kDa), due to the absence of the N-terminal DNA-binding domain. This provides miniTurbo additional advantages in terms of reducing both the background and interference of the localization and function of the targeted protein (Branon *et al.*, 2018).

In 2020, AirID was introduced as a novel biotin ligase and it was developed by combining ancestral enzyme reconstruction and site-directed mutagenesis. Despite sharing 82% protein sequence with BioID, AirID has better biotinylation activity. However, a direct comparison of AirID and the most active PDB enzyme, TurboID, demonstrated that AirID necessitates a minimum of 3 hours to achieve adequate biotin labelling, in contrast to TurboID's 1-hour requirement. This disparity in enzymatic

kinetics positions AirID below TurboID in this aspect (Kido *et al.*, 2020). Most recently, two more PDB enzymes have been developed: microID and ultraID. MicroID is the N-terminal fragment of BioID2, extending up to the amino acid K¹¹⁷. It has a size of 19.7 kDa and performs biotinylation labelling as early as 10 minutes. Interestingly, a single mutation (L41P) in microID resulted in the development of ultraID, which exhibits at least 5 times higher *in vivo* biotinylation activity compared to microID. It is speculated that L41P substitution in ultraID promotes the destabilisation of the biotin-binding site, facilitating the release of biotinyl-5'-AMP. Although ultraID exhibits notably superior activity compared to microID, its enzymatic efficacy is comparable with that of TurboID. Furthermore, ultraID displays a reduced background signal in the absence of exogenous biotin compared to TurboID, thereby enhancing the specificity of its biotinylation labelling. Lastly, the compact size of microID and ultraID reduces the likelihood of interfering with the function, trafficking, and interaction of the fused protein (Kubitz *et al.*, 2022).

3.1.3 Proximity Dependent Biotinylation in Kinetoplastids

Different PDB approaches were also used to investigate the interacting protein networks of various proteins in kinetoplastids (reviewed in Geoghegan *et al.*, 2022). The first reported application of PDB in kinetoplastids was by Morriswood *et al.* (2013), where they used a tetracycline-inducible BioID system in *T. brucei* to investigate the protein composition of the discrete cytoskeletal structure known as bilobe. Another PDB enzyme used in *T. brucei* was BioID2, which revealed the interaction between the inner mitochondrial membrane insertase Oxa1 and ZapE2 that is conserved in other eukaryotes (Pyrih *et al.*, 2020). In addition, as discussed previously, PDB labelling methods performed by peroxidases such as APEX2, can be toxic, particularly in whole-organism studies. Despite this concern, Vélez-Ramírez *et al.* (2021) successfully employed APEX2 as a PDB approach in *T. brucei* to characterise protein interactomes in various flagellum subdomains, including the axoneme and the flagellum tip. In *T. cruzi*, TurboID was utilized to investigate the flagellar membrane and/or associated proteins of the two main replicative stages of the parasite - epimastigote and amastigote. This study led to the discovery of 218 flagellar proteins in the epimastigote stage and 99 flagellar proteins in the amastigote stage. Among these, the flagellar localization of three proteins was validated via immunofluorescence (Won *et al.*, 2023). Finally, our group used PDB to gain insights into fundamental aspects of chromatin biology in *Leishmania*. Specifically, we investigated the interactomes of the bromodomain factor 5 (BDF5) and the kinetoplastid kinetochore proteins KKT2, KKT3 and KKT19 using XL-BioID (Jones *et al.*, 2022; Geoghegan *et al.*, 2022). XL-BioID is a novel PDB approach that was introduced by Geoghegan *et al.* (2022), which involves an *in vivo* DSP crosslinking step following proximity biotinylation. This additional step significantly improved the proximal protein signal intensity by approximately 10-fold, which led to the identification of 16 out of the 25 predicted inner KKT proteins and the discovery of two novel ones. In the same study, we also utilized the miniTurbo PDB enzyme to characterise the dynamic interactions of kinetochore proteins throughout the cell cycle of hydroxyurea-synchronized *L. mexicana* promastigotes.

3.1.4 Aims

In this study, we are interested to investigate the proximal protein interacting network of the *L. mexicana* DUB2. The direct protein interactome of this protein has been previously investigated using *in vivo* crosslinking AP-MS, which revealed that DUB2 interacts with various proteins involved in diverse biological processes such as: RNA splicing/capping (e.g. CYC12); RNA binding (e.g. GCD10p); transcription (e.g. NIF3); DNA replication (e.g. PCNA); endosome trafficking (e.g. VPS4); ubiquitination

(e.g. polyubiquitin) and phosphorylation (e.g. MKK1). These interacting partners of DUB2, along with its reported DUB2 nuclear localization, placing DUB2 near actively transcribed genes (Damianou *et al.*, 2020). However, as it has already been mentioned AP-MS is prone to losing weak and transient protein-protein interactions. Thus, in this study performed XL-BioID using the miniTurbo enzyme to provide a holistic protein profiling of DUB2 that would complement the previously mapped protein interactome. The PDB miniTurbo enzyme was chosen as the most suitable enzyme for this project due to its: high activity with a restricted promiscuous biotinylation; absence of DNA binding domain, which makes the enzyme smaller and less likely to interfere with the nuclear localization and function of the bait protein; use of non-toxic labelling conditions; and ideal function for dynamic cellular processes, such as enzymatic cleavage. At this point, it is worth mentioning that ultraID and microID were not available at the given time that the experiment was performed. Nonetheless, in the end, the dataset containing the proximal interacting proteins of DUB2 will be compared with other extensive -omics data to potentially identify substrates of DUB2 (Liu *et al.*, 2018; chapter 4).

In brief, we performed the following steps in the given order to achieve our goal in this chapter:

- Generated an endogenously miniTurbo-C-terminal-tagged DUB2 promastigote cell line and an endogenously miniTurbo-N-terminal-tagged CLK1 control.
- Optimized the XL-BioID using miniTurbo protocol to minimize background biotinylation in the absence of exogenous biotin.
- Identified proximal interacting partners of DUB2
- Investigated interaction between DUB2 and its proximal interacting proteins via co-IP.
- Checked the overlap between IP-derived interactome (Damianou *et al.*, 2020) and miniTurbo-derived proximal interactome
- Re-investigated DUB2 localization

3.2 Results

3.2.1 Generation and Validation of MiniTurbo-Tagged Cell Lines

In order to investigate the protein interacting network of the DUB2 in the *L. mexicana* promastigote stage, we endogenously double allele tagged the *DUB2* encoding gene (LmxM.08_29.2300) with a 3xMyc-tagged miniTurbo expressing sequence to its C-terminus (DUB2::miniTurbo::Myc). In addition, to ensure that both alleles were successfully tagged, we integrated a different drug resistance marker allowing selection with either blasticidin or puromycin - in each allele. This was performed on a T7Cas9 expressing promastigote cell line (parental line) using the CRISPR-Cas9 approach developed by Beneke *et al.* (2017). At this point is worth mentioning that DUB2 was thought to be a nuclear protein, therefore we selected *L. mexicana* CDC2-like kinase 1 (CLK1; LmxM.09.0400), which localizes in the same specific subcellular compartment, as a control for this approach (Damianou *et al.*, 2020; Geoghegan *et al.*, 2021). The reasons of using “compartment-specific” controls were threefold. Firstly, it allows for subtraction of nonspecific proximal labelling in the nucleus. Secondly, it facilitates the identification of endogenously biotinylated proteins and lastly, it helps with the removal of proteins associating with the protein biogenesis machinery. Thus, an N-terminally double allele tagged with a 3xMyc-tagged miniTurbo CLK1 (Myc::miniTurbo::CLK1) cell line was also generated.

To select successfully transformed promastigotes, we performed dual antibiotic selection using BSD and PUR antibiotics. Subsequently, we carried out a genomic validation that the *miniTurbo* expressing gene and antibiotic resistance cassette for *puromycin acetyltransferase (PAC)* and *blasticidin S deaminase (BSD)* were indeed integrated in the expected genomic regions via three independent diagnostic PCRs (Fig. 4A). Furthermore, we confirmed through an α -Myc western blotting (Fig. 4B) that both mutant cell lines were expressing their baits DUB2 (untagged size: 81kDa; with fusion: ~110 kDa) and CLK1 (untagged size: 53 kDa; with fusion: ~82 kDa) fused to the 3xMyc miniTurbo (29.2 kDa). This indicated that regardless the size of the tag the target specific protein remained stable. However, we observed additional bands in both samples, suggesting either a partial degradation of the tagged proteins or non-specific binding of the α -Myc primary antibody. The absence of positive and negative controls, such as another myc-tagged cell line and the parental cell line, respectively, precludes the justification of either of these conclusions. Moreover, DUB2 is known for its vital role in the promastigote-to-amastigote differentiation process of *L. mexicana*. Thus, we conducted an AlamarBlue assay to address whether the presence of the 3xMyc-miniTurbo was interfering with the DUB2 function during this differentiation process (Damianou *et al.*, 2020). Upon calculating the percentage difference of fluorescence intensities between treated and untreated (T7Cas9) cells, we found out through the one-way ANOVA analysis that there was no significant difference between the treated and untreated samples, at 10 h, 56 h or 128 h after induction of differentiation (Fig. 4C). Therefore, we concluded that the presence of the 3xMyc-miniTurbo does not affect the metabolic activity pattern, viability and proliferation capacity of the cells during differentiation, indicating that the essential function of DUB2 remains intact.

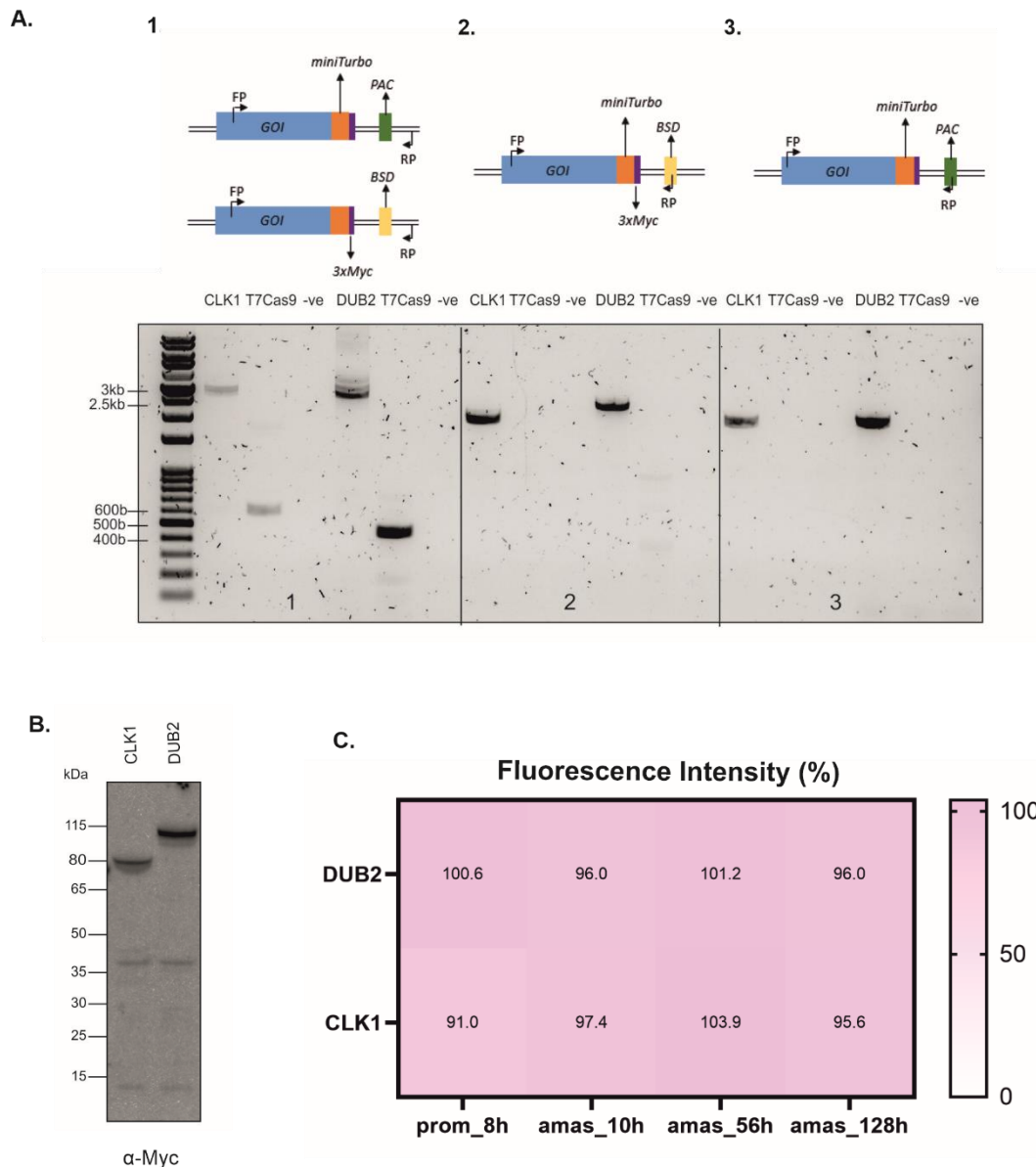


Figure 4: Generation and validation of DUB2 and CLK1 tagged with miniTurbo cell lines. A. PCRs performed on genomic DNA from T7Cas9 (control), DUB2::miniTurbo::Myc and Myc::miniTurbo::CLK1 promastigotes, followed by agarose gel electrophoresis (1% w/v, 45 min, 100 V). Illustration for each given PCR is also included, using N-terminally tagging of gene of interest (GOI) with 3xMyc-miniTurbo as an example. **A1.** This PCR investigates any miniTurbo-untagged targeted GOI within the genome, with primers designed to amplify regions within the GOI and upstream (for N-terminal tagging) or downstream (C-terminal tagging) of the PAC/BSD resistance cassette. If an untagged gene is present, then a DNA fragment of equal size with the T7Cas9 version of the gene was expected. Tagged DNA fragments are ~2.7 kb- 3.3 kb and the untagged ones (only present in T7Cas9 promastigotes) are <1 kb. **A2&3.** Successful integration of the BSD and PAC resistance cassettes respectively, with primers designed to anneal to the BSD/PAC resistance cassette and GOI. Successful integration for both resistance cassettes was revealed in the genome of both miniTurbo-tagged promastigotes with expected products of ~2-3 kb being observed. Negative control (-ve; just reagents) was used in each PCR to test for any possible contamination. PCR BIO Ladder I (5 μ l) was used as a DNA ladder. **B.**

Expression of 3xMyc-miniTurbo tagged proteins DUB2 (110 kDa) and CLK1 (82 kDa) was validated via a western blot analysis using promastigote cell extracts. The α -Myc clone 4A6 (mouse monoclonal IgG1) antibody (1:5000; EMD Millipore) was used as a primary antibody and the α -mouse IgG HRP conjugate antibody (1:5000; Promega) was used as a secondary antibody. For ladder, the Spectra™ Multicolor Broad Range Protein Ladder (10 μ l) was added. **C.** Averaged percentage difference of fluorescence intensity per indicated miniTurbo cell line against T7Cas9 control, at the given time points post-induction of promastigote-to-axenic amastigote differentiation (n=3). One-way ANOVA was performed for each time point, with no significant difference being reported between T7Cas9 and miniTurbo-tagged cell lines ($p > 0.05$). Abbreviations: FP; forward primer, RP; reverse primer, BSD; blasticidin S deaminase, PAC; puromycin acetyltransferase, GOI; gene of interest, % of FI; percentage of fluorescence intensity of tagged over control cell lines, P; promastigotes, A_10h; axenic amastigotes 10h post-differentiation induction.

3.2.2 Optimization of MiniTurbo Workflow Using BioLock

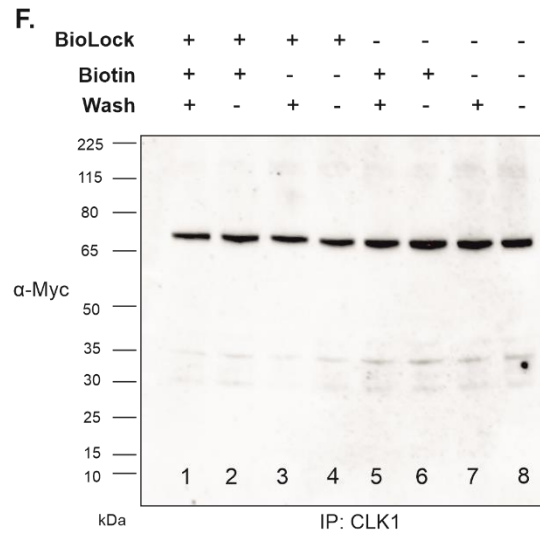
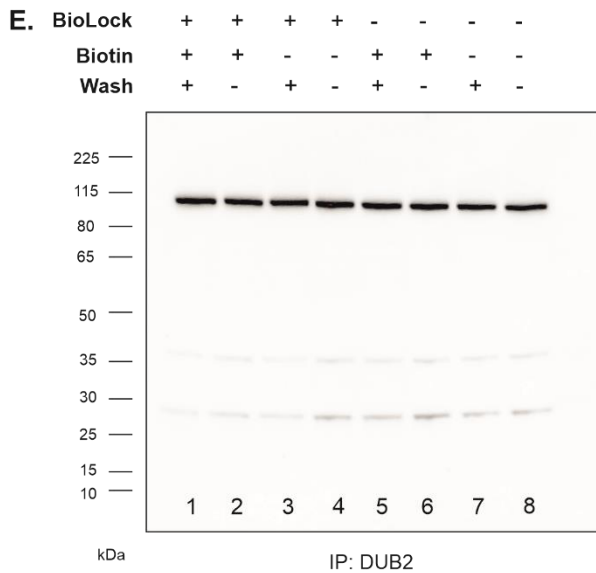
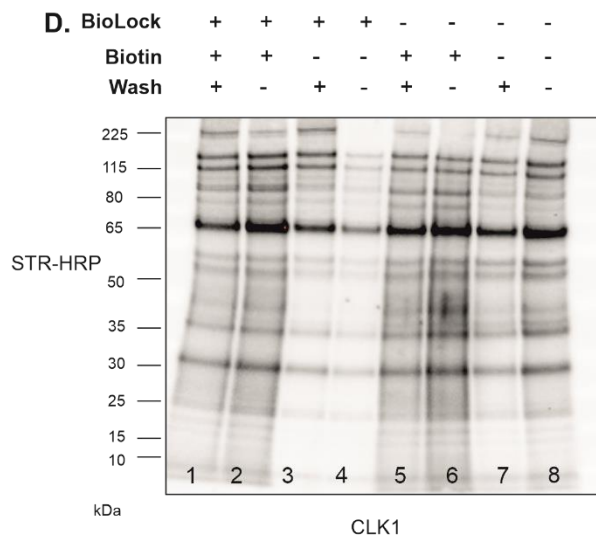
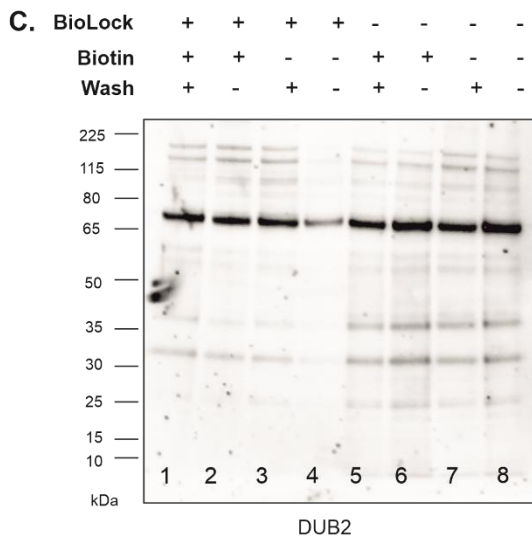
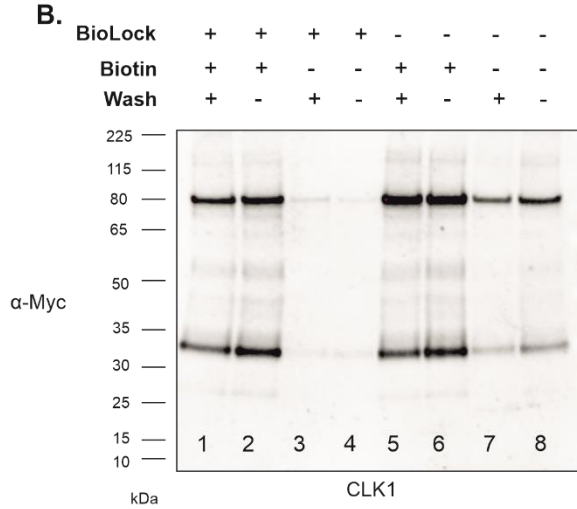
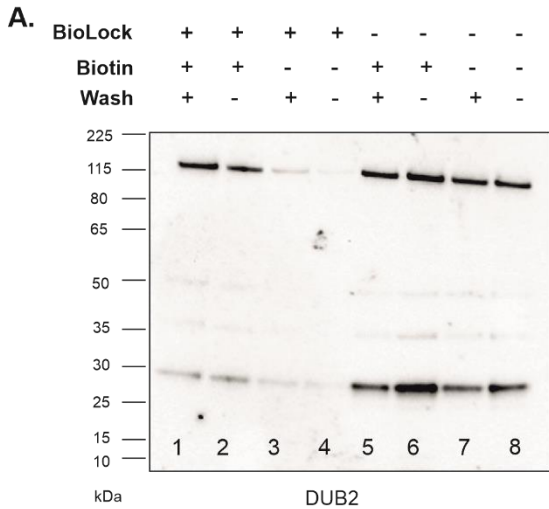
Next, we tested for evidence of *in-vivo* miniTurbo-mediated biotinylation in *L. mexicana* promastigotes. Biotin is the substrate of the miniTurbo enzyme that is required to perform biotinylation *in vivo*, thus we added exogenous biotin in the media. Due to the high enzymatic activity of the enzyme, 500 μ M of exogenous biotin and 30 min of biotin labelling was enough for the enzyme to perform proximity biotinylation in *Leishmania* promastigote cultures (Geoghegan *et al.*, 2021). We then affinity purified the DUB2::miniTurbo::Myc (110 kDa) and Myc::miniTurbo::CLK1 (82 kDa) via an over-night (o/n) pulldown using streptavidin-coated beads (lane 6 in Fig. 5A&B). Notably, we observed promiscuous biotinylation of both bait proteins in eluate samples even without the addition of the exogenous biotin (lane 8 in Fig. 5A&B). This is explained by the high catalytic activity of the miniTurbo that allows the utilization of low biotin levels present in both the growth medium and the cell itself. Degradation products of both baits (30 kDa for DUB2::miniTurbo::Myc and 35 kDa for Myc::miniTurbo::CLK1) were also captured in both conditions, indicating that the o/n pulldown or cell lysis could have somehow affected the protein stability in the cells. In addition to the self-biotinylation of the bait proteins, we also examined for evidence of the miniTurbo-mediated biotinylation protein profiling, using a streptavidin blot analysis by re-probing the same membrane with streptavidin - horseradish peroxidase (HRP) conjugate. However, in both promastigote cultures, the biotinylated protein profiling in the presence or absence of exogenous biotin was identical, supporting further the high enzymatic activity of miniTurbo (lines 4 to 8 in Fig. 5C&D). Taken together, these results suggest that miniTurbo-dependent biotinylation is efficient in living *Leishmania* promastigotes.

This uncontrolled biotinylation by miniTurbo in the absence of exogenous biotin was expected. Therefore, under the same experiment we tried to minimize this phenomenon by depleting the exogenous biotin in the medium of the growing cultures. This was carried out by adding BioLock (IBA Lifesciences), a biotin-blocking solution that contains avidin, 18 h before performing the *in-vivo* biotin labelling. Interestingly, both DUB2::miniTurbo::Myc and Myc::miniTurbo::CLK1 proteins were affinity purified by streptavidin-coated beads only when exogenous biotin was added to the culture after the 18 h depletion (compare lanes 2 and 4 in Fig. 5A&B). This indicates that indeed the activity of the miniTurbo is affected by the presence of biotin in the medium and also that BioLock solution could be used as an optimization step to reduce uncontrolled miniTurbo biotinylation. Furthermore, the presence of BioLock solution in the growing cultures could have affected the proximity labelling by depleting some of the added exogenous biotin. Therefore under the same experiment, we also examined whether washing off the growing medium of the cultures containing BioLock with 1 x PBS and then replacing it with fresh medium before biotin labelling took place would improve the biotin labelling induction. However, it did not increase the self-biotinylation of the DUB2::miniTurbo::Myc

and Myc::miniTurbo::CLK1 proteins (compare lanes 1 and 2 in Fig. 5A&B), indicating that adding exogenous biotin to a final concentration of 500 μ M is enough to support miniTurbo biotinylation without being depleted by BioLock. Similarly, washing off of the BioLock containing media did not have any obvious impact on the promiscuous miniTurbo-derived biotinylation of both baits in the absence of biotin (compare lanes 3 and 4 in Fig. 5A&B), supporting that this optimization step might not be necessary.

In addition to the self-biotinylation of the bait proteins, we also examined for evidence of the biotinylated protein profiling under the different conditions, using a streptavidin blot analysis, where the same membranes were re-probed with STR-HRP conjugate. Both BioLock-treated promastigotes, expressing either DUB2::miniTurbo::Myc or Myc::miniTurbo::CLK1, revealed identical protein patterns in the presence of exogenous biotin, regardless whether the washing step was applied or not (compare lanes 1 and 2 in Fig. 5C&D). Similarly, in the absence of exogenous biotin, the same biotinylated protein profiling is observed when the washing step was applied for the DUB2::miniTurbo::Myc culture (lane 3 in Fig. 5C). In contrast, under the same condition, there is an absence of a 45 kDa protein in the Myc::miniTurbo::CLK1 culture (lane 3 in Fig 5D), indicating that the particular protein is a promising interacting protein of CLK1 that has been biotinylated by miniTurbo. Interestingly, the persistency of the particular protein pattern in both streptavidin blots under those three conditions, indicates that all these proteins might be either endogenously biotinylated proteins, proteins associated with the protein biogenesis machinery or compartment specific proteins. Notably, in the absence of both of the washing step and the exogenous biotin, there was a decrease of these biotinylated proteins (lane 4 in Fig. 5C&D). This supports the conclusion from the previous results in Fig. 5A&B that the overnight treatment with BioLock solution can reduce the promiscuous miniTurbo biotinylation activity in the absence of exogenous biotin. Furthermore, these results suggest that replacing the BioLock-containing growing medium with a fresh one, which contains some exogenous biotin, is enough to recover some endogenously- and/or miniTurbo-biotinylated captured proteins in a short time window. However, we cannot exclude the possibility that the addition of exogenous biotin in the presence of BioLock might affect adversely the identification of the transient and weak protein-protein interactions via miniTurbo in the *Leishmania* promastigotes. Thus, the washing step was included in downstream experiments.

For all the studied conditions, input samples were collected before the streptavidin pulldowns to show that both the baits (Fig. 5E&F) and other biotinylated proteins (Fig. 5.G&H) were present beforehand, and that the absence or presence of successful biotinylation defined by the different applied conditions determined the already mentioned observations. Oligopeptidase B (OPB; 83.5 kDa) was used as a loading control (Fig. 5I&J).



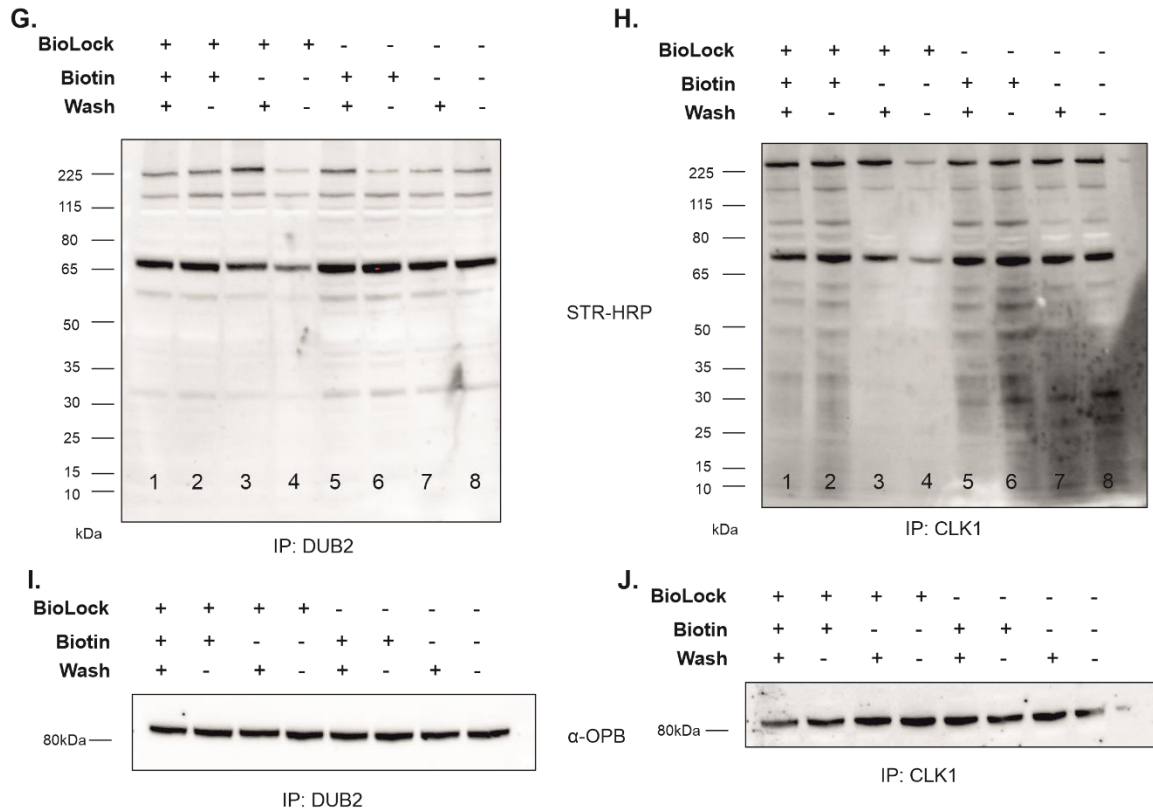
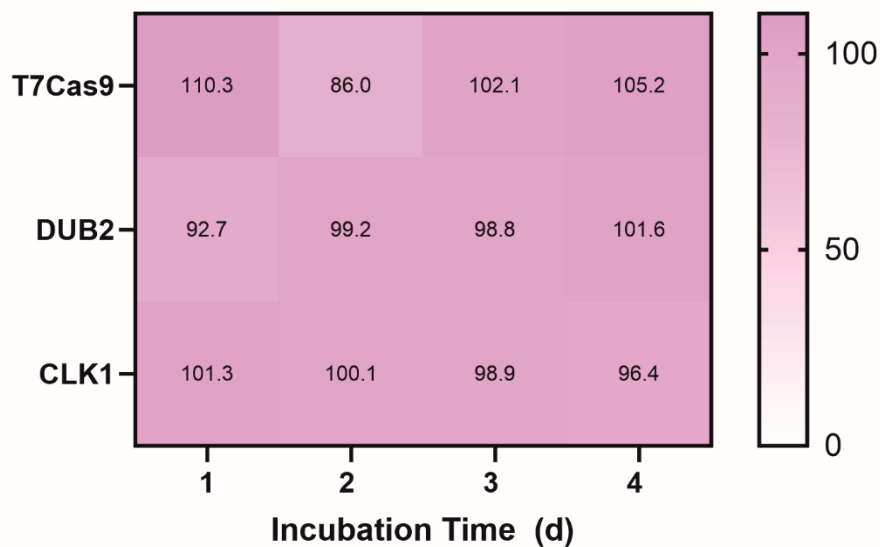


Figure 5: Optimization of XL-BioID using miniTurbo workflow using BioLock. Briefly, promastigote cells expressing DUB2::miniTurbo::Myc and Myc::miniTurbo::CLK1 were cultured in HOMEM medium; just before cells reached log-phase (2×10^6 cells mL^{-1}), BioLock solution was added (BioLock: +) or not (BioLock: -) in the growing cultures for 18h; BioLock-containing medium was washed off and replaced with fresh HOMEM medium (wash: +) or not (wash: -); 500 μM final concentration of exogenous biotin was added (biotin: +) or not (biotin: -) for 30 min to induce miniTurbo biotinylation; in vivo crosslinking was performed using DSP; cells were lysed using RIPA buffer and biotinylated proteins were affinity purified using streptavidin-coated beads. A portion of each cell lysate (called input sample) was extracted before streptavidin pull-down was performed (IP: DUB2, IP: CLK1). **A&B.** Western blot analysis using α -Myc tag clone 4A6 (mouse monoclonal IgG1) antibody (1:5000; EMD Millipore) as a primary antibody and α -mouse IgG HRP conjugate antibody (1:5000; Promega) as secondary antibody revealed the presence or not of DUB2::miniTurbo::Myc (110 kDa) and Myc::miniTurbo::CLK1 (82 kDa) upon streptavidin pull-down, under the different examined conditions. **C&D.** Re-probed the same two membranes (A&B) with streptavidin-horseradish peroxidase (HRP) conjugate (1:5000; Thermo Fisher Scientific) to observe the biotinylated protein profile of the differently-treated eluates derived from the two miniTurbo-tagged cell lines. **E&F.** Pre-streptavidin pull-down input samples were also analysed as in A&B to prove that the 3xMyc miniTurbo-tagged proteins were successfully expressed in the cell lines, and that the absence of proteins in A&B was due to their unsuccessful biotinylation by the miniTurbo enzyme. **G&H.** Biotinylated protein profile of input samples pre-pull-down, as performed in C&D. **I&J.** Oligopeptidase B (OPB; 83.5 kDa) was used as loading control for input. The membranes from C&D were re-probed with the primary α -LmjOPB (sheep) antibody (1:20,000; Munday et al., 2011) and secondary EasyBlot α -sheep IgG (HRP) antibody (1:5000; GeneTex). Abbreviations: STR-HRP; streptavidin-horseradish peroxidase conjugate, IP; input.

Biotin (a.k.a. vitamin H) is a micronutrient (244 g mol^{-1}) that is essential for all organisms. Biotin is either synthesised *de novo* such as in most prokaryotes, fungi and plants, or it is uptaken by biotin transporters (e.g. sodium multivitamin transporter SMVT), like in mammalian cells and yeasts (reviewed in Tong, 2013; Azhar *et al.*, 2015). *Leishmania* belongs in the latter group, making them auxotrophic for biotin (Naderer & McConville, 2008). Depletion of biotin from the growing medium of the promastigote cultures by using BioLock could affect adversely the metabolic activity, cell proliferation and viability of the cells. Therefore, to investigate this, we perform an AlamarBlue assay, in which we grew DUB2::miniTurbo::Myc and Myc::miniTurbo::CLK1 promastigote cultures in the presence of BioLock (treated) or not (untreated) for 4d. Every 24h, we recorded the fluorescence intensity of the 3 replicates that were used in each condition and calculated the percentage difference of fluorescence between BioLock-treated promastigotes and untreated ones. Fig. 6A illustrates the averaged percentages of the fluorescence difference in a heat map, with a gradient of grey spanning between 85% and 110% respectively. One-way ANOVA analysis revealed no significant difference between the metabolic activity of BioLock-treated and untreated promastigotes for both miniTurbo-tagged cell lines at every tested time-point, indicating that the presence of BioLock does not negatively impact the metabolic activity of the cells. Contrastingly, 4-day growth curve revealed a profound defect on the cell growth of the BioLock-treated DUB2::miniTurbo::Myc and Myc::miniTurbo::CLK1 promastigotes compared to BioLock untreated, but only 48 h post-BioLock treatment (Fig. 6B). This suggests that biotin depletion via BioLock permits the sufficient growth of cells until they reach $\sim 4 \times 10^6 \text{ cells mL}^{-1}$ (early log-phase). However, beyond that growing point (late log phase) the available biotin in the growing medium is not enough to sustain comparable growth rates as the ones observed in the untreated promastigotes. Collectively, we showed BioLock is acceptable to be used as an overnight biotin-depletion treatment to minimize miniTurbo-mediated uncontrolled biotinylation.

A. Fluorescence Intensity (%)



B.

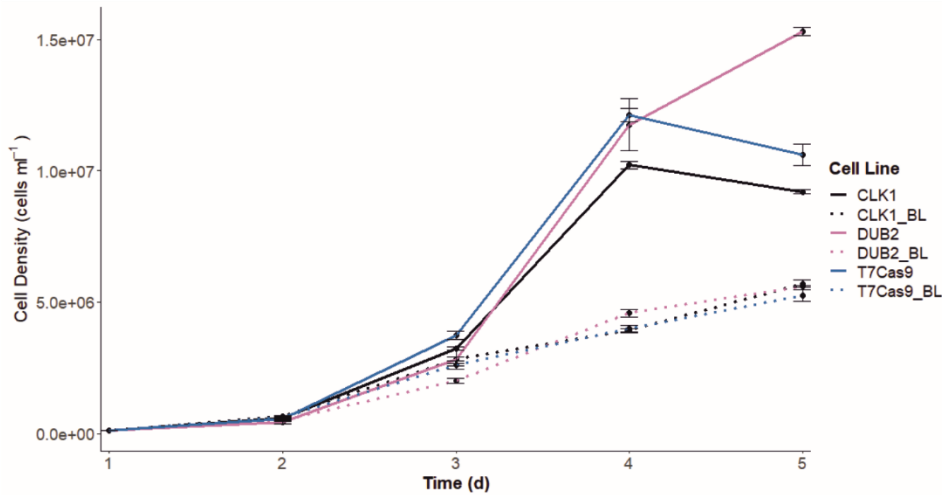


Figure 6: Impact of BioLock in the metabolism and growth of the *Leishmania* promastigotes. A. BioLock treatment had no significant effect on the metabolic activity of the treated DUB2::miniTurbo::Myc (DUB2), Myc::miniTurbo::CLK1 (CLK1) and T7Cas9 promastigote cells relative to the untreated ones, per investigated incubation period (days; d). 3 replicates were used for each case, and each given value represent the averaged percentage difference of fluorescence intensity between treated and untreated samples taken in each time point. **B.** Treatment with BioLock for up to 2 days (d) of incubation had no significant effect on the growth of the investigated promastigote cell lines. Promastigotes were grown in the presence or absence of BioLock for 4 days, cell density was measured every 24h, and the mean \pm S.E. of three replicates was plotted. Cells treated with BioLock are depicted with a dashed line and labelled as _BL (=BioLock; e.g.CLK1_BL).

3.2.3 Identification of DUB2 Proximal Interactome

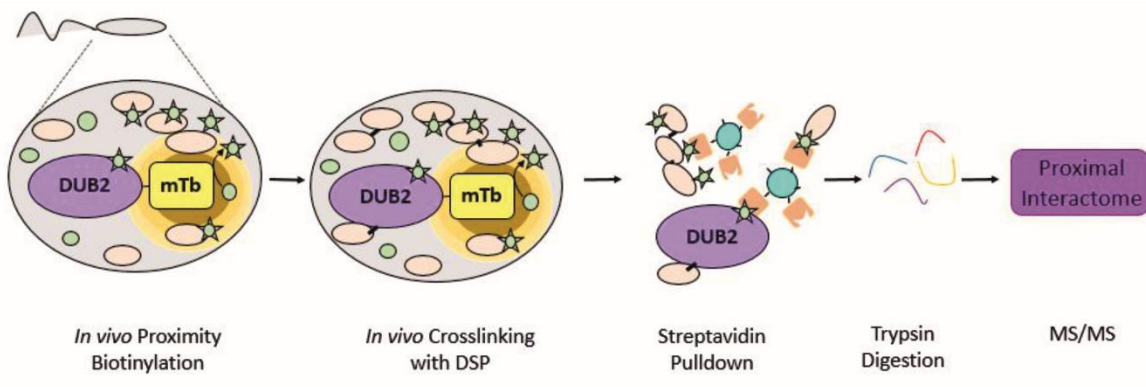
Upon generating and validating our miniTurbo-tagged promastigote cell lines and optimizing the miniTurbo workflow using BioLock, we performed label-free tandem mass-spectrometry (MS/MS) to identify the proximal interacting proteins of DUB2. For the MS/MS analysis, we prepared three independent samples from each cell line, as described in the schematic in Fig. 7A. Briefly, we added BioLock solution o/n to the growing promastigotes, and then, 18 h post incubation we washed out the BioLock-containing growing medium and replaced it with fresh one. Then, we added exogenous biotin to a final concentration of 500 μ M for 30 min, washed it off and then cross-linked the promastigotes with dithiobis (succinimidyl propionate; DSP). We then extracted lysates from 1×10^9 cells; affinity purified biotinylated proteins using streptavidin-coated beads; performed on-bead trypsin digestion and then sent them for MS/MS.

Label free quantification by mass-spectrometry, combined with downstream limma-based enrichment analysis revealed 73 and 165 proteins to be significantly enriched for DUB2 and CLK1 respectively (5% FDR; $n=3$; Fig. 7B). Confidence in the quality of our MS data was provided through a principal component analysis (PCA). The PCA plot revealed distinct clustering of Myc::miniTurbo::DUB2 and CLK1::miniTurbo::Myc samples, with biological replicates per condition to cluster together. This result indicates that there is variation between the samples of the two tested cell lines, however this variation is not as high between the biological replicates, showing reproducibility and robustness of the data (Fig. 7C & D). This conclusion was further supported through a Pearson correlation coefficient analysis, where strong and positive correlation was observed

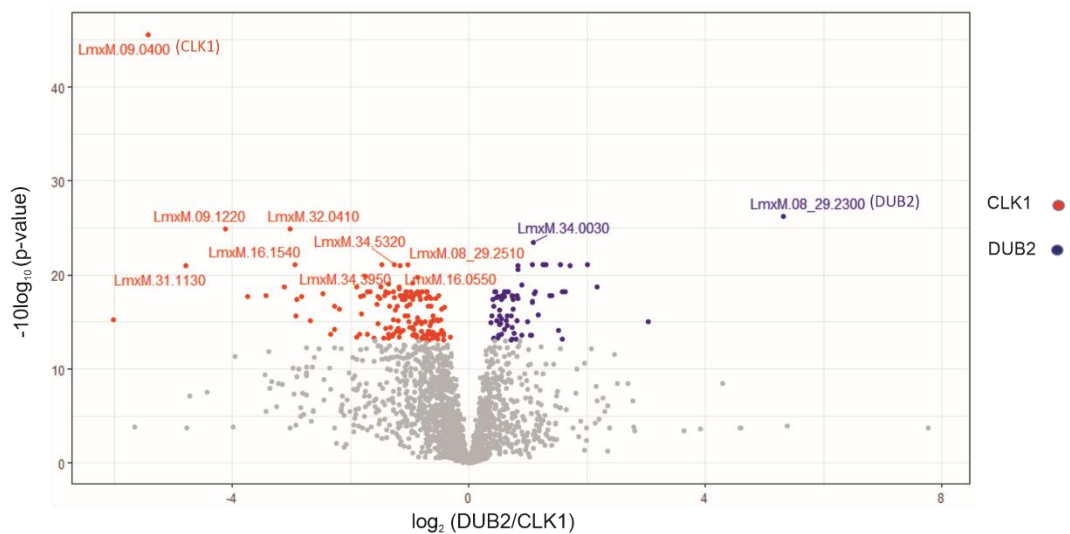
between the biological replicates per cell line ($PCC > 0.98$). The significant proximal interacting proteins of DUB2 are listed in Table 3, of which the top three proteins with the highest fold-change (FC) enrichment over the CLK1 proximal interactome were: the ubiquitin carboxyl-terminal hydrolase DUB2 (LmxM.08_29.2300; $\text{Log}_2\text{FC} = 5.31$), kinesin K39 (LmxM.14.1120; $\text{Log}_2\text{FC} = 3.04$) and the 50S ribosome-binding GTPase (LSG1; LmxM.05.0200; $\text{Log}_2\text{FC} = 2.17$). As for the CLK1 proximal interactome, the three top proteins were: the hypothetical protein LmxM.06.0430 ($\text{Log}_2\text{FC} = -6.02$), CLK1 (LmxM.09.0400; $\text{Log}_2\text{FC} = -5.43$) and the hypothetical protein LmxM.31.1130 ($\text{Log}_2\text{FC} = -4.78$; data not shown). At this point it is worth mentioning that the kinetoplastid kinetochore protein 2 (KKT2), KKT5 and KKT24, which are known interactors of CLK1, were identified in our CLK1 proximal interactome, providing validation that our approach was successful (data not included).

Next, we carried out a gene ontology (GO) enrichment analysis to categorise the proximal interacting proteins of DUB2 based on their biological processes. This was performed via manual inspection through literature combined with the GO enrichment tool provided by TriTrypDB. The GO analysis categorised the proximal interactome in 17 different biological processes, with protein translation having the most hits (41%), followed by RNA binding/processing (8%), cytoskeletal-associated proteins (7%) and glycolysis (7%; Fig. 8).

A.



B.



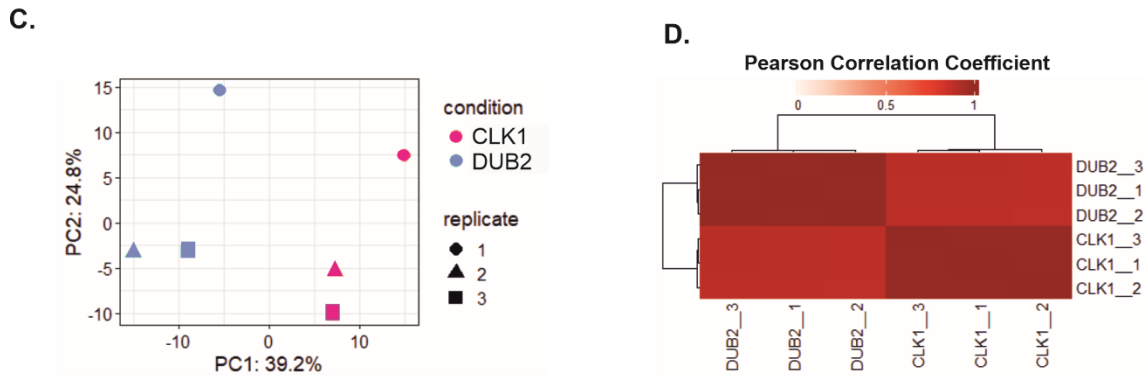


Figure 7: Investigation of the proximal interactome of DUB2. **A.** Schematic of PDB using miniTurbo enzyme. MiniTurbo-tagged DUB2 promastigote was used as an example. MiniTurbo-tagged CLK1 promastigote cell line was concomitantly subjected to the same conditions. **B.** Identification of the proteins significantly enriched in the DUB2 (73 hits; blue) and CLK1 (165 hits; red) datasets. Enrichment analysis performed using limma package in Rstudio ($p < 0.05$). In grey are the non-significant detected proteins. False Discovery Rate was set up at 5% and 3 biological replicates were used. **C.** Variation between DUB2 and CLK1 datasets is observed, however not across replicates, as calculated by PCA. Each symbol represents a different replicate per condition, while colours distinguishes the conditions used (blue for DUB2::miniTurbo::Myc-derived data; pink for Myc::miniTurbo::CLK1-derived data). **D.** Strong and positive correlation observed across replicates within each condition, whereas the correlation between conditions is weaker but still positive. Correlation was calculated using PCC, of which dark red indicates very strong and positive correlation (PCC=1) and light red means no correlation (PCC=0). The three replicates per sample are numbered as _1, _2 and _3.

Table 3 Proximal interacting proteins of DUB2. For each protein the following information were included: accession number, Log₂ Fold Change value, acronyms used in literature, description as given in TritypDB, and whether the protein is present in the immunoprecipitation-derived DUB2 interactome dataset (Damianou et al., 2020) and the ubiquitinomics datasets from chapter 4.

Proximal Interactome of DUB2				IP-Derived Interactome of DUB2 (Damianou et al., 2020)	Ubiquitinome (Chapter 4)
Accession	Log ₂ FC	Description	Acronym		
LmxM.08_29.2300	5.31	DUB2	Deubiquitinase 2	Yes	Yes
LmxM.14.1120	3.04	K39	kinesin 39		
LmxM.05.0200	2.17	LSG1	50S ribosome-binding GTPase		
LmxM.11.0820	2.01	hypothetical protein			Yes
LmxM.15.0170	1.71	PP2C/PDP	Protein phosphatase 2C/pyruvate dehydrogenase phosphatase (PDP)		Yes
LmxM.21.0550	1.62	DLAT	dihydrolipoamide acetyltransferase		
LmxM.29.0880	1.59	ADK	adenosine kinase		Yes

LmxM.34.2950	1.57	KPAF1	kinetoplast polyadenylation/uridylation factor		
LmxM.31.2730	1.54	hypothetical protein			
LmxM.18.0300	1.52	RAN/NTF2/MASP	RAN protein binding protein, Nuclear transport factor 2/mucin-associated surface protein		Yes
LmxM.36.3470	1.39	e1 of 2-OGDH (E1o-h) OR α -KDE1	2-oxoglutarate dehydrogenase E1 component		
LmxM.19.0190	1.36	MBF-1	Multiprotein bridging factor -1		Yes
LmxM.36.3910	1.30	AdoHcy or SAHH	S-adenosylhomocysteine hydrolase - not clear localization in trypanosomes...		Yes
LmxM.13.1210	1.25	NT3	nucleobase transporter 3 (purine)		Yes
LmxM.18.1380	1.18	PDHA1	pyruvate dehydrogenase E1 alpha subunit		
LmxM.33.1520	1.12	TPPP-like	p25-alpha; Tubulin Polymerization Promoting Protein (TPPP)-like protein		Yes
LmxM.33.0820	1.11	EF-1b	Elongation Factor 1-beta		
LmxM.34.0030	1.09	PYK	pyruvate kinase		
LmxM.36.6650	1.08	iPGMA	2,3-bisphosphoglycerate-independent phosphoglycerate mutase		Yes
LmxM.21.0840	1.07	MetAP2	methionyl aminopeptidase 2		Yes
LmxM.36.1940	1.07	NT2	inosine-guanosine transporter		Yes
LmxM.16.1470	1.06	KLIF	Kinesin Localized to the Ingressing Furrow (based on T.brucei)		
LmxM.15.1440	1.05	GlnRS	glutaminyl-tRNA synthetase		Yes
LmxM.19.0160	0.99	MetAP	methionyl aminopeptidase		Yes
LmxM.28.0490	0.90	PCCB	Propionyl-CoA carboxylase beta chain		
LmxM.31.2950	0.89	NDKb	Nucleoside-diphosphate kinase b		Yes
LmxM.36.0180	0.83	EF-2	elongation factor 2		
LmxM.28.2555	0.83	RPS17	40S ribosomal protein S17		
LmxM.26.2330	0.83	RPL35	60S ribosomal protein L35		
LmxM.28.2420	0.82	E2 of 2-OGDH (E2o-h) or α -KDE2	2-oxoglutarate dehydrogenase, E2 component,		

			dihydrolipoamide succinyltransferase,		
LmxM.08_29.2380	0.81	kinesin		Yes	Yes
LmxM.20.1700	0.79	non-specific S/T-kinase	non-specific Serine/Threonine-kinase		
LmxM.34.4940	0.76	hypothetical protein			Yes
LmxM.27.0880	0.75	e1 of 2-OGDH (E1o-h) OR α -KDE1	2-oxoglutarate dehydrogenase E1 component		Yes
LmxM.27.0670	0.74	aATP11	Putative amino acid transporter aATP11		Yes
LmxM.26.1630	0.74	RPS33	40S ribosomal protein S33		
LmxM.09.1010	0.73	Hypothetical (POMP10-disagree)	(Present in the outer mitochondrial membrane proteome 10)		Yes
LmxM.10.0070	0.73	RPL35a	ribosomal protein L35a, putative		Yes
LmxM.14.1270	0.73	RPS27A	putative ubiquitin/ribosomal protein S27a		Yes
LmxM.13.0570	0.72	RPS12	40S ribosomal protein S12		Yes
LmxM.14.1160	0.71	ENO	enolase		Yes
LmxM.07.0500	0.67	RPL7A	60S ribosomal protein L7a		
LmxM.34.1670	0.67	RPL26	60S ribosomal protein L26, putative		Yes
LmxM.05.0680	0.65	CTP	tricarboxylate carrier or citrate transport protein		
LmxM.03.0200	0.64	P5CDH	Delta-1-pyrroline-5-carboxylate dehydrogenase		Yes
LmxM.34.0240	0.64	RPL30	60S Ribosomal protein L30	Yes	Yes
LmxM.22.1360	0.63	FPPS	Farnesyl pyrophosphate synthase		Yes
LmxM.15.0950	0.61	RPS3	putative 40S ribosomal protein S3		Yes
LmxM.29.0460	0.61	aspRS	Aspartyl tRNA synthetase		
LmxM.16.0590	0.60	Gln-dependent CPS/CPSase	Putative glutamine-dependent carbamoyl-phosphate synthetase		Yes
LmxM.36.5010	0.60	RPSA	40S ribosomal protein SA		Yes
LmxM.34.1880	0.58	RPL5	60S ribosomal protein L5		
LmxM.33.2790	0.56	SRP68?	Signal-recognition-particle 68		Yes
LmxM.34.3760	0.55	RPL27A/L29	60S ribosomal protein L27A/L29		Yes
LmxM.31.2690	0.55	RPL27	Ribosomal protein L27		
LmxM.15.0200	0.54	RPL13a	putative 60S ribosomal protein L13a	Yes	Yes
LmxM.21.1720	0.53	RPL32	60S ribosomal protein L32		

LmxM.31.0950	0.52	TSN	Tudor staphylococcal nuclease (TSN, also known as Tudor-SN, SND1 or p100)		Yes
LmxM.08_29.2460	0.52	RPL13	60S ribosomal protein L13		
LmxM.01.0050	0.50	MCC	3-methylcrotonyl-CoA carboxylase alpha subunit		
LmxM.30.0640	0.50	REMC5/REMC5A	RNA editing mediator complex protein 5		
LmxM.21.0730	0.50	RPL36	60S ribosomal protein L36		
LmxM.18.0510	0.48	ACO	acotinase or Aconitate hydratase		Yes
LmxM.32.1955	0.47	RPL37	60S ribosomal protein L37		Yes
LmxM.24.2110	0.46	HMGS	3-hydroxy-3-methylglutaryl-CoA synthase		Yes
LmxM.26.0170	0.45	RPL7	60S ribosomal protein L7	Yes	
LmxM.34.0600	0.44	RPL18a	60S Ribosomal protein L18a	Yes	
LmxM.22.1520	0.42	RPL14	40S ribosomal protein L14	Yes	
LmxM.11.0960	0.42	RPS5	40S ribosomal protein S5		
LmxM.24.0040	0.42	RPL17	60S ribosomal protein L17		Yes
LmxM.31.3130	0.41	RPL3	60S ribosomal protein L3		Yes
LmxM.07.0680	0.39	RPS9	40S ribosomal protein S9		Yes
LmxM.36.3750	0.37	RPS27-1	40S ribosomal protein S27-1		

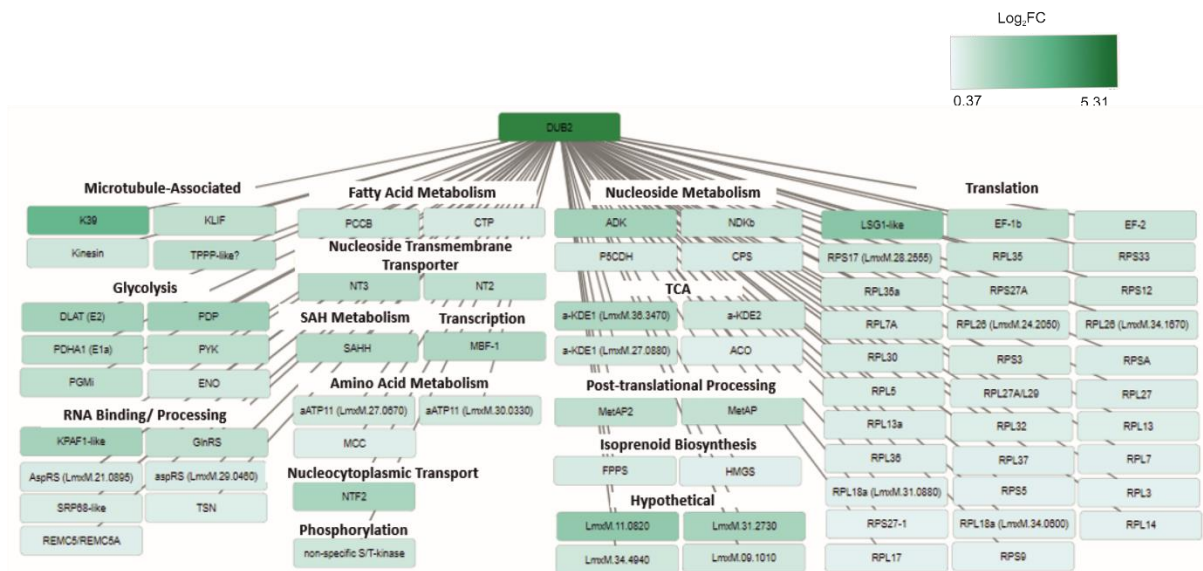


Figure 8: Proximal interactome of DUB2. Proteins were clustered based on their main biological process, in descending order from the protein with the highest Log₂ Fold Change (FC; darker green) to the one with the lowest Log₂ FC (light green). The extended version of the protein acronyms and their exact Log₂ FC value can be found in Table 3. Abbreviations: SAH; S-Adenosylhomocysteine, TCA; tricarboxylic acid cycle.

3.2.4 Comparison of DUB2 Interactomes Generated via XL-BioID using miniTurbo and Immunoprecipitation

Sequentially, we compared the interactome previously generated by Damianou *et al.* (2020) via immunoprecipitation (IP interactome) with our XL-BioID proximal interactome. As previously mentioned, there were 110 statistically significant enriched proteins in the DUB2 IP interactome compared to the RDK2 interactome, with RDK2 being used as the control. From these 110 interacting proteins of DUB2, we found the following seven proteins, to be also present in our proximal interactome (Fig. 9; Table 3): ubiquitin carboxyl-terminal hydrolase (DUB2; LmxM.08_29.2300), kinesin (LmxM.08_29.2390), 60S ribosomal protein L13a (RPL13a; LmxM.15.0200), 60S ribosomal protein L14 (RPL14; LmxM.22.1520), 60S ribosomal protein L7 (RPL7; LmxM.26.0170), 60S ribosomal protein L30 (RPL30; LmxM.34.0240) and 60S ribosomal protein L18a (RPL18a; LmxM.34.0600).

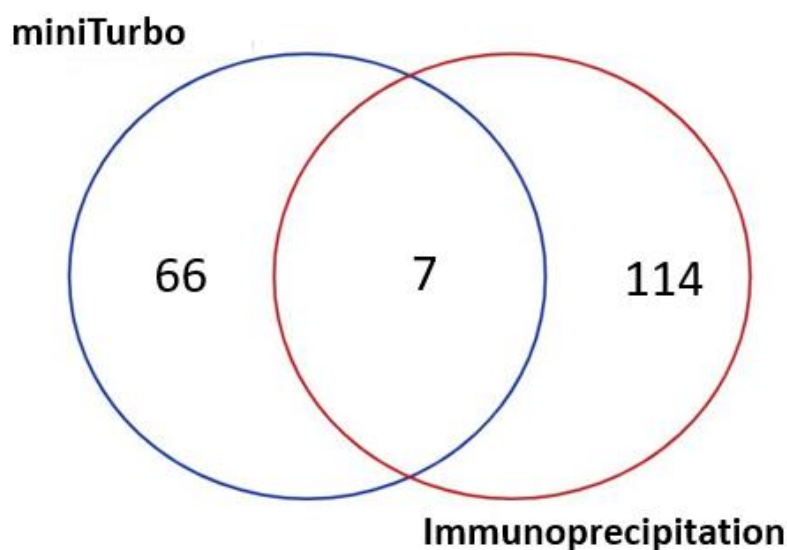


Figure 9: Investigation of the overlapping proteins between the two DUB2 interactomes derived from XL-BioID using miniTurbo and immunoprecipitation (Damianou *et al.*, 2020).

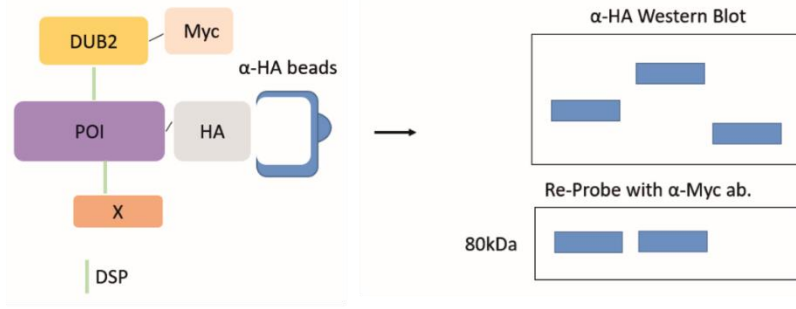
3.2.5 Investigation of DUB2-Interacting Proteins Relationship via Co-Immunoprecipitation

Next, we investigated whether DUB2 forms strong and stable interactions with some of the proximal interacting proteins. Overall, 15 proteins were selected from the proximal interactome of DUB2 and co-immunoprecipitation was conducted. Selection of this subset of proteins was performed based on at least one of the following criteria: fold enrichment value, ubiquitination state (based on ubiquitinomics datasets generated in Chapter 4) and whether the protein had been identified in the previously published DUB2 interactome (Table 3; Damianou *et al.*, 2020). Cyclin 12 (CYC12) and NGG1 interacting factor 3-like protein (NIF3) were included in this experiment, as two of the most highly enriched interacting partners of DUB2 identified in the Damianou *et al.* (2020) study.

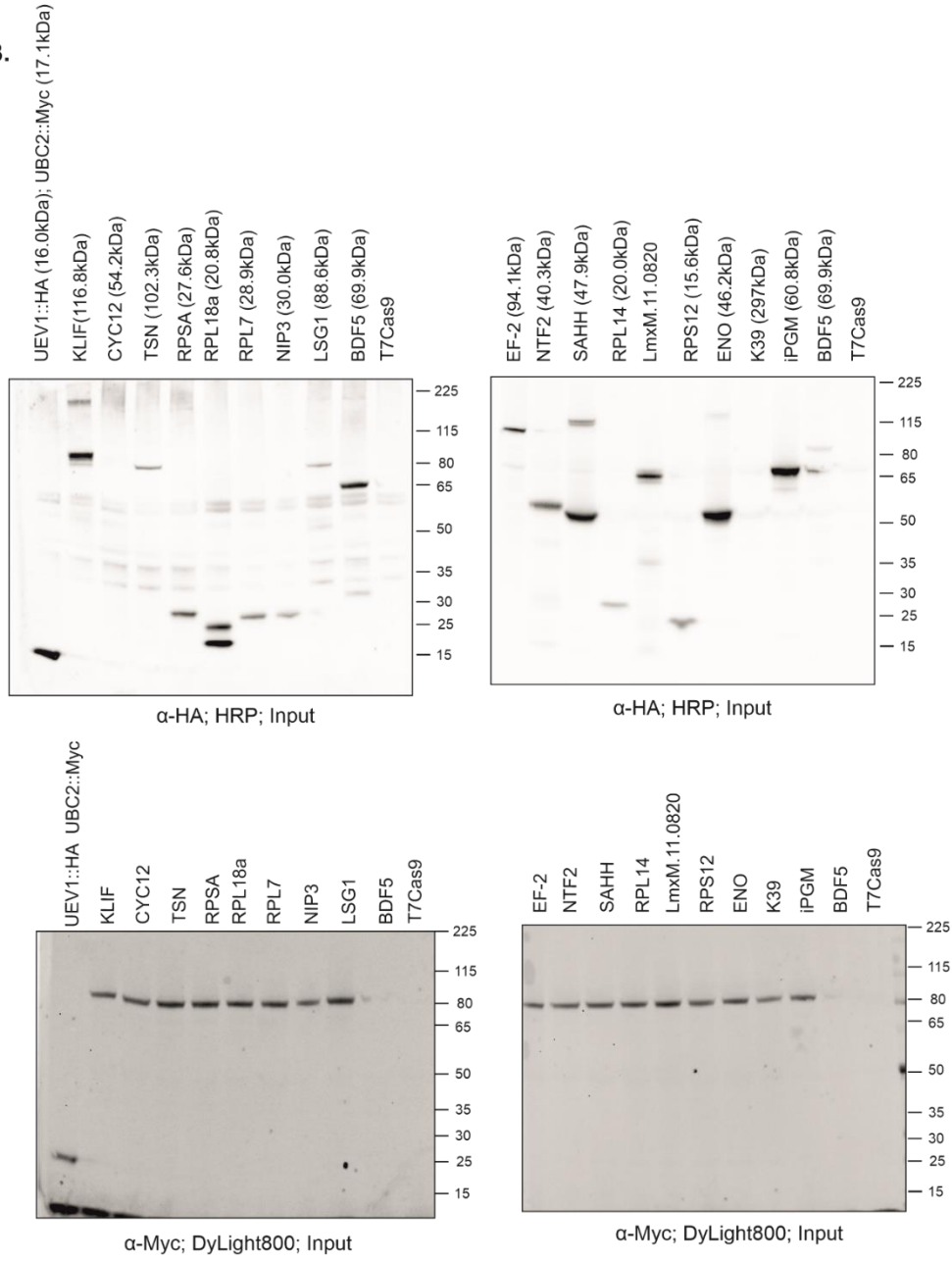
The principle behind co-immunoprecipitation is firstly to immunoprecipitate a protein of interest (POI) along with its interactive proteins using a specific antibody against that POI, and secondly to validate the presence of this protein complex in the enrichment solution via western blot. In our case, we aimed to immunoprecipitate the HA::POI, along with the DUB2::Myc protein, using α -HA antibodies

conjugated on magnetic beads and then test for the presence of HA::POI and DUB2::Myc proteins in the eluate, via western blot by using α -HA and α -Myc as primary antibodies respectively (summarized in Fig. 10A). To perform this experiment, we first generated cell lines expressing the POI and DUB2 with an HA tag and 3xMyc tag, respectively. This was achieved via the simultaneous endogenous tagging of the *POI* and *DUB2* gene, in T7Cas9 promastigote cells. Successful expression of both HA-tagged POI and DUB2::Myc was validated by western blot, prior immunoprecipitation (Fig. 10B). Sequentially, co-immunoprecipitation combined with an *in-vivo* cross-linking was performed for each cell line. Cross-linking was performed for two reasons: firstly, to enhance the stability of any possibly transient interactions and secondly, to imitate the cross-linking conditions used in the XL-BioID. All the POI were successfully immunoprecipitated, apart from K39, however none of the investigated proteins co-immunoprecipitated with DUB2 (Fig. 10C). As a positive control, we used the well characterised heterodimer complex of UBC2-UEV1, where the UBC2::Myc was successfully co-immunoprecipitated with the UEV1::HA (Burge *et al.*, 2021).

A.



B.



C.

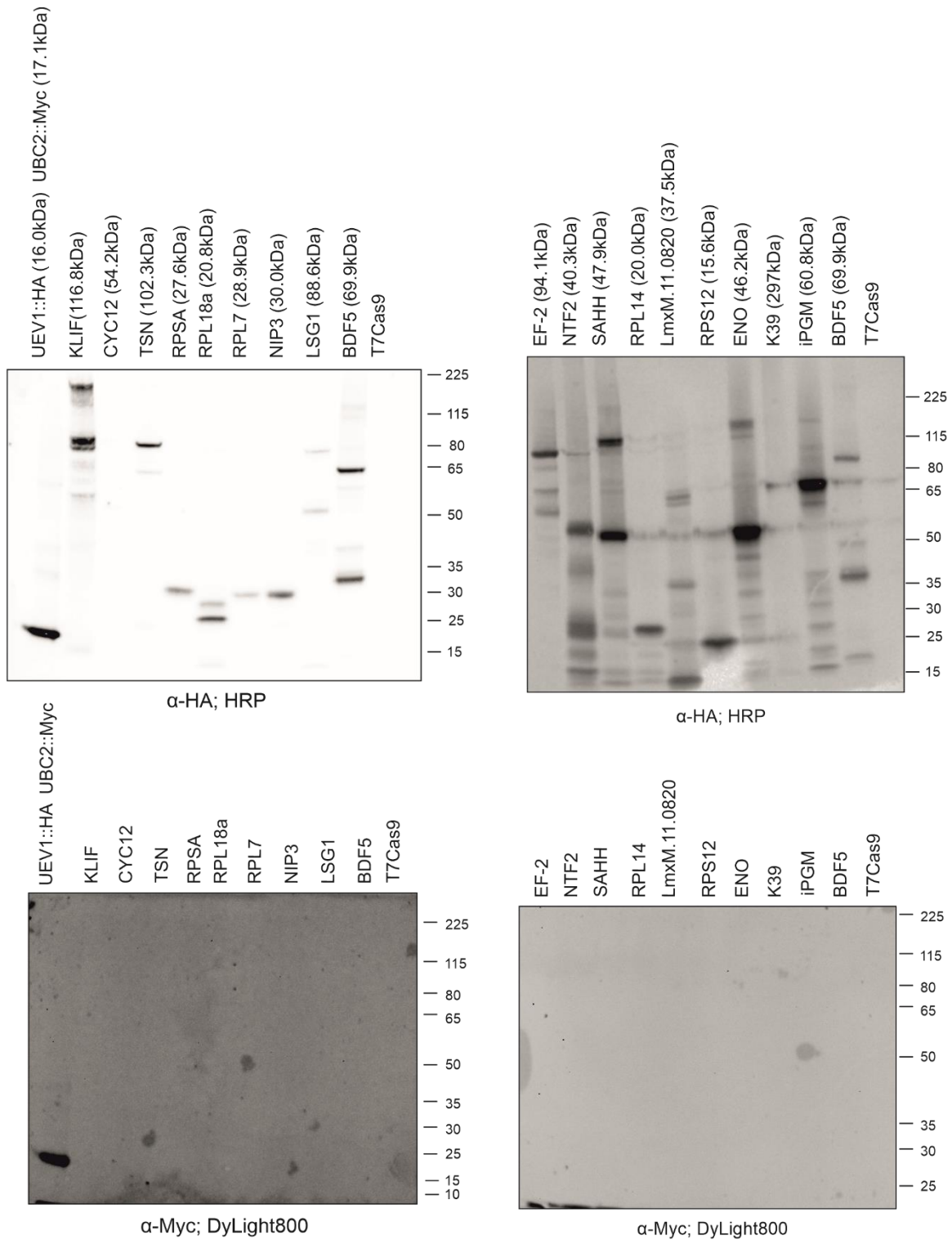


Figure 10: Use of co-IP to explore the interacting relationship between selected proteins and DUB2.
A. Experimental workflow of co-immunoprecipitation. Briefly, HA-tagged POI, upon in vivo crosslinking using DSP (DSP (dithiobis(succinimidyl propionate)) crosslinker), were immunoprecipitated via α-HA antibody coated magnetic beads along with its interacting partners. Eluates were run on a western blot, and the presence of the HA-tagged POI and the DUB2::Myc (~81.5 kDa) was investigated. α-HA primary antibody and α-Myc primary antibody was used respectively for each case. **B.** Immunoprecipitation was performed against 17 selected HA-tagged POI – 15 of them derived from the DUB2 miniTurbo interactome and 2 (CYC12 and NIP3) from the DUB2 immunoprecipitation-derived interactome. All 17 HA-tagged POI promastigote cell lines were also expressing DUB2::Myc.

The top western blots are probed with an α -HA antibody and they show the presence of the HA-tagged POI prior immunoprecipitation. These samples are known as input. The same membrane was re-probed with an α -Myc antibody to show the presence of DUB2::Myc (~81.5 kDa) in the cell lysate, prior immunoprecipitation (bottom western blots). UEV1 and UBC2, which are known interacting proteins in *L. mexicana*, were used as positive controls and the parental T7Cas9 as a negative control. HA::BDF5 expressing cell line was used as an additional α -HA control. The expected molecular weight for each POI is included in kDa next to the name of each POI (e.g. KLIF (116.8kDa)) C. α -HA immunoprecipitation was performed, eluates were run on SDS-PAGE gel and protein investigation was performed via western blotting. The top two western blots were probed with α -HA antibody to show the successful immunoprecipitation of the HA-tagged POI. The same membranes were then re-probed with α -Myc antibody to investigate whether DUB2::Myc was co-immunoprecipitated with the HA-tagged POI (bottom two western blots). The significance of each control that was included is described in B. Abbreviations: DSP; dithiobis(succinimidyl propionate)) crosslinker, DUB2; deubiquitinase 2, UEV1; ubiquitin-conjugating enzyme E2 variant 1 ,UBC2; ubiquitin-conjugating enzyme E2 2 , KLIF; kinesin localized to the ingressing furrow , CYC12; cyclin-12 , TSN; tudor staphylococcal nuclease, RPSA; 40S ribosomal protein SA , RPL18a; 60S ribosomal protein L18a, RPL7; 60S ribosomal protein L7, NIP3; NGG1 interacting factor 3-like protein , LSG1; 50S ribosome-binding, GTPase, BDF5; bromodomain factor 5 , EF-2; elongation factor 2 , NTF2; Nuclear transport factor 2 , SAHH; S-adenosylhomocysteine hydrolase , RPL14; 40S ribosomal protein L14 , RPS12; 40S ribosomal protein S12, ENO; enolase, K39; kinesin 39; iPGMA; 2,3-bisphosphoglycerate-independent phosphoglycerate mutase.

3.2.6 DUB2 Localization

Even if DUB2 had previously been characterised as nuclear protein, there were no nuclear proteins as proximal interacting partners of DUB2. Thus, we decided to re-investigate the protein localization of DUB2 via immunofluorescence. Firstly, we endogenously HA-tagged *DUB2* at its C-terminal (DUB2::HA) in the parental T7Cas9 cell line and *PAC* resistance cassette was used for drug selection. Secondly, to ensure that both *DUB2* alleles were tagged, we cloned out DUB2::HA cells and tested for homozygotes using diagnostic PCR (Fig. 11A). 75% of the clones were homozygous for the HA-tag and upon the PCR validation, we tested the homozygote Clone 11 (Cl11) for the expression of DUB2::HA, using α -HA western blotting. Indeed, a single protein was detected at ~81.5 kDa, confirming the successful expression of DUB2::HA (Fig. 11B). Finally, we investigated the localization of DUB2 by conducting α -HA-based immunofluorescence analysis using the DUB2::HA promastigotes. The results revealed consistent presence of DUB2 in both the cytoplasm and nucleus throughout the cell-cycle of the *Leishmania* promastigote. However, DUB2 was not detected associated with the kinetoplast or in the flagellum (Fig. 11C).

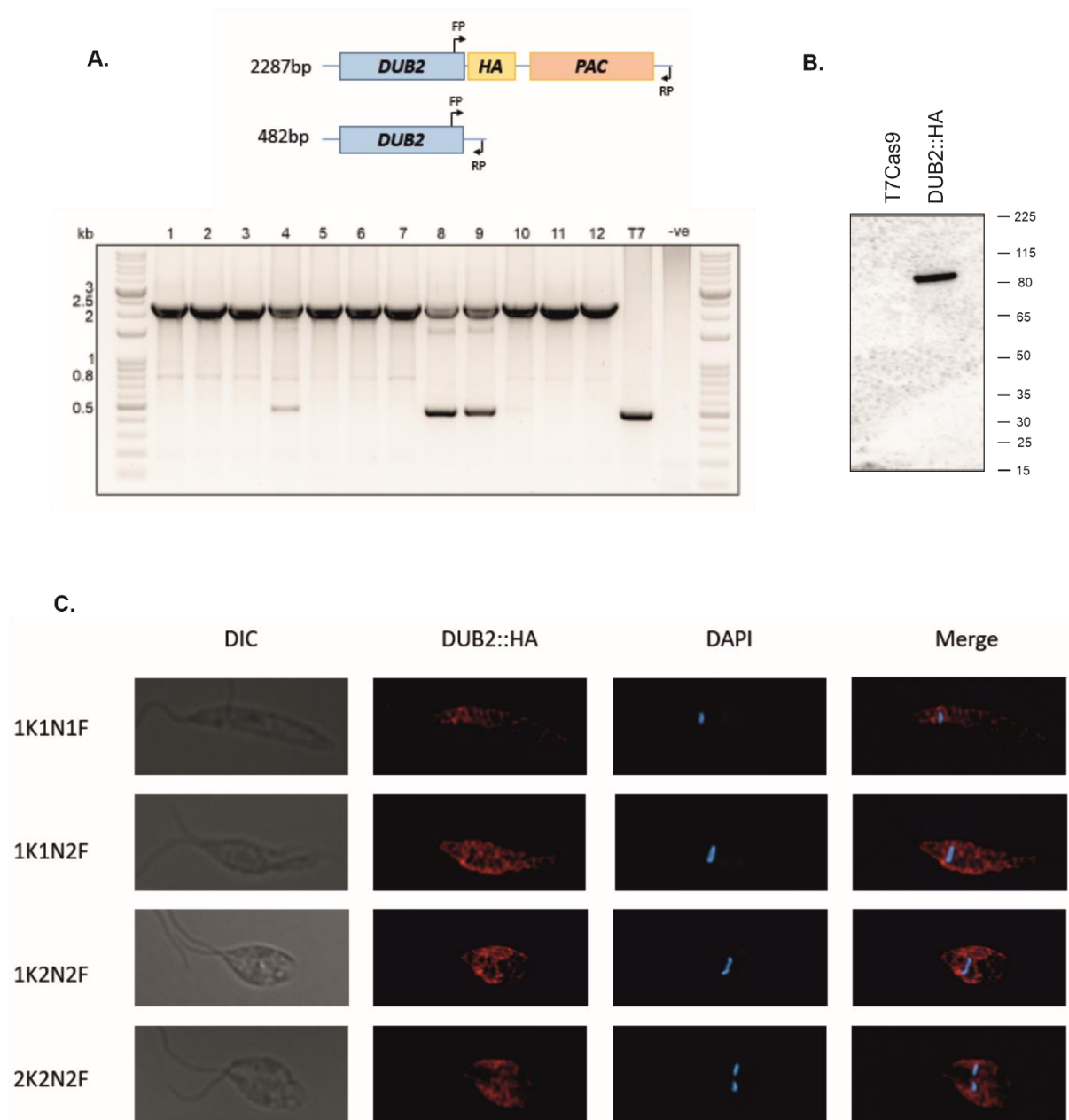


Figure 11: Localization of DUB2. **A.** Diagnostic PCR of cloned *DUB2::HA* promastigotes with a *PAC* resistance cassette. Homozygote mutants were selected based on not having the wild-type untagged version of *DUB2* gene (482bp). **B.** Detection of successful *DUB2*-HA protein expression was achieved through western blotting (1:5000; α -HA.11 mouse – I6B12; BioLegend). Only Clone 11 was tested for this experiment and the T7Cas9 promastigote cell line was used as a negative control. **C.** *DUB2::HA* is localised predominantly in the nucleus and cytoplasm of *L. mexicana* promastigote cells. This was investigated through immunofluorescence, in which cells were fixed with 4% w/v formaldehyde. α -HA.11 mouse – I6B12 (BioLegend) at 1:100 dilution and Goat α -Mouse IgG-Alexa Fluor® 647 (SouthernBiotech) at 1:500 dilution were used as primary and secondary antibodies respectively. DAPI was used for DNA staining. Images were deconvolved using Microvolution™, a plug-in for ImageJ and Fiji.

3.3 Discussion

Overall, the emerged role of proximity dependent biotinylation in the field of interactomics provides an insightful understanding of the function and localization of the protein, including transient and weak interactions, such as in the case of deubiquitinases and their substrates. In this study, we were able to investigate the proximal interactome of the *L. mexicana* DUB2 using the XL-BioID approach, with miniTurbo being the PDB enzyme of choice (Geoghegan *et al.*, 2022).

We have successfully generated an endogenously miniTurbo-tagged DUB2 promastigote cell line, with both of the *DUB2* alleles being tagged as a result of dual antibiotic selection (BSD and PUR). Despite the size of the miniTurbo enzyme (28 kDa), C-terminal tagging of DUB2 with miniTurbo did not interfere with the essential function of the DUB2 enzyme. Conversely, three attempts at double allele tagging DUB2 with miniTurbo at the N-terminus were unsuccessful, with promastigote cells being unable to recover. From the latter observation, it is suggested that there are either regulatory elements at the 5' end of the *DUB2* gene required for the successful expression of the gene or the expression of DUB2 enzyme fused with miniTurbo could affect its essential function and/or localization. Nevertheless, it supports previous conclusions that expression of DUB2 is essential for the survival of the *Leishmania* promastigotes (Damianou *et al.*, 2020).

The miniTurbo is known to be one of the best PDB enzymes in terms of labelling kinetics, allowing biotinylation to be performed both in less time and in the presence of less exogenous biotin. Despite miniTurbo's reputation for causing less background biotinylation (Branon *et al.*, 2018), there was still quite a significant amount of background biotinylation in both the miniTurbo-tagged DUB2 and CLK1 cell lines even when exogenous biotin was absent. Similar observations of miniTurbo-derived biotinylation in the absence of exogenous biotin were reported for the investigation of both the proximal interacting partners of KKT3 throughout the cell cycle of the *Leishmania* promastigotes and of its compartment-specific miniTurbo-tagged control BDF5 as well (Geoghegan *et al.*, 2022). This phenomenon was also observed in other studying systems, such as in the case of NCI-H295R adrenal cells, of which PDB using miniTurbo was performed to characterise the proximal interacting proteins of the protein kinase A catalytic subunit (Omar *et al.*, 2023). A possible reason to explain this miniTurbo-derived background biotinylation, at least for the case of *Leishmania*, is the presence of biotin in the growing medium of the biotin-auxotrophic promastigote cells. The small quantities of biotin combined with the high sensitivity and activity of the constantly expressed miniTurbo enzyme could lead to background labelling.

The impact of biotin concentration in the growing medium for the performance of PDB using TurboID was also addressed in a study conducted in *Saccharomyces pombe*. Interestingly, when the TurboID-tagged Rmt3 strain was cultivated in a biotin-free medium, there was a substantial decrease in Rmt3 biotinylation compared to the same strain grown in a biotin-supplemented medium (Larochelle *et al.*, 2019). Indeed, we demonstrated that to be the case in our experiment. Depletion of biotin from the growing media using the avidin-containing BioLock solution, resulted in reduction of background biotinylation. These results are consistent with a recent application of BioLock as a biotin scavenger to counteract the TurboID-dependent background biotinylation of the bait, ER-resident chaperon CNPY3. This uncontrollable biotinylation was inhibiting the essential function of CNPY3 in monocyte cells due to the presence of biotin in the growing media of the cells, making the PDB using the TurboID enzyme toxic for the cells (Garloff *et al.*, 2023). Nevertheless, we developed an optimized XL-BioID protocol, of which background biotinylation by the miniTurbo enzyme in the absence of exogenous biotin was successfully minimized.

Focusing on the proximal interacting proteins of DUB2, we identified 73 significantly enriched proteins, of which DUB2 was the protein with the highest fold-change enrichment over the control dataset. This validated that PDB using miniTurbo has worked successfully, and that our dataset and statistical analysis were reliable. The next two most enriched proteins were the kinesin K39 and the 50S ribosome-binding GTPase (LSG1). Kinesins are known ATP-dependent motor proteins that interact with microtubules, playing a pivotal role in a range of cellular processes. In kinetoplastids, they contribute to vital functions such as cellular growth and differentiation. K39 is a kinesin containing a tandem series of 39 amino acid repeat units and in *L. donovani*, it has a cell-cycle dependent localization with a predominant enrichment at the posterior pole of the cell. This suggested that K39 is involved with intracellular trafficking during cell-dependent morphological events (Gerald *et al.*, 2007). K39 is also known to interact with the microtubule-associated regulator coronin 12, which is involved in the microtubule remodelling during the *Leishmania* cytokinesis (Sahasrabudde *et al.*, 2009). Interestingly, the human kinesin orthologue KIF16B, which is involved in the transport of early endosomes to the plus end of microtubules, was found to be regulated via ubiquitination. However, the exact functionality of this PTM was not investigated further (Lohraseb *et al.*, 2022). Nevertheless, it is suggested that DUB2 might involve in the regulation of the cell-cycle dependent intracellular trafficking and cytokinesis of the *Leishmania* promastigotes.

On the other hand, the third highly enriched LSG1 protein is not well studied in kinetoplastids. Nonetheless, insights to its biological function were taken from its bacterial and eukaryotic orthologues. In the former case, the LSG1-bacterial orthologue EngA is involved in numerous biological processes, including ribosomal biogenesis and cell- cycle progression (Bharat & Brown, 2014). In the latter case, the *S. cerevisiae* LSG1 is involved solely in the ribosomal biogenesis and cytoplasmic maturation of the 60S ribosomal subunit (Kargas *et al.*, 2019). However, there are no evidence of any kind of interaction between LSG1 and components of ubiquitination machineries, such as DUBs. Despite the lack of such evidence, DUB2 might still regulate either directly or indirectly LSG1, suggesting the possible role of DUB2 in regulating ribosomal-associated processes. It is worth pointing out that there is a possibility of a ribosomal-associated protein, such as LSG1, to be biotinylated during the translation of the DUB2 fusion protein. However, this scenario is discounted due to the use of the CLK1 control, which is also translated in fusion with miniTurbo.

As well as the top enriched proteins, another proximal interacting protein of DUB2 worth mentioning is the Kinesin Localized to the Ingressing Furrow (KLIF). KLIF is an orphan kinesin that its name was given due to its localization pattern along the furrow ingression. The so-far characterised function of KLIF in *T. brucei* suggests that it is an essential kinetoplast-specific protein, which is involved in the completion of cytokinesis via facilitating the furrow to completely ingress. The reason we are focusing on this high confidence interactor is twofold: a) *T. brucei* DUB2 protein was present in the same proximal interactome of TOEFAZ1 where KLIF was discovered, increasing the chances that KLIF and DUB2 are somehow associated (Hilton *et al.*, 2018) and b) the KLIF protein was identified as one of the ubiquitinated proteins from my DiGly dataset. Therefore, this supports the first hypothesis that DUB2 regulates microtubule-associate events, such as cytokinesis, through the regulation of kinesin proteins, including KLIF and the already mentioned kinesin K39.

Furthermore, another hypothesis is that DUB2 might be involved in regulating the secretion pathway of *L. mexicana*, due to the presence of known secreting proteins in the proximal interactome of the DUB2. For instance, enolase and nuclease-diphosphate kinase b are two proximal interacting proteins of DUB2 that were previously verified as secreted proteins. The former is a glycolytic and gluconeogenic enzyme that is also involved in binding plasminogen/plasmin on the surface of the parasite to break down macrophage-derived fibrin and the latter in preventing the ATP-mediated

cytolysis of the macrophages (Kolli *et al.*, 2008; Gómez-Arreaza *et al.*, 2014). Furthermore, the signal-recognition-particle 68 (SRP68) protein was also identified as one of the proximal interacting proteins of DUB2. SRP68 is a known eukaryotic protein that targets newly synthesised proteins containing a secretion signal from the cytoplasm to the membrane of endoplasmic reticulum (Pool *et al.*, 2022). Thus, interaction of DUB2 with SRP68, enolase and nuclease-diphosphate kinase indicate that DUB2 might regulate protein secretion and intracellular trafficking of *L. mexicana* promastigotes.

Nevertheless, insights into the biological function of the proximal interacting proteins of DUB2 indicated that are involved in 17 different biological processes. Thus, it is suggested that DUB2 might have a pleiotropic function in the *Leishmania* promastigote cells. Interestingly, the vast majority of these interacting proteins participate in ribosomal-associated processes, suggesting that the predominant role of DUB2 is to regulate translation. This statements is additionally supported from the comparison of the DUB2 proximome with the DUB2 IP-derived interactome generated by Damianou *et al.* (2020). Surprisingly, six out of the seven overlapping proteins (DUB2 is excluded) are r-proteins, which are part of the large ribosomal subunit. For instance, the eukaryotic 60S ribosomal protein L14 (RPL14), which was identified as part of the secretome of *L. mexicana* promastigotes (Hamilton, 2019), is involved in the stable assembly of r-proteins that are located either in a close proximity with it or at the solvent-exposed part of the peptide exit tunnel. These properties of RPL14 contribute to the sufficient availability of 60S subunits within the cell and also to the effective maturation of pre-rRNAs to rRNAs (Espinár-Marchena *et al.*, 2018). Another example is the 60S ribosomal protein 7 (RPL7), which is an r-protein that assembles to the early nucleolar ribosome precursors containing 27S pre-rRNAs (Babiano *et al.*, 2013). Depletion of RPL7 led to the significant reduction of the levels of 60S subunits, 80S ribosomes, precursor rRNAs (e.g.12S rRNA) and mature rRNAs (e.g. 5.8S rRNA), supporting that RPL7 is important for ribosomal biogenesis and rRNA processing (Robledo *et al.*, 2008). Collectively, these possible interactions of these r-proteins with DUB2 indicate that DUB2 regulates translation through ribosomal biogenesis and rRNA maturation.

Previous studies have highlighted the direct regulation of ribosomal proteins and protein synthesis by DUBs. For instance, yeast Ubp3p deubiquitinase (human orthologue of USP10) regulates the proteasome-mediated degradation of aberrant nascent polypeptides during the ribosome-associated quality control (RQC) process, through the mono-ubiquitinated state of ribosomal protein S3 (RPS3; present in my hits too; Jung *et al.*, 2017). In addition, USP10 is involved in rescuing from proteasomal degradation the mono-ubiquitinated but still functional ribosomal subunits that are stalled in translation (Meyer *et al.* 2020). Interestingly, DUB2 and USP10 are both ubiquitin-specific-processing proteases (USP), however based on phylogenetic analysis performed by Damianou *et al.* (2020), the two DUB proteins are relatively distinct. Ubp3 and Otu2 were also identified as DUBs regulating translation through the association with the 40S ribosome. Specifically, Ubp3 maintains the monoubiquitination state of the r-protein eS7 for efficient translation, and upon translation termination, Otu2 associates with the 40S ribosome and deubiquitinates the monoubiquitinated eS7. This leads to the release of the translated mRNAs, allowing the formation of a new functional 80S ribosome and the re-imitation of a new round of translation (Takehara *et al.*, 2021). Thus, it is understood that DUBs can regulate ribosomal proteins through various approaches, ensuring the efficient translation of proteins within the cell. These examples support further our hypothesis that DUB2 is somehow involved in the regulation of translation.

At this point it is worth mentioning that variation between the IP and XL-BioID approaches can be attributed to three reasons: firstly, the two approaches are mainly used complementary and not interchangeably due to the small overlap they have (Baudouin *et al.*, 2020; McCoy *et al.*, 2023); secondly, different controls were used for each approach (RDK2 for IP and CLK1 for XL-BioID) that

might affected the statistically determined interactomes per case; and thirdly, the endogenous single-allele N-terminus tagging of *DUB2* might had somehow mis-localized the protein to the nucleus and the lysosome and therefore the co-immunoprecipitated hits observed by Damianou *et al.* (2020) might not be reliable. The latter argument is support by our previously mentioned unsuccessful attempts to endogenously N-terminally double allele tag the *DUB2* with *miniTurbo* expressing cassette. The promastigotes were never able to recover upon the N-terminus tagging. However, due to the lack of robust evidence justifying this hypothesis, both datasets were equally treated in this thesis.

Overall, some deubiquitinases are known to be part of a stable complex and their activity is regulated within that complex. For instance, the yeast DUBs Ubp8 and Rpn11 are components of the histone-modifying complex SAGA and the 26S proteasome respectively and association with their interacting partners (e.g. Sgf11 and Rpt1 respectively) induces their activation (Morgan *et al.*, 2016; Dambacher *et al.*, 2016). This is not the case for DUB2. Out of the 14 distinct interacting proteins identified with statistical enrichment in either one or both interactomics datasets (XL-BioID, IP), none co-immunoprecipitated DUB2 during their immunoprecipitation. This implies, firstly, that DUB2 operates independently within the cell without establishing stable complexes. Secondly, despite employing *in vivo* DSP cross-linkers during the affinity purification process (as described in methods), the interaction between these proteins and DUB2 may be transient or weak. This underscores the significant advantage of proximity labelling approaches in capturing these protein-protein interactions, compared to the less sensitive immunoprecipitation techniques. Finally, this observation gains additional support from the effective co-immunoprecipitation of UBC2 together with its bait, UEV1. UBC2 and UEV1 were used as control since they have previously been demonstrated to form a stable heterodimer complex *in vitro* (Burge *et al.*, 2020). In summary, the evidence supports the notion that DUB2 functions autonomously within the cell, and the examined interacting proteins are more likely to serve as substrates of DUB2 due to their transient and weak interaction with it.

However, it is crucial to acknowledge that this affinity purification experiment was executed only once, thus any conclusions inferred from it should be treated with caution. Furthermore, promastigote cells underwent the affinity purification process without prior incubation with BioLock. Consequently, the immediate interactome of DUB2 might display variations under biotin-depletion conditions in comparison to normal circumstances. In opposition, it is worth considering that the impact of BioLock on the overall proteome of promastigotes is likely to be minimal due to protocol optimization and the identification of established interacting proteins through the *miniTurbo* control, CLK1 (data not shown; Geoghegan *et al.*, 2022).

Moving towards the localization of DUB2, it was previously suggested that DUB2 is mainly localized in the nucleus of the *Leishmania* promastigotes. However, occasional lysosomal localization was also reported under the same study. To characterise the localization of DUB2, Damianou *et al.* (2020) used live cell imaging on promastigote cells expressing N-terminally-tagged mNeonGreen DUB2. However, these cells were not cloned out to ensure tagging in both DUB2 alleles. This, combined with our previous unsuccessful double-allele tagging attempts at the N-terminus of DUB2 suggests that the previously reported localization pattern might be wrong. In addition, based on the significantly enriched proteins in our proximal interactome of DUB2, there were no evidence of any nuclear-specific localized proteins except for certain proteins like ribosomal proteins that are situated in the nucleolus during pre-ribosomal assembly. Re-investigation of the cellular localization of DUB2 revealed that DUB2 is localized in the cytoplasm and partially in the nucleus throughout the cell-cycle of the promastigotes. However, DUB2 was absent from the flagellum and the kinetoplast. Taken together, this ubiquitous localization of the DUB2 protein within *Leishmania* promastigotes validates

the anticipated pleiotropic role of DUB2 and provides a rationale for the array of interacting hits identified in both XL-BioID and IP interactomics datasets.

To summarize, our efforts have successfully mitigated the background biotinylation stemming from the highly active PDB miniTurbo enzyme, resulting to the optimization of the XL-BioID protocol in *Leishmania* promastigotes. This accomplishment was made possible through the implementation of BioLock solution. Additionally, we have effectively generated stable miniTurbo-tagged DUB2 and CLK1 cell lines, where the fusion of proteins did not disrupt their essential function within *Leishmania* cells. Our investigation encompassed the characterisation of the proximal interactome of DUB2, a comparison with the pre-existing IP-based interactome established by Damianou *et al.* (2020), and an assessment of whether selected interacting proteins form stable complexes with DUB2. Our findings indicated that such stable complexes were not formed; nonetheless, further inquiry is warranted to ascertain if these proteins form weak or transient interactions. This might be achieved through the use of milder lysis buffer (such as NP40-based) when working with *in vivo* cross-linked promastigote cells. Furthermore, it could be valuable to replicate the affinity purification experiment under conditions of biotin depletion induced by BioLock. Lastly, a re-evaluation of DUB2 localization uncovered its prevalent presence throughout the promastigote cell, dispelling the prior notion of exclusive localization to the nucleus and lysosome, as previously reported.

4 Investigation of Total Ubiquitinomics and Proteomics Changes in *L. mexicana* Promastigotes in Response to DUB2 Depletion

4.1 Introduction

4.1.1 Identification of DUB Substrates

It is currently well-established that deubiquitinases (DUBs) are involved in a broad-range of biological processes, such as controlling protein quality and regulating gene expression. However, many of the insights into the function of a DUB is provided through the identification of its ubiquitinated substrates. The most conventional way of identifying substrates of DUBs is by observing changes in the total ubiquitinome of the cell in response to a type of modulation that affects the protein levels of the investigated DUB. For instance, ubiquitinated proteins that are deubiquitinated by a DUB will remain ubiquitinated upon knockout, or knockdown of that DUB. Thus, upon quantification, more ubiquitinated proteins will be detected in the knockout/knockdown DUB sample compared to the wild-type control (Elu *et al.*, 2022).

Despite the fact that the overall ideology on how to identify DUB substrates is consistent, there are variations on how to perform each step. For instance, in the case of investigating substrates for the ubiquitin-specific peptidase 14 (USP14), modulation of the protein levels of USP14 in HEK293T cells was achieved via the ectopic expression of USP14 WT or catalytic inactive (C114A) USP14 and identification of changes in the overall ubiquitinome was performed. Specifically, ubiquitinated proteins were firstly enriched via immunoprecipitation using K63, K48 and FK2 antibodies that recognise K63-linked, K48-linked and mono-/ poly- ubiquitinated proteins respectively and secondly sent for label free proteomics analysis (Chadchankar *et al.*, 2019). On the other hand peptide-centric approaches are more popular. They utilize immunoaffinity enrichment of ubiquitinated peptides (K-GG) using branch-specific di-glycine (DiGly) antibodies coupled with proteomics analysis. These branched-DiGly containing peptides are generated via the tryptic miscleavage of ubiquitinated lysine residues of the targeted protein combined with the concomitant cleavage of the C-terminally arginine of the conjugated ubiquitin (-VLRLRGG). Bingol *et al.* (2014) used such peptide-centric approach to identify substrates of USP30 in response to RNAi-induced USP30 knocked down in HEK293 cells.

Nevertheless, both of these examples contain an enrichment step of ubiquitinated moieties. This is attributed to the low stoichiometry of ubiquitinated proteins in physiological conditions, which makes them challenging to be detected by MS in the presence of abundant non-ubiquitinated peptides. Furthermore, certain types of ubiquitination targets proteins to the proteasome for degradation, which contributes to their quick turnover, making their detection even more difficult. The use of proteasome inhibitors, such as MG132, can prevent this phenomenon from taking place, leading to an up-to three-fold increase of ubiquitinated proteins within the sample (Wagner *et al.*, 2011). For the proteomics, most of the ubiquitinomics workflows use data-dependent acquisition (DDA) as a data collection mode in tandem mass spectrometry (MS/MS). However, the introduction of data-independent acquisition (DIA) mass-spectrometry combined with a neural network-based data processing improved further the depth and precision of *in-vivo* ubiquitinomics and therefore of DUB substrate identification. For instance, Steger *et al.* (2021) investigated changes in the total ubiquitinome of HCT116 cells upon inhibition of USP7 with the specific covalent inhibitor FT671 using DIA-MS. Strikingly, they were able to detect 8087 ubiquitinated proteins, of which 552 were upregulated upon 15 min of FT671-treatment.

4.1.2 DUB Substrates and Ubiquitinomics in Parasitology

In the field of parasitology, despite the identification of numerous DUBs in various organisms, there have been no studies investigating substrates of DUBs using ubiquitinomics (Kumar *et al.*, 2022). Instead, there are two proteomics analyses that provided insights into the molecular targets of the trypanosomal DUB orthologues USP7 and VDU, characterising them as essential mediators of surface protein turnover and endocytic activity. This was achieved via observing the alterations in the total proteomes of *Trypanosoma cruzi* and *T. brucei* in response to USP7 and VDU silencing (Zoltner *et al.*, 2015; Souza-Melo *et al.*, 2023). However, application of ubiquitinomics in the field of parasitology is not unprecedented. Overall, there are three ubiquitinomics-based studies in four different parasites - *Plasmodium berghei* (*P. berghei*), *L. mexicana*, *T. brucei* and *T. evansi* – of which *P. berghei* has the highest number of identified ubiquitinated sites (=2183), corresponding to 519 proteins (Rashpa *et al.*, 2023; Harris, 2022; Zhang *et al.*, 2020). Focusing on the only available ubiquitinomics study in the *Leishmania* parasite conducted by Harris (2022), he attempted to characterise the total ubiquitinome of the promastigote. At a 1% false discovery rate (FDR) he was able to identify 8 and 5 ubiquitination sites under MG132 and DMSO conditions respectively. However, the ubiquitinome of eukaryotic cells is expected to be the 5-10% of their total proteome, which is not the case for this study, addressing the need of developing an optimized ubiquitinomics workflow in *Leishmania*.

4.1.3 Aims

The aim of the research described in this chapter was to identify changes in the overall ubiquitinome and proteome of *L. mexicana* promastigotes upon inducible deletion of DUB2. These results, combined with the two available interactomes of DUB2, should reveal promising substrates of DUB2. Our approach is based on the study conducted by Liu *et al.* (2018), in which a comprehensive proteome, ubiquitinome and interactome analysis revealed substrates of USP14. In brief, we performed the following steps in the given order to achieve our goal:

- Developed an optimized peptide-centric ubiquitinomics workflow using *L. mexicana* promastigote cells via testing
 - a. Lysis buffers
 - b. Protein input
 - c. The usage of MG132 proteasome inhibitor
 - d. The use of different DDA-MS/MS database search engines, DIA-MS/MS and different mass-spectrometers
- Generate an inducible DUB2-HA^{FLOX/+} *Leishmania* promastigote cell line using a modified version of the recently developed inducible diCre/Cas9 system, to knock out DUB2 (Yagoubat *et al.*, 2020).
- Identify changes in the total ubiquitinome and proteome of *Leishmania* promastigotes in response to DUB2 knock out, using both total ubiquitinomics and total proteomics.

4.2 Results

4.2.1 Optimization Steps of the Ubiquitinomics Workflow in *L. mexicana* Promastigotes

4.2.1.1 Buffers and Loading Input

The first question that we tried to answer is which cell lysis buffer releases the highest number of ubiquitinated proteins into the buffer? We tested three different cell lysis buffers, including 5% sodium dodecyl sulphate (SDS) buffer, sodium deoxycholate (SDC) buffer and radioimmunoprecipitation assay (RIPA) buffer, in the presence or absence of protease inhibitors. Based on a western blot analysis using the anti-FK2 primary antibody, which detects mono- and poly-ubiquitinated proteins, we found out that SDS buffer without the peptidase inhibitors releases the highest number of ubiquitinated proteins compared to the other tested conditions (Fig. 12A). This was validated quantitatively by comparing band intensities between the lanes, which were normalized using the band intensity of the house-keeping enzyme oligopeptidase B (OPB; data not shown). Furthermore, almost no ubiquitinated proteins were observed when using the SDC buffer. To sum up, SDS buffer without protease inhibitors was found to be the best buffer for lysing promastigote cells.

The second optimization step we performed was to identify how many ubiquitinated proteins are in *L. mexicana* promastigotes compared to Henrietta Lacks (HeLa) cells. The reason we performed this experiment was because we are using the customized DiGly-conjugated magnetic beads (CST), which suggests using 1-2mg of input protein. However, these kits were developed using human cells, therefore we needed to find out the amount of input required from *L. mexicana* promastigotes. To test that, we compared, via a western blot analysis using the α -FK2 primary antibody, the band intensities of ubiquitinated proteins derived from SDS-lysed *L. mexicana* promastigotes and HeLa cells, treated or not with MG132 proteasome inhibitor (Fig. 12B). MG132 is used broadly in ubiquitination studies, to prevent the proteasomal degradation of the ubiquitinated proteins, which facilitates the accumulation and identification of transiently ubiquitinated proteins. Based on western blot analysis we found out that HeLa cells have ~ 3.5 times more ubiquitinated proteins than *L. mexicana*, in both MG132 and DMSO-treated conditions (n=1). Thus, it was concluded that for investigating the total ubiquitinome of *L. mexicana* promastigotes, ~ 7 mg of protein input should be used.

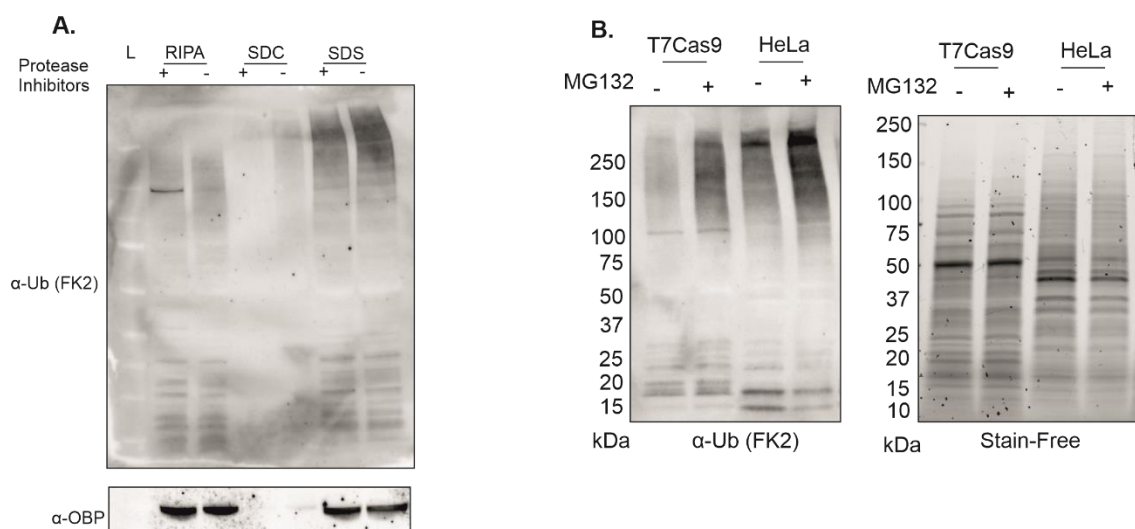


Figure 12: Optimization steps for the ubiquitinomics workflow in *L. mexicana* promastigotes. **A.** Western blot analysis of *L. mexicana* promastigote T7Cas9 extracts lysed with the indicated lysis buffer, in the presence (+) or absence (-) of protease inhibitors. The anti-Ubiquitin FK2 antibody was used in 1:5000 dilution. The same blot was re-probed with α -OBP antibody (1:20000) as a loading and normalization control. **B.** Western blot analysis of ubiquitinated proteins from cell extracts derived from T7Cas9 promastigotes and HeLa cells, treated or not with MG-132 proteasome inhibitor. 1:5000 α -Ub (FK2) antibody was used as a primary antibody. The total proteome identified by the stain-free gel, was used as loading and normalization control.

4.2.1.2 Mass-spectrometer, Acquisition Mode and MG132 Proteasome Inhibitor

Upon optimization of the ubiquitinomics workflow, we performed a preliminary experiment using a single DiGly-enriched sample of *L. mexicana* promastigotes, which was treated with MG132 (Fig. 13A). Briefly, we harvested and lysed 1.5×10^9 cells using 5% SDS buffer and we isolated and purified 7mg of promastigote proteins. We then performed an overnight protein digestion using trypsin/Lys-C and sequentially we confirmed by Coomassie staining that the proteins were digested successfully to peptides (Fig. 13B). We chose to use the Trypsin/Lys-C mix because it minimizes the trypsin-derived missed cleavages and improves several aspects of the mass spectrometry analysis of complex protein mixtures, including enhancing the identification of peptides and proteins (Savelien *et al.*, 2013). Following that, we enriched the DiGly-conjugated peptides using the anti-DiGly conjugated magnetic beads and then we sent them for label-free DDA-MS/MS, using the Orbitrap Fusion mass-spectrometer. At 1% False Discovery Rate (FDR), we identified 4384 unique peptides, of which 2209 contained the DiGly remnant (Fig. 13C). These 4384 peptides correspond to 1240 different proteins, of which the 881 are ubiquitinated. To confirm that the identified peptides are indeed ubiquitinated, we manually inspected the MS2 spectra and observed a shift of 114.0423 Da in the presence of the DiGly remnant (data not shown). Therefore, it is concluded that we have developed a robust workflow to investigate the total ubiquitinome of *L. mexicana* promastigotes.

Next, we were interested to test whether the newly acquired TimsTOF HT mass-spectrometer outperforms the Orbitrap Fusion in identifying DiGly-conjugated *Leishmania* peptides. At the same time, we were also interested in whether DIA mode improves protein coverage over DDA mode, as proved previously in human cells (Hansen *et al.*, 2021; Steger *et al.*, 2021). Thus, we ran an MG-132-treated and a DMSO-treated DiGly-enriched sample using either DDA or DIA workflows established on the TimsTOF HT. To avoid biological variation across samples, we loaded 50% per sample per acquisition mode.

Once we acquired the raw data for each condition, we needed to identify peptides possessing the characteristic DiGly-remnant. Therefore, we firstly analysed the DiGly-enriched raw-data acquired in DDA mode using three different database search engines: Mascot, PEAKS11 and FragPipe. FragPipe identified 7848 and 12917 ubiquitination sites in WT and MG132 treated samples, outperforming both Mascot and PEAKS11 that identified respectively from the WT sample 6714 and 7175 ubiquitination sites and from the MG132-treated sample 10880 and 8210 ubiquitination sites (Fig. 13D). Secondly, to process the DIA raw data, we used DIA-NN. Due to the lack of a spectral library for DiGly-modified peptides, we used DIA-NN in a library-free mode. Overall, DIA-NN classified as ubiquitinated peptides 5826 for the WT sample and 6740 for the MG132 control (Fig. 13D). At this point is worth mentioning that we set the FDR of all the analyses at 1%. Nevertheless, under the tested conditions, DDA and not DIA performed better at the identification of ubiquitinated peptides for both MG132-treated and WT samples, with FragPipe software giving the deepest coverage. Despite the data acquisition mode, the overall performance of TimsTOF HT mass-spectrometer for identifying ubiquitination sites in MG-132-

treated samples is around twenty times better than the previously used Orbitrap Fusion mass-spectrometer (Fig. 13E). Thus, we decided to proceed with DDA TimsTOF HT as mass-spectrometer and acquisition mode, and FragPipe as database search engine for identifying peptides with a DiGly-remnant from *L. mexicana* promastigotes. Even if the use of the proteasome inhibitor MG132 increased the number of ubiquitinated proteins, we decided to not use it for reasons explained in the discussion.

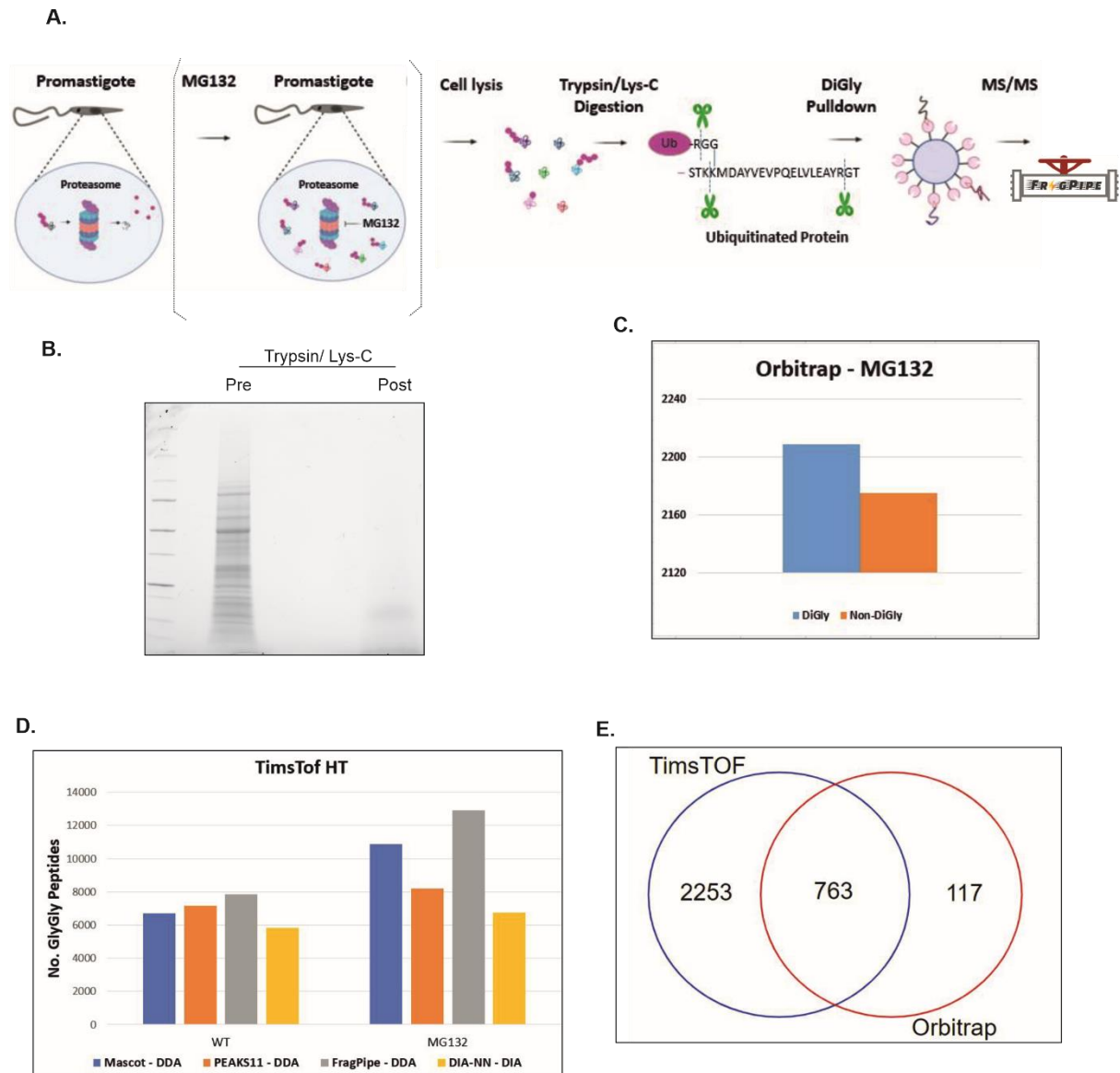


Figure 13: Continuation of the optimizations for the ubiquitinomics workflow. A. Schematic of the experimental ubiquitinomics workflow. Parenthesis around MG132-treated promastigote cells indicates that this step can be excluded if desired. **B.** Coomassie staining of gel containing *Leishmania* promastigote protein sample pre- (proteins) and post- (peptides) trypsin/ Lys-C digestion. **C.** Number of peptides with and without branched DiGly motif identified by the Orbitrap Fusion (n=1; 1% FDR). **D.** Number of DiGly peptides identified from a single MG132-treated sample and a single DMSO-treated (WT) sample, of which half of each was loaded for DDA- and DIA-MS/MS, using the TimsTOF HT mass-spectrometer. Raw data were searched with Mascot, PEAKS11 and FragPipe for DDA and with DIA-NN for DIA (1% FDR). **E.** Comparison of the two mass-spectrometers TimsTOF HT and Orbitrap Fusion in terms of coverage of *Leishmania* ubiquitinated proteins. Data of the MG132-treated samples

from A. and D. were compared. For the case of TimsTOF HT, data analysed by FragPipe – DDA were the best and therefore used for this analysis.

4.2.2 Generation of DUB2-HA^{FLOX+/+} *Leishmania* Promastigote Cell Line

The primary aim of the research described in this chapter was to identify changes in the total ubiquitinome and proteome of the *Leishmania* promastigotes in response to DUB2 deletion. However, *DUB2* is an essential gene required for the survivability of the *Leishmania* promastigote cells. Thus, the only available way to study the cellular function of such gene is through the use of an inducible diCre system. For the purposes of this study, we decided to generate inducible *DUB2* knockouts (iKO) using a modified approach inspired by the rapamycin-DiCre-based inducible CRISPR-Cas9 system developed by Yagoubat *et al.* (2019). Briefly, we decided to replace the endogenous *DUB2* gene with a LoxP-flanked *DUB2HA* C-terminally tag construct, which we generated via Gibson assembly (Fig. 14A). Furthermore, downstream of the 3' LoxP site is a puromycin resistance gene for selection. In both approaches, insertions were achieved using homologous recombination via the CRISPR-Cas9 system.

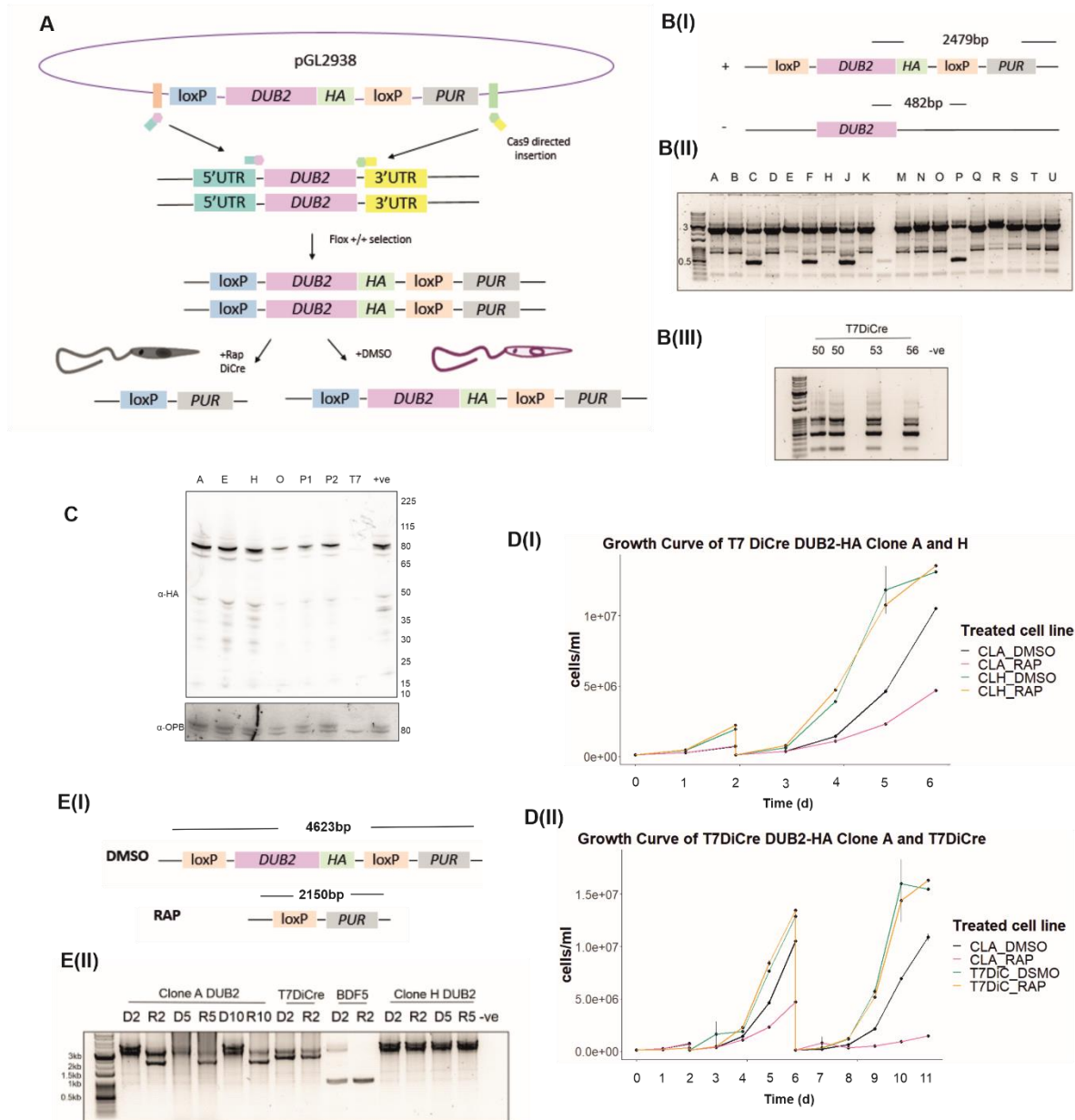
To ensure maximum depletion of DUB2 from the promastigotes, we first needed to select for homozygous mutants having both of their *DUB2* alleles replaced with the floxed versions. Thus, we performed cloning followed by PCR validations. Overall, 78% of the clones had both of their alleles successfully replaced (Fig. 14B (I-III)). We showed via western blotting that four of these homozygous mutants expressed HA-tagged DUB2 proteins (Fig.14C) and that allowed us to proceed to the follow up investigation of whether the DiCre system was active in the presence of rapamycin and how that affected the growth pattern of the promastigotes. By observing the growth-rate of two homozygous mutants treated either with DMSO or rapamycin for six days, we found out that clone A had a profound defect in its growth after four days of incubation with rapamycin (Fig. 14D (I)). In addition, there was a small delay in the growth rate of DMSO-treated clone A compared to the parental T7DiCre control (Fig. 14D (II)). Nevertheless, these results suggested that *DUB2* excision was successful. Indeed, we confirmed both at the genomic and protein level that the *DUB2* gene and DUB2 protein was successfully excised (>2 days; Fig. 14E (I-II)) and degraded (> 4 days; Fig. 14F) respectively. Based on these results, we concluded that we have generated a functional inducible DUB2-HA^{FLOX+/+} cell line, which responded efficiently to rapamycin.

Next, we investigated whether the use of the proteasome inhibitor MG132 prevents the degradation of DUB2 after four and five days of rapamycin incubation. At both time-points the DUB2 protein levels of rapamycin-treated samples were reduced compared to the DMSO-treated controls, regardless of whether they have been treated with the MG132 inhibitor (Fig. 14G). To be more specific, there is a 0.88 and 0.89 fold decrease of the DUB2 signal upon incubation with rapamycin for four and six days respectively, despite the presence of MG132. Thus, the use of MG132 at these given time points would not have interfered with the degradation process of DUB2.

Lastly, we were also interested to observe whether there are any profound changes in the total ubiquitinated protein profile of *Leishmania* promastigotes upon deletion of DUB2. To do that, we quantified and compared the intensities of ubiquitinomes observed on a western blot probed with the anti-ubiquitin FK2 antibody. A 96h rapamycin treatment of DUB2^{FLOX+/+} promastigotes increased the intensity of the ubiquitinome profile by ~1.5 fold-change (n=1; Fig. 14G). Data were normalized against the intensity of the house keeping protein oligopeptidase-B (OPB). Thus, it is expected in the downstream ubiquitinomics experiment to observe higher number of identified ubiquitinated

proteins in rapamycin-treated samples, where *DUB2* is knocked out. However, this preliminary conclusion has the caveat of being conducted once.

To summarize, we successfully created a homozygous *DUB2*^{FLOX/+} promastigote cell line that responds to rapamycin, with four days of incubation being the optimal time-point for the *DUB2*-KO ubiquitinomics.



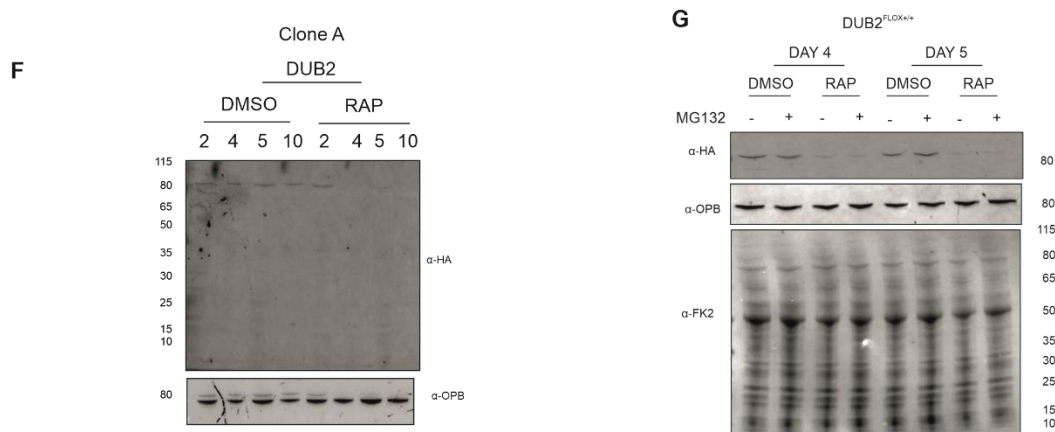


Figure 14: Generation of T7Cas9 DUB2-HA^{Flox+/+} *L. mexicana* promastigote cell line. A. Schematic of how the inducible DUB2 cell line was generated and how the rapamycin (RAP) - induced excision of DUB2 is achieved. **B.** Diagnostic PCR for identifying homozygote clones carrying the *LoxP-DUB2-HA-LoxP-PUR* cassette. **B (I)** Schematic of the PCR design and the expected DNA sizes with or without the DNA cassette. **B (II)** 17 clones were tested via this PCR and amplicons were run on a 1% Agarose gel. **B (III)** The parental T7DiCre cell line was used as control. **C.** Selected clones and cell populations were tested for expression of DUB2::HA via western blot. 1:5,000 of α-HA rabbit and 1:5,000 α-Rabbit (Promega) were used as primary and secondary antibodies. As a loading control, OPB was used. Membrane was stripped off and re-probed with the primary α-LmjOPB (sheep) antibody (1:20,000; Munday et al., 2011) and sequentially with the secondary antibody EasyBlot α-sheep IgG (HRP) antibody (1:5,000; GeneTex). **D.** Growth curve of inducible DiCre DUB2::HA promastigote cell line in response to DMSO and rapamycin (RAP). **D (I)** Triplicates of clone A (CLA) and clone H (CLH) were incubated for 6 days in either DMSO or RAP (300 nM), at a starting concentration of 1×10^5 cells mL^{-1} . At day 2, cells were re-seeded in fresh media at concentration of 1×10^5 cells mL^{-1} and 300 nM of RAP and DMSO were re-added. **D (II)**. At the same time the parental cell line was used as control (n=3). In this case, both clone A and parental cell line were grown for 11 days, and cells were re-seeded at day 2 and 6 as described in D (I). **E.** Investigation of whether DUB2 gene is excised in response to rapamycin using PCR. **E (I)** Schematic of the designed PCR, which also indicates the expected sizes of the DNA amplicons per treatment. **E (II)** PCR analysis and run of DNA amplicons on 1% agarose gel of samples derived from clone A, clone H, parental cell line T7DiCre and the positive BDF5^{FLOX+/-} control. DNA derived from promastigote cells at the indicated time points (e.g. D2 = DMSO-treated for 2 days). Only reagents were used as negative control (-ve). **F.** Time-course of DUB2 protein levels in the presence of RAP or DMSO, using western blot. For probing, the primary α-HA rabbit antibody (1:5,000) and secondary α-rabbit donkey Dylight650 (1:5,000) were used. OPB was used as loading control and it was detected using the α-LmjOPB antibody as a primary (1:20,000) and the α-sheep donkey Dylight488 (1:5,000) antibody as a secondary. **G.** To test whether MG132 proteasome inhibitor prevents degradation of DUB2 after 4 and 5 days of DMSO/RAP treatment, DUB2 protein levels were investigated via western blot. The probing conditions used for both DUB2::HA and the loading control OPB were identical with F. Changes in the total ubiquitinome were also investigated by re-probing the same membrane with the primary α-ubiquitin mouse antibody FK2 (1:5,000) and the secondary α-mouse HRP rat antibody (1:5,000; Promega).

4.2.3 Identification of Changes in the Total Ubiquitinome of *Leishmania* Promastigotes upon Inducible Deletion of DUB2

So far, we have developed an optimized label-free quantitative mass-spectrometry workflow for investigating ubiquitinated proteins in *L. mexicana* promastigotes and we have generated an inducible DUB2^{FLOX/+} cell line, with four days of rapamycin incubation being the optimal incubation period for depleting DUB2 protein levels. Combining the two, we are going to investigate changes in the total ubiquitinome and proteome of *Leishmania* promastigotes in the presence and absence of DUB2.

Overall, we treated *Leishmania* promastigotes either with DMSO or rapamycin for 96h. For each condition, we used three independent biological replicates, of which cells were grown up in a cell density of 5×10^6 cells mL⁻¹. We then harvested 1.5×10^9 cells per replicate and lysed them in 5% SDS buffer. Upon alkylation and reduction of proteins, we desalted the proteins using Strap columns. Sequentially, we performed trypsinisation and isolated 100 µg of peptides per sample for investigating alterations in the total proteome in response to inducible deletion of DUB2. The rest of the peptides underwent DiGly-enrichment and were sent for DDA-MS/MS using timsTOF HT in order to identify and quantify ubiquitinated peptides in each sample (Fig. 15A). For performing statistical tests, we used the Rstudio package DEP, which stands for Differential Enrichment analysis of Proteomics data.

Across all six DiGly-enriched samples, we identified 12026 distinct peptides, of which 7771 were ubiquitinated (Fig. 15B). These ubiquitinated peptides consist the ~68% of the overall identified peptides, indicating efficient enrichment of peptides carrying the DiGly remnant. However, not all DiGly peptides were present in all six replicates, with 1438 of them being detected in a single replicate (Fig. 15C). Inclusion of peptides with too many missing values will affect adversely both the downstream imputation methodology and statistical analysis. Therefore, we selected peptides that were detected in at least two out of three replicates in at least one of the two treated conditions (Hansen *et al.*, 2021). By doing that, we ended up with 5918 DiGly peptides in total, with the exact remained numbers per sample spanning from 4454 (D_1) to 5304 (R_1; Fig. 15D). Overlapping analysis of these 5918 DiGly peptides indicated that most of them (=3352) were present in all six samples, with the smallest number (=393) being quantifiable in two samples of a single condition (Fig. 15E). Sequentially, we applied variance stabilizing transformation to correct the background and normalize the data and we found that it had no effect in the data distribution across the samples (Fig. 15F). Moreover, there is no variance-mean dependence across the data and this was depicted as horizontal red line, of which red line represents the running median estimator (Fig. 15G).

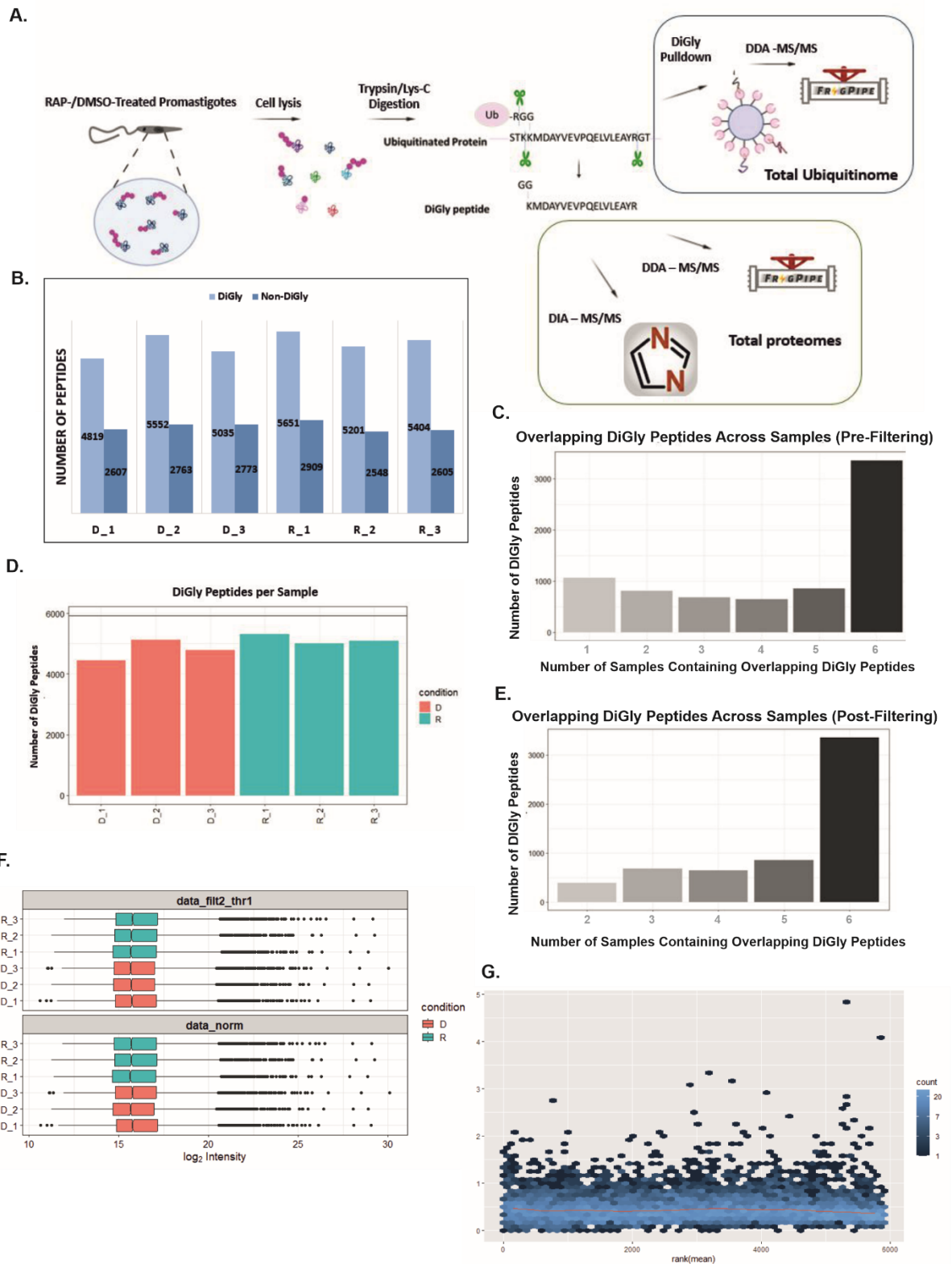


Figure 15: Insights into the ubiquitinomics data in response to the DUB2 KO. **A.** Schematic of the ubiquitinomics and proteomics workflow, using the inducible deletion DUB2^{Flox+/+} promastigote cell line. Biological triplicates were used per DMSO and rapamycin (RAP) treatment. **B.** Number of identified DiGly and non-DiGly peptides per sample. R= rapamycin; D= DMSO. **C.** Number of DiGly

peptides being present in one or more samples. For instance, if a DiGly peptide is present in only one of the six samples, then it will be allocated in number of samples containing overlapping DiGly peptides 1, but if a DiGly peptide is present in all six samples, then it will be allocated in number of sample containing overlapping DiGly peptides 6. No filtering was applied in this dataset. **D.** Number of DiGly peptides remained per sample after applying the following threshold: peptides that were detected in at least two out of three replicates in at least one of the two treated conditions were kept for downstream analysis. **E.** Same as C., however of DiGly peptides meeting the condition mentioned in D. **F.** Comparison of distribution between normalized and not normalized data, which were labelled as `data_norm` and as `data_filt2_thr1` respectively. **G.** Rank of the means of the abundance of the ubiquitinated peptides plotted against standard deviations. Each point represents several ubiquitinated peptides with similar SD and mean. The red line depicts the running median estimator.

Despite the “cleaning” of the data, there were lots of missing values (Fig. 16A). Thus, imputation was needed. At this point is worth introducing the categorisation of missing values, with the two main classes be: missing at random (MAR) and missing not at random (MNAR). In brief, MAR missing values are when peptides are detected in some but not all samples across different conditions. This could be due to technical limitations such as in the case of the semi-stochastic selection of peptides under DDA-MS/MS. As about MNAR, they are the missing values being solely present in samples of a specific condition. This might be due to biological significance. MNAR and MAR missing values are imputed differently, thus we first categorise the type of missing values being present in our ubiquitinomics dataset. Based on the heatmap of Fig. 16A, some missing values are only present in rapamycin-treated samples making them possible MNAR missing values. However, some others are observed randomly across both treatments, categorising them as possible “MAR” missing values.

Despite the first observations from the heatmap, further analyses are required to understand better the nature of these missing values. Firstly, we checked the densities and the cumulative fractions of the peptides with and without missing values. Missing values are primarily from peptides with lower intensity, suggesting that these missing values should be treated as MNAR and a left-censored-imputation method should be applied (Fig. 16B&C). Nevertheless, DEP package allows you to test different imputation approaches at the same time, including MAR-centric, MNAR-centric or even combined (Fig. 16D). The imputation method of missing values that outperformed the rest by scoring the highest number of limma-derived significant hits was the one using random minimal draws derived from the left end of Gaussian distribution (labelled as manual imputation; Fig. 16E). This approach is known for favouring MNAR datasets, which agrees with the previous conclusions for the nature of the missing values, and therefore it was selected as the imputation method for this dataset.

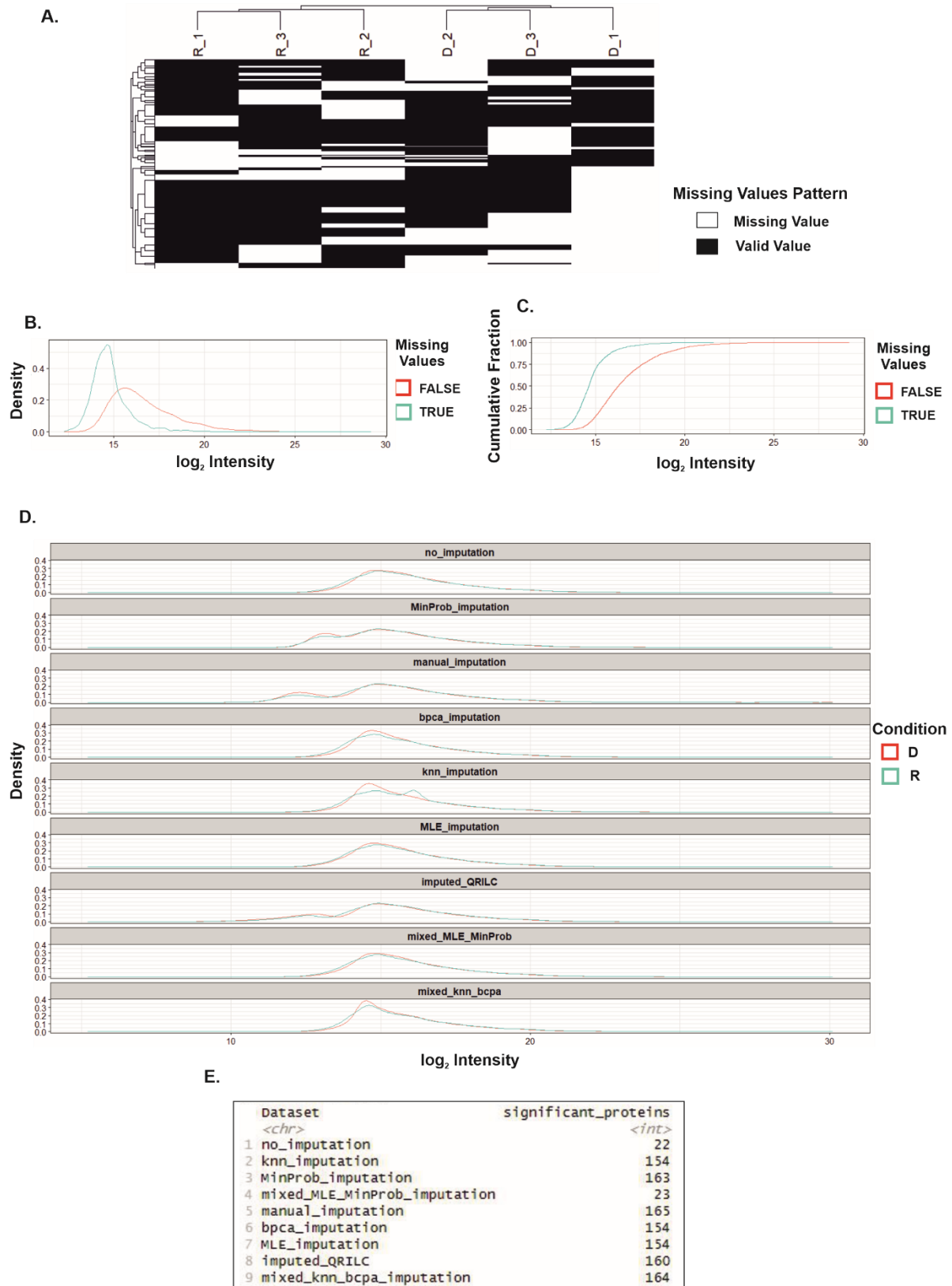


Figure 16: Exploration and imputation of missing values. **A.** Heatmap of missing values per sample. Each line represents an ubiquitinated peptide, which is missing in at least one of the six samples. White box indicates missing value (no quantifiable value) and black box indicates quantified value. **B.**

Intensity distributions (=density) of proteins with and without missing values. Y-axis indicates the “density of probability”, meaning the chance of obtaining X-axis-related values. **C.** Cumulative fraction of proteins with and without missing values. Y-axis indicates the probability of a random variable having values less than or equal to x. For the following 3 plots different imputation methods were tested concomitantly. **D.** Distribution of intensities, before and after imputation. **E.** Significantly differentiated ubiquitinated peptides (limma; $p < 0.05$) between the two treatments, rapamycin and DMSO, upon replacing missing values using the given imputation approach.

First insights into the quality of our data were revealed via principal component analysis (PCA). PCA of the top 500 variable ubiquitination sites revealed that DMSO- and RAP-treated samples are well-separated in two different clusters (Fig. 17A). Noticeably, DMSO sample 1 (D1) is not tightly clustered with the rest of the replicates, suggesting that the sample is relatively variable. However, based on Pearson correlation coefficient (PCC) analysis, all three DMSO-treated samples, including D1, have a strong and positive correlation (Fig. 17B). Therefore, we decided to keep the D1 sample to maintain statistical power for the downstream analysis. Overall, combining PCA and PCC results, we concluded that the variance across the samples is driven primarily by the difference in DUB2 protein levels.

To identify significant changes in the total ubiquitinome in response to deletion of DUB2, we used limma analysis, which combines protein-wise linear models and empirical Bayes statistics. Collectively, we identified 165 ubiquitination sites to be significantly different, of which 122 ubiquitination sites corresponded to 113 proteins that were upregulated in the absence of DUB2 ($p < 0.05$, Fig. 17C). Due to the application of a statistical significance threshold at a p-value less than 0.05, we decided to exclude a fold change threshold in all statistical analysis in this chapter (Elu *et al.*, 2022). Nevertheless, all these significant ubiquitinated peptides were solely enriched in replicates per condition, supporting the robustness of our conclusions (Fig. 17D).

From these significant proteins, we are interested in the 113 ubiquitinated proteins that are significantly upregulated in the absence of DUB2. The reasoning behind this is that if an ubiquitinated protein is a substrate of DUB2, then in the absence of DUB2 this substrate will remain ubiquitinated. These changes are translated in our experiment as upregulation of ubiquitination sites in rapamycin-treated samples, compared to the DMSO-treated controls. Therefore, for the needs of this study to identify substrates of DUB2 we focused only on these significant ubiquitinated peptides. We listed all the significantly upregulated ubiquitinated proteins in Table 4 and we highlighted known proteins that are ubiquitinated (e.g. root hair defective 3; RDH3) and/or are part of the ubiquitin-proteasome pathway (e.g. proteasomal BETA6 protein). Nevertheless, the top three upregulated ubiquitinated proteins are: the serine-threonine kinase receptor-associated protein (STRAP; LmxM.27.1250; $\text{Log}_2\text{FC} = -5.23$), a hypothetical protein with a coiled coil domain based on HMMER analysis (LmxM.34.3240; $\text{Log}_2\text{FC} = -4.68$) and the amino acid transporter (AA19; LmxM.07.1160; $\text{Log}_2\text{FC} = -4.55$).

To get insights into the biological processes, the cellular compartment, and the molecular function of the significantly upregulated ubiquitinated proteins, we performed gene ontology enrichment analysis using TritypDB ($p < 0.05$; Fig. 17E-G). Through this analysis, we revealed that these proteins are involved in diverse biological processes, with most of them being involved in cellular localization and transporting (GO: 0051179 & GO: 0006810; proteins=17), but also in cell projection organisation (GO: 0030030; proteins=4; Fig. 17E). Furthermore, cellular compartment analysis revealed that most of the hits are localized at the posterior of the cell, such as in the cell projection (GO: 0042995, proteins=26), with a particular contribution to the cytoskeleton of the cell (GO: 0005856; protein=14; Fig. 17F). Finally, in regards to the molecular function of the hits, the analysis suggested that

transporter activity (GO: 0005215) and nucleoside-triphosphatase activity (GO: 0017111) are the top two, with seven and six proteins being involved in each function respectively (Fig. 17G).

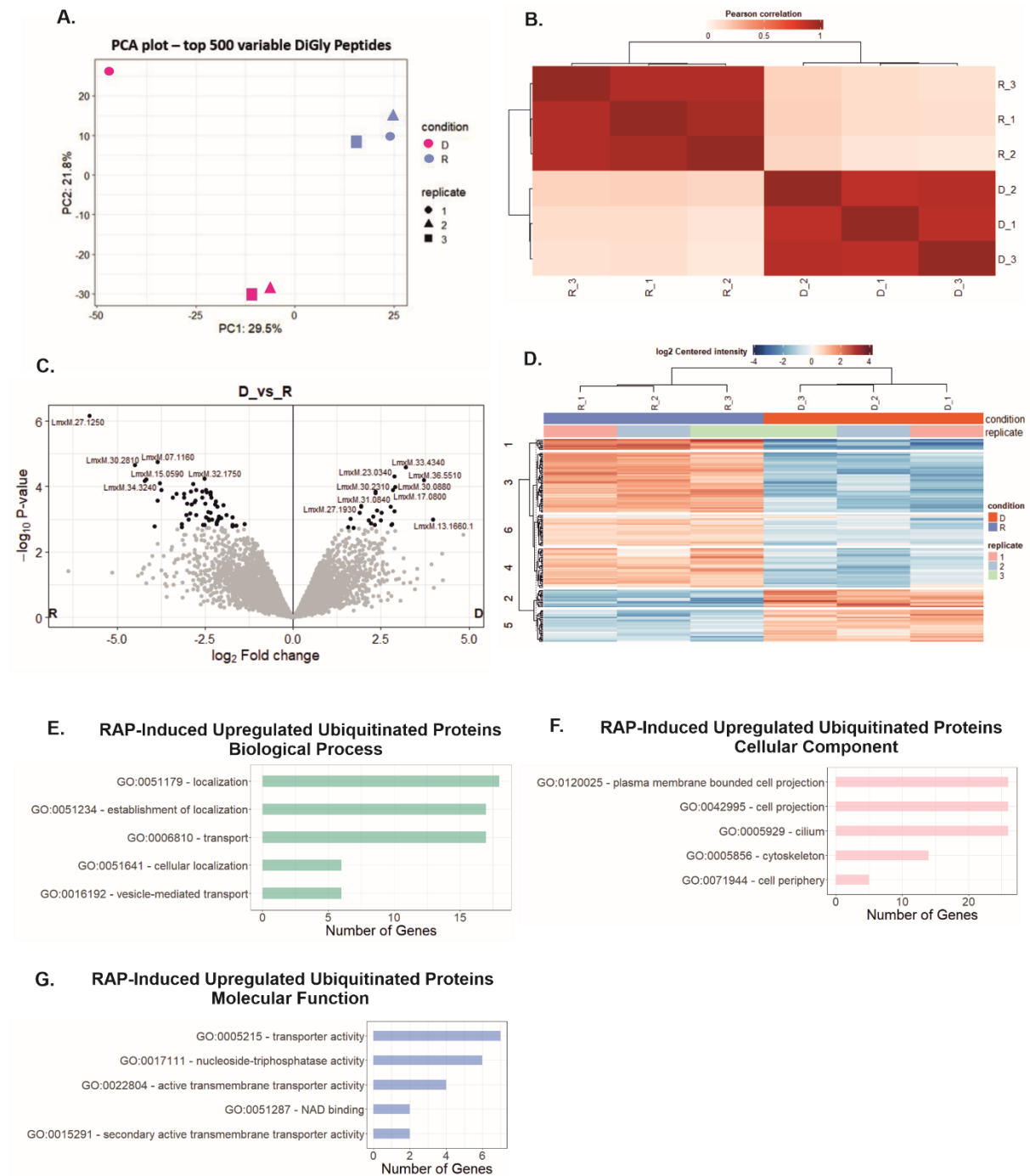


Figure 17: Exploration of the significantly different ubiquitinated peptides between DUB2-depleted and wild-type samples. A. PCA plot of the top 500 variable DiGly peptides. Each symbol represents a different replicate per condition, of which condition is coloured with red for DMSO (D) and blue for RAP (R). **B.** PCC matrix, of which dark red indicates very strong and positive correlation (PCC=1) and light red means no correlation (PCC=0). **C.** Volcano plot depicting the significantly different ubiquitinated peptides in black, while in grey are the non-significant hits. On the right site are the ones upregulated in the DMSO samples, while on the left site are the ones upregulated in the RAP samples. **D.** Heatmap of all significant ubiquitinated peptides (rows) per sample (column). Red

indicates significant ubiquitinated peptide upregulation while blue significant downregulation. Gene Ontology analyses of significantly upregulated ubiquitinated proteins in response to RAP-induced DUB2 depletion. The top 10 GO terms, with the highest number of proteins are presented in **E.** for biological processes, **F.** for cellular component and **G.** for molecular function.

Table 4: Significantly upregulated ubiquitinated peptides in DUB2 depleted samples. For each significantly upregulated ubiquitinated peptide derived from the DUB2 depleted samples, the following information were listed: Gene ID, product description, which was taken from TriTrypDB, the amino acid sequence of the ubiquitinated (DiGly) peptide, the Log₂Fold Change (Log₂FC) between DMSO-treated and rapamycin-treated samples and whether the particular protein or its homologues in other organisms was previously reported as ubiquitinated. In the DiGly peptide column, the lysine residues, where ubiquitination occurs with a mass shift of 114.0423 Da, were represented as “K”. Other PTMs were also included: oxidation of methionine = M [15.9949]; phosphorylated serine = S [79.9663]; phosphorylated threonine = T [79.9663] and alkylated thiol groups of protein cysteines = C [45.9877].

Gene ID	Product Description	DiGly Peptide	Log ₂ FC	Ub. In Literature
LmxM.27.1250	serine-threonine kinase receptor-associated protein, putative	VAPAAPAADNGVADITKVK	-5.23	
LmxM.34.3240	hypothetical protein, conserved	SVAIADVQAQLSQKK	-4.68	
LmxM.30.2810	KH domain/Domain of unknown function (DUF1771)/Smr domain containing protein, putative	VPGLSEGVLSKPEDGDKAPTCLK	-4.55	
LmxM.07.1160	amino acid transporter 19, putative	QDDNPELTKKPHAGAEDTNTGEAL DEEDAEEVPRK	-4.50	
LmxM.15.0590	hypothetical protein, conserved	HEAYVNPENPELYSTLYKK	-4.09	
LmxM.34.3890	calmodulin-like protein	AAGLNPSEKIK	-3.85	
LmxM.08_29.1640	ABC transporter domain protein, putative	LESYTKYLAAK	-3.78	
LmxM.31.0370	root hair defective 3 GTP-binding protein (RHD3), putative	VQELKTFR	-3.76	Sun <i>et al.</i> , 2020
LmxM.13.1530	phospholipid-transporting ATPase 1-like protein	ILPGKLSK	-3.67	
LmxM.09.1490	cytochrome b5-like protein, putative	YYIGDVHPDDADKVK	-3.47	
LmxM.32.1110	hypothetical protein, conserved	SSADPATAPVAEVTQLPHAKK	-3.41	
LmxM.33.2420	glycosyltransferase-like protein	NPDGTFKSPGSGVAPWHETYR	-3.26	
LmxM.36.5010	40S ribosomal protein SA, putative	GIKS[79.9663]IGMM[15.9949]YW LLAR	-3.18	Blazejewski <i>et al.</i> , 2022
LmxM.26.2120	hypothetical protein, conserved	EPPSPPPLPTAAHKR	-3.18	
LmxM.19.1010	WD domain, G-beta repeat, putative	SAAASKISDPSQITAPDGAGTK	-3.17	
LmxM.34.4180	bardet-biedl syndrome 1 protein	KLESLLDSGVQTSSR	-3.16	
LmxM.08_29.0500	Ca ²⁺ -ATPase N terminal autoinhibitory domain containing protein, putative	SLSQLKALSSIAR	-3.15	
LmxM.08.0070	Putative zinc finger motif, C2HC5-type/ASCH domain containing protein, putative	DGAVTEAGAEEDEPHDADESVVPT GAEPLPSLLQKIWYSPDGTR	-3.11	
LmxM.31.2030	Ras-related protein RAB2B, putative	LISIQGKSVK	-3.08	Zhang <i>et al.</i> , 2021
LmxM.27.1750	dynein heavy chain, putative	GDSM[15.9949]WQNSHSSLKLEP ALAK	-2.94	Lee <i>et al.</i> , 2008

LmxM.30.1180	hypothetical protein, unknown function	GKSYLIPK	-2.93	
LmxM.26.2120	hypothetical protein, conserved	YGKGLDPAAVAANR	-2.92	
LmxM.25.0080	poly(A)-binding protein, putative	LDTAVNAKELQAAFTK	-2.90	Li <i>et al.</i> , 2021
LmxM.08_29.0620	ABC transporter, putative	AISDDDELHSASFANGS[79.9663]LKM[15.9949]NGK	-2.89	
LmxM.25.0280	hypothetical protein, conserved	M[15.9949]EVVQVSQEKEQLR	-2.89	
LmxM.16.0970	hypothetical protein, conserved	DAVAELQHLPKPPPPLEPAAQR	-2.86	
LmxM.23.0547	hypothetical protein, conserved	DKVVAGSAASAALR	-2.85	
LmxM.08_29.1160	tryparedoxin 1, putative	LQKQNE[M[15.9949]VDM[15.9949]SSLSGK	-2.82	
LmxM.13.1620	squalene monooxygenase-like protein	ILVDYNKPTLPSLEKQSEWLIQDVAPR	-2.80	Foresti <i>et al.</i> , 2013
LmxM.23.1020	hypothetical protein, unknown function	DVEETDDAAKDVEAADDAAKDVEAADGEAK	-2.80	
LmxM.25.1430	Putative intraflagellar transport protein A1	EDAM[15.9949]LEEQETKLIK	-2.78	
LmxM.27.0970	ABC transporter, putative	LLAAVDLEDKAHYM[15.9949]SK	-2.76	
LmxM.36.6650	2,3-bisphosphoglycerate-independent phosphoglycerate mutase	IDDEHETFKEVPSDR	-2.74	
LmxM.10.0400	pteridine transporter ft5, putative	DLKQDATAATPQQKPATNVGLQS[79.9663]PVDEK	-2.73	
LmxM.29.2740	TPR domain protein, conserved	AKATGLSAGGGM[15.9949]GGFPEMGGMPDMGQFANMMS[79.9663]NPQFM[15.9949]ETAQR	-2.73	
LmxM.29.0490	hypothetical protein, conserved	TEDIIVWKR	-2.70	
LmxM.34.2110	hypothetical protein, conserved	AAATAQEALAEAQKYR	-2.69	
LmxM.32.0400	serine peptidase, putative	EALLSGKPLTDAAKASGDSFNR	-2.68	
LmxM.33.1050	TPR repeat/SET domain containing protein, putative	DIEASKQESSDAANSPATM[15.9949]AK	-2.67	
LmxM.33.3760	actin-like protein, putative	VLPYQGGTGGGTSAAAGKGSPTAVKEAPVR	-2.65	
LmxM.08_29.0650	phosphate transporter, putative	DLSFFKSR	-2.63	
LmxM.08_29.1490	asparagine synthase, putative	LVNAAATTTPELSPKK	-2.62	
LmxM.29.0380	phosphatase 2C, putative	GGKM[15.9949]IFATEDHKPYIPEETER	-2.61	
LmxM.31.2120	hypothetical protein, conserved	GGGWLSSM[15.9949]LDKGVNAASGLFLEPR	-2.59	
LmxM.23.0630	exocyst complex component Sec10, putative	FYTTVISTAAPASAKK	-2.58	
LmxM.36.5150	kinesin-D	LADEVKDLQVEK	-2.55	
LmxM.16.0930	Snf7, putative	KYELVASLEHEK	-2.55	
LmxM.09.0100	flagellar pocket cytoskeletal protein bilbo1	ETKLM[15.9949]SEASSYLGNM[15.9949]R	-2.54	

LmxM.25.2020	hypothetical protein, conserved	FGAGAVKQLSADGYNVILEGR	-2.47	
LmxM.32.1750	macrophage migration inhibitory factor-like protein	VESWGEYPPSPKPKM[15.9949]M[15.9949]TPR	-2.46	
LmxM.27.1750	dynein heavy chain, putative	VFGSTDVLTEKVTAHAR	-2.40	
LmxM.08.0070		VQQSYFEDDVEVFAEETVEAEKTK	-2.39	
LmxM.36.1390	hypothetical protein, conserved	NLLFLSKEAEDK	-2.39	
LmxM.04.0680	ubiquitin-conjugating enzyme E2, putative	LELFLPEEYPM[15.9949]KPPK	-2.37	McKenna <i>et al.</i> , 2001; Burge <i>et al.</i> , 2020
LmxM.10.0400	pteridine transporter ft5, putative	SAVSHEVALDAAQPDDS[79.9663]EENT[79.9663]SSLEAAGVVTKDLOAEK	-2.36	
LmxM.03.0030	D-3-phosphoglycerate dehydrogenase-like protein	PSLIDPPYHALLEGVNPAAKELLESK	-2.34	Wang <i>et al.</i> , 2020
LmxM.32.2440	KH-associated protein 1	VVASQESM[15.9949]VKR	-2.33	
LmxM.19.1150	hypothetical protein, conserved	TPLITAKELAE LR	-2.30	
LmxM.08_29.0780	U-box domain protein, putative	LLSEIPPLRPKR	-2.28	
LmxM.05.0350	trypanothione reductase	NDAVLVDAYSKTSM[15.9949]DNIYAIGDVTSR	-2.23	
LmxM.08_29.2160	rab-GDP dissociation inhibitor, putative	NAYYGESASLNLEQLYQKFNK	-2.21	
LmxM.27.1210	translation initiation factor eIF2B delta subunit, putative	ILDVIEAELKM[15.9949]SFK	-2.21	
LmxM.27.0480	Nucleolar protein 60, putative	SKPFM[15.9949]SSPVLR	-2.20	
LmxM.10.0400	pteridine transporter ft5, putative	SAVSHEVALDAAQPDDS[79.9663]EENTS[79.9663]SLEAAGVVT[79.9663]KDLOAEK	-2.19	
LmxM.16.0080	Galactose oxidase, central domain/Domain of unknown function (DUF4110), putative	EREEAKFFR	-2.17	
LmxM.36.5140	VHS domain containing protein, putative	VQLSLIEIKDKALR	-2.17	
LmxM.22.0730	cytoskeleton associated protein, putative	EEEELKELK	-2.16	
LmxM.23.1300	lathosterol oxidase-like protein	AGDPKYVDPVYASYHEEK	-2.14	Jaenicke <i>et al.</i> , 2011
LmxM.08.0470	small ubiquitin protein, putative	AEAAAASVSAQQISLKVVNADGAEM[15.9949]FFK	-2.14	Lecona <i>et al.</i> , 2016; Pfeiffer <i>et al.</i> , 2017
LmxM.23.1020	hypothetical protein, unknown function	DVEAADGEAKC[45.9877]AEAVDMEEK	-2.13	
LmxM.34.2810	hypothetical protein, conserved	M[15.9949]FVHPSLRPTEQLGTTASTKGGQNTNGSR	-2.13	
LmxM.36.1340	N-acetyltransferase subunit Nat1, putative	QEEGYESIKQAILLNPK	-2.12	
LmxM.08.0090	adaptor complex protein (AP) 3 delta subunit 1, putative	HIADTKNEVNVADPR	-2.09	
LmxM.16.1420	hypothetical protein, conserved	TGGSVGSKAFLPR	-2.08	
LmxM.20.0690	hypothetical protein, conserved	LIAETAAYETVKNSFIR	-2.05	

LmxM.28.1990	Leucine-rich repeat protein 1, putative	NVDEDIDVLTDELQDTPGDAHTTKIL K	-1.97	
LmxM.27.0680	amino acid permease, putative	KLESS[79.9663]SLT[79.9663]DDG ESAAK	-1.97	Soetens <i>et al.</i> , 2001
LmxM.10.0510	glycerol-3-phosphate dehydrogenase [NAD+], glycosomal/mitochondrial	GFFQKSGGNLIAYAK	-1.96	
LmxM.31.0250	hypothetical protein, conserved	VAVGHGPGSSQLDVPSSKR	-1.95	
LmxM.09.0220	hypothetical protein, conserved	GKLSIPTDAEGSQVDFRR	-1.94	
LmxM.08_29.21 60	rab-GDP dissociation inhibitor, putative	NAYYGESASLNLEQLYQKFNK	-1.91	
LmxM.14.0490	Amastin surface glycoprotein, putative	M[15.9949]KSLVAEQK	-1.90	
LmxM.30.2020	succinyl-diaminopimelate desuccinylase-like protein	ILEADPPYGAKVTFK	-1.88	
LmxM.36.1580	hypothetical protein, conserved	M[15.9949]PHPSADALLAPPSVQE WVKLQEALTR	-1.86	
LmxM.33.0480	ion transporter, putative	FLDPYTNASTAKNDM[15.9949]Y NSAAALR	-1.86	
LmxM.27.0790	MatE, putative	RPTSISLDASPAASAIKK	-1.85	
LmxM.28.2250	glycosomal membrane protein-like protein	ENLLGKNFDDAHLR	-1.83	
LmxM.24.2180	Trypanosome basal body component protein	EKDGTIAALR	-1.82	
LmxM.34.1760	proteasome complex subunit Rpn13 ubiquitin receptor, putative	TTVNLEDFKKILASVSK	-1.81	Besche <i>et al.</i> , 2014
LmxM.29.1790	DNAJ domain protein, putative	ESVAAVTGASNGTEVEGKK	-1.80	
LmxM.33.0350	eukaryotic translation initiation factor 5, putative	VAPIVSWLGM[15.9949]DAKADA	-1.80	
LmxM.36.4320	hypothetical protein, conserved	VSLYSDEVGHNYEVDM[15.9949]K LEDAFTGR	-1.80	
LmxM.10.0400	pteridine transporter ft5, putative	DLQAEKKLV	-1.71	
LmxM.27.1710	eukaryotic translation release factor, putative	GM[15.9949]GTSVISVYM[15.994 9]TPKEQIAGM[15.9949]VAK	-1.71	
LmxM.03.0890	NLI interacting factor-like phosphatase, putative	DGQGS GDGAVEVEPQNSLKASDDD AGGTLEER	-1.67	
LmxM.30.2170	ARM-like helical domain-containing protein	LLNKNILSNPVDLLSM[15.9949]LP EAR	-1.56	
LmxM.10.1150	Cilia- and flagella-associated protein 45, putative	M[15.9949]AEYIKQK	-1.53	
LmxM.27.1980	FtsJ cell division protein, putative	YVFNDDDDLDPWFVKDEQR	-1.53	
LmxM.17.0910	acyltransferase, putative	FAEKELLSR	-1.51	
LmxM.26.1890	hypothetical protein, conserved	FLGKLESHR	-1.47	
LmxM.13.0450	ALBA-domain protein 1	NQGVVEVKK	-1.40	
LmxM.08.0470		VVNADGAEM[15.9949]FFKIK	-1.40	
LmxM.30.0440	cytoskeleton-associated protein CAP5.5, putative	APSAKAISDT[79.9663]VS[79.9663]AEEEEPK	-1.38	
LmxM.10.1290	Beta-1,2 mannoside phosphorylase	DEFTAVPELSWELEDPIQNVKR	-1.36	
LmxM.24.0140	ankyrin/TPR repeat protein	LDPTNKDLQQVK	-1.33	

LmxM.09.1020	LEM3 (ligand-effect modulator 3) family / CDC50 family, putative	KLIPDFVHEYGR	-1.32	
LmxM.31.0330	hypothetical protein, unknown function	SSQALATPTSGEEGTWLETPLFKTTR	-1.30	
LmxM.31.1330	PPPDE putative peptidase domain containing protein, putative	ITTKEVPSR	-1.27	
LmxM.18.1100	Ankyrin repeats (3 copies), putative	SVAEFAAHM[15.9949]KQK	-1.24	
LmxM.33.3430	cleavage and polyadenylation specificity factor, putative	DVDYDAPEVQKLIK	-1.24	Lee <i>et al.</i> , 2020; Liu <i>et al.</i> , 2022
LmxM.36.3210	14-3-3 protein 1, putative	LPDDLAELIYM[15.9949]AKLAEEAER	-1.17	Sato <i>et al.</i> , 2011
LmxM.09.0640	hypothetical protein, conserved	M[15.9949]LTEDLKGLYDR	-1.17	
LmxM.06.0140	proteasome beta 6 subunit, putative	VQLQQM[15.9949]LKYR	-1.04	
LmxM.36.0260	xylulokinase, putative	HEPEIFAKVDK	-1.01	
LmxM.01.0120	hypothetical protein, conserved	AQTAVSKFK	-1.01	
LmxM.20.1140	protein transport protein YIF1, putative	NYFAVDNTYVKR	-1.01	
LmxM.13.1130	Uncharacterised ACR, YagE family COG1723, putative	ETLEVDDNFKAR	-0.89	
LmxM.06.0240	Present in the outer mitochondrial membrane proteome 34	AAASAAEDDEAAVAKWGQR	-0.89	
LmxM.36.0460	vacuolar protein sorting-associated protein, putative	AVGQFGKDVQNVLTQHVPVLR	-0.68	MacDonald <i>et al.</i> , 2017
LmxM.16.1550	Component of motile flagella 6, putative	IAEAKSLQGR	-0.22	
LmxM.14.0660	fatty acid elongase, putative	AAAGESAPATAPAGKK	-0.03	

4.2.4 Identification of Changes in the Total Proteome of *Leishmania* Promastigotes upon DUB2 Knockout

In addition to identifying differences in the total ubiquitinome of the *Leishmania* promastigotes, we were also interested to observe how the total proteome changed in response to deletion of *DUB2*. As described in Fig. 15A, we extracted ~100 µg of protein from each sample prior to DiGly enrichment and then, upon sample processing, we loaded them for both label-free DDA- and DIA-MS/MS. Usage of both acquisition modes ensures a deeper protein coverage and therefore a better overlap between the proteomics and ubiquitinomics datasets. One of the benefits of such proteomics datasets is that it provides further insights in the regulatory function of *DUB2*, such as preventing proteins from being degraded by the proteasome. However, the primary reason of performing such experiment is to receive information on the stoichiometry (=occupancy) of the unmodified (=non-DiGly) peptides, and thus of the overall protein within the sample. Comparison of such data with the stoichiometry of DiGly-modified peptides could explain possibly changes observed in ubiquitinomics data. For instance, if the number of the ubiquitinated sites of a protein increases in the absence of *DUB2* but also the overall abundance of the same protein increases, then it is more likely the former observation to be explained simply by the increase in the abundance of the protein itself.

Focusing on the DIA dataset first, the data were searched against a theoretical library using DIA-NN and analysed by Rstudio using the DEP package. In total, there were 6225 proteins in the DIA data, covering more than the 67% of the predicted proteome of the parasite (Rogers *et al.*, 2011). Overlap across the three rapamycin-treated was striking, with only 8 proteins not being present in all three

samples. However, in the case of DMSO-treated samples, 258 out of the 6225 identified proteins were not quantified in all 3 samples, with sample 3 (D3_DIA) missing 251 of these proteins (Fig. 18A&B). Comparison across all 6 samples revealed that 5961 proteins were quantified in all 6 samples, with only 2 proteins being measured in just 3 out of 6 samples. Thus, there was no need of filtering the data for downstream analysis (Fig. 18C&D). Background correction and normalization of the data via variance stabilizing transformation did not affect the data distribution across the samples, however there is a variance-mean dependency by proteins with smallest intensities (mean<1000; Fig. 18E&F).

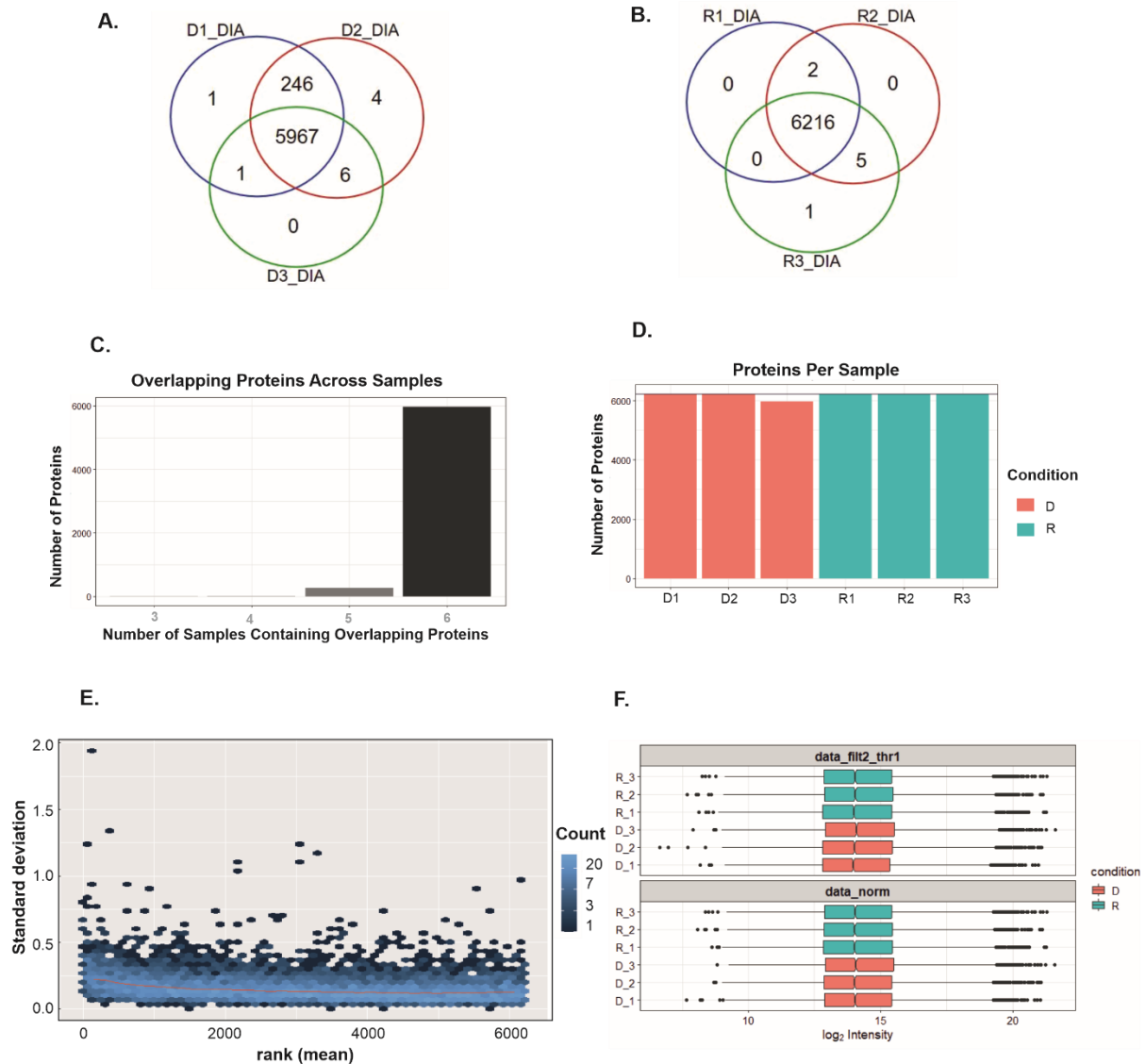


Figure 18 DIA-dependent proteomics data in response to deletion of DUB2. A. Proteins identified by DIA A. 3 DMSO-treated samples and **B.** 3 RAP-treated samples identified using TimsTOF HT mass-spectrometer in DIA mode. **C.** Overlapping proteins across all 6 samples. Each bar represents the overall number of samples containing an overlapping protein. For example a protein that is present in three out of six samples will be distributed in the bar called 3. **D.** Summarized identified proteins per sample. **E.** Rank of the means of the abundance of the ubiquitinated peptides plotted against standard deviations. Each point represents a number of ubiquitinated peptides with similar SD and mean. The

red line depicts the running median estimator. **F.** Data distribution based on protein intensity of normalized data (data_norm) and not (data_filt2_thr1).

Nevertheless, some missing values remained across the samples with DMSO-treated sample 3 having the highest number (251 missing values; Fig. 19A). After examining the nature of these missing values, we discovered that they fall under the category of “MAR” missing values. To address this issue, we determined that the K-nearest neighbour approach was the most effective imputation method (data not shown). Sequentially, limma analysis identified 111 significantly differentially expressed proteins, of which 72 were significantly downregulated in the DUB2 knocked out samples ($p < 0.05$, limma, Fig. 19B). Samples per treatment are clustered together (Fig. 19C) and their profiles for the significant proteins matching with the rest of the replicates (Fig. 19D). This, combined with the strong and positive Pearson correlation coefficient that the replicates have per condition, support that the samples per experimental condition are very similar making the analysis robust (Fig. 19E).

At this point, it is worth mentioning that we were solely interested in the significantly downregulated proteins in response to rapamycin treatment. Downregulated proteins indicate that these proteins were being degraded by proteasome in the absence of DUB2. Thus, it supports the hypothesis that these proteins are substrates of DUB2, by which DUB2 prevents their proteasomal degradation (Liu *et al.*, 2018). From the 72 downregulated proteins in response to DUB2 knock out, the top 3 hits are: ubiquitin carboxyl-terminal hydrolase (DUB2; LmxM.08_29.2300; $\text{Log}_2\text{FC} = 2.24$); hypothetical protein (LmxM.08.0020; $\text{Log}_2\text{FC} = 1.28$) and nucleoside transporter 1 (LmxM.15.1240; $\text{Log}_2\text{FC} = 1.10$; Table 5). At this point it is worth mentioning that 25 of these significantly downregulated proteins were identified as ubiquitinated based on our total *L. mexicana* promastigote ubiquitinomics dataset (Table 5). However, none of them had a significant upregulation in their ubiquitinated state in the presence or absence of DUB2.

Insights into the biological processes of the significantly downregulated proteins in response to the knockout of DUB2 revealed that most of these proteins were involved in a DNA-related process such as DNA metabolism (GO: 0006259; proteins = 6), DNA repair (GO: 0006281; proteins = 5) and DNA replication (GO: 0006260; proteins = 3; Fig. 19F). This is further supported by the cellular component analysis, where two out of the six GO Terms are involved at the site of DNA damage (GO: 0090734; protein = 1) and site of double-strand break (GO: 0035861; protein = 1; Fig. 19G). Finally, gene ontology analysis of these hits in regards of their molecular function indicated that 3 proteins have dioxygenase activity (GO: 0051213), while 3 other proteins have a catalytic activity against DNA (GO: 0140097). The rest 27 GO terms span from deubiquitinase activity (GO: 010100; proteins = 2) to protein phosphatase regulatory activity (GO: 0019888; protein = 1; Fig. 19H).

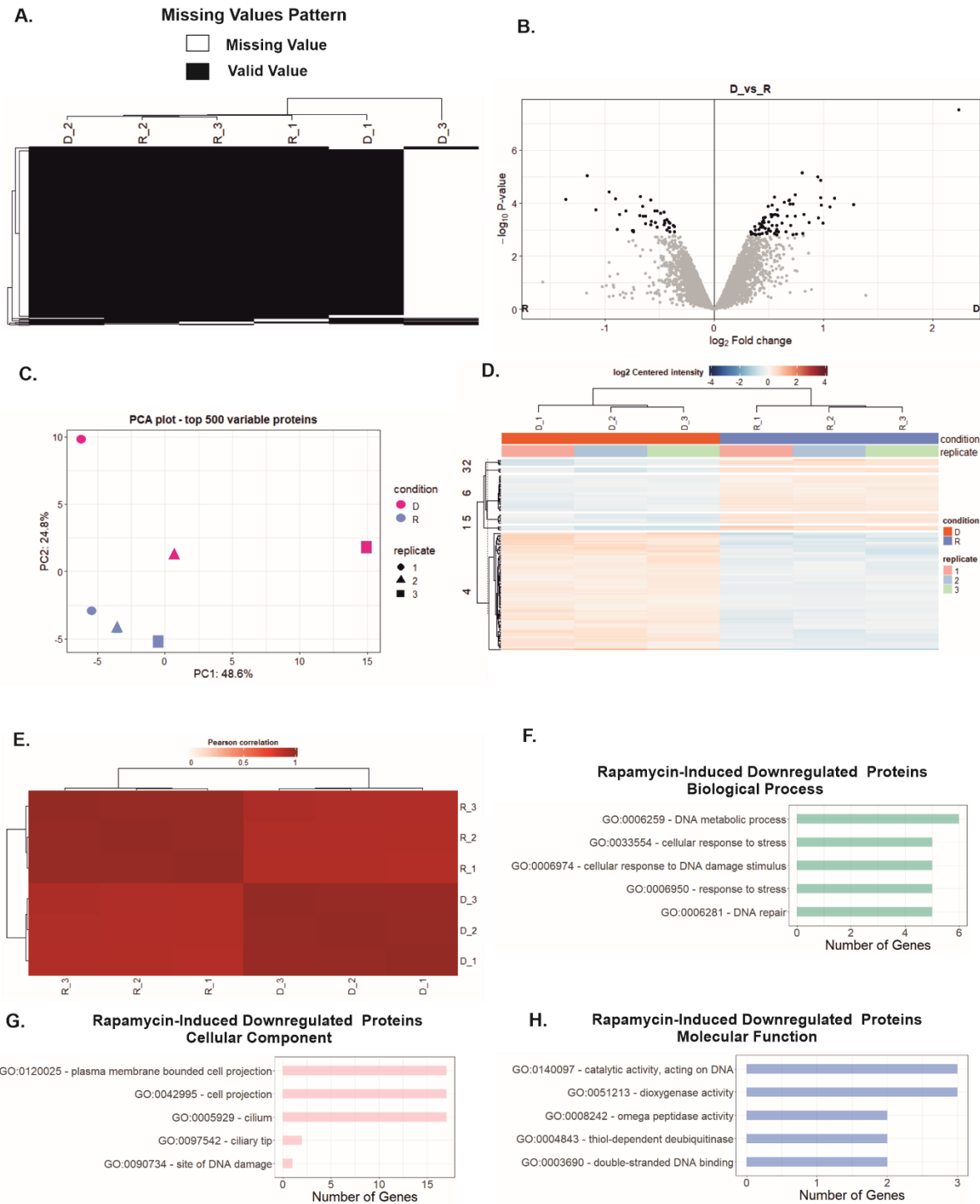


Figure 19: Insights into the significantly different proteins identified via DIA-MS/MS. **A.** Heatmap of missing values per sample. Each line represents a protein, which is missing in at least one of the six samples. White box indicates missing value (unique peptides <2) and black box indicates quantified value (unique peptides ≥ 2). **B.** Volcano plot depicts the significantly different proteins in black, of which the ones on the right were upregulated in DMSO-treated samples and the ones on the left were upregulated in RAP samples. **C.** PCA plot of the top 500 variable proteins. Different symbols indicate different sample, with red and blue representing DMSO (D) and rapamycin (R) treatments respectively. **D.** Heatmap of all significantly different proteins (rows) in each sample (column). Red = upregulation; Blue = downregulation. **E.** PPC matrix, of which dark red means very strong and positive correlation (PCC=1) and light red means very weak and negative correlation (PCC=-1). **F.** Top 10 GO

terms with the highest number of proteins for biological processes, **G.** cellular component and **H.** molecular function.

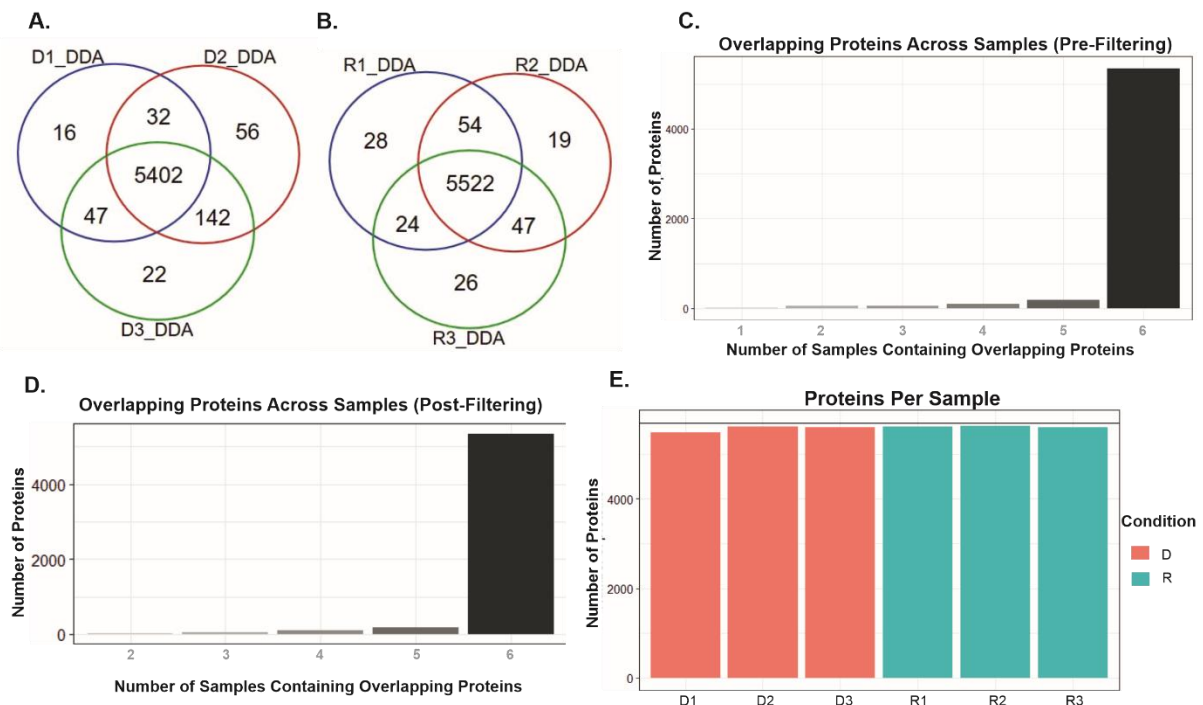
Table 5: Significantly downregulated proteins in response to deletion of DUB2 derived from the DIA dataset. For each significantly downregulated proteins (limma; $p < 0.05$) derived from the DUB2 depleted samples, the following information were listed: Gene ID, product description, which was taken from TriTrypDB, the Log₂Fold Change (Log₂FC) between DMSO-treated and rapamycin-treated samples and whether they are ubiquitinated based on our *L. mexicana* promastigote ubiquitinomics dataset from section 4.3.

Gene ID	Product Description	Log ₂ FC	Ubiquitinated
LmxM.08_29.2300	ubiquitin carboxyl-terminal hydrolase, putative	2.24	Yes
LmxM.08.0020	hypothetical protein, conserved	1.28	
LmxM.15.1240	nucleoside transporter 1, putative	1.10	
LmxM.19.1030	hypothetical protein, conserved	1.06	
LmxM.28.0550	DNA repair protein RAD51, putative	0.98	
LmxM.06.1060	2OG-Fe(II) oxygenase superfamily, putative	0.97	
LmxM.36.3160	tubulin binding cofactor c, putative	0.97	
LmxM.31.3280	hypothetical protein, conserved	0.95	
LmxM.13.1450	EF hand-like protein	0.95	
LmxM.10.0740	hypothetical protein, conserved	0.87	
LmxM.14.0050	hypothetical protein, conserved	0.82	
LmxM.30.0760	hypothetical protein, unknown function	0.81	
LmxM.30.2860	protein kinase, putative	0.80	Yes
LmxM.28.1830	DNA repair protein-like protein	0.75	Yes
LmxM.36.6360	Protein of unknown function (DUF2962), putative	0.74	
LmxM.07.0743	protein phosphatase inhibitor, putative	0.74	
LmxM.31.1990	hypothetical protein, conserved	0.72	
LmxM.33.1340	hypothetical protein, conserved	0.72	Yes
LmxM.36.2760	Nodulin-like, putative	0.70	Yes
LmxM.16.0770	hypothetical protein, conserved	0.70	
LmxM.23.0010	hypothetical protein, conserved	0.69	Yes
LmxM.31.3030	chaperone protein DnaJ, putative	0.68	Yes
LmxM.08_29.1850	pre-RNA processing PIH1/Nop17, putative	0.67	Yes
LmxM.10.0030	phosphate-Repressible Phosphate Permease-like protein	0.66	
LmxM.24.0760	DNA repair and recombination protein RAD54, putative	0.64	
LmxM.29.3110	S-adenosylmethionine decarboxylase proenzyme	0.62	
LmxM.03.0410	hypothetical protein	0.58	Yes
LmxM.13.1070	hypothetical protein, unknown function	0.58	Yes
LmxM.36.0750	hypothetical protein, conserved	0.58	Yes
LmxM.34.0180	Kinetoplastid kinetochore protein 24, putative	0.57	Yes
LmxM.33.3160	hypothetical protein, conserved	0.57	
LmxM.22.0360	hypothetical protein, conserved	0.57	

LmxM.33.3010	rhodanese-like domain containing protein, putative	0.57	
LmxM.33.4600	1,2-Dihydroxy-3-keto-5-methylthiopentene dioxygenase, putative	0.56	
LmxM.29.3440	DNA ligase I, putative	0.55	
LmxM.33.3580	hypothetical protein, conserved	0.55	
LmxM.23.1370	mitochondrial carrier protein-like protein	0.53	
LmxM.31.3070	MIZ/SP-RING zinc finger, putative	0.53	
LmxM.06.1260	pteridine transporter, putative	0.53	Yes
LmxM.22.1400	hypothetical protein, conserved	0.52	
LmxM.22.1340	Putative S-adenosyl-L-methionine-dependent methyltransferase, putative	0.52	
LmxM.36.3150	ADP-ribosylation factor GTPase activating protein, putative	0.52	
LmxM.36.1950	DNA mismatch repair protein MSH6, putative	0.50	
LmxM.15.0110	hypothetical protein, conserved	0.50	
LmxM.08_29.2260	DNA replication complex GINS protein SLD5, putative	0.50	
LmxM.34.3540	pre-rRNA-processing protein PNO1, putative	0.50	Yes
LmxM.34.4650	protein phosphatase, putative	0.48	
LmxM.26.2150	hypothetical protein, conserved	0.48	
LmxM.13.0990	hypothetical protein, conserved	0.47	
LmxM.36.0890	eukaryotic translation initiation factor 6 (eIF-6), putative	0.47	Yes
LmxM.30.0790	c2 domain protein, putative	0.46	
LmxM.32.1895	LisH domain-containing protein FOPNL, putative	0.45	
LmxM.10.0200	Mitogen-activated protein kinase 10, putative	0.45	Yes
LmxM.27.2450	hypothetical protein, conserved	0.45	
LmxM.10.1130	hypothetical protein, conserved	0.45	
LmxM.22.0500	hypothetical protein, conserved	0.44	Yes
LmxM.31.3990	GIPL galf transferase, putative	0.44	Yes
LmxM.36.4230	paraflagellar rod component, putative	0.44	Yes
LmxM.13.0460	hypothetical protein, conserved	0.43	Yes
LmxM.18.0480	uracil-DNA-glycosylase, putative	0.43	
LmxM.33.0410	hypothetical protein, conserved	0.42	Yes
LmxM.15.0770	protein kinase, putative	0.42	Yes
LmxM.27.1360	hypothetical protein, conserved	0.41	
LmxM.27.1480	cyclic nucleotide-binding domain containing protein, putative	0.41	
LmxM.31.1210	pentatricopeptide repeat domain containing protein, putative	0.41	
LmxM.24.0620	ubiquitin carboxyl-terminal hydrolase, putative	0.38	Yes
LmxM.16.0360	hypothetical protein, conserved	0.38	
LmxM.30.2710	phosphatidylinositol-4-phosphate 5-kinase-like protein	0.37	Yes
LmxM.05.0130	protein kinase, putative	0.37	
LmxM.34.4870	hypothetical protein, conserved	0.35	
LmxM.30.2530	hypothetical protein, conserved	0.34	Yes

LmxM.05.0200	50S ribosome-binding GTPase, putative	0.33	
--------------	---------------------------------------	------	--

We were also interested to investigate whether the mode of data acquisition of mass-spectrometry affects the coverage of total protein profiles and consequently the overlap with the ubiquitinomics data. Thus, we ran the same six samples (3 x DMSO & 3 x RAP) that we used for generating DIA data on DDA-dependent label-free quantitative mass-spectrometry. For the *de novo* search of the DDA data, we used FragPipe, where we filtered the peptides at 1% false discovery rate (FDR) and accepted proteins that have at least two unique peptides. In total, we identified 5738 proteins that corresponds to ~62% of the total *Leishmania* proteome (Rogers *et al.*, 2011). From the DMSO-treated samples, we quantified 5717 proteins, of which the 5402 were present in all three samples, 221 in two samples and 94 in just one of the samples (Fig. 20A). For the case of rapamycin-treated samples, we identified in total 5720 proteins, of which 5522 were quantified in all three replicates, 125 in just two replicates and 73 in only one (Fig. 20B). Comparison of all six samples revealed an overlap of 5342 proteins across all six, however 16 proteins were present in just one of the samples (Fig. 20C). Thus, we filtered the DDA data using the condition that detected proteins in at least two of the samples of a single treatment would be kept. 5697 proteins passed the conditioning (Fig. 20D&E) and the proteins with lower ranked intensity means having overall higher calculated standard deviation compared to the rest (Fig. 20F). Nevertheless, normalization and transformation of the data had no impact in the sample distribution (Fig. 20G) and missing values were still counted in all the samples (Fig. 20H). Downstream investigation revealed that these missing values were MNAR, and the best imputation approach was the quantile regression imputation of left-censored data (QRILC) approach, which utilizes random draws from truncated distribution generated under quantile regression parameters.



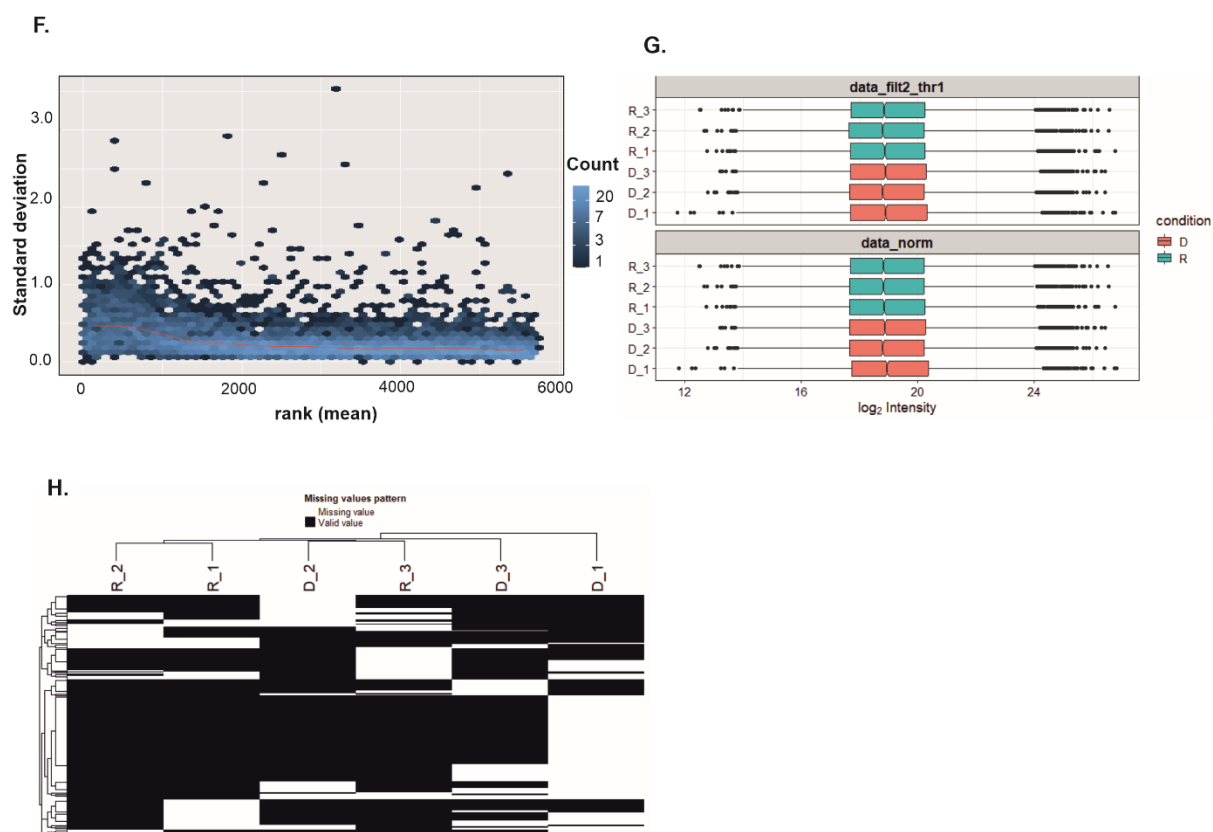


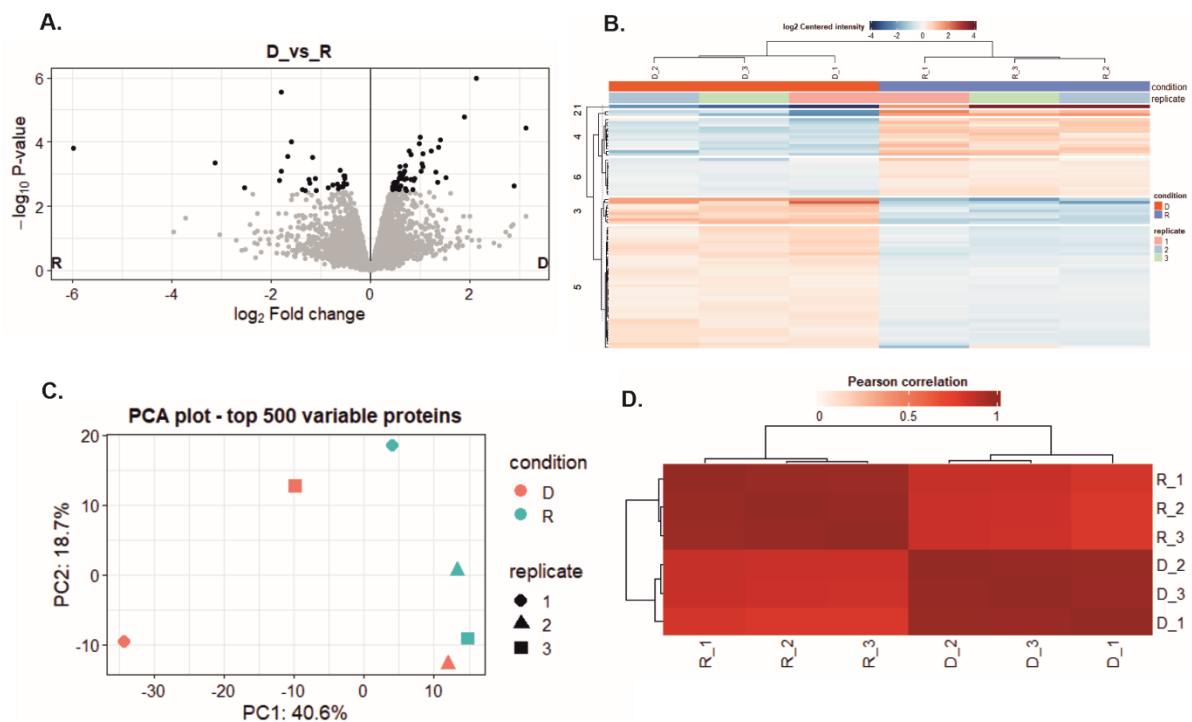
Figure 20: Insights into the DDA proteomics data in response to deletion of DUB2. Overlapping proteins across **A.** DMSO-treated samples and **B.** RAP-treated samples identified using TimsTOF HT mass-spectrometer at DIA mode. **C.** Number of proteins being present in one or more samples. For instance, if a protein is present in only one of the six samples, then it will be allocated in bar with number 1. No filtering was applied in this dataset. **D.** Number of proteins remained per sample after applying the following threshold: proteins that were detected in at least two out of three replicates in at least one of the two treated conditions were kept for downstream analysis. **E.** Same as C., however for proteins meeting the condition mentioned in D. **F.** Rank of the means of the abundance of the ubiquitinated peptides plotted against standard deviations. Each point represents a number of ubiquitinated peptides with similar SD and mean. The red line depicts the running median estimator. **G.** Data distribution based on protein intensity of normalized data (data_norm) and not (data_filt2_thr1). **H.** Heatmap of missing values per sample. Each line represents a protein, which is missing in at least one of the six samples. White box indicates missing value and black box indicates quantified value.

50 out of the 82 differentially expressed proteins were significantly downregulated in response to rapamycin-induced deletion of *DUB2* (Fig. 21A). Moreover, all the significant proteins have similar intensity patterns across their replicates, with replicates clustered together, making the data analysis consistent and therefore robust (Fig. 21B). In addition, to investigate whether there is variation across the samples, we performed Pearson correlation coefficient and principal component analysis (Fig. 21C&D). The former approach indicated that the replicates per condition have a strong and positive correlation ($PCC > 0.98$), while the latter approach showed that samples are clustered in a treatment-

dependent manner. Thus, samples per condition are very similar to each other, which further enhances the confidence to the treatment-dependent significant observations.

The top three hits that were significantly downregulated upon DUB2 knockout are: ubiquitin carboxyl-terminal hydrolase (DUB2; LmxM.08_29.2300; $\text{Log}_2\text{FC}=3.14$), hypothetical protein (LmxM.33.2485; $\text{Log}_2\text{FC} = 2.15$) and Tetratricopeptide repeat (TPR) containing protein (LmxM.36.2070; $\text{Log}_2\text{FC} = 1.90$; Table 6). Broader investigation to the biological importance of the downregulated proteins in response to the decreased protein levels of DUB2 suggests that these proteins are involved in various biological processes such cellular responses to stress (GO: 0006950; proteins = 4) and DNA repair (GO: 0006281; proteins = 3; Fig. 21E). Moreover, cellular component analysis performed in TritypDB indicates that these proteins are found in five distinct components: cell tip (GO: 0051286; proteins= 2), pellicle (GO: 0020039; protein =1), site of DNA damage (GO: 0090734; protein =1), ubiquitin ligase complex (GO: 0000151; protein = 1) and mitochondrial intermembrane space (GO: 0005758; protein = 1; Fig. 21F). In regards of the molecular function, hits are variable, with three proteins having ligase activity (GO: 0016874) and two proteins having an enzyme regulator activity (GO: 0030234; Fig. 21G). Furthermore, from these significantly downregulated proteins, 14 were also identified as ubiquitinated in *L. mexicana* promastigotes, however none of their ubiquitination sites was significantly upregulated in response to DUB2 depletion (Table 6).

Subsequently, we wanted to directly compare the two significantly altered DUB2-KO proteomes generated using either DIA or DDA mass-spectrometry mode. This would help us decide with which total proteome dataset we will proceed to downstream analyses. Focusing only on the significantly downregulated proteins of each dataset for reasons mentioned previously, there is an overlap of 21 proteins between the two sets, including the AP-2 associated kinase 1 (AAK1) and DNA ligase I (LigI; Table 7; Fig. 21H). However, this number does not even cover the 75% of significant downregulated hits of the less abundant DDA-derived downregulated proteome. Thus, we utilized both datasets in downstream analyses, to increase the possibilities of identifying promising DUB2 substrates.



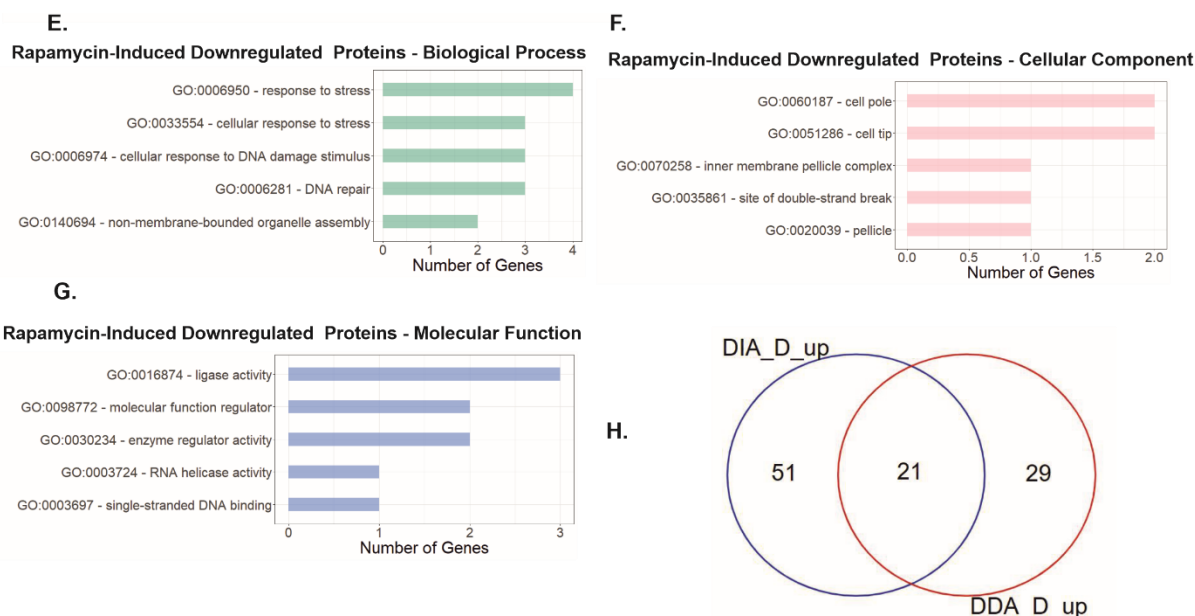


Figure 21: Changes in the total proteome upon DUB2 knockout (DIA-datasets)). A. Significantly enriched proteins in rapamycin (R)-treated and DMSO (D)-treated cells from DIA-derived datasets. Enrichment analysis was performed using limma (FDR= 5%). Significant and non-significant proteins were depicted in black and grey, respectively (n=3). B. Heatmap of significantly different proteins per sample (red = upregulation; blue = downregulation) C. PCA plot of the top 500 variable proteins. Each sample is represented with different symbol, while red indicates DMSO treatment and blue RAP-treatment. D. PCC matrix of significantly different proteins across samples. GO analysis of significantly downregulated proteins in DUB2 depleted samples only focusing on their E. biological function F. cellular component and G. molecular function. H. Overlapping significantly downregulated proteins in DUB2 depleted samples between DDA and DIA generated datasets.

Table 6: Significantly downregulated proteins in response to DUB2 depletion derived from the DDA dataset. For each significantly downregulated proteins (limma; $p < 0.05$) derived from the DUB2 depleted samples, the following information were listed: Gene ID, product description, which was taken from TriTrypDB, the Log_2FC between DMSO-treated and rapamycin-treated samples and whether they are ubiquitinated based on our *L. mexicana* promastigote ubiquitinomics dataset (section 4.3).

Gene ID	Product Description	Log_2FC	Ubiquitinated
ubiquitin carboxyl-terminal hydrolase, putative	LmxM.08_29.2300	3.14	Yes
hypothetical protein, conserved	LmxM.33.2485	2.14	
TPR repeat/Tetratricopeptide repeat, putative	LmxM.36.2070	1.90	
Family of unknown function (DUF572), putative	LmxM.08_29.1220	1.53	
rhodanese-like domain containing protein, putative	LmxM.32.0990	1.41	
Ecotin-like protein	LmxM.15.0300	1.41	
DNA repair protein RAD51, putative	LmxM.28.0550	1.38	
hypothetical protein, conserved	LmxM.27.1410	1.36	
hypothetical protein, conserved	LmxM.10.0740	1.32	

hypothetical protein	LmxM.03.0410	1.06	Yes
50S ribosome-binding GTPase, putative	LmxM.29.0840	1.06	
hypothetical protein, conserved	LmxM.31.1990	1.04	
S-adenosylmethionine decarboxylase proenzyme	LmxM.29.3110	1.03	
2OG-Fe(II) oxygenase superfamily, putative	LmxM.06.1060	1.01	
hypothetical protein, conserved	LmxM.17.1300	1.00	
hypothetical protein, conserved	LmxM.36.0750	0.99	Yes
hypothetical protein, conserved	LmxM.28.2150	0.90	
Protein of unknown function (DUF2962), putative	LmxM.36.6360	0.89	
WD domain, G-beta repeat/Sof1-like domain containing protein, putative	LmxM.34.3880	0.88	
hypothetical protein, conserved	LmxM.25.2310	0.86	
hypothetical protein, conserved	LmxM.36.5030	0.82	
hypothetical protein, conserved	LmxM.26.2150	0.82	
protein kinase, putative	LmxM.30.2860	0.79	Yes
hypothetical protein, unknown function	LmxM.30.0760	0.74	
hypothetical protein, conserved	LmxM.27.2450	0.73	Yes
tubulin binding cofactor c, putative	LmxM.36.3160	0.72	
glucose transporter 2	LmxM.36.6290	0.72	Yes
hypothetical protein, conserved	LmxM.16.0770	0.69	
Putative GTPase activating protein for Arf, putative	LmxM.28.1770	0.68	
hypothetical protein, conserved	LmxM.28.2830	0.67	
hypothetical protein, conserved	LmxM.20.1700	0.66	
RNA-binding protein, putative	LmxM.08_29.1340	0.63	
phosphate-Repressible Phosphate Permease-like protein	LmxM.10.0030	0.61	
hypothetical protein, conserved	LmxM.25.0600	0.60	Yes
deoxyuridine triphosphatase, putative	LmxM.06.0560	0.60	Yes
hypothetical protein, conserved	LmxM.28.2890	0.59	Yes
calmodulin, putative	LmxM.13.1160	0.59	
DNA ligase I, putative	LmxM.29.3440	0.59	
Suppressor of G2 allele of SKP1, putative	LmxM.20.1640	0.58	Yes
hypothetical protein, conserved	LmxM.13.0990	0.55	
transcription like protein nupm1, putative	LmxM.30.1940	0.53	Yes
hypothetical protein, conserved	LmxM.31.2090	0.52	
Cytokine-induced anti-apoptosis inhibitor 1, Fe-S biogenesis, putative	LmxM.07.0230	0.52	
hypothetical protein, conserved	LmxM.13.0460	0.49	Yes
ubiquitin-conjugating enzyme E2, putative	LmxM.33.0900	0.48	
protein kinase, putative	LmxM.15.0770	0.47	Yes
eukaryotic translation initiation factor 6 (eIF-6), putative	LmxM.36.0890	0.46	Yes
hypothetical protein, conserved	LmxM.34.0610	0.46	

folypolyglutamate synthetase	LmxM.36.2610	0.46	
hypothetical protein, conserved	LmxM.02.0690	0.45	
pre-mRNA splicing factor ATP-dependent RNA helicase, putative	LmxM.36.0870	0.44	

Table 7: Overlapping significantly downregulated hits in response to DUB2 depletion between DDA and DIA datasets. Product description taken from TriTrypDB

Gene ID	Product Description
LmxM.03.0410	hypothetical protein
LmxM.06.1060	2OG-Fe(II) oxygenase superfamily, putative
LmxM.08_29.2300	ubiquitin carboxyl-terminal hydrolase, putative
LmxM.10.0030	phosphate-Repressible Phosphate Permease-like protein
LmxM.10.0740	hypothetical protein, conserved
LmxM.13.0460	hypothetical protein, conserved
LmxM.13.0990	hypothetical protein, conserved
LmxM.15.0770	protein kinase, putative
LmxM.16.0770	hypothetical protein, conserved
LmxM.26.2150	hypothetical protein, conserved
LmxM.27.2450	hypothetical protein, conserved
LmxM.28.0550	DNA repair protein RAD51, putative
LmxM.29.3110	S-adenosylmethionine decarboxylase proenzyme
LmxM.29.3440	DNA ligase I, putative
LmxM.30.0760	hypothetical protein, unknown function
LmxM.30.2860	protein kinase, putative
LmxM.31.1990	hypothetical protein, conserved
LmxM.36.0750	hypothetical protein, conserved
LmxM.36.0890	eukaryotic translation initiation factor 6 (eIF-6), putative
LmxM.36.3160	tubulin binding cofactor c, putative
LmxM.36.6360	Protein of unknown function (DUF2962), putative

4.2.5 Overlapping Proteins Across Datasets of Interest

Next, we were interested to investigate whether any of the significant proteins are present in more than one of the following datasets that we have generated: proximal interacting proteins of DUB2 identified by XL-miniTurboID (DUB2 proximome dataset); significantly downregulated proteins in response to DUB2 depletion identified via DDA- and DIA-MS/MS (DDA- and DIA-dependent downregulated DUB2-KO proteome datasets) and significantly upregulated ubiquitinated proteins in response to DUB2 depletion (DDA-dependent upregulated DUB2-KO ubiquitinome dataset). To be more specific, we were only interested in overlapping hits between an interactome, ubiquitinome and/or proteome datasets. These overlapping hits would be classified as the most promising substrates of DUB2 and they would be prioritized for future validation. In the same analysis, we also included the interactome of DUB2 that was generated previously using immunoprecipitation (IP dataset; Damianou *et al.*, 2020). As it was mentioned in the previous chapter, the XL-miniTurbo and

the IP interactome datasets have a small overlap (7 proteins; Fig. 9), so we concluded that the two approaches are complementary to each other. Therefore, the reason of including the IP dataset in this analysis was to increase the possibility of identifying promising DUB2 substrates.

Overall, from all 5 datasets there were 391 significant proteins, of which 73 derived from the DUB2 proximome, 121 from the IP interactome, 72 from the DIA-dependent downregulated DUB2-KO proteome, 51 from the DDA-dependent downregulated DUB2-KO proteome and 112 from the DDA-dependent upregulated DUB2-KO ubiquitinome. The overlapping hits across datasets, which are listed in Fig. 22, are as follows: a) the ubiquitin carboxyl-terminal hydrolase (DUB2; LmxM.08_29.2300) spans across all datasets apart from the upregulated DUB2-KO ubiquitinome, b) an “orphan” hypothetical protein (LmxM.20.1700) is present in the XL-miniTurboID proximome and DDA-derived downregulated DUB2-KO proteome, c) the 50S ribosome-binding GTPase (LSG1; LmxM.05.0200) protein is present in the DIA-derived downregulated DUB2-KO proteome and DUB2 proximome, while d) 40S ribosomal protein SA (RPSA; LmxM.36.5010) and 2,3-bisphosphoglycerate-independent phosphoglycerate mutase (iPGMA; LmxM.36.6650) are significant hits for the DUB2 proximome and the upregulated DUB2-KO ubiquitinome. Moreover, e) the ubiquitin-conjugating enzyme E2 (UBC2; LmxM.04.0680), cleavage and polyadenylation specificity factor (CPSF73; LmxM.33.3430), small ubiquitin protein (SUMO; LmxM.08.0470) and rab-GDP dissociation inhibitor (GDI; LmxM.08_29.2160) are overlapping hits of the IP interactome and DUB2-KO upregulated ubiquitinome. f) The 7 overlapping proteins between the XL-miniTurboID proximome and IP interactome and g) the 20 hits being significant in both downregulated DUB2-KO proteomes were listed and discussed previously (Fig. 9 & Table 7).

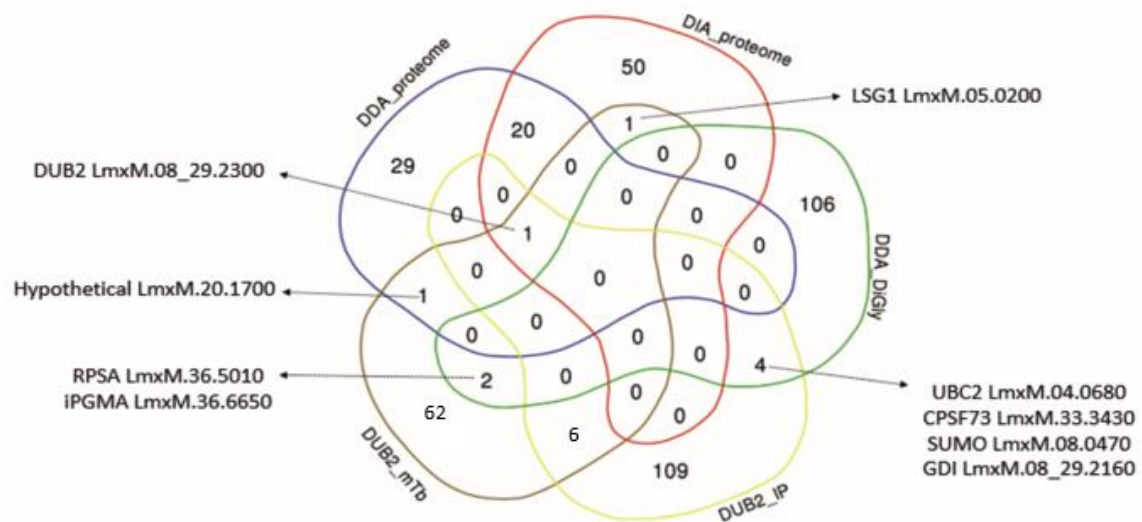


Figure 22: Overlapping proteins across all the generated datasets. DUB2 proximome interactome using miniTurboID (DUB2_mTb); DUB2 interactome via immunoprecipitation (DUB2_IP); proteins with upregulated ubiquitination sites in DUB2 depleted samples (DDA_DiGly); downregulated proteins in DUB2 depleted samples (DIA_proteome for DIA-derived data; DDA_proteome for DDA-derived data). The 7 hits present in both interactomes and the 21 proteins present in both downregulated proteomes were not listed because they were mentioned in Fig. 9 and Fig. 21H, respectively.

4.3 Discussion

4.3.1 Ubiquitinomics Workflow Optimization

In general, ubiquitinomics studies are widely employed to detect ubiquitinated peptides in various organisms through the utilization of mass spectrometry. It is anticipated that approximately 5-10% of the eukaryotic proteome undergoes ubiquitination. Nevertheless, this expectation did not hold true in the sole available study conducted on the *Leishmania* promastigotes (Harris, 2022). In that study, only 8 ubiquitinated peptides were identified in MG132-treated promastigotes, and 5 ubiquitinated peptides were identified in DMSO-treated promastigotes. These identifications were made while maintaining a stringent 1% false discovery rate (FDR). Regarding the incomplete coverage of the *Leishmania* ubiquitinome, it could be attributed to several factors, including the utilization of low protein input (0.35 mg), the use of RIPA as a lysis buffer, and the application of a home-made kit for enriching DiGly peptides. Thus, it was required to develop an optimized ubiquitinomics workflow for identifying ubiquitinated peptides in *L. mexicana* promastigotes.

Comparison of 5% SDS and RIPA buffer revealed that the former is a better lysis buffer for maintaining higher amount of ubiquitinated proteins in *L. mexicana* promastigotes. SDS is a very strong ionic detergent that can completely solubilize even the hardest to-be solubilize proteins such as membrane proteins. The high protein denaturing capacity of SDS deactivates cellular proteases, including cysteine peptidases such as DUBs (Shevchenko *et al.*, 2006). Therefore, both proteins and their post-translational modifications, including ubiquitination, are maintained intact inside the lysate. This is further supporter by our observation that protease inhibitors do not improve the ubiquitination signal derived from 5% SDS-lysed samples. Conversely, protease inhibitors improved the ubiquitination signal of RIPA-lysed cells, indicating that some proteases remain active in that buffer. Despite the fact that RIPA buffer contains 0.1% SDS, its protein denaturing capacity is limited, especially for proteins derived from the cytoskeleton and extracellular matrix (Ngoka, 2008; Janes, 2015). Subsequently, its capacity to improve the maintenance and solubility of ubiquitinated proteins is limited. In regards of SDC lysis buffer, it has been recently shown that it improves the ubiquitinome profile extracted from human colorectal carcinoma HCT116 cells (Steger *et al.*, 2021). However, in *Leishmania* promastigotes this could not be confirmed. Lack of evidence could be attributed to the misuse of SD, which has a high pH and is temperature sensitive. This may have caused precipitation of proteins during sample preparation, preventing them from being identified via western blot.

Despite showing that 5% SDS buffer is the most efficient lysis buffer, two things are worth pointing out: firstly, SDS at a concentration of more than 0.1% affects adversely trypsin digestion and secondly, the presence of the strong surfactant SDS into a MS sample can cause various problems during the electrospray, including ion suppression (Zhang *et al.*, 2007; Botelho *et al.*, 2010). Therefore, SDS needs to be removed prior to trypsinisation. A filter-based strategy using suspension traps (S-Traps) were chosen as the most efficient and quickest way to remove SDS remnants (Sharma *et al.*, 2012; Ludwig *et al.*, 2018). However, even with these filters some proteins and peptides can be lost during the desalting step. Nevertheless, despite these limitations we have successfully showed that 5% SDS lysis buffer is the most efficient way to release ubiquitinated proteins from *L. mexicana* promastigote cells.

Furthermore, we showed that 7mg proteins from *Leishmania* promastigote cells are enough to acquire a deep coverage of its ubiquitinome. The recommended input protein for the customized anti-DiGly antibody conjugated magnetic beads (CST) is 1-2mg. However, this was optimized on human cells. The proteome and therefore the ubiquitinome of the *Leishmania* parasite is smaller compared to the human HeLa cells, which justifies the need of at least three times more protein input for such experiments (Paape *et al.*, 2010; Meier *et al.*, 2020; van der Wal *et al.*, 2022). The overall requirement of such low protein inputs is attributed to the highly efficient anti-DiGly antibody conjugated magnetic

beads (CST). Previous DiGly-enrichment kits required at least 30mg as protein input for a deep ubiquitinome coverage, making them fifteen times less efficient compared to the ones we used (Fulzele & Bennett, 2018). Furthermore, another advantage of using CST magnetic beads is that the antibodies are already conjugated on the beads, which saves time in terms of optimizing and performing this step. Moreover, due to the covalently and irreversibly bound antibodies to the magnetic beads, prevents contamination of the MS sample with peptides derived from the DiGly-enriching antibodies. Finally, the use of magnetic racks to isolate the magnetic beads makes the procedure easier compared to the previously used agarose beads.

Despite optimizing the preparation of the DiGly-enriched samples, we also showed that TimsTOF HT is the best available mass-spectrometer in our MS facility to identify *Leishmania* ubiquitinated peptides. The overall outperformance of TimsTOF, which is 19-fold against Orbitrap Fusion and 171-fold against maXis (data not shown), could be attributed to the additional ion mobility separation step, which separates gas-phased ions based on their collisional cross section (CCS; Meier *et al.*, 2015; Meier *et al.*, 2018). This additional dimension improves the selectivity of our analysis but also the overall speed, which reaches sequencing rates above 100 Hz compared to ~20 Hz of Orbitrap (Gravel *et al.*, 2023). Furthermore, it contributes to the precursor-based mass resolution of resulting spectra, facilitating the identification of modified peptide ions such as phosphopeptides (Oliinyk & Meier, 2023). Therefore, it could justify the improved identification of *Leishmania* peptide ions modified with the DiGly remnant. The main caveat of our conclusion that TimsTOF HT mass spectrometer outperformed the rest is that the comparison of datasets is based on only three independent experiments. Thus, additional variation due to biological factors and sample preparation are possible. Collectively, the striking difference in the ubiquitinomics datasets and the advantages of using TimsTOF HT mass-spectrometer shows for the first time the improved applicability of such mass-spectrometer in proteomics-related studies, including ubiquitinomics, for the *Leishmania mexicana* parasite.

Previous ubiquitinomics studies proved that DIA-MS/MS can triple the number of identified ubiquitination sites compared to DDA-MS (Steger *et al.*, 2021; Hansen *et al.*, 2021). However, the opposite was observed for the case of DiGly-enriched *Leishmania* promastigote samples. This unexpected observation could be attributed to the utilization of a library-free DIA-NN approach, which is the fastest, cheapest and least efficient way to identify modified peptides with DiGly remnants. To cancel out this possibility there is a need to develop an empirical spectral library using DDA-mode derived data. Empirical spectral libraries combined with theoretical ones are known to improve DIA-MS/MS ubiquitinomics coverage in human samples. However, such libraries require time and sources to be developed. Furthermore, other MS-related parameters might have contributed to the poorer performance of DIA-MS/MS on DiGly-enriched samples. For instance, the fixed 400-1200 m/z isolation window of DIA-MS/MS could have prevented the identification of *Leishmania* ubiquitination sites outside that range, limiting its performance compared to the DDA-MS/MS. Nevertheless, due to the lack of time, additional optimizations were not performed. In conclusion, we have showed for the first time that DIA-MS/MS is applicable for identifying ubiquitination sites of *Leishmania* promastigotes, with DDA-MS/MS performing better under the investigated parameters.

In terms of which database search software is the best for analysing our ubiquitinomics DDA-MS/MS raw data, FragPipe outcompeted both Mascot and PEAKS11. Overall, all three software utilize a *de novo* sequencing tag approach, which firstly identifies the most accurately alignment of spectrum to a peptide and secondly detects mass shifts (“mass offset”) that probably corresponds to PTMs of amino acids from this peptide. Thus, all three software are ideal for identifying PTMs from DDA-derived raw data (Creasy & Cottrell, 2002; Han *et al.*, 2011; Polasky *et al.*, 2023). However, a great

advantage of PEAKS11 and FragPipe is that they also use a dynamic programming algorithm, which considers the coexistence of both modified and unmodified forms (=base forms) of the same peptide in the same sample. Inevitably this feature increases the robustness of identified PTMs due to the independent identification of the same peptide in two forms. Some PTMs, such as ubiquitination, SUMOylation and phosphorylation, are classified as labile modifications. In tandem MS, labile modifications refer to those that undergo fragmentation either instead of or in addition to peptide backbone fragmentation. FragPipe is ideal on identifying both neutral losses from such modifications and even modifications being completely lost during fragmentation, which subsequently cannot be detected in MS2. This is achieved via the labile search, which uses “open”/ “offset” search that identifies differences between the MS1-derived mass of the observed precursor and the mass of the peptide sequence. This has improved the spectral assignment rate for our ubiquitination sample, as it was previously observed for other PTMs, including phosphorylation (Polasky *et al.*, 2023). Thus, FragPipe outperformed the other two database search engines for analysing DDA-derived *L. mexicana* ubiquitinomics raw data.

The usage of proteasomal inhibitors such MG132 is well established to rescue ubiquitinated proteins from being degraded by the proteasome, leading to the increase of their stoichiometry. Our ubiquitinomics results proved that this is also the case in *L. mexicana* promastigote cells, where incubation of cells with MG132 increased the number of identified ubiquitination sites by ~61% (n=1; data not shown). Previous studies have also confirmed the impact of MG132 on the ubiquitinome of *Leishmania*, however through western-blotting (Martel, 2019; Petersen *et al.*, 2021). Such approach prevents the accurate identification and quantification of specific ubiquitinated proteins being accumulated in response to MG132. Harris (2022) was the only person who attempted to identify ubiquitinated proteins in *Leishmania* using a similar ubiquitinomics approach, however he only identified 8 and 5 high confident hits (1% FDR) in the presence and absence of MG132. Nevertheless, despite of showing that MG132-treated samples increase indeed the number of DiGly peptides in our sample, there were more than 300 DiGly peptides that were identified only in the DMSO-treated sample and not in the MG132 one (n=1; data not shown). This comes in agreement with previous observations in other type of cells such as U2OS, where more than 1,900 ubiquitination sites were identified only in the untreated and not in the MG132-treated DiGly-enriched sample (Hansen *et al.*, 2021). Therefore, it is probable that MG132 treatment indeed increases the stoichiometry of proteins that undergo post-translational modification with ubiquitin linkages that are associated with proteasomal degradation, such as K48 and K63, which in turn reduces the detection of ubiquitinated proteins with other ubiquitinated linkages.

Furthermore, another limitation of MG132 was addressed in the case of MV4-11 cells, of which treatment with MG132 induced a two-fold decrease of 15% of the quantified ubiquitinated sites, including the biologically important ubiquitination site K120 on histone H2B (Wagner *et al.*, 2011). In addition, MG132 proteasomal inhibitor is known to induce cell apoptosis through various different pathways. For instance, it induces formation of reactive oxygen species and depletion of glutathione that leads sequentially to mitochondrial dysfunction, cytochrome c release and eventually to cell death (Guo & Peng, 2013). This could justify the identification of ubiquitination sites of stress responsive proteins, including heat shock proteins DNAJ, HSP90 and HSP20, observed in our MG132-derived dataset (data not shown). Similarly, such ubiquitination sites have been upregulated in *Drosophila melanogaster* Schneider's line 2 cells upon MG132 treatment (Sap *et al.*, 2017). Collectively, these undesired side effects caused by MG132 proteasomal inhibitor reported in the literature in combination with the sufficient identification and quantification of ubiquitination sites in MG132-untreated DiGly enriched samples supported our decision of not using a proteasomal

inhibitor. Nevertheless, it is the first ubiquitinomics study which characterised in such extent the ubiquitinome of *L. mexicana* promastigote under both MG132 and DMSO conditions.

4.3.2 Advantages of DUB2^{FLOX/+} Promastigote Cell Line

Upon optimizing the ubiquitinomics workflow for the *Leishmania* promastigote cells, we also needed to generate an inducible KO system for *DUB2*. In this study, we have successfully created a homozygous DUB2^{FLOX/+} promastigote cell line that excises the *DUB2* gene in responses to rapamycin. The diCre inducible system has been used previously to study the essentiality of *DUB2* in the parasite, however our approach has two main advantages: firstly, *DUB2* is tagged C-terminally with an HA tag and secondly, it has a functional T7Cas9 system incorporated inside the parasite (Damianou *et al.*, 2020). The presence of HA tag facilitates detection of *DUB2* in both immunofluorescence and western blotting studies, as used here to detect optimal time-point of *DUB2* rapamycin-induced depletion, but it can also be used to investigate interacting partners of *DUB2* via co-immunoprecipitation (Jones *et al.*, 2022). Moreover, the presence of a T7Cas9 system allows easier manipulation of the parasite's genome, such as tagging promising *DUB2* substrates, which will be beneficial for downstream validation experiments. Nevertheless, four days is the optimal incubation time point with rapamycin for this cell line and the reason for that is two-fold: the vast majority of *DUB2* proteins were degraded up-to that point, with the growth rate of promastigote cells remaining the same. Therefore, we achieved maximum *DUB2* depletion, with minimal induction of promastigote cell-death (Duncan *et al.* 2016). By ensuring that these criteria are met, we increased the chances that the observed alterations in the total ubiquitinome and proteome were driven primarily by the absence of *DUB2* and not due to the activation of downstream cellular-death pathways.

4.3.3 Insights into the Most Promising Substrates of *DUB2*

Focusing firstly on the ubiquitinomics data, there was a significant upregulation in ubiquitination at 122 specific sites upon *DUB2* depletion (limma; $p < 0.05$). Therefore, it is suggested that all these proteins directly or indirectly could be regulated by *DUB2*. An ubiquitination site of the serine-threonine kinase receptor-associated protein (STRAP) had the highest significant increase in its ubiquitination state upon *DUB2* depletion ($\log_2FC = -6.60$), making it the most likely substrate of *DUB2* from this dataset. STRAP is a WD40 domain-containing protein that has cytoplasmic localization in *T. brucei*. However, under sinefungin treatment, which inhibits the trans-splicing process, STRAP is translocated to nuclear periphery granules (Goos *et al.*, 2019). STRAP has been extensively studied in other systems, which collectively suggested that STRAP is involved primarily in antiapoptotic process under normal conditions and in proapoptotic process under stress conditions (Manoharan *et al.*, 2018). Interestingly, STRAP is also part of the Cul4A-DDB1-STRAP E3 ligase complex that is involved in the regulation of cellular resistance to oxidative DNA damage through the stabilization of the polynucleotide kinase phosphatase (PNKP; Parsons *et al.*, 2012). Despite STRAP being associated with this E3 ligase complex, there is no evidence that STRAP is ubiquitinated itself.

The next most likely *DUB2* substrate is the hypothetical protein LmxM.34.3240 ($\log_2FC = -5.80$), of which has no predicted conserved domains apart from a coiled-coil domain, and it was found to be secreted from *L. mexicana* amastigotes (Hamilton, 2019). The *T. brucei* homologue of this protein, Tb927.9.12310, was identified as a cell-cycle-regulated transcript, but this finding has not been validated at the proteomics level (Crozier, 2016). The third most promising *DUB2*-regulated ubiquitination site was found in the amino acid transporter 19 (AAT19). Previously, transcriptomic profiling of AAT19 of *L. amazonensis* revealed a significant upregulation of AAT19 upon differentiation

to axenic amastigote (Aoki *et al.*, 2017). AAT19 is a homologue of sodium-coupled neutral amino acid symporter 1 (SNAT1), which is a transmembrane protein responsible for facilitating the cellular uptake of neutral amino acids, dependent on both sodium and pH levels. SNAT1 contributes in the anabolism and particularly in the synthesis of glutathione, but it is also involved in various cellular signalling pathways, including the mTOR pathway (Yamada *et al.*, 2019). However, neither the hypothetical protein LmxM.34.3240 nor AAT19 was previously reported as ubiquitinated. Therefore, this evidence is the first to suggest that these proteins might be regulated via ubiquitination. In addition, these three proteins will be prioritized for downstream investigations as substrates of DUB2, as they exhibit the highest fold change enrichment in the DUB2-depleted ubiquitinomics dataset.

Nevertheless, all these significantly upregulated ubiquitinated proteins expanding in different biological processes, suggesting that DUB2 might have pleiotropic functions. Interestingly, most of these hits are involved in intracellular localization and trafficking processes. For instance root hair defective 3 (RHD3) is an atlastin GTPase that facilitates the formation of interconnected endoplasmic reticulum (ER) via the formation of homotypic fusions between the ER tubules (Sun *et al.*, 2020). Another three example involved in this biological process are: RAB2B, dynein heavy chain 2 (DHC2.2) and vacuolar protein sorting-associated 45b protein (Vsp45b). RAB2B belongs to the family of Rab-type small GTPases and in its GTP-activated form is responsible to translocate vesicular carriers from donor to acceptor organelles required primarily for the maintenance of a compacted Golgi (Aizawa & Fukuda, 2015; Zhang *et al.*, 2021). Dyneins are eukaryotic motor proteins involved in the intracellular transporting of vesicles using ATP-driven microtubule-based motion. Specifically, DHC2.2 is one of the two cytoplasmic *Leishmania* dynein-2 isoforms participating in flagellum assembly and in the maintenance of the promastigote's cell shape (Adhiambo *et al.*, 2015). Finally, Vps45 is an endosomal Sec1/SM protein involved in the transport of vesicles to vacuoles and in the coordination of SNARE-mediated fusion. Vps45b is one of the two Vsp45 homologues in *L. mexicana*, of which is exact function needs be deciphered (MacDonald *et al.*, 2017; Spence, 2022). Collectively, all these hits are known to be ubiquitinated in other systems, with DHCs being a validated DUB substrate (Lee *et al.*, 2008). This increases the robustness of our ubiquitinomics dataset but it also enhances the hypothesis that DUB2 has a primarily regulatory role in intracellular protein/vesicle trafficking.

From the ubiquitinomics dataset, it is also worth mentioning that some of the significantly upregulated ubiquitinated proteins are also part of the ubiquitin proteasome pathway. Rpn13 and BETA6 (Pup1) are members of the proteasomal 19S regulatory particle and 20S core particle respectively. The former is involved in the binding of ubiquitin-conjugated proteins targeted in the proteasome, of which function is eradicated either under stress conditions or proteasome malfunction via poly-ubiquitination of Rpn13 (Besche *et al.*, 2014). The latter one has a protease activity, resembling trypsin due to the C-terminal cleavage of peptide bonds after basic residues (Arendt & Hochstrasser, 1997). However, there is no evidence that it is regulated via ubiquitination. As well as proteasome components, there are also three proteins involved in the ubiquitination machinery, which are: the E2 conjugating enzyme UBC2, an U-box E3 ligase and the RING-type P197 E3 ligases. UBC2 is one of the most promising substrates of DUB2, thus it is discussed later on. Focusing on the E3 ligases, both U-box and RING-type classes are known to act as scaffold to place E2 and substrate in the optimal orientation to achieve the direct transfer of ubiquitin (Burge 2020; Yang *et al.*, 2021). However, not much is known about their intracellular function in kinetoplastids, apart from RING-type E3 ligase (called P197), which is localized at the tripartite attachment complex and acts as a linking component between basal bodies and the kinetoplast, which is required for a successful kinetoplast division (Gheiratmand *et al.*, 2013). Nevertheless, it is well established that various E3 ligases are regulated via ubiquitination. For instance, the ERAD ubiquitin E3 ligase Hrd1 undergoes autoubiquitination to form

an activated ubiquitin-gated channel, by which its stability and activity is regulated via the deubiquitinase enzyme Ubp1 (Peterson *et al.*, 2019). Finally, the permutated papain-fold peptidases of dsRNA viruses and eukaryotes 4 (PPPDE4) is the last significant upregulated ubiquitinated hit involved in the UPS pathway. PPPDE4 is cysteine peptidase possessing DUB activity and it is localized in two sites of the *L. mexicana* promastigotes: at the endomembrane system and as a distinct punctum at the posterior tip (Grewal *et al.*, 2019). Generally, several DUBs are known to be regulated post-translationally, with ubiquitination affecting substrate interactions, localization and function of the enzyme (Snyder & Silva, 2021). Therefore, it is hinted that DUB2 regulates the UPS at various points, with one possible function being the direct regulation of ubiquitin-dependent proteasomal degradation.

Moving towards the changes in the total proteome of *Leishmania* promastigotes in response to DUB2 depletion, 72 and 50 proteins were identified as significantly downregulated from the DIA and DDA datasets respectively ($p < 0.05$; limma). Comparison of the two datasets revealed an overlap of 21 proteins, which supported our initial hypothesis that the two approaches are complementary. This variation could be attributed to the standardised and shorter isolation window of DIA and the semi-stochastic selection of abundant precursors of DDA. This justification is further supported by the absence of biological and sample-preparation variations due to the usage of equal peptide fractions from the same samples for each replicate per MS mode. Nevertheless, use of both approaches expanded the number of promising hits that their protein levels could be regulated via DUB2 and the ubiquitin-proteasome pathway. Furthermore, the presence of 21 overlapping proteins supports two additional conclusions: firstly, that our datasets are robust, and secondly that these overlapping proteins are likely to be true statistically significant hits, despite exhibiting relatively small fold-change enrichments in the DUB2-depleted proteomics datasets. Moreover, at this point it is worth highlighting that DUB2 was significantly downregulated at both datasets, confirming the successful knockdown of the DUB2 protein in the cell population in response to rapamycin.

In addition, insights into the function of these 21 overlapping proteins highlights the support of two ubiquitinomics-derived statements: DUB2 might play crucial role in the intracellular transport pathway and DUB2 might be an important regulator of various DNA-related events of *L. mexicana* promastigotes. For instance, two of the overlapping hits are the AP-2 associated kinase 1 (AAK1), which is involved in clathrin-mediated endocytosis, and the essential tousel-like kinase 2 (TLK2) that facilitates various nuclear processes, including DNA repair and replication. Interestingly, the former is known to be ubiquitinated and the latter to interact with several E3 ligases, suggesting that these proteins are regulated through the ubiquitination system (Gupta-Rossi *et al.*, 2011; Correia *et al.*, 2019). Moreover, RAD51 and DNA ligase I (LigI) are two other overlapping hits worth mentioning. RAD51 is a recombinase involved in DNA repair but also in the genetic exchange of *T. cruzi* and its presence at the DNA site is regulated through ubiquitination (Inano *et al.*, 2017; Alves *et al.*, 2018). Similarly, LigI is also involved in the DNA repair and replication and its protein levels are regulated via the ubiquitin-proteasome pathway (Peng *et al.*, 2016). Collectively, it is understood that DUB2 could participate in the ubiquitin-dependent proteasomal degradation of these proteins, which has as a subsequent effect at different biological processes such as DNA repair and clathrin-mediated cargo uptake.

4.3.4 Insights into the Overlapping Proteins across Datasets

Apart from selecting STRAP, the hypothetical protein LmxM.34.3240 and AAT19 as the most promising substrates of DUB2 based on their fold-change enrichment in the ubiquitinomics dataset, we also

identified eight more proteins as potential DUB2 substrates. These eight proteins were present in at least two of the following datasets: interactome (IP or proximome), downregulated proteome in response to DUB2 depletion (DDA- or DIA-derived dataset) and/or upregulated ubiquitinome in response to DUB2 depletion (Fig. 22).

Focusing first on the hypothetical protein LmxM.20.1700, it is exclusively found in *Leishmania* species without any identifiable conserved domains, classifying it as an “orphan” protein. In addition, there is no available information regarding this protein, which limits the extraction of any conclusions about DUB2’s function in relation to it. Similarly, no specific studies targeting the 50S ribosome-binding GTPase *Leishmania* protein or its orthologues in other kinetoplastids are available. Nevertheless, insights into its function were gained through its BLAST-derived bacterial orthologue EngA and eukaryotic orthologue LSG1. EngA is an essential GTPase protein primarily involved in ribosomal-associated functions, including the regulation of ribosomal biogenesis, but it is also associated with non-ribosomal functions, such as cell cycle progression and DNA replication (Bharat & Brown, 2014). On the other hand, the eukaryotic homologue LSG1 is exclusively involved in ribosomal biogenesis, contributing to the completion of the peptidyl transferase centre, which leads to the cytoplasmic maturation of the 60S ribosomal subunit (Kargas *et al.*, 2019). Both the hypothetical protein LmxM.20.1700 and the LSG1 protein were the only proteins among these eight overlapping hits that show no ubiquitination sites in any of our ubiquitinomics datasets. Thus, it is more likely that DUB2 has a regulatory effect on the function and abundance of both the hypothetical protein LmxM.20.1700 and the LSG1 protein, rather than them being direct substrates of DUB2. As a result, these proteins are excluded from downstream validation experiments.

The next two promising substrates - rab-GDP dissociation inhibitor (GDI) and the 2, 3-bisphosphoglycerate-independent phosphoglycerate mutase (iPGMA) - were found significantly enriched in the interactomics and upregulated ubiquitinomics datasets. So far, these proteins have never been identified to possess ubiquitination sites, making this study the first to report them as ubiquitinated. iPGMA is responsible for interconversion of 2- and 3- phosphoglycerates during glycolysis and gluconeogenesis. The cytosolic function of iPGMA relies on the presence of a divalent metal ion, with cobalt being the most favoured choice in the parasites *T. brucei* and *L. mexicana* (Chevalier *et al.*, 2000; Guerra *et al.*, 2004). It is also worth mentioning that there are no orthologues of this enzyme in humans, making it a selective target for drugs (Crowther *et al.*, 2014). On the other hand, GDI is an evolutionary conserved paralogue of Rab escort proteins (REP) that exhibits a higher affinity for GDP-bound and geranyl-geranylated Rab proteins. Specifically, GDI facilitates the extraction of the GDP-bound inactive Rab proteins from their associated membrane into the cytosol and also contributes to the delivery of GTP-bound active Rab proteins back to the targeted membrane (Pylypenko *et al.*, 2018). Similarly, the overall role of GDI in the intracellular trafficking is conserved in the *Leishmania* parasite with the only difference that it has only one GDI isoform instead of three, which is the case in mammals (Alory and Balch, 2003; Kumar *et al.*, 2016). Collectively, DUB2 is highly possible to regulate directly both of these proteins, expanding the contribution of DUB2 into carbohydrate metabolism and intracellular protein trafficking.

In regard of the remaining four promising substrates, there is previous evidence of them possessing ubiquitination sites either in *Leishmania* or other eukaryotes. For instance, the *Leishmania* ubiquitin-conjugating enzyme E2 (UBC2), which functions in the cellular transformation of the parasite from promastigote to amastigote, might be auto-regulated. This was hypothesised due to the identification of an *in-vitro* auto-ubiquitination event. Similarly, an *in-vitro* auto-ubiquitination event has also been identified in its human orthologue UBE2N on residue K92, which corresponds to K90 in UBC2 (McKenna *et al.*, 2001; Burge *et al.*, 2020). Indeed, in our ubiquitinomics dataset we have identified

K90 to be ubiquitinated, but also K80 and K63, of which only K63 ubiquitination site was significantly upregulated in response to DUB2 KO. Regardless, it is suggested that UBC2 is regulated at different levels *in vivo*, as previously observed in its yeast homologue Ubc13, and DUB2 might have an activating regulatory function (reviewed by Hodge *et al.*, 2016). At this point it is worth mentioning that UBC2 forms K63-linked di-ubiquitin chains *in vitro* but only when it is in a heterodimer complex with the E2 inactive variant UEV1 (Burge *et al.*, 2020). Interestingly, UEV1 was also found to be ubiquitinated and upregulated upon DUB2 KO, however it was not significant.

The cleavage and polyadenylation specificity factor (CPSF73) is another promising substrate of DUB2 that is known to be ubiquitinated in both yeast and humans (Lee *et al.*, 2020; Liu *et al.*, 2022). This ubiquitination event is performed by the HECT-like E3 ligase UBE3D and it is responsible to target the CPSF73 protein for proteasomal degradation. However, multiple ubiquitination sites have been identified on CPSF73 and the one involved in ubiquitin-dependent proteasomal degradation has not been characterised (Chen *et al.*, 2014). Nevertheless, multi-ubiquitination sites have been also identified in our ubiquitinomics dataset, with only one of the sites being significantly upregulated in response to DUB2 KO. This combined with the conserved function of CPSF73 across eukaryotes as an essential endonuclease, which is responsible of cleaving pre-mature mRNAs in order to become polyadenylated and then exported as mature mRNAs in the cytoplasm, suggests that the regulation of CPSF73 post-translationally is also evolutionary conserved (Koch *et al.*, 2016). DUB2 might contribute in the stability of CPSF73 by rescuing it from proteasomal degradation, providing DUB2 an additional cellular role in RNA editing.

Next, 40S ribosomal protein SA (RPSA) is another promising substrate of DUB2 that is overall found in two forms: the 37-kDa and 67-kDa. The former form is found in both the nucleus and cytoplasm and interacts with the 40S small ribosomal subunit (Malygin *et al.* 2011). The latter form is found embedded in the plasma membrane, enriched in lipid rafts, and it is involved in various signalling pathways contributing to early cortical development and neuromorphogenesis. The PEDF-RPSA-Itga6 signalling pathway is one of them, of which membrane stability of RPSA is determined by the competitive relation of Itga6 with the Nedd4 HECT type E3 ligase. For instance, if Itg6 protein is not present in the membrane then RPSA is getting ubiquitinated and destabilised and vice versa (Blazejewski *et al.*, 2022). In kinetoplastids, RPSA was found to co-immunoprecipitate with the RNA-binding proteins Alba1 and Alba3 in *Leishmania* promastigotes and amastigotes respectively, and with the telomerase subunit homolog La in *T. brucei* (Dupé *et al.*, 2015; Shan *et al.*, 2019). This might suggest that RPSA is involved in both the control of the developmental gene expression and the maintenance and modification of chromatin in *Leishmania*. Furthermore, RPSA proteins levels significantly decreased in response to LeishF3d KO, supporting the interlinking of RPSA between the cap-dependent activity and protein synthesis of the *Leishmania* parasite (Bose *et al.*, 2023). Collectively, regulation of RPSA through DUB2 could affect all the stated RPSA cellular functionalities, supporting further the so-far pleiotropic function of DUB2.

Finally, the last promising substrate of DUB2 is the small ubiquitin protein (SUMO), of which has two ubiquitination sites (K39 and K51) that were significantly upregulated in response to DUB2 depletion. SUMOylation is an ubiquitin-like eukaryotic post-translational modification involved in various biological processes as reviewed elsewhere (Celen & Sahin, 2020). However, the hybrid ubiquitin/SUMO chains have been studied in a smaller extent and such chains are predominantly occurred upon specific stressors (Pérez *et al.*, 2020). For instance, ubiquitination of the SUMOylated protein xeroderma pigmentosum C (XPC) drives the recruitment of XPC at UV-damaged DNA sites (Poulsen *et al.*, 2013). In addition, Ub/SUMO chains are also involved in maintaining genome stability

and in targeting proteins for proteasomal degradation (Guzzo *et al.*, 2012; Erker *et al.*, 2013). However, no such hybrid chains have been reported in the SUMOylome of *T. cruzi* and *T. brucei* (Bayona *et al.*, 2011; Iribarren *et al.*, 2015). Interestingly, DUBs such USP7, USP11 and Ataxin-3 (ATX3) have the ability to detect poly-SUMOylated proteins and then sequentially to modify the ubiquitin chains on these SUMOylated targets via deubiquitination. These DUBs are known as SUMO-targeted ubiquitin proteases (STUPs) and so far their action has been associated with DNA replication, regulation of nuclear bodies and DNA maintenance (Hendriks *et al.*, 2015; Lecona *et al.*, 2016; Pfeiffer *et al.*, 2017). Therefore, it is suggested that DUB2 might also be a STUP involved in various nuclear processes that are regulated by hybrid ubiquitin/SUMO chains.

At this point, it is worth mentioning that these conclusions were based on independent analyses of the total ubiquitinomics and proteomics datasets in response to DUB2 depletion. Therefore, the occupancy of each protein was not taken into consideration, introducing the first limitation of this chapter. Manual inspection of the significantly modified proteins in both the ubiquitinomics and proteomics datasets revealed 4 overlapping proteins: macrophage migration inhibitory factor-like protein (LmxM.32.1750), glycosomal membrane protein-like protein (LmxM.28.2250), ARM-like helical domain-containing protein (LmxM.30.2170), and ubiquitin carboxyl-terminal hydrolase (DUB2; LmxM.08_29.2300; data not shown). The first three were significantly upregulated in response to DUB2 depletion in both the ubiquitinomics and proteomics data, while the latter, as expected, was significantly downregulated in both datasets. As a result, conclusions regarding the significant changes in their ubiquitination levels were treated with caution, leading to the deprioritization of the first three proteins for future DUB2 substrate investigations. Further analysis of the significantly modified proteins in response to DUB2 depletion revealed that 64 were ubiquitinated, however without a significant change (data not shown). Focusing specifically on the significantly downregulated proteins, 26 and 13 proteins from the DIA and DDA datasets, respectively, were found to be ubiquitinated (Tables 6 & 7). Considering the occupancy of these proteins, it is suggested that the ubiquitination levels were increased in response to DUB2 depletion, making them potential DUB2 substrates. However, recognising the importance of occupancy, additional bioinformatics analysis is required for finalizing these conclusions, which can be conducted using Perseus (Tyanova *et al.*, 2016).

To summarize, we developed a robust ubiquitinomics workflow in *L. mexicana* promastigotes, which facilitated in the identification of changes in the total ubiquitinome of the parasite in response to loss of DUB2. Taken together these results with the ones from the proteomics and interactomics experiments, we concluded that DUB2 has a pleiotropic function with the most likely contribution into the regulation of the intracellular trafficking, DNA maintenance and ubiquitin proteasome pathway. For future work, these substrates could be validated as follows; substrates could be endogenously tagged in the T7Cas9 DUB2^{FLOX/+} promastigote cell line; treat cells with DMSO or rapamycin; perform immunoprecipitation against the substrate; observe changes on the ubiquitination state of the immunoprecipitated substrate. It is expected that in the absence of DUB2, there would be an increase in ubiquitination on the substrates.

5 Biochemical Assays against *Leishmania* DUBs and Small Molecule Inhibitor Discovery against DUB2

5.1 Introduction

Overall, many proteases, including cysteine proteases, are expressed as inactive precursors. To become proteolytic active, the inactive proteases require to undergo an irreversible or reversible activation. The former activation process involves proteolysis of the inhibitory prodomains from the inactively expressed zymogen, and the latter one can be carried out via PTMs, pH or localization change, and interaction with other proteins (Sanman & Bogyo, 2014). Similar regulation mechanisms are applied to the activity of many DUBs (Lange, Armstrong & Kulathu, 2022). For instance, the binding of WDR20 and WDR48 proteins to the USP46 has a synergistic effect on the structural conformation around the catalytic centre of the DUB, enhancing the substrate-binding and allosterically activating the USP46 (Zhu *et al.*, 2019). Thereby, the thiol group of the active site cysteine performs a nucleophilic attack against the isopeptide bond that links the C-terminus of the ubiquitin with its substrate, causing cleavage of the ubiquitin. To study the activation state of DUBs, as well as their enzymatic activity, various assays utilizing either activity-based probes (ABPs) or ubiquitin-based substrates have been developed (Gui, Paudel & Zhuang, 2020; Gorka, Magnussen, & Kulathu, 2022; Huppelschoten, 2022).

5.1.1 Activity-Based Probes

Focusing first on the DUB-targeting ABPs, the vast majority of them are ubiquitin-based molecules, which act as a DUB substrate and covalently attach at the active site of the DUB (Gorka, Magnussen, & Kulathu, 2022). However, the ABP itself does not get cleaved by the DUB, facilitating the detection of ABP-labelled DUBs. This irreversible attachment is achieved via one of the three ABP components, the reactive group (a.k.a. warhead). The reaction group is an electrophile that reacts with the nucleophilic catalytic cysteine of DUBs through one of the following reaction mechanisms: direct addition (e.g. ubiquitin-propargylamide; Ub-PA; Ekkebus *et al.*, 2013), conjugate addition (e.g. ubiquitin-vinyl methyl ester; Ub-VME; Borodovsky *et al.*, 2002), nucleophilic substitution (e.g. ubiquitin-bromoethyl; Ub-Br₂; Borodovsky *et al.*, 2002), or disulfide exchange (ubiquitin-disulfide; Ub-DiS; de Jong *et al.*, 2017). The other two components of the DUB-specific ABP are the recognition element and the reporter tag, which are also referred to as targeting group and label or handle, respectively. The former component of an ubiquitin-based ABP consists of either a full-length mono- or multi-ubiquitin molecule, and it is responsible for recruiting the ABP to the ubiquitin-binding domain of the DUBs, and therefore it provides specificity and selectivity (Ekkebus *et al.*, 2013; Mulder *et al.*, 2014). Furthermore, the attachment of ubiquitin at the ubiquitin-binding domain of the DUB facilitates structural rearrangements of the DUB catalytic site, ensuring accessibility of the electrophilic reactive group at the nucleophilic catalytic cysteine (Hu *et al.*, 2002; Hu *et al.*, 2005). In regards of the latter ABP component, the reporter tag allows the detection and enrichment of APB-labelled DUBs. Fluorophores, including Cyanine5 (Cy5), and affinity tags, including HA, are utilized for detecting ABP-labelled DUBs through *in-gel* fluorescence and immunoblotting analysis, respectively. Additionally, HA and biotin are among the reporter tags that are used for enriching and purifying ABP-bound DUBs, which DUBs can be then identified via MS (Gorka, Magnussen, & Kulathu, 2022).

5.1.2 Applications of ABPs

Ubiquitin-based ABPs have been used extensively in various applications. For instance, ABPs lacking the reporter group (e.g. Ub-VME) have been utilized in crystallographic studies as a non-cleavable DUB substrate to promote ordering and stabilization of the investigated DUB, and also to provide better understanding of their catalytic mechanism. This approach facilitated the structural characterisation of either full-length or the catalytic domain of multiple active DUBs, as reviewed by (Gorka, Magnussen, & Kulathu, 2022). The *Legionella pneumophila* Lem27 is a specific example of a truncated protein characterised structurally while in complex with Ub-PA probe (Liu *et al.*, 2020). The introduction of a reporter tag leads to the second application of ubiquitin-based ABPs, which is known as activity-based protein profiling (ABPP). ABPP identifies the active DUBome that is present in the extracts of studied cells. For instance, a chemoproteomics-based ABPP workflow, combining the enrichment of HAUbPA-labelled DUBs via anti-HA immunoprecipitation, followed by a high-pH pre-fractionation post-trypsinisation and label-free quantitative analysis by LC-MS/MS, revealed the presence of 74 active DUBs in MCF7 crude extracts (Pinto-Fernández *et al.*, 2019). Similarly, ABPP has been used extensively in detecting active DUBs in pathogenic organisms extending from parasitic protozoa, such as *Toxoplasma gondii* and *L. mexicana*, to viruses, including *Adenoviridae* and *Herpesviridae* (Balakirev *et al.*, 2002; Kattenhorn *et al.*, 2005; Frickel *et al.*, 2007; Damianou *et al.*, 2020). Furthermore, it has contributed in the tracking of DUB activities in response to various *in vivo* conditions. For example, Damianou *et al.* (2020) utilized Cy5UbPA-based ABPP to show that the active DUBome of *L. mexicana* remain constant through the life cycle of the parasite. Additionally, ABPPs led to the discovery of novel DUBs, including the OTU DUB family in HeLa cells, underscoring once more the essential function of ABPs (Balakirev *et al.*, 2003).

Ub-based ABPs have also been utilized in the identification of candidate DUB inhibitors. This assay is known as competitive-ABPP, in which intact cells or cell extracts are incubated with a compound of interest, and then its cell lysate is treated with an ABP. If the investigated compound inhibits the activity of a DUB, then the ABP will not be able to bind to this DUB, leading to the reduction of detected ABP-bound DUB compared to the untreated control. Therefore, this compound would be categorised as promising DUB inhibitor. This approach is ideal for compounds inhibiting DUBs either allosterically or by binding covalently (irreversible inhibitor) to their active catalytic site. However, if the tested compound has lower binding affinity to the DUB (reversible inhibitor) than the ABP, then it will be most likely outcompeted by the ABP, unless the incubation time of the ABP is reduced (Altun *et al.*, 2011; Reverdy *et al.*, 2016; Harakandi *et al.*, 2021). Two striking applications of competitive-ABPP, combining immunoblotting and quantitative mass spectrometry, led to the characterisation of specific inhibitors FT671/FT827 and FT206 against the MFC7-breast cancer cell - derived USP7 and NCI-H520 lung squamous cell carcinoma cell-derived USP28, respectively (Turnbull *et al.*, 2017; Ruiz *et al.*, 2021). However, in both cases the competitive-ABPP was used as a late-stage drug characterisation. To overcome this, the high-throughput-compatible ABPP (ABPP-HT) was developed. Briefly, a liquid handling platform was used to performed ABPP-targeted immunoprecipitations and sample preparations, and timsTOF LC-MS/MS was utilized at runtimes as short as 15 min, to identify and quantify the enriched ABP-bound DUBs. This advanced ABPP approach allowed the screening of 100 samples per day, increasing the throughput of competitive-ABPP and thereby, making it ideal for HT compound screening in early stages of DUB-targeted drug discovery (Jones *et al.*, 2021; Jones *et al.*, 2022).

5.1.3 Cleavable Ubiquitin-Based Substrate

At this point, it is worth mentioning that cleavable ubiquitin-based substrates have also been incorporated in high-throughput screening (HTS) of small molecule libraries against recombinant DUBs. The first cleavable substrate, which was amenable for HTS-based DUB activity profiling, was the ubiquitin-7-amino-4-methylcoumarin (Ub-AMC) substrate. The AMC moiety is directly attached to the C-terminus of ubiquitin via an amide bond, and cleavage of that bond via an active DUB leads to the release of the AMC dye (Dang *et al.*, 1998). The free AMC dye has an enhanced fluorescence, and changes in fluorescence levels can be monitored via fluorescence spectroscopy (excitation 380 nm, emission 460 nm; Dang *et al.*, 1998). Ub-AMC was used in the first HTS, which was conducted against the recombinant UCHL1 protein, using a library of 42,000 compounds. As in the case of competitive-ABPP, the principle of distinguishing inhibitor compounds was as follows: if the compound inhibited the recombinant DUB, then the Ub-AMC will not be cleaved and no change in fluorescence will be detected. False positives were eliminated through a demonstration of the absence of AMC quenching in the sole presence of the compound, as well as through a dose-response investigation. Through this study, a competitive UCHL1 inhibitor, known as LDN-57444, was discovered (Liu *et al.*, 2003).

Nevertheless, the excitation wavelength of AMC falls in the same UV range of many compounds used in a screen, leading to the recording of no or unreliable signal. This case is predominant for enzymes with low K_m , in which less substrate is used (Hassiepen *et al.*, 2007). As an alternative, ubiquitin-rhodamine110-glycine (Ub-Rho110-G or Ub-Rho) was developed. Ub-Rho is a non-fluorescent substrate which, upon cleavage of ubiquitin by an active DUB, becomes fluorescent due to the release of monosubstituted rhodamine (excitation/emission at 485 nm / 535 nm; Hassiepen *et al.*, 2007). Chen *et al.* (2011) incorporated Ub-Rho in a HTS for the first time, in which a library of ~10k bioactive small molecules was screened against the recombinant USP1/UAF1 complex (UAF1 is an essential interacting partner required for the USP1 DUB activity). Each compound was tested in a dose-response manner, and the most active compounds were validated as DUB inhibitors via an orthogonal diubiquitin cleavage assay. Subsequently, compounds were tested for DUB selectivity, and two compounds, pimozone and GW7647, were identified as USP1/UAF1-specific inhibitors (Chen *et al.*, 2011). An Ub-Rho-based HTS was also employed by the Buhrlage group in collaboration with Novartis, which led in the identification of several highly selective DUB inhibitors. However, instead of prioritizing HTS compounds solely on their potency, they incorporated DUB selectivity as an additional early priority factor. Specifically, they screened in parallel ~50k small molecules against 8 different human DUBs. Compounds inhibited the catalytic activity of only one of the tested DUBs, with IC_{50} less than 10 μ M and maximum DUB inhibition of more than 80%, were selected as starting points for downstream medicinal chemistry optimization (Varca *et al.*, 2021).

5.1.4 Aims

In this chapter, we aimed to develop a competitive-ABPP to investigate whether chemical compounds provided by Cobb's lab inhibit active DUB proteins extracted from *L. mexicana* promastigote cells. This assay was developed utilizing the already established Cy5UbPA-based ABPP method (Damianou *et al.*, 2020). In addition, we expressed and purified the recombinant *LmDUB2* protein, as described elsewhere (Damianou *et al.*, 2020). Previous biochemical assays showed that this protein is catalytic active and has broad di-ubiquitin cleavage specificity (apart from Lys27 and Met1; Damianou *et al.*, 2020). Nevertheless, we provided further insights into its biochemical properties, including preferential ABP-binding conditions and oligomerization state. Furthermore, as previously mentioned, DUB2 is one of the four essential DUBs in *L. mexicana*, making the protein a promising therapeutic

target. Thereby, we performed in collaboration with Novartis an Ub-Rho-based HTS against the *LmDUB2* recombinant protein, using a curated library of ~50k small molecules.

In short, we completed the subsequent actions in a specific sequence to accomplish our objective:

- Development of competitive-ABPP using the Cy5UbPA probe.
- Test and validate whether 8 chemical compounds are inhibitors of *L. mexicana* promastigote DUBs.
- Purification of recombinant *LmDUB2* expressed using the baculovirus expression system.
- Investigate oligomerization state of *LmDUB2* using SEC-MALLS and native-PAGE gel.
- Optimize incubation conditions and Ub-PA probe-to-*LmDUB2* ratio.
- Optimize Ub-Rho-based HTS conditions for *LmDUB2*, including buffers and substrate/protein concentrations.
- Perform a screen of ~50k compounds against *LmDUB2*.
- Perform dose response screens of compounds identified as inhibitors against *LmDUB2* and *TcDUB2*, to identify the potency of the true inhibitors.

5.2 Results

5.2.1 Competitive Activity Based Protein Profiling for *Leishmania* DUBs

As mentioned in the introduction, one way of investigating whether a chemical compound is inhibiting active DUBs *in vivo* is by performing competitive activity based protein profiling (ABPP), using an activity based probe (ABP; Fig. 23A; Turnbull *et al.*, 2017). To apply this methodology in *L. mexicana*, we modified the already established protocol developed by Damianou *et al.* (2020), which utilizes the Cy5-ubiquitin-propargylamide (Cy5UbPA) probe. We firstly reduced the incubation time of the probe, minimizing the possibility of future tested non-covalent inhibitors to be outcompeted by the ABP. From the investigated incubation times of the probe with T7/Cas9 *L. mexicana* promastigote cell extracts, we found that 5 min is the minimal incubation time of the probe, which preserves sufficient labelling of active DUBs (Fig. 23B). Next, we introduced an incubation step prior to the addition of ABP, in which we added the tested compound at 30 μ M for up to 1 h. To test whether our competitive ABPP is applicable, we incubated our cell extracts with HBX 41 108, a known non-specific covalent DUB inhibitor (Colland *et al.*, 2009; Ritorto *et al.*, 2014). Indeed, HBX 41 108 inhibited most of the active *Leishmania* DUBs compared to the DMSO-treated samples (Fig. 23C). We also included a DMSO-treated cell extract in the assay as a reference of the expected active DUB profile of the T7/Cas9 promastigotes, and also, to show that the DMSO, which was used as the solvent for the inhibitors, is not the one responsible for any observed DUB inhibition (Fig. 23C).

Finally, we screened 8 potential DUB inhibitors, which were provided by Steve Cobb's lab, against the cell extracts of T7/Cas9 promastigotes. Previously, Kaiser *et al.* (2015) developed a drug repurposing strategy, which investigated whether 100 approved and established drug and drug-like molecule have an antiprotozoal activity. A similar approach was performed by Steven Cobb's lab against *Leishmania* promastigotes and amastigotes and they discovered several significant compounds inhibiting the *Leishmania* growth, including zinc pyrithione (unpublished data). Zinc pyrithione (ZnPT) is a Food and Drug Administration (FDA) – approved antidandruff agent that is selectively cytotoxic against various cancer cell lines (Zhao *et al.*, 2017). Its mechanism of action involves the inhibition of the human proteasome-associated DUBs, USP14 and UCHL5. Ciclopirox and piroctone olamine share similar functional groups to pyrithione, and therefore we tested whether all these compounds, including 4 derivatives of pyrithione, inhibit any *Leishmania* DUBs. DMSO and HBX 41 108 were used as negative and positive controls, respectively. We further loaded only the ABP mixed in lysis buffer, to detect possible oligomerization of the probe.

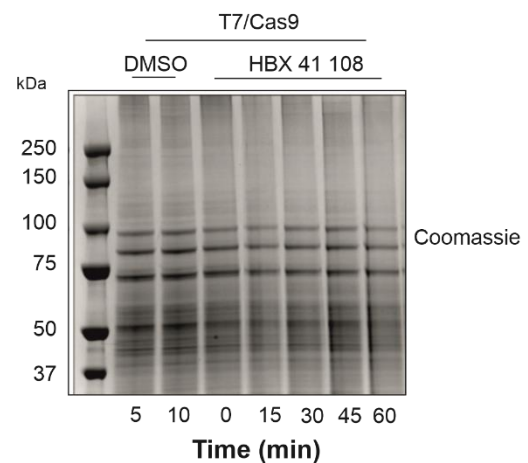
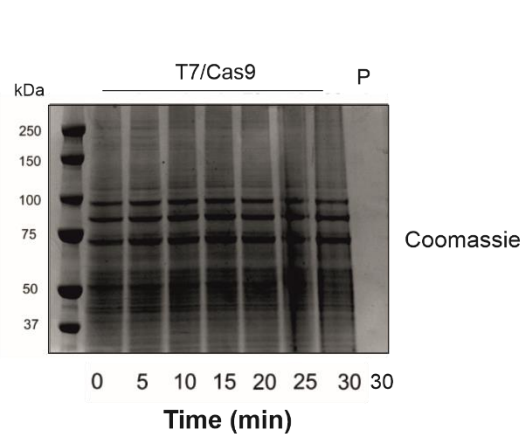
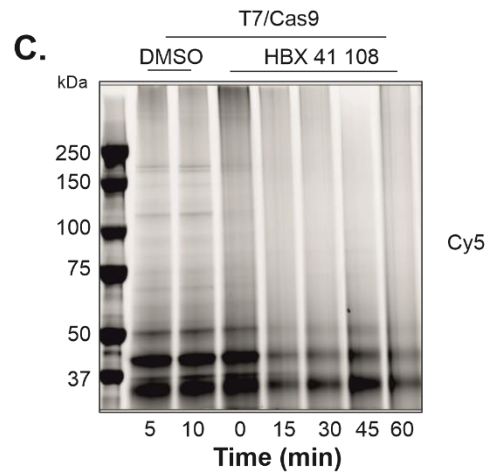
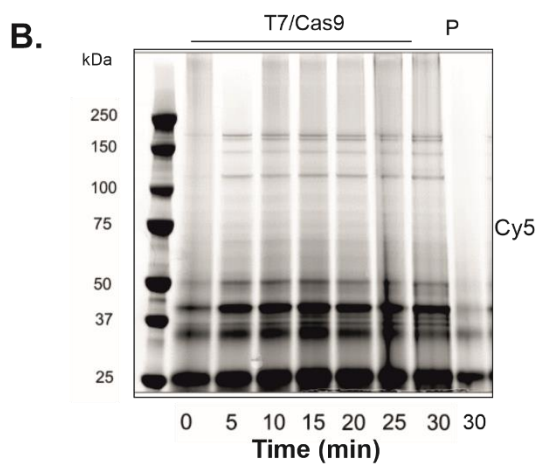
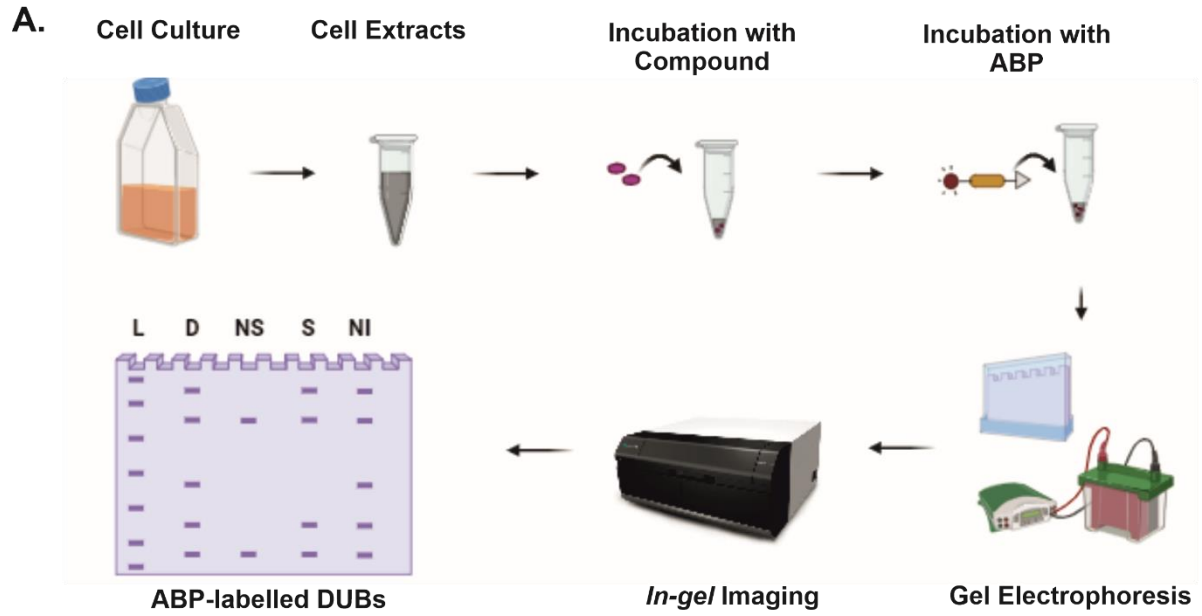


Figure 23: Development of competitive ABPP. **A.** Workflow of competitive ABPP, in which *L. mexicana* promastigote cells are lysed and a fraction of their cell extract is incubated with a compound of interest. Then, the ABP is added. The mixture is loaded onto a SDS gel and a gel electrophoresis is performed, followed by in gel imaging using the Typhoon gel imager. ABP-labelled DUBs (= active

DUBs) are visualized and the band profile determines whether the investigated compound is a DUB inhibitor. The four possible results are as follow: no change in the labelling pattern (DMSO = D, non-inhibitor = NI), absence of several bands (non-specific DUB inhibitor; NS), and a single band is missing (specific DUB inhibitor; S). Ladder (L) was also included in the schematic. **B.** Investigation of shortest incubation time for Cy5UbPA probe, using *L. mexicana* promastigote T7/Cas9 cell extracts. Subsequent of in gel Cy5 imaging, the gel was stained with Coomassie Blue to observed total protein loading per sample. Probe treated with lysis buffer (P) was used as a control, to observe whether the probe oligomerizes under the investigated conditions. **C.** Various incubation times of HBX 41 108 with *L. mexicana* promastigote T7/Cas9 cell extracts, prior Cy5UbPA addition. DMSO was used as a negative control. Coomassie Blue was used as loading control.

Nevertheless, pyrithione (PYR) and its four derivatives HP05, HP12, HP13 and HP16, inhibited clearly at least two DUBs (~40 kDa and ~50 kDa; Fig. 24A). The 40 kDa band was expected to be DUB16 due to its molecular weight (~25kDa the protein itself and ~9kDa the attached probe) and its band position, as determined by the previous mapping of ABP-labelled DUBs (check: Damianou *et al.*, 2020). Similarly, the 50 kDa band was predicted to be the DUB15 (~34 kDa). DUB15 is a non-essential DUB, while DUB16 is one of the four essential DUBs in *L. mexicana*. Thus, DUB16 inhibition could explained the anti-leishmanial activity of the compound. Focusing on DUB16, we validated its identity onto the gel by including a DMSO-treated cell extract derived from the T7/Cas9 DUB16-overexpressing ([DUB16]) cell line (Fig. 24A). Next, we repeated the competitive ABPP against all the investigated compounds three times independently (Fig. 24B&C) and we quantified the intensities for the DUB16 and DUB17 bands. We selected DUB17 (band at ~45kDa) as a control, since no obvious inhibition was observed from the tested compounds. We normalized the band intensities using the quantified intensity of the total proteome, which was revealed upon staining the same gels with Coomassie Blue (Fig. 24A-C). Kruskal-Wallis analysis revealed a significant inhibition of DUB16 upon treatment with PYR, PYR-derivatives and the HBX 41 108 positive control (Fig. 24D). On the other hand, DUB17 is only inhibited by HBX 41 108 (Fig. 24E). Therefore, it was concluded that PYR and its derivatives significantly inhibit the essential DUB16 of *L. mexicana*.

PYR and its derivatives were found by Cobb's lab to inhibit *L. mexicana* growth. Thus, our next question was whether the inhibition capacity of these compounds was solely attributed to the targeting of the essential DUB16. To investigate that, we calculated the EC₅₀ of PYR and its derivative, HP13, against log-phase T7/Cas9 (basic DUB16 protein levels) and T7/Cas9 [DUB16] promastigote cells, using the AlamarBlue assay (check chapter 3). If the compounds target the essential DUB16 and not any other essential proteins, then we expected that the DUB16 overexpression will increase the EC₅₀ values of the compounds, indicating resistance. As a positive and negative control, we included miltefosine and DMSO, respectively. The calculated EC₅₀ for HP13 was 0.41 μM for T7/Cas9 promastigotes and 0.45 μM for T7/Cas9 [DUB16] promastigotes (n=3; Fig. 24F). As about PYR, the EC₅₀ values were 0.21 μM and 0.22 μM, respectively (n=3; Fig. 24G). Similar observations between the two cell lines were recorded in response to miltefosine and DMSO (Fig. 24H&I). Collectively, these results show that PYR and HP13 affect almost identically the survival growth of the two cell lines, despite the overexpression of DUB16 protein levels in one of them. Therefore, it was concluded that these compounds inhibit other essential processes within the *Leishmania* promastigotes, including the deubiquitination activity of the essential DUB16.

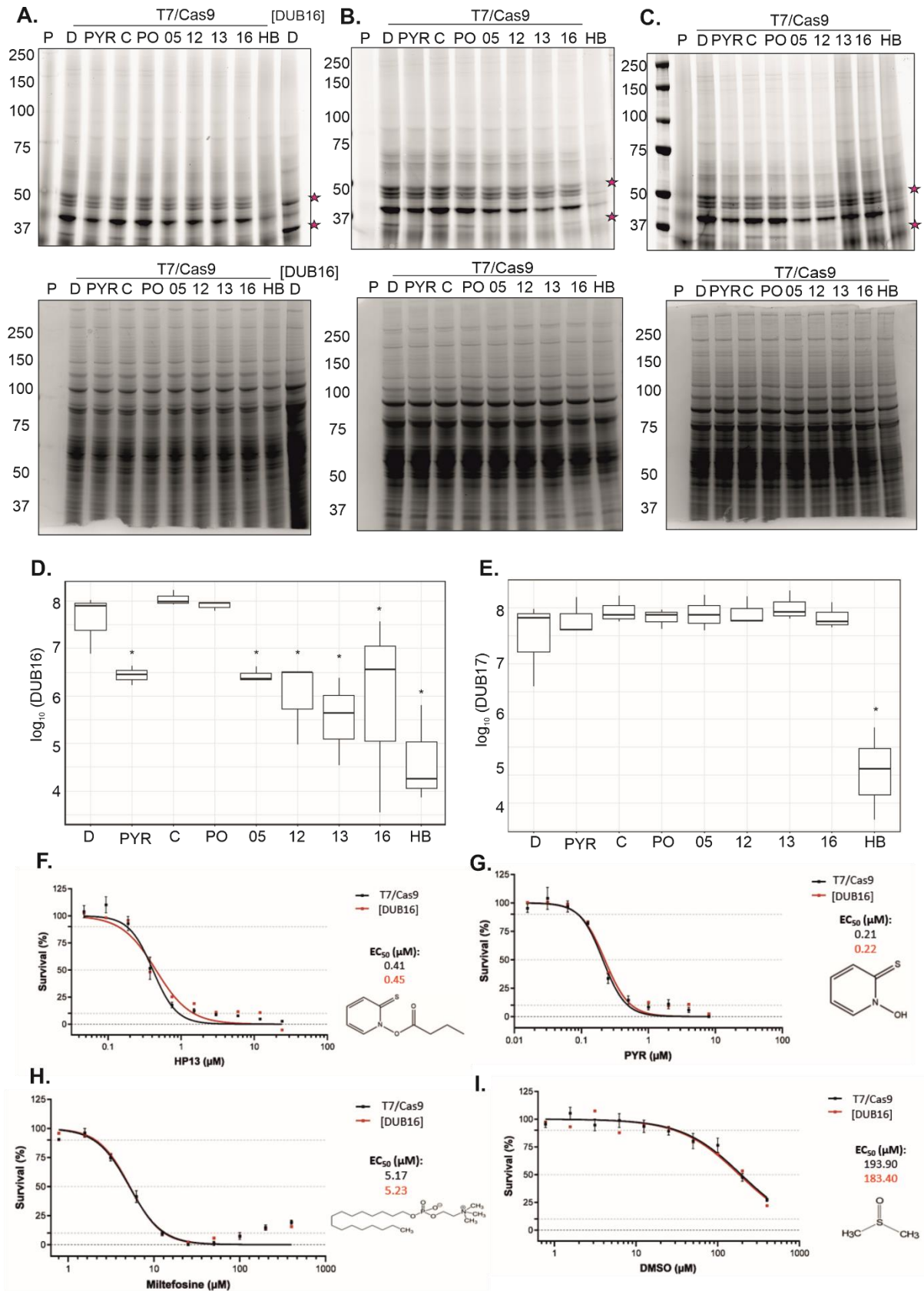


Figure 24: Investigation of possible *L. mexicana* DUB inhibitors. A. The 8 compounds provided by Steve's Cobb lab were tested whether they are DUB inhibitors, using the Cy5UbPA-based competitive-

ABPP against *L. mexicana* T7/Cas9 cell extracts. DMSO and HBX 41 108 were used as negative and positive control respectively. T7/Cas9 [*DUB16*] cell line was used as a reference for identifying the ABP-bound DUB16 band. All investigated compounds were tested at a final concentration of 30 μ M. Post in gel imaging, the gel was stained with Coomassie Blue to detect total protein load per sample. **B. & C.** The same experiment described in A. was repeated twice more, however the T7/Cas9 [*DUB16*] cell line was omitted. The stars indicate the 50 kDa and 40 kDa inhibited DUB15 and DUB16, respectively. **D.** The intensity of Cy5UbPA-labelled DUB16 bands were quantified for each compound, for all three independent experiments and normalised against the Coomassie Blue loading control. Values were plotted in \log_{10} (y-axis). Kruskal-Wallis was used as a statistical method, which revealed significant inhibition of DUB16 in the presence of pyruvate (PYR), its derivatives (HP05, HP12, HP13, HP16) and of the positive control HBX 41 108 (HB), compared to the DMSO negative control (D). Stars indicate compounds that significantly inhibited DUB16 and the p-value of the analysis was 0.01. **E.** The same analysis was repeated for the DUB17 band. Kruskal-Wallis analysis revealed no significant inhibition of DUB17 from any of the investigated compounds, apart from the HBX 41 108 positive control. Stars indicate compounds that significantly inhibited DUB17. **F.** AlamarBlue assay was used to calculate EC₅₀ of HP13 compound against *L. mexicana* T7/Cas9 and T7/Cas9 [*DUB16*] promastigote cell cultures. Fluorescence intensity values for each tested concentration of the inhibitor, per cell line, were converted to percentages of survival and fitted to a sigmoid curve. For 100% survival, the fluorescence values detected in the absence of the inhibitor were used, and for 0% survival, the fluorescence values detected from the highest concentration of the inhibitor were employed. Each data point represents the mean of 3 replicates, and the error bars represent a standard error of the mean. This analysis was performed in Prism (GraphPad). Similarly, the same experiment was performed to test the impact of **G.** pyriithione (PYR), **H.** miltefosine (positive control) and **I.** DMSO against both T7/Cas9 and T7/Cas9 [*DUB16*] promastigote cells.

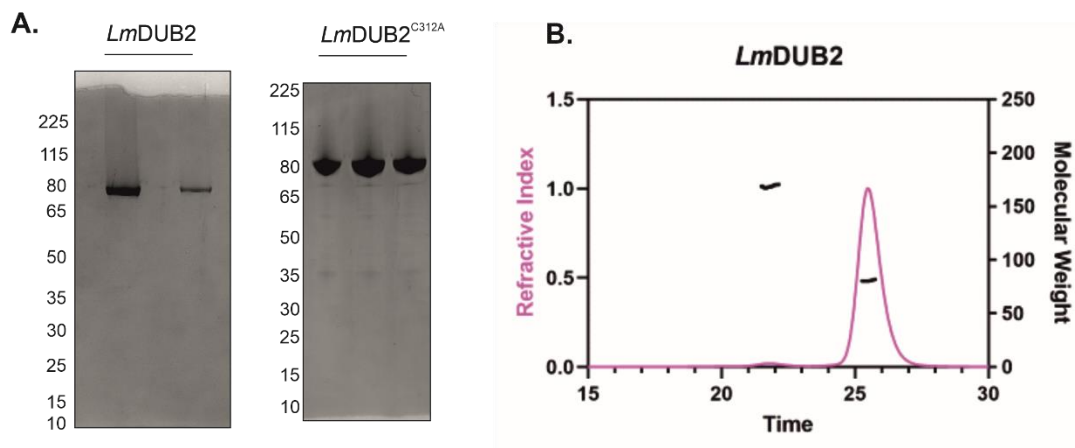
5.2.2 Expression and Characterisation of *LmDUB2* Recombinant Protein

Previously, Damianou *et al.* (2020) successfully expressed and purified recombinant *L. mexicana* DUB2 (*LmDUB2*) and its catalytic inactive mutant (*LmDUB2*^{C312A}) using the baculovirus expression system. The reason of selecting this expression system was two-fold: firstly, due to previous unsuccessful attempts of expressing full-length *LmDUB1* protein in *E. coli* (unpublished), and secondly, due to previous successful recombinant expression of its trypanosomal orthologue DUB1 using the same system (unpublished). Nevertheless, we managed to express and purify both recombinant *LmDUB2* and *LmDUB2*^{C312A} proteins, using the same protocol (Fig. 25A; Damianou *et al.*, 2020).

Next, we were interested on investigating the oligomerization state of *LmDUB2*. To do that, we performed a size-exclusion chromatography multi-angle laser light scattering (SEC-MALLS) approach, which combines measurements of the refractive index and multi-angle laser light scattering to estimate the molecular weight of recombinant proteins. According to the chromatograms, there are two peaks in the refractive index: one major and one minor. The major peak has an estimated MW of 82 kDa, consistent with monomer (Fig. 26B). This makes up about 95% of the material eluted, with about 2.5% present in the minor peak which has MW consistent with a dimer (Fig. 25B). There is a small amount of higher MW material eluting as a mixture (just visible in the chromatograms; data not shown). Therefore, it was concluded that *LmDUB2* predominantly exists in a monomeric form. Subsequently, we tested whether the presence of reducing agent affects the conformation of the recombinant *LmDUB2*, using native PAGE. Regardless the presence of DTT (2 mM, 5 mM and 10 mM), TCEP (2 mM, 5 mM and 10 mM) or β -mercaptoethanol (5 mM), the migration pattern of the recombinant *LmDUB2* protein was identical to the sample without any reducing agents (Fig. 25C). We also concluded that

LmDUB2 is predominantly found as a monomer due to the detection of a single protein per condition, supporting the SEC-MALLS results (Fig. 25C).

Subsequently, we tested whether the recombinant *LmDUB2* was catalytic active using the ABPP assay. Briefly, we incubated the recombinant *LmDUB2* for 15 min in an activation buffer containing reducing agent to fully reduce the catalytic cysteine. Subsequently, we added the ABP (Ub-PA in our case), incubated the mixture for 1 h, ran it on an SDS PAGE and imaged the Coomassie Blue-stained gel. Ultimately, we detected a ~10 kDa shift of the *LmDUB2* band (from ~80 kDa to 90 kDa), suggesting binding of the ABP (size of probe is ~9 kDa; Fig. 25D). In the same experiment, we also tested Ub-PA and *LmDUB2* ratio, and optimal incubation temperature, and we found that 2:1 and room temperature (RT) improved by ~90% the ABP labelling (Fig. 25D). However, we also observed a weaker secondary band at ~100 kDa, suggesting either oligomerization of the *LmDUB2*-attached probe or a binding of a second probe on *LmDUB2* (Fig. 25D). To answer whether the ABP binds predominantly at the active catalytic site of *LmDUB2*, we repeated the experiment using the catalytic inactive *LmDUB2*^{C312A}. The overall profile of *LmDUB2*^{C312A} in the presence and absence of Ub-PA is identical (Fig. 25E). Therefore, we proved that Ub-PA selectively binds at the active catalytic cysteine of the *LmDUB2*, and the secondary ~100 kDa band observed at the *LmDUB2* is due to a dimerization of the Ub-PA probe.



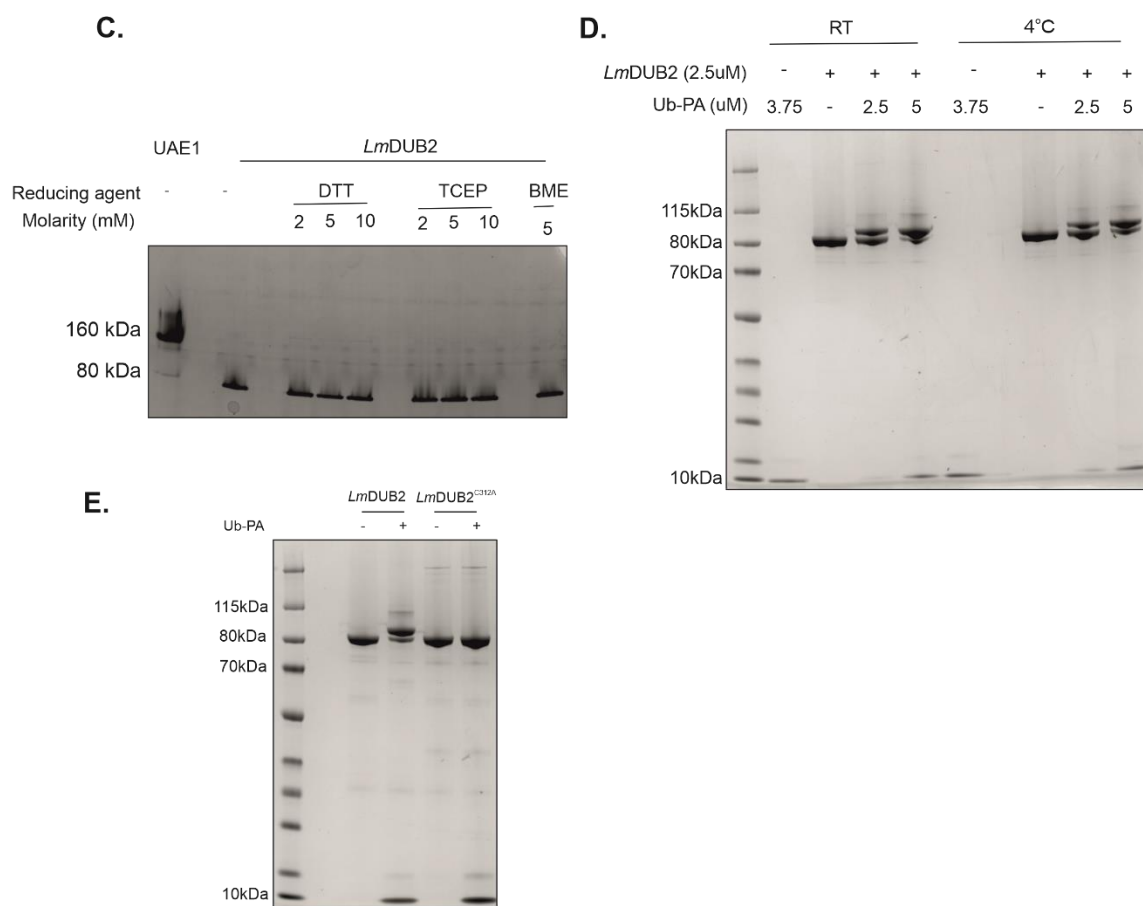


Figure 25: Biochemical characterisation of recombinant *LmDUB2* protein. **A.** Exploration of the significantly different ubiquitinated peptides between DUB2-depleted and wild-type samples. The purity of recombinant *LmDUB2* and its catalytic inactive mutant were assessed using SDS-PAGE, followed by Coomassie Blue staining. **B.** Elution profile of *LmDUB2* presented as changes in refractive index over time (curved purple line). The calculated molecular weight (kDa) of *LmDUB2* protein, based on the light scattering data, is indicated as a black line. **C.** To investigate possible conformational changes of *LmDUB2*, Native-PAGE was performed and the migration pattern of the protein in the presence of different reducing agents - DTT, TCEP and BME - was observed. The recombinant UAE1 (153 kDa) protein was used as a control. **D.** Investigation of optimal conditions for binding of Ub-PA probe to *LmDUB2*. The probe was mixed with *LmDUB2* either at 1:1 or 2:1 ratio, and incubated for 1h either at room temperature (RT) or 4°C. Samples were then analysed on SDS-PAGE and gel was subsequently stained with Coomassie Blue. Quantification of bands was performed in Image Lab. **E.** Investigation of whether the Ub-PA probe binds specifically at the active catalytic site of *LmDUB2*. Ub-PA was incubated for 1h at RT either with *LmDUB2* or *LmDUB2*^{C312A} and then analysed by SDS-PAGE, followed by Coomassie Blue staining.

5.2.3 High-Throughput Drug Screening Against DUB2

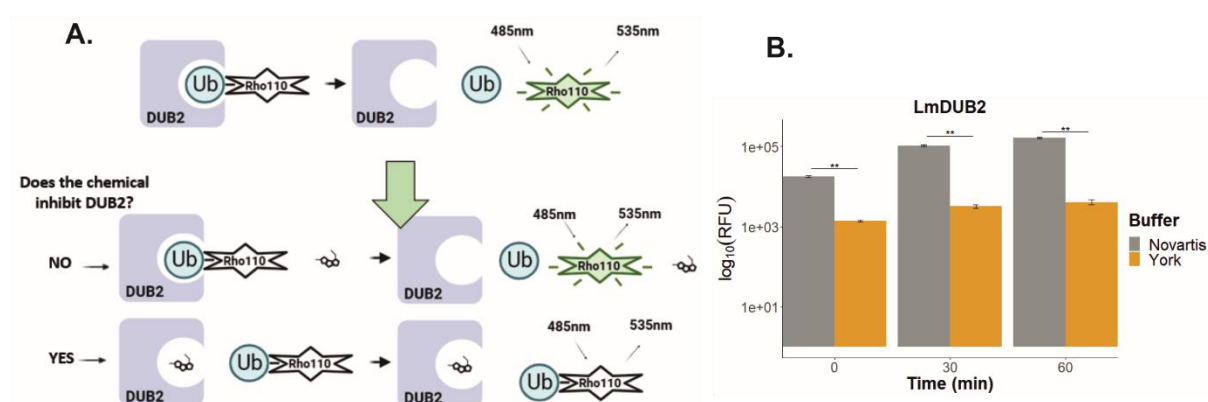
5.2.3.1 Experimental Workflow

Following the characterisation of the recombinant *LmDUB2* protein, combined with the essential nature of the protein in *L. mexicana*, we decided to perform a high-throughput drug screening against the recombinant *LmDUB2*. This was performed in collaboration with the Novartis Institute for Biomedical Research (NIBR), which through their FAST Lab program allows academic labs to get access

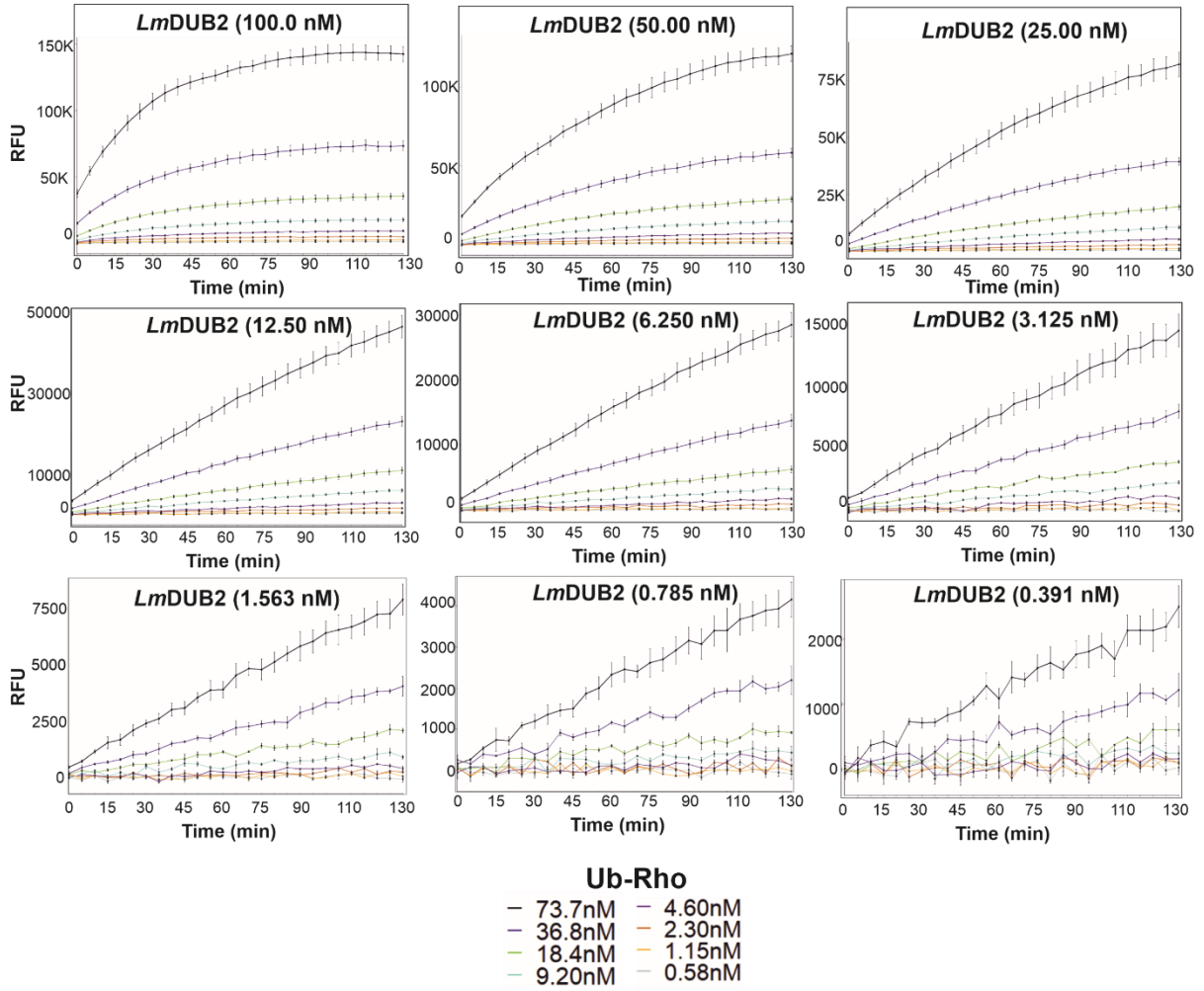
to a non-proprietary compound library assembled by them. For screening the compounds against the recombinant DUB, we employed the fluorogenic DUB substrate, ubiquitin-rhodamine110 (Ub-Rho), and we followed an already developed protocol provided by NIBR (Fig. 26A; Varca *et al.*, 2021). As previously described in the introduction, Ub-Rho, upon cleavage by an active recombinant DUB, releases fluorescence signal. However, prior incubation of the DUB with an inhibitor, will prevent cleavage of the ubiquitin from rhodamine 110, thereby no fluorescence signal will be detected (Fig. 26A).

5.2.3.2 Optimization

Before performing the primary HT-screening, we needed to optimize the protocol against *LmDUB2*. Initially, we compared two buffers to determine which one improves the cleavage of the fluorogenic Ub-Rho by *LmDUB2*. The first buffer consisted of 50mM Tris (pH 8), 50mM NaCl, 0.002% Tween-20 and 5mM DTT and it was referred to as ‘Novartis buffer’ due to its use as part of the previous DUB screen conducted by Novartis (Varca *et al.*, 2021). The second buffer, contained 25mM Tris (pH 7.6), 150mM NaCl and 10mM DTT, and we named it the ‘York buffer’ (Pruneda & Komander, 2019). Direct comparison of the two buffers revealed that the ‘Novartis buffer’ increased significantly the relative fluorescence units (RFU) detected by the Ub-Rho – *LmDUB2* reaction (p-value = 0.0023; n-6; Fig. 26B). Specifically, we detected a 13-fold, 28-fold and 33-fold increase in the fluorescent intensity following 0 min, 30 min and 60 min of incubation time, respectively (Fig. 26B). Ub-Rho mixed with either the ‘Novartis’ or ‘York’ buffer was used as background control for each condition, and therefore each recorded value was normalized against the control. Subsequently, we carried out a titration of *LmDUB2* and Ub-Rho to minimize reagent consumption, while maintaining the production of fluorescence values beyond 5-fold signal-to-noise ratio after 1 h of incubation. We found that the optimal combination was 25nM of *LmDUB2* mixed with 73.7 nM of Ub-Rho primarily due to its 10-fold signal-to-noise ratio provided at 1 h of incubation, while the reaction at the given time point was far from reaching saturation (Fig. 26C). All these optimization steps conducted in a 384-well plate, with a final volume of 10 μ l per reaction. To reduce even further the consumption of reagents, we performed assay miniaturization in a 1536-well plate. We scaled down the final volume of the reaction to 5 μ l, while maintaining both the DUB-substrate ratio and the ~11-fold signal-to-noise ratio (Fig. 26D).



C.



D.

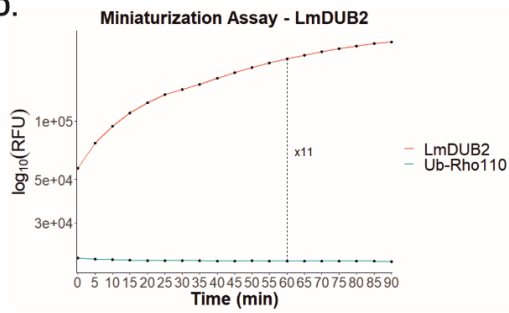


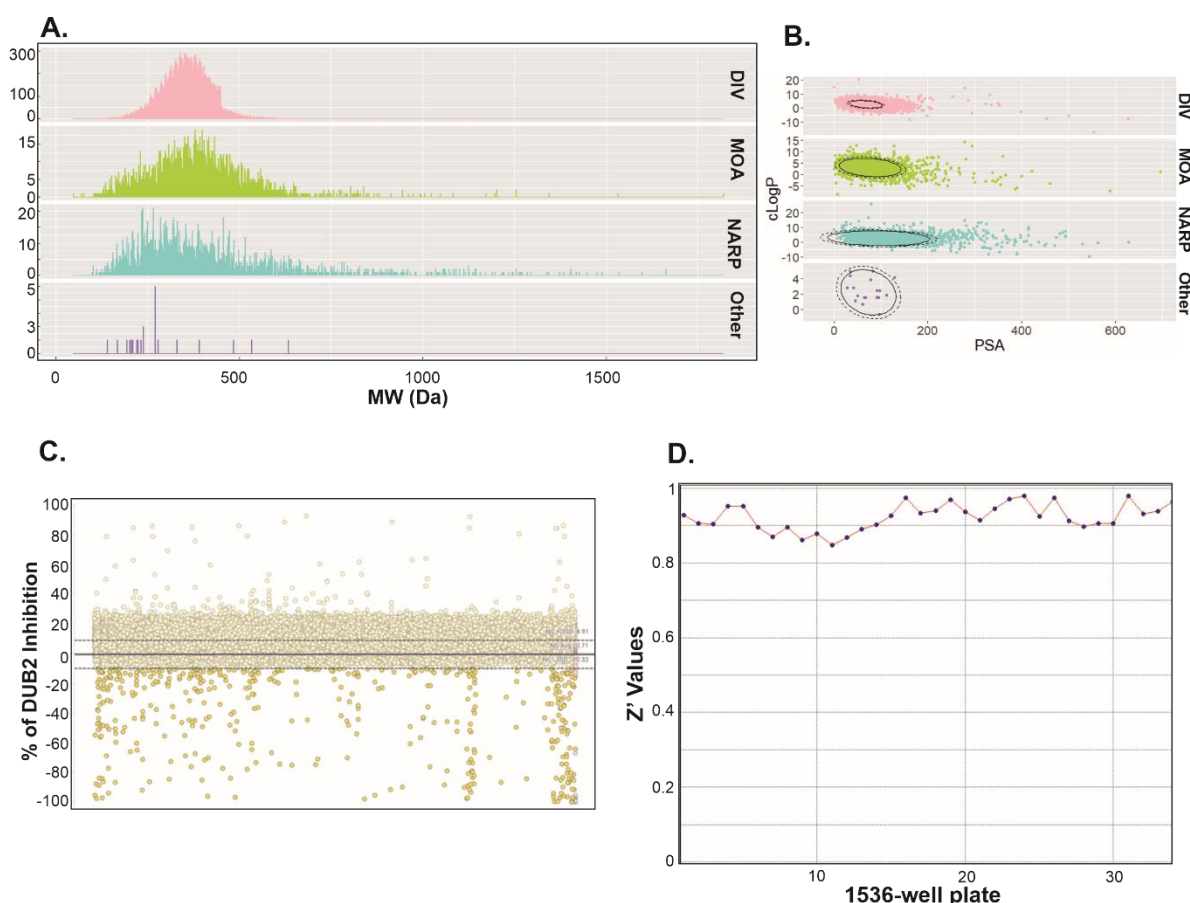
Figure 26: Optimization of High-Throughput Drug Screen conditions against *LmDUB2*. **A.** Schematic of the HT screen against *LmDUB2*. Briefly, incubation of *LmDUB2* recombinant protein with the fluorogenic Ub-Rho, will lead to the cleavage of the ubiquitin and the release of the fluorescent rhodamine 110. This change in the fluorescence state of the substrate is detected at excitation/emission wavelengths of 485nm/535nm using the PheraStar fluorescence plate reader, and it signifies that the DUB is catalytically active. If *LmDUB2* is incubated with a compound that inhibits its catalytic activity, then the subsequently added Ub-Rho will not be cleaved, and therefore no fluorescence will be detected. Conversely, if *LmDUB2* is incubated with a compound that does not inhibit its catalytic activity, then after cleavage of ubiquitin from rhodamine 110, fluorescence will be detected. **B.** Comparison of relative fluorescence units (RFU) detected when *LmDUB2* and Ub-Rho were incubated for 0 min, 30 min and 60 min, in either Novartis or York Buffer. Pairwise Wilcoxon test was used to show that the Novartis Buffer improved significantly the DUB2-driven Ub-Rho cleavage (p-values= 0.0023, n=6). Ub-Rho mixed in either Novartis or York buffer was used as a normalization control. Stars indicate that the difference between the fluorescence intensities of the two buffers per given time point was significant. **C.** Titration assay to identify minimal *LmDUB2* and Ub-Rho concentrations, which will still provide a >5 signal-to-noise ratio. RFU were recorded every 5 min for a time interval of 130 min and 3 replicates were used per condition. The mean and its standard error were plotted per time point. Ub-Rho mixed with buffer at the given concentrations was used as a normalization control. **D.** Investigation of the signal-to-noise ratio detected over 90 min of *LmDUB2*/ Ub-Rho reaction, at miniaturization conditions. These conditions included: 1536-well plate instead of 384-well plate and the final volume of the reaction was 5 μ l instead of 10 μ l. Ub-Rho was used as negative control (n=6). At 60 min of incubation, the fluorescence intensity recorded from the DUB2/Ub-Rho reaction was 11 times higher than the control.

5.2.3.3 Primary HT Drug Screen against DUB2

The primary HT Drug Screen against DUB2 contains ~50,000 compounds, which are divided into four categories: the curated diversity set addressing all possible targets, compounds with a known mechanism of action, natural products, and others. Insights into the physicochemical properties of the compounds revealed that the vast majority of them have a molecular weight in the range of 150 Da and 600 Da, molecular polar surface area (PSA) lower than 200 and calculated logP (cLogP; P = partition coefficient) values between 0 and 6 (Fig. 27A&B). These values indicate that the compounds meet the criteria of drug-like properties, such as lipophilicity and permeability, making them good starting compounds for the development of an applicable drug against *L. mexicana* DUB2 (Bickerton *et al.*, 2012; Schuffenhauer *et al.*, 2020). We screened the entire library at a concentration of 10 μ M against *LmDUB2*, and we found that 438 compounds inhibited our target (n=1; Fig. 27C). Overall, compounds reducing the *LmDUB2* activity by ~10.3% were assigned as inhibitors, while the ones increasing it beyond 8.91% were assigned as activators (Fig. 27C). We defined these separation bands through the subtraction of the threshold value for active controls (Ub-Rho mixed with DMSO), which is defined as the sum of the mean signal of the active control and its three times standard deviation, from the threshold value of the neutral control (*LmDUB2* mixed with Ub-Rho and DMSO), which is the sum of the mean signal of the neutral control and its three times standard deviation. As a quality control of the data, we calculated the Z' value of each 1536-well plate. Z' value indicates whether the difference of the neutral and active control are significantly different from each other in terms of mean and standard deviation, with Z' values between 0.5 and 1 considered as excellent (Zhang *et al.*, 1999). All our Z' values were beyond 0.85, indicating that our data were of high quality, making them robust (Fig. 27D).

5.2.3.4 Dose-Response Screens

Subsequently, an 8-point half-log dose response screen was performed for all the 438 inhibitory compounds, at a highest concentration of 20 μM . The reason of performing this assay was two-fold: firstly, to validate that the compounds are truly inhibitors and not false positives, and secondly, to identify the concentration of the compound required for inhibiting 50% of the *LmDUB2* maximum activity (IC_{50}). The dose-response experiment unveiled that among these 438 compounds, 86 exhibited high potency as inhibitors ($\text{IC}_{50} < 10 \mu\text{M}$), while 66 demonstrated weaker inhibitory effects ($10 \mu\text{M} < \text{IC}_{50} < 20 \mu\text{M}$; $n=3$). To assess the potential of these compounds in addressing other human parasitic models, we also subjected the same 438 compounds to testing against the catalytic active recombinant *Trypanosoma cruzi* DUB2 (*TcDUB2*) homologue (57% protein sequence similarity; Fig. 26E). This additional dose-response screening led to the identification of 41 and 61 highly potent and weak *TcDUB2* inhibitors, respectively ($n=3$). A direct comparison of the two screens revealed 63 overlapping *LmDUB2* and *TcDUB2* inhibitory compounds, out of which 41 are highly potent and 22 are weaker against both proteins (Fig. 27E). We also compared these inhibitors with previously gathered data on 8 human DUBs, and it became evident that 23 of our compounds exhibited selective inhibition, targeting either *LmDUB2*, or both *LmDUB2* and *TcDUB2* (Fig. 27E). In regards of the quality of the data, both screenings provided highly reliable data due to their Z' values be beyond 0.8 (Fig. 27F&G). The top 3 compounds with the lowest IC_{50} against *LmDUB2* and *TcDUB2* are listed in Table 8.



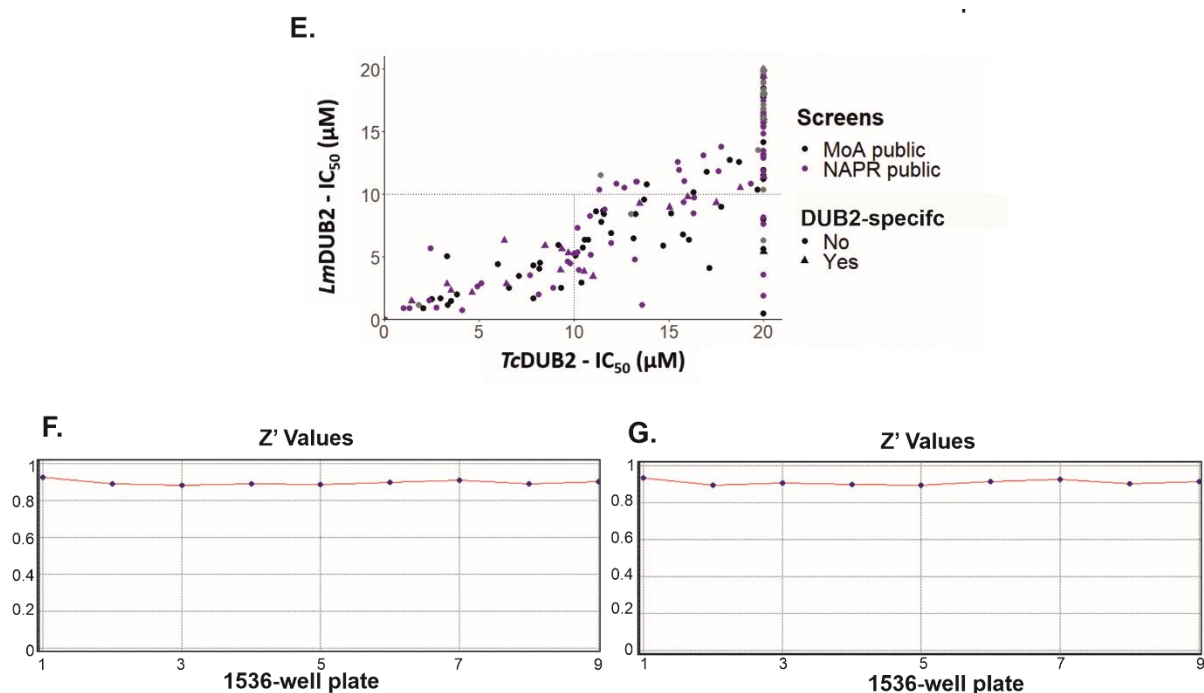


Figure 27: Primary and secondary HT drug screens. **A.** Distribution of the molecular weight (Da) of compounds used from each of the four sets: DIV= diversity, MOA = mechanism of action, NAPR = natural product, and other. **B.** Distribution of compounds per screening set based on their cLogP value against their polar surface area value. Confidence ellipse shows where the 95% of the compounds are located on the graph. **C.** Primary screen composed of ~50,000 compounds was performed against *LmDUB2*. Each compound was added at a final concentration of 10 μM , and incubated for 10 min with *LmDUB2*, prior the addition of Ub-Rho, which was incubated for 1 h ($n=1$). As a neutral and active control, *LmDUB2* mixed with Ub-Rho and DMSO, and Ub-Rho mixed with DMSO, were used respectively ($n=3$). Compounds that reduced the activity of *LmDUB2* by 10.3% were assigned as qualified inhibitors and highlighted in yellow. The separation bands assigned in the graph were calculated as previously described. Each investigated compound was depicted as a dot, and plotted across the x-axis. **D.** Z' values calculated for the 34 x 1536-well plates that were used for screening the entire compound library. **E.** A dose-response analysis of each qualified inhibitor (438) was performed against *LmDUB2* and *TcDUB2* ($n=3$). The IC_{50} of each compound was calculated against both recombinant proteins. Upon filtering (i.e., the sigmoid curve must pass through the 50% DUB2 activity threshold), IC_{50} s for each qualified compound against *LmDUB2* and *TcDUB2* were plotted against each other. Compounds with an IC_{50} less than 10 μM were categorised as potent inhibitors, while compounds with an IC_{50} between 10 μM and 20 μM were categorised as weak inhibitors. Compounds that are natural products are depicted in black, while the ones with a known mechanism action are depicted in purple. Compounds inhibiting DUB2 and the 8 previously investigated human DUBs are represented with a triangle and assigned as DUB2-specific. **F & G.** Z' values calculated per 1536-well plate that was used for the dose-response secondary screen of the 438 promising inhibitors against *LmDUB2* and *TcDUB2*, respectively.

Table 8 Top 3 inhibitors for *LmDUB2* and *TcDUB2*. The top 3 inhibitors of *LmDUB2* are listed in ascending IC_{50} in the first half of the table, and their values are in bold. Similarly, the top 3 inhibitors of *TcDUB2* are listed at the bottom half of the table. Additional information for each compound, including the name of the compound, PubChem compound ID (CID) number, structure, the qualified

IC₅₀ against the other DUB2, and whether they are DUB2-specific (not inhibiting the 8 previously screened human DUBs), was included.

Compound	PubChem CID	Structure	Screening Set	Qualified IC ₅₀ TcDUB2	Qualified IC ₅₀ LmDUB2	DUB2-specific
Haloquinone	133561	<chem>CC(=O)c1cc2c(c(O)c1C)C(=O)C(=O)c1c(O)cccc1-2</chem>	NAPR public	0.008392	0.006293	No
NBI-31772	135543997	<chem>OC(=O)c2cc1cc(O)c(O)cc1c(n2)C(=O)c3ccc(O)c(O)c3</chem>	MoA public	20	0.49	No
Theaflavin-3-gallate	169167	<chem>Oc1cc(cc(O)c1O)C(=O)O[C@@H]3Cc2c(cc(O)cc2O)O[C@@H]3C7C=C(O)C(=O)c6c(O)c(O)cc([C@H]5O)c4cc(O)cc(O)c4C[C@H]5O)c6C=7</chem>	NAPR public	4.09	0.77	No
Compound	PubChem CID	Structure	Screening Set	Qualified IC ₅₀ TcDUB2	Qualified IC ₅₀ LmDUB2	Human Selective
Haloquinone	133561	<chem>CC(=O)c1cc2c(c(O)c1C)C(=O)C(=O)c1c(O)cccc1-2</chem>	NAPR public	0.008392	0.006293	No
Ellagic acid	5281855	<chem>Oc1cc2C(=O)Oc4c(O)c(O)cc3C(=O)Oc(c1O)c2c34</chem>	NAPR public	1.01	0.926	No
Asperugin B	6449979	<chem>CC(C)=CCC/C(/C)=C/CC/C(/C)=C/COc1c(O)cc(C=O)c(C=O)c1O</chem>	NAPR public	1.3	0.88	No

5.3 Discussion

5.3.1 Development of a Robust Competitive-ABPP in *L. mexicana*

Overall, activity-based protein profiling (ABPP) using non-cleavable ubiquitin-based probes is a well-established approach for characterising the active DUBome of a studied organism. In the case of *L. mexicana*, ABPP using the fluorescent Cy5UbPA probe revealed that all twenty identified DUBs are catalytic active, including the four essential DUB1, DUB2, DUB12, and DUB16 (Damianou *et al.*, 2020). Interestingly, it was also concluded that the active DUBome does not change throughout the life cycle of the parasite, underscoring another application of the ABPP of tracking changes in the activity of DUBs under various conditions (Damianou *et al.*, 2020). Nevertheless, ABPP is also used as a crucial assay for identifying compounds inhibiting the active DUBs, and this assay is known as competitive-ABPP. Competitive-ABPP has been used extensively in the past for identifying several human DUB inhibitors, such as the UCHL1-specific inhibitor LDN-57444 and USP1/UAF1-specific GW7647 inhibitor (Liu *et al.*, 2003; Chen *et al.*, 2011). However, this assay has not been employed in *Leishmania*, limiting the characterisation of compounds as *Leishmania* DUB inhibitors.

In this chapter, we developed a competitive-ABPP using the already published Cy5UbPA-based ABPP protocol established by our lab. Briefly, the finalized protocol involved an additional 1 h incubation step, in which the investigated compound was added in the promastigote cell extract, followed by a 5 min incubation with the Cy5UbPA probe. Reduction of the latter incubation step from 1 h to 5 min was crucial for preventing the ABP from outcompeting compounds that inhibited the *Leishmania* DUBs reversibly. Validity to our developed protocol was provided through the testing of a known human non-specific DUB inhibitor, HBX 41 108. HBX 41 108 is a cyano-indenopyrazine derivative compound that was initially thought to inhibit specifically USP7, however, it was later confirmed as a non-specific DUB inhibitor (Colland *et al.*, 2009; Ritorto *et al.*, 2014). Interestingly, we showed that HBX 41 108 also inhibits the activity of several *Leishmania* DUBs, making it the first characterised *Leishmania* DUB inhibitor. Despite this valuable conclusion, we also showed that the competitive ABPP we developed is a robust tool for identifying inhibitors targeting the active DUBome of *Leishmania*.

5.3.2 Pyrithione and its Derivatives as Inhibitors of *Leishmania* DUB16

Nonetheless, using this competitive-ABPP we characterised pyrithione and its four derivatives as inhibitors of at least two *Leishmania* promastigote DUBs. The two DUBs were DUB15 and DUB16, which the former is a non-essential *Leishmania* DUB, while the latter is essential. Inhibition of DUB16 could explain the previously identified *in vivo* anti-leishmanial activity of these compounds by Cobb's lab. However, overexpression of DUB16 did not provide any resistance to these compounds, indicating that there are other essential targets for these compounds in the parasite. Therefore, we conclude that pyrithione and its derivatives prevent the *Leishmania* growth via inhibiting the essential activity of DUB16, among other essential processes within the parasite.

5.3.3 *LmDUB2* – a catalytic active monomeric DUB

We successfully expressed and purified recombinant *LmDUB2* and its catalytic inactive mutant, *LmDUB2*^{C312A} using a baculovirus expressing system. The methodology has been previously developed by Damianou *et al.* (2020), however it is worth mentioning that this eukaryotic expression system was selected due to the unsuccessful attempts of expressing the full length *LmDUB2* in *E.coli* (unpublished). Similarly, *TbDUB1* and *LmDUB1* recombinant proteins were also expressed using the

same system, indicating the necessity of a eukaryotic environment for expressing trypanosomatid DUBs (unpublished). On the other hand, successful expression of the recombinant *TcDUB2* was achieved through the use of another eukaryotic system, the HEK293 cells (Protein Production, UoY). HEK293 cells were selected because they are more resilient (i.e. can be frozen down and regrown), and the overall expression of the protein is less time-demanding and less laborious compared to the baculovirus expression system. In regards of the human orthologues of DUB2, USP5 (95 kDa) and USP13 (98 kDa), successful recombinant expression was achieved through both *E. coli* and eukaryotic expression systems, including HEK293 cells (Zhang *et al.*, 2011; Zhao *et al.*, 2013). Nonetheless, we concluded that eukaryotic expression systems, such as baculovirus / insect cells and HEK293 cells, are ideal for expressing trypanosomatid DUBs.

To investigate whether a recombinant DUB is catalytic active, there are several biochemical assays that can be performed. For instance, if di-/poly-ubiquitin molecules are incubated with a recombinant DUB, and mono-ubiquitin or smaller poly-ubiquitin chains are observed, then it means that the DUB is catalytic active. This assay was previously used to show that *LmDUB2* is catalytic active, as well as to characterise the broad linkage specificity of the enzyme (Damianou *et al.*, 2020). Another way to validate that a DUB is catalytic active is through the use of a non-cleavable ubiquitin-based ABP probes. Covalent binding of an ABP (~9 kDa) to the active catalytic site of the investigated DUB increases its molecular weight, and therefore a shift in its SDS-PAGE migration pattern is observed. Damianou *et al.* (2020) performed this additional assay, utilizing the Cy5UbPA probe, to confirm that *LmDUB2* is catalytic active. In this experiment, the catalytic inactive DUB2^{C312A} was included as a control, to show that the probe binds selectively to the active catalytic site of the recombinant protein and not elsewhere (Damianou *et al.*, 2020).

Similarly, we showed that the Ub-PA probe binds selectively to the catalytic active recombinant *LmDUB2* and not to the *LmDUB2*^{C312A}, validating that our recombinant *LmDUB2* is also catalytic active. For this experiment, we decided to use the Ub-PA probe instead of the Cy5UbPA probe, due to its lower cost, absence of light-sensitivity and no-need of specialised equipment (e.g. Typhoon gel scanner). We also demonstrated that the Ub-PA probe binds to the recombinant *TcDUB2* protein, however whether the binding was at the catalytic site was unclear as we had not made a catalytically inactive *TcDUB2* control. Nonetheless, we demonstrated that *TcDUB2* is catalytic active through an Ub-Rho assay, in which fluorescence was detected in the presence of *TcDUB2* over the control (only Ub-Rho; data not shown). Collectively, we successfully expressed and purify catalytic active *LmDUB2* and *TcDUB2*.

Overall, DUBs have several mechanisms of regulating their activity, and one of them depends on their oligomerization state. For instance in HEK293T cells, USP35 forms a homodimer through its C-terminal domain, which activates its deubiquitinase activity, allowing the deubiquitination of its substrate, Aurora B, and the ultimate control of mitosis (Park *et al.*, 2023). Conversely, USP25 forms a tetramer in solution, which results in its auto-inhibition. Despite the presence of an ubiquitinated substrate, the tetrameric USP25 remained inhibited, suggesting that the tetramer might be activated by external factors, such as other proteases (Sauer *et al.*, 2019). In regards to *LmDUB2*, we revealed that it is predominantly found as a monomer in solution, through the combination of SEC-MALLS and native-PAGE gel analyses. The latter analysis has further shown that treatment of recombinant *LmDUB2* with any reducing agents does not affect its physiochemical properties, making the reducing agents applicable for future structural studies. Nonetheless, we also identified that *TcDUB2* is predominantly a monomer in solution, indicate the first experimental similarity with *LmDUB2*. These conclusions are in accordance with their human homologues, USP5 and USP13, which have been reported as monomeric in solution (Zhang *et al.*, 2011; Avvakumov *et al.*, 2012). However, the *in vitro* catalytic

activity of USP13 is very poor compared to USP5, *LmDUB2*, and *TcDUB2*, suggesting that USP13 activity might be controlled via PTMs or other external factors. To sum up, we demonstrated that *LmDUB2* and *TcDUB2* are catalytic active in their monomeric forms, and we hypothesize that their *in vivo* activity is controlled by a similar regulation mechanism as USP5.

5.3.4 Identification of Promising DUB2 Inhibitors

It is well-established that DUBs are associated with a spectrum of diseases, including neurodegeneration and cancer, making them promising therapeutic targets (Celebi *et al.*, 2020; Bello *et al.*, 2022). Indeed, selective inhibitors of USP7 and USP28 led to the elimination of cancerous cells, primarily due to the subsequent degradation of their substrate proteins (Turnbull *et al.*, 2017; Ruiz *et al.*, 2021). Several of these selective inhibitors have been identified through HTS against recombinant DUBs, in which DUB activity was assessed through a biochemical assay using fluorogenic ubiquitin-based substrate (Ub-AMC or Ub-Rho; Liu *et al.*, 2003; Chen *et al.*, 2011). For this reason, we employed an Ub-Rho based HTS against *LmDUB2*, to identify DUB2-specific inhibitors. Before performing the primary screen against *LmDUB2*, we successfully optimized the screening conditions, as previously described by Varca *et al.* (2021), ensuring that the Ub-Rho-derived signal was 5 times higher than the background noise, while the consumption of valuable reagents was minimal.

The primary screen conducted against *LmDUB2* consisted of ~50k curated compounds. This screening deck was previously arranged by NIBR with the primary aim of increasing the chemical diversity of the included compounds while maintaining drug-like properties. This was accomplished while ensuring that the overall number of compounds remained relatively low, given the availability of around 2 million compounds at NIBR (Schuffenhauer *et al.*, 2020). Indeed, insights into the physicochemical properties of the screened compounds revealed that they fulfil several drug-like criteria, including lipophilicity and permeability, making them suitable for downstream applications against the *Leishmania* parasite. In regards of the primary screen, we identified 438 compounds inhibiting *LmDUB2* activity by at least ~11%, categorising the 0.88% of the library as promising DUB2 inhibitors. At this point, it is worth mentioning that the same library of compounds was previously explored against the human DUBs USP7, USP8, USP10, USP17, USP28, USP30, UCHL1 and OTU3, producing variable hit rates ranging from 0.4% to 6.9% (Varca *et al.*, 2021). Direct comparison of the compounds identified as inhibitors between *LmDUB2* and the human DUBs revealed that 23 compounds inhibited solely *LmDUB2*, making them selective, and also placed *LmDUB2* as the fourth DUB with the most promising inhibitors that were identified from this primary screen.

We further categorised these 438 compounds as strong ($IC_{50} < 10 \mu M$) and weak inhibitors ($10 \mu M < IC_{50} < 20 \mu M$) using dose-response screens against the recombinant *LmDUB2* protein. Interestingly, we found that 86 compounds are highly potent inhibitors and 66 are weaker inhibitors, with haloquinone being the most potent inhibitor ($IC_{50} = 0.006 \mu M$). Haloquinone is a compound naturally produced by *Streptomyces venezuelae* ssp. and has an antibiotic activity against gram positive bacteria, including halobacteria and arthrobacteria (Wersmeyer-Wenk *et al.*, 1981). Haloquinones and its derivatives have been used extensively as drinking water disinfectants, however toxicological studies showed that their disinfection by-products are cytotoxic and carcinogenic (Zhao *et al.*, 2010; Xu *et al.*, 2021). Nevertheless, a haloquinone, PKF118-744, was previously found to inhibit the interaction between β -Catenin/Tcf complex and DNA in epithelial cells (Lepourcelet *et al.*, 2004). The aberrant wnt/ β -Catenin signalling pathway has been associated with the formation of several human cancers, thereby PKF118-744 was utilized as a good starting point for the production of promising novel inhibitors (Halbedl *et al.*, 2013).

Next, the second and third most potent inhibitors of *LmDUB2* were NBI-31772 and theaflavin-3-gallate, respectively. NBI-31772 is a known non-peptide ligand that binds to insulin-growth factor-I (IGF) binding proteins. As a result, endogenous IGF is displaced from the IGF-binding proteins. This release of IGF leads to the increase of bioavailable IGF, meaning that it could be explored as a therapeutic treatment for diabetes and other IGF-responsive diseases (Liu *et al.*, 2001). An interesting application of NBI-31772 in mice showed that the injected compound induced anxiolytic and antidepressant-like effect in mice. These behavioural changes were attributed to the NBI-31772 mechanism of action as a displacer of IGF-1, which subsequently activates IGF-1 receptors (Malberg *et al.*, 2007). Similarly, the activity of NBI-31772 on IGF-signalling promoted cardiomyocyte proliferation (Choi *et al.*, 2013). On the other hand, theaflavin-3-gallate is a polyphenol compound that belongs in the family of theaflavin monogallates, which are natural occurring red pigments derived from black tea. Interestingly, theaflavin monogallates have an anti-HIV-1 activity. A study showed that it prevents the formation of the gp41 six-helix bundle of the HIV and thereby, its subsequent entry into the targeted cell (Liu *et al.*, 2005). In addition, theaflavin monogallates possess anti-oxidant activities due to their ability on scavenging reactive oxygen species and preventing hydroxyl radical-induced DNA oxidative damage *in vitro* (Wu *et al.*, 2011). Finally, it was evidenced that they also have anti-carcinogenic properties due to the inhibition of the cyclooxygenase enzyme Cox-2, which is known to implicate in intestinal carcinogenesis through prostaglandin biosynthesis, and the direct inhibition of Caco-2 colon cancer cell growth (Lu *et al.*, 2000).

In regards of the recombinant *TcDUB2* protein, for which the same dose-response screens were performed against it, we identified 41 and 61 compounds demonstrating high and weak inhibition, respectively. The top three inhibitors with the lowest calculated IC_{50} values were haloquinone ($IC_{50} = 0.008 \mu\text{M}$), ellagic acid ($IC_{50} = 1.01 \mu\text{M}$) and asperugin B ($IC_{50} = 1.30 \mu\text{M}$). Haloquinone was the most potent inhibitor of *LmDUB2*, thereby it has already been discussed. As about ellagic acid, it is a chromene-dione derivative that is present in many fruits (e.g. pomegranates and peaches), seeds (e.g. walnuts and almonds) and vegetables. It has several properties, including antioxidant, anti-inflammatory, anti-diabetic and anti-tumor activities (Ríos *et al.*, 2018). Among the many molecular targets of ellagic acid, including cyclin-dependent kinase 6 and aldehyde oxidase, it has been found that ellagic acid inhibits the Hepatitis C virus (HCV) helicase and serine protease activity of HCV NS3/4A protease, preventing HCV replication (Reddy *et al.*, 2014; Siah *et al.*, 2016; Yousuf *et al.*, 2020). Asperugin B is a prenyloxybenzaldehyde isolated by the mycelium of *Aspergillus rugulosus*, as a secondary metabolite (Ballantine *et al.*, 1967). Unfortunately, it is a poorly characterised natural product and there are no available information regarding its biological activity. Despite that none of the top 3 inhibitors of both *TcDUB2* and *LmDUB2* being established DUB inhibitors, we have demonstrated that these compounds hold the potential for further exploration in that regard.

To summarize, we have identified promising compounds that inhibit DUB2 activity, either strongly or weakly, with some compounds being DUB2-selective. These compounds have been used as a reference for the generation of an additional expansion screen, which includes chemically-related compounds that will be screened against both *LmDUB2* and *TcDUB2*. Subsequently, the top 10 compounds exhibiting the strongest inhibition will be tested against the parasites and human cells. This assays will indicate whether the compounds are cell permeability and selective against the parasite. Eventually, the parasite-selective compounds would be tested for inhibiting other DUBs via competitive-ABPP experiments and EC_{50} would be further determined. Validated selective compounds could be explored for therapeutic purposes and/or as tools for improving the molecular understanding of DUBs within the two parasites (e.g. design of PROTACs, DUBTACs and cell-permeable DUB ABPs). Furthermore, these compounds, as well as the Ub-PA probe, could facilitate in the deciphering of the

apo-DUB2 protein structure in future studies. As well as several compounds inhibiting *LmDUB2* from the primary screen, there were several others activating it. All these activating compounds could be equally explored, as the inhibiting compounds, for future DUB2-specific applications.

In regards of the limitations of this piece of work, the reproducibility of the competitive-ABPP coupled with in-gel fluorescence was poor, probably due to the utilization of the unstable and light-sensitive Cy5UbPA. The use of Cy5UbPA reduces the experimental time, however it requires specialised equipment (Typhoon) for imaging the gel. To overcome these limitations, the use of HA-tagged UbPA probe in future experiments is recommended. This probe allows for the visualization of ABP-bound DUBs via western blot, providing more robust and stronger signal, and can also be enriched with anti-HA antibody for additional characterisation via MS. However, both of these probes are not cell permeable, thus they only capture the active DUBome under lysed conditions. Furthermore, one of the 7 known families of DUBs is called JAMM. JAMM DUBs are classified as Zn-dependent metalloproteases, and based on their mechanism of action they do not form a substrate-enzyme covalent intermediates as in the case of cysteine protease DUBs (Shrestha *et al.*, 2014). Thus, ABP cannot attach covalently to them and therefore development of JAMM-specific ABPs is required (Morell *et al.*, 2013). Moreover, the ABPs have additional adduct sites proteomes, such as non-catalytic cysteine residues and non-DUB proteins, therefore additional experiments (e.g. competition assay coupled with MS) required to validate which ABP-bound DUBs are truly active (Pinto-Fernández *et al.* 2019). As about the DUB2-HTS, the primary screen was conducted once. Therefore, false negative compounds were not detected, introducing the first and only major limitation of this experiment. Conversely, false positive compounds were identified through the follow up dose-response screens, and excluded for future investigations.

6 General Discussion

6.1 DUB2 has a Pleiotropic Function in *L. mexicana* Promastigotes.

The ubiquitination system has attracted a lot of attention in the recent years, due to its importance in many diseases, including cancer and neurological disorders (Celebi *et al.*, 2020; Bello *et al.*, 2022). Similarly, great efforts have been attained by the Mottram lab to decipher the importance of this system in the eukaryotic pathogenic parasite, *Leishmania mexicana* (Burge *et al.*, 2020; Damianou *et al.*, 2020). Overall, in the parasite there are predicted to be 3 ubiquitin-expressing genes, 2 E1 ubiquitin activating enzymes, 13 E2 ubiquitin conjugating enzymes, 79 E3 ubiquitin ligases, and 20 deubiquitinases (DUBs; Burge *et al.*, 2020; Damianou *et al.*, 2020). Focusing on the *Leishmania* DUBs, DUB4, DUB7 and DUB13, exhibited significant contribution in the differentiation cycle of the parasite, while DUB1, DUB2, DUB12 and DUB16, were categorised as essential for the survival of *Leishmania* promastigotes (Damianou *et al.*, 2020). In this study, we were interested to understand why the activity of DUB2 is so important for the parasite. To achieve that goal, we investigated the substrates of DUB2 at the promastigote stage, through exploring its interactome via biotin proximity labelling, and changes in the total ubiquitinome and proteome in response to DUB2 depletion.

Focusing on the interactomics aspect of the project, we investigated the proximal interacting partners of DUB2 using XL-BioID. XL-BioID is a biotin proximity labelling approach that incorporates *in vivo* crosslinking (Geoghegan *et al.*, 2022). Previously, it was shown that this approach is the most efficient way for investigating the proximome of *L. mexicana* proteins (e.g. CLK2), however the exact mechanism on how or why this is happening is unclear (Geoghegan *et al.*, 2022; Jones *et al.*, 2022). We selected miniTurbo as the best biotin ligase for accomplishing our goal primarily due to its high enzymatic activity that facilitates the labelling of dynamic cellular processes, and the lack of DNA binding domain that makes the enzyme smaller, and thereby, less likely to interfering with the localization and function of the bait protein (Branon *et al.*, 2018). Despite miniTurbo being known for its reduced background biotinylation, we showed that this was not the case in *Leishmania*. This was attributed to the utilization of biotin that was present in the growing medium, combined with the high catalytic activity of the constantly expressed and active miniTurbo, which was fused to the bait (DUB2 and CLK1). To minimize this uncontrollable biotinylation, we introduced the use of BioLock, an avidin-containing biotin depletion solution, which was added directly to the growing culture, under optimized conditions. However, it is crucial to acknowledge that prolonged biotin depletion is toxic for the growth of the parasite. Thus, incubation of the growing culture with BioLock might modify the proteome of the parasite, and therefore the proximal interacting proteins of the bait protein. For future experiments, it might be worth generating an inducible miniTurbo system in *Leishmania* that will prevent unregulated background biotinylation, without concern about cytotoxic conditions (May *et al.*, 2020; Herfurth *et al.*, 2023).

Next, we found that 73 proteins were significantly enriched in BioLock-treated miniTurbo tagged DUB2 promastigote samples compared to BioLock-treated miniTurbo-tagged CLK1 ones. These 73 proteins comprise the proximal interactome of DUB2, with kinesin K39 and ribosomal LSG1 proteins being the most highly enriched. Interaction of DUB2 with these two proteins suggests that DUB2 could be involved in the regulation of the cell-cycle dependent intracellular trafficking and cytokinesis, as well as in ribosomal-associated processes (Gerald *et al.*, 2007; Sahasrabudde *et al.*, 2009; Kargas *et al.*, 2019). At this point, it is worth mentioning that the human DUB2 homologues, USP13 and USP5, have also been associated with cytokinesis, suggesting a potential conserved *in vivo* functional role among these three proteins (Esposito *et al.*, 2020; Halcrow *et al.*, 2022). Nonetheless, we revealed that these

73 proximal interacting proteins are involved in 17 different biological processes, ranging from glycolysis to RNA processing, suggesting that DUB2 has a pleiotropic function in *L. mexicana* promastigotes. The same conclusion was given previously by Damianou *et al.* (2020), upon identifying the broad ubiquitin linkage specificity of the recombinant DUB2. At this point it is worth reminding that the overall number of *Leishmania* DUBs is five times less than human DUBs, supporting further the hypothesis that the parasitic DUBs, such as DUB2, developed pleiotropic functions to satisfy, efficiently, the needs of this eukaryotic organism. Nonetheless, the vast majority of the proximity hits are involved in translation and other ribosomal-associated processes, indicating that the primary role of DUB2 is to regulate these processes within the cell. This will not be the first example of a DUB associated with ribosomes, as USP10 was found to act as ribosome-associated quality control, ensuring the rescue of functional ribosomal proteins from proteasomal degradation (Jung *et al.*, 2017; Meyer *et al.*, 2020).

Interestingly, comparison of the miniTurbo-derived proximal interactome with the previously published DUB2 interactome that was generated through XL - co-immunoprecipitation revealed an overlap of only 8 proteins, including DUB2 (Damianou *et al.*, 2020). This shows that the two approaches are complementary to each other and not interchangeable. Thereby, both approaches should be performed, if possible, for characterising future interactomes. Despite knowing that some DUBs forming stable complexes with other proteins, DUB2 acts independently within the cell. This was attributed to the lack of formation of stable complexes with any of the selected interacting proteins identified with statistical enrichment in either one or both interactomics datasets. However, the major caveat of this conclusion is that the experiment was performed only once, thus ideally these interactions should be re-examined using either the same or less harsh lysis conditions, in the presence or absence of BioLock.

Prior to the investigation of changes in the total ubiquitinome and proteome in response to DUB2 endogenous depletion, we needed to develop a peptide-centric ubiquitinomics workflow in *L. mexicana*. We tested various conditions and we found that the most optimal ones were: 5% SDS as lysis buffer, 7 mg of protein as input from *L. mexicana* promastigotes, TimsTOF HT in DDA mode for acquiring mass spectrometry data of DiGly-enriched samples and FragPipe to analyse MS-derived raw data. Our optimized ubiquitinomics pipeline was able to identify at least 5,000 DiGly peptides in a single run, corresponding to more than 1700 *Leishmania* proteins. This comprises the ~19% of the total proteome of the parasite, exceeding the expected number of ubiquitinated proteins identified in other eukaryotic cells (5% - 10% of their overall proteome). This could be attributed to the relatively small proteome of the parasite combined with the utilization of an optimized peptide-centric ubiquitinomics workflow (Paape *et al.*, 2010). Furthermore, this workflow provides sufficient exploration of ubiquitinated proteins without the need of using proteasomal inhibitors, such as MG132, allowing the investigation of the total ubiquitinome under native conditions. Despite the high efficiency of our ubiquitinomics workflow, there is one important limitation. We used a mixture of trypsin and Lys-C to hydrolyse proteins to peptides, and thereby to convert ubiquitinated proteins to DiGly-peptides. However, proteins possessing the ubiquitin-like modification NEDD8 (ISG15 not present in *Leishmania*) are also hydrolysed to DiGly-peptides (Vogl *et al.*, 2020; Burge *et al.*, 2020). Therefore, our datasets display a combination of ubiquitin- and NEDD8-modified *Leishmania* proteins. It is also worth mentioning that the monoclonal DiGly-specific antibodies, used in our DiGly-enrichment step, do not recognise the DiGly-remnants found on the N-terminal Met1 of the protein, suggesting more ubiquitinated *Leishmania* proteins are to be revealed. To counteract both of these limitations, the UbiSite strategy is recommended. This approach involves protein cleavage with Lys-C only, which generates 13-residue (ESTLHLVLR)GG remnant peptides derived from ubiquitinated

proteins. These peptides can be then enriched using a specific antibody that recognises this 13-residue long remnant motif and identified via mass-spectrometry (Akimov *et al.*, 2018).

Upon optimizing the ubiquitinomics workflow for the *Leishmania* promastigote cells, we investigated changes in the overall ubiquitinome and proteome of the parasite in response to DUB2 depletion. To do that, we generated a DUB2^{FLOX+/-} promastigote cell line that utilizes the inducible diCre system to excise the *DUB2* gene in responses to rapamycin (Yagoubat *et al.*, 2020; Damasceno *et al.*, 2020). The optimal incubation period of rapamycin was 4 days due to the sufficient depletion of DUB2 from within the cell and the minimal DUB2-induced promastigote cell-death. Furthermore, it is worth acknowledging that the inducible diCre system is the only available method for depleting the expression levels of an essential gene within *L. mexicana* and it was previously used to validate the DUB2 essentiality in *L. mexicana*. Nonetheless, DUB2-depletion led to the significant increase in ubiquitination of 122 specific sites in promastigote cells, corresponding to 113 different proteins. Gene ontology analysis revealed that these proteins are involved in various biological functions, including intracellular trafficking and the ubiquitination system, supporting the previous conclusion that DUB2 has a pleiotropic function. The top three ubiquitination sites with the highest upregulation were identified on the serine-threonine kinase receptor-associated protein (STRAP), the hypothetical protein LmxM.34.3240 and the amino acid transporter 19 (AAT19). In the case of the hypothetical protein, its role is unknown within the cell. An insight into the function of the other two proteins is taken by their eukaryotic homologues. For instance, STRAP is known to be involved primarily in anti-apoptotic process under normal conditions and in pro-apoptotic process under stress conditions, while AAT19 is involved in anabolism and various signalling pathways through the uptake of neutral amino acids, which is regulated by pH and sodium levels (Manoharan *et al.*, 2018; Yamada *et al.*, 2019). None of these three proteins were previously identified as ubiquitinated, thus it will be interesting to see how this dynamic process regulates their function. Nevertheless, STRAP, the hypothetical protein LmxM.34.3240 and AAT19 will be prioritized for future experimental validation as substrates of DUB2.

Under the same experimental conditions, we also investigated changes in the total proteome of promastigote cells, and we found 72 and 50 proteins being significantly downregulated from the DIA and DDA respectively. . At this point it is worth highlighting that from a single DIA-MS/MS run, we were able to identify up to ~6000 proteins, which corresponds to the ~66% of the proteome, making it the most efficient MS pipeline available in the literature for identifying *L. mexicana* promastigote proteins. Nonetheless, 21 proteins were overlapped between the two datasets, indicating the complementarity of the approaches, as well as providing confidence that our data are reliable. Insight into the biological role of these 21 proteins, we extracted the following additional conclusion: DUB2 might play a crucial role in regulating various DNA-related events, through proteins like the DNA ligase I, the recombinase RAD51 and the essential tousel-like kinase 2 that is involved in numerous DNA-associated processes. However, it is worth pointing out that the log₂FC values of most significantly downregulated proteins were very low (log₂FC <1), suggesting that might not have any biological significance. This further introduce the hypothesis that DUB2 might not be actively involved in rescuing ubiquitinated proteins from protein degradation. At this point it is worth mentioning that there is no rapamycin-induced control of a different gene, which will facilitate the identification of gene excision-associated changes at both the proteome and ubiquitinome level.

Nonetheless, our ubiquitinomics and proteomics conclusions are solely based on the independent analysis of each dataset, with significant hits across the ubiquitinomics and proteomics datasets having minimal overlap. The last step for completing this analysis is to directly combine these datasets (e.g. through Perseus) and calculate the occupancy per protein. This will indicate proteins of which their ubiquitinated state change due to the absence of DUB2, and not due to variation of the levels of

the protein itself within the sample. It will also introduce new significantly upregulated/downregulated ubiquitination events in response to DUB2 depletion, as well as removing some of the already identified significantly modified ubiquitination sites.

As previously mentioned, the primary goal of this thesis was to understand the function of DUB2 within the *L. mexicana* promastigotes, through the identification of its substrates. From these generated interactomics, ubiquitinomics and proteomics datasets, there are several proteins that are worth following in future substrate validation experiments. However, we recommend prioritizing hits that fulfil the following criteria: most enriched proteins in the DUB2 proximome (and IP-interactome by Damianou *et al.*, 2020), proteins with the most significantly upregulated ubiquitination sites in the absence of DUB2, most significantly downregulated proteins upon DUB2 depletion, which are present in both DIA and DDA datasets, and proteins that are present in at least two of the already mentioned datasets. For the latter case, there are eight proteins fulfilling these criteria: the orphan hypothetical protein LmxM.20.1700, the ribosomal-associated LSG1, the rab-GDP dissociation inhibitor (GDI), the 2, 3-bisphosphoglycerate-independent phosphoglycerate mutase (iPGMA), the ubiquitin-conjugating enzyme E2 (UBC2), the cleavage and polyadenylation specificity factor (CPSF73), the 40S ribosomal protein SA (RPSA) and the small ubiquitin-like modifier (SUMO). All these proteins are promising substrates of DUB2, contributing in a diversity of biological processes within the cell, ranging from carbohydrate metabolism to RNA editing. This underscores, once more, the pleiotropic function of DUB2. The evaluation of these promising substrates will involve enriching each of these proteins from cells expressing DUB2 or not, followed by the subsequent characterisation of their ubiquitination state via western blot. It is expected that in the absence of DUB2, there would be an increase in their ubiquitination state.

6.2 DUB2 - an anti-Leishmanial Drug Target

Leishmania is one of the causing agent of cutaneous Leishmaniasis, affecting ~220K people around the world (WHO, 2023). Current treatments are suffering from various-side effects. For instance, in the case of miltefosine, the only available orally administrated drug, is known to be teratogenic (Soni *et al.*, 2022). Therefore, the need of identifying new molecular targets and better drugs is urgent. DUB2 is a promising candidate due to its essential role in *Leishmania* promastigotes, and its requirement for establishing and maintaining infection (Damianou *et al.*, 2020). Thus, we explored DUB2 as a therapeutic target for the first time. A library of ~50K curated compounds was screened against the recombinant *Lmx*DUB2, and through the utilization of the fluorogenic Ub-Rho substrate, we were able to determine 438 potent inhibitors. Follow up dose-response screens revealed 86 compounds to be *Lmx*DUB2-potent inhibitors ($IC_{50} < 10 \mu M$), and 66 to be weak inhibitors ($10 \mu M < IC_{50} < 20 Mm$). Among them, the top three compounds were haloquinone, NBI-31772 and theaflavin-3-gallate, which are known to inhibit different non-DUB cellular targets. Similarly, the same dose-response screen was tested against the recombinant *Tc*DUB2, a homologue of *Lmx*DUB2, and it was revealed 41 and 61 compounds demonstrating high and weak inhibition, respectively. As in the case of *Lmx*DUB2, haloquinone was the most potent inhibitor, while ellagic acid and asperugin B were the follow-up two hits. Again, none of these compounds have been previously reported to inhibit DUBs *in vivo*, however they were all identified as non-selective inhibitors against human DUBs *in vitro* (Varca *et al.*, 2021). Nonetheless, all the potent compounds, including the 23 compounds inhibiting selectively DUB2, were selected as model compounds for generating an additional expansion screen that will be tested against both proteins (in progress). The top hits will be eventually assessed against human, *L. mexicana* and *T. cruzi* cells for permeability and parasite-selectivity. Subsequently, the DUB-specificity

of the compounds will be evaluated via an in gel based competitive-ABPP that we have successfully developed in this project. Eventually, selective compounds can be explored for the generation of anti-leishmanial drugs and/or for generating DUB-selective tools, such as cell-permeable probes, DUBTAC and PROTAC molecules, to further understand the functionality of DUBs within the parasite (Mullard, 2019; Conole *et al.*, 2019; Henning *et al.*, 2022).

6.3 Impact and Future Perspectives

In this thesis, our efforts have successfully mitigated the background biotinylation stemming from the highly active PDB miniTurbo enzyme, resulting in the optimization of the XL-miniTurboID protocol in *Leishmania* promastigotes. This achievement was carried out through the depletion of biotin from the media of cultured cells using BioLock. Implementation of this optimized protocol allowed the characterisation of 73 proximal interacting proteins of the essential *L. mexicana* DUB2. Interestingly, these proteins are involved in a plethora of biological functions, spanning from translation to phosphorylation, underscoring the pleiotropic role of DUB2. We also investigated how the total ubiquitinome and proteome of *L. mexicana* promastigotes change in response to DUB2 depletion. For the former approach, we developed an optimized ubiquitinomics workflow, which involves the use of 7 mg of protein input, 5% SDS as lysis buffer, customized anti-DiGly antibody conjugated magnetic beads (CST) for DiGly-enrichment, timsTOF as an ideal mass spectrometer, DDA as a mode of acquisition, and FragPipe as database search software. Overall, we identified for the first time 122 ubiquitination sites to be upregulated and more than 50 proteins to be downregulated in response to DUB2. Insights into their biological function supported, as the PDB-derived statement, that DUB2 has a pleiotropic function.

The conclusions from the ubiquitinomics and proteomics datasets were driven independently of their relative occupancy. Thus, as a follow-up step, we are going to integrate the proteomics and ubiquitinomics data and represent them in a scatter plot. This will help discriminate DUB2-dependent effects on protein levels versus the degree of ubiquitination for each individual site identified, facilitating the substrate selection of DUB2. Regarding the validation of substrates of DUB2, we are planning to endogenously tag the substrates in the T7Cas9 DUB2^{FLOX^{+/+}} promastigote cells, treat cells with DMSO or rapamycin, perform immunoprecipitation against the substrate, and observe changes in the ubiquitination state of the immunoprecipitated substrate. It is expected that in the absence of DUB2, there would be an increase in ubiquitination of the substrate. Alternatively, gradient centrifugation or size exclusion chromatography can be used to identify higher molecular DUB2 containing complexes and their exact content.

Finally, we have identified more than 40 promising compounds that inhibit either or both *L. mexicana* and *T. cruzi* DUB2. Next, the most potent compounds will be tested for selectivity in parasites over human cells, and the parasite-selective compounds would be eventually tested for whether they inhibit *Leishmania/ Trypanosoma* DUBs using competitive ABPP. Validated parasite-specific DUB inhibiting compounds could be explored for therapeutics and/or for improving the molecular understanding of DUBs in the parasites.

Abbreviations

AAK1 = AP-2 associated kinase 1

AAT19 = amino acid transporter 19

ABP = activity based probe

ABPP = activity-based protein profiling

ACN = acetonitrile

AD = adenylation domain

AmB = Amphotericin B

AP-MS = affinity purification mass spectrometry

AXA = axenic amastigotes

A. aeolicus = *Aquifex aeolicus*

a.k.a = as known as

BCA = Bicinchoninic acid

BDF5 = bromodomain factor 5

BLASTp = protein-protein BLAST

BSD = blasticidin S deaminase

Cas9 = CRISPR-associated gene 9

CCD = catalytic cysteine domain

CCS = collisional cross section

CL = cutaneous leishmaniasis

CPSF73 = cleavage and polyadenylation specificity factor

CRISPR = clustered regularly interspaced short palindromic repeats

CYC12 = cyclin-12

Cy5 = Cyanine5

DCL = diffuse cutaneous leishmaniasis

DDA = data-dependent acquisition

DEP = Differential Enrichment analysis of Proteomics data

DIA = data-independent acquisition

DiCre = dimerizable Cre recombinase

DiGly = GlyGly

DMEM = Dulbecco's Modified Eagle Medium
DTT = Dithiothreitol
DUB = deubiquitinase
DUB2 = deubiquitinase 2
ERAD = endoplasmic reticulum-associated degradation
E. coli = *Escherichia coli*
FBS = fetal bovine serum
FC = fold-change
FDR = false discovery rate
GDI = rab-GDP dissociation inhibitor
GO = gene ontology
HCT116 = human colorectal carcinoma
HECT = homologous to E6AP C terminus
HeLa = Henrietta Lacks
HRP = horseradish peroxidase
HSP70 = heat shock protein 70
IGF-1 = insulin-like growth factor 1
iKO = inducible knockout
IP = immunoprecipitation
iPGMA = 2, 3-bisphosphoglycerate-independent phosphoglycerate mutase
IRS-2 = insulin receptor substrate
 K_d = dissociation constant
kDNA = kinetoplast DNA
KKT = kinetoplastid kinetochore protein
KLIF = kinesin localized to the ingressing furrow
KO = knockout
LB = Luria Broth
LC-MS/MS = Liquid Chromatography with Tandem Mass Spectrometry
LigI = DNA ligase I
loxP = locus of crossover of bacteriophage P1

L. mexicana = *Leishmania mexicana*

MAR = missing at random

MCL = mucocutaneous leishmaniasis

MNAR= missing not at random

MS/MS = tandem mass spectrometry

MWCO = molecular weight cut-off

NIF3 = NGG1 interacting factor 3-like protein

NTDs = neglected tropical disease

OPB = oligopeptidase-B

o/n = over-night

PAC = puromycin acetyltransferase

PASEF = Parallel Accumulation–Serial Fragmentation

PBS = phosphate-buffered saline

PCA = principal component analysis

PCC = Pearson correlation coefficient

PCR = polymerase chain reaction

PDB = proximity dependent biotinylation

PKDL = post-kala-azar dermal leishmaniasis

PFR = paraflagellar rod

PTM = post-translational modification

P. berghei = *Plasmodium berghei*

RBR = RING between RING

RDK2 = Repressor of differentiation kinase 2

REP = Rab escort proteins

RING = really interesting new gene

RIPA = Radioimmunoprecipitation assay buffer

RPSA = 40S ribosomal protein SA

SDC = sodium deoxycholate

SDS = sodium dodecyl sulfate

SEC = size-exclusion chromatography

SEC-MALLS = size-exclusion chromatography-multi angle laser light scattering

Sf21 = ovarian cells isolated from *Spodoptera frugiperda*
sgRNA = single guide RNA
SNAT1 = sodium-coupled neutral amino acid symporter 1
SPD = sample per day
SRP68 = signal-recognition-particle 68
STRAP = serine-threonine kinase receptor-associated protein
STUPs = SUMO-targeted ubiquitin proteases
S-trap = suspension trap
TBST = Tris-buffered saline with 0.1% Tween 20 detergent
TEAB = triethyl ammonium bicarbonate
TFA = trifluoroacetic acid
TimsTOF = trapped ion mobility spectrometry coupled to a time-of-flight mass spectrometer
TLK2 = tousled-like kinase 2
T. brucei = *Trypanosoma brucei*
T. cruzi = *Trypanosoma cruzi*
T. evansi = *Trypanosoma evansi*
Ub-PA = ubiquitin-propargylamide
Ub-Rho = Ubiquitin Rhodamine 110
Ub-VME = ubiquitin-vinyl methyl ester
USP = ubiquitin-specific peptidase
VL = visceral leishmaniasis
WHO = World Health Organization
XPC = xeroderma pigmentosum C

References

- Aalto, A., Martínez-Chacón, G., Kietz, C., Tsyganova, N., Kreutzer, J., Kallio, P., Broemer, M. and Meinander, A., 2022. M1-linked ubiquitination facilitates NF- κ B activation and survival during sterile inflammation. *The FEBS Journal*, 289(17), pp.5180-5197.
- Adams, T., Ennusun, N.A.A., Quashie, N.B., Futagbi, G., Matrevi, S., Hagan, O.C., Abuaku, B., Koram, K.A. and Duah, N.O., 2018. Prevalence of Plasmodium falciparum delayed clearance associated polymorphisms in adaptor protein complex 2 mu subunit (pfap2mu) and ubiquitin specific protease 1 (pfubp1) genes in Ghanaian isolates. *Parasites & vectors*, 11, pp.1-12.
- Adhiambo, C., Forney, J.D., Asai, D.J. and LeBowitz, J.H., 2005. The two cytoplasmic dynein-2 isoforms in Leishmania mexicana perform separate functions. *Molecular and biochemical parasitology*, 143(2), pp.216-225.
- Adler-Moore, J.P. and Proffitt, R.T., 1993. Development, characterization, efficacy and mode of action of Ambisome, a unilamellar liposomal formulation of amphotericin B. *Journal of Liposome Research*, 3(3), pp.429-450.
- Aizawa, M. and Fukuda, M., 2015. Small GTPase Rab2B and its specific binding protein Golgi-associated Rab2B interactor-like 4 (GARI-L4) regulate Golgi morphology. *Journal of Biological Chemistry*, 290(36), pp.22250-22261.
- Akimov, V., Barrio-Hernandez, I., Hansen, S.V., Hallenborg, P., Pedersen, A.K., Bekker-Jensen, D.B., Puglia, M., Christensen, S.D., Vanselow, J.T., Nielsen, M.M. and Kratchmarova, I., 2018. UbiSite approach for comprehensive mapping of lysine and N-terminal ubiquitination sites. *Nature structural & molecular biology*, 25(7), pp.631-640.
- Alory, C. and Balch, W.E., 2003. Molecular evolution of the Rab-escort-protein/guanine-nucleotide-dissociation-inhibitor superfamily. *Molecular biology of the cell*, 14(9), pp.3857-3867.
- Alsford, S., Eckert, S., Baker, N., Glover, L., Sanchez-Flores, A., Leung, K.F., Turner, D.J., Field, M.C., Berriman, M. and Horn, D., 2012. High-throughput decoding of antitrypanosomal drug efficacy and resistance. *Nature*, 482(7384), pp.232-236.
- Altun, M., Kramer, H.B., Willems, L.I., McDermott, J.L., Leach, C.A., Goldenberg, S.J., Kumar, K.S., Konietzny, R., Fischer, R., Kogan, E. and Mackeen, M.M., 2011. Activity-based chemical proteomics accelerates inhibitor development for deubiquitylating enzymes. *Chemistry & biology*, 18(11), pp.1401-1412.
- Alvar, J., Yactayo, S. and Bern, C., 2006. Leishmaniasis and poverty. *Trends in parasitology*, 22(12), pp.552-557.
- Alvar, J., Aparicio, P., Aseffa, A., Den Boer, M., Canavate, C., Dedet, J.P., Gradoni, L., Ter Horst, R., López-Vélez, R. and Moreno, J., 2008. The relationship between leishmaniasis and AIDS: the second 10 years. *Clinical microbiology reviews*, 21(2), pp.334-359.
- Alves, C.L., Repolês, B.M., da Silva, M.S., Mendes, I.C., Marin, P.A., Aguiar, P.H.N., Santos, S.D.S., Franco, G.R., Macedo, A.M., Pena, S.D.J. and Andrade, L.D.O., 2018. The recombinase Rad51 plays a key role in events of genetic exchange in Trypanosoma cruzi. *Scientific reports*, 8(1), p.13335.

- Ambrosio, F.A., Costa, G., Gallo Cantafio, M.E., Torcasio, R., Trapasso, F., Alcaro, S., Viglietto, G. and Amodio, N., 2023. Natural Agents as Novel Potential Source of Proteasome Inhibitors with Anti-Tumor Activity: Focus on Multiple Myeloma. *Molecules*, 28(3), p.1438.
- Abi Habib, J., Lesenfans, J., Vigneron, N. and Van den Eynde, B.J., 2022. Functional differences between proteasome subtypes. *Cells*, 11(3), p.421.
- Akimov, V., Barrio-Hernandez, I., Hansen, S.V., Hallenborg, P., Pedersen, A.K., Bekker-Jensen, D.B., Puglia, M., Christensen, S.D., Vanselow, J.T., Nielsen, M.M. and Kratchmarova, I., 2018. UbiSite approach for comprehensive mapping of lysine and N-terminal ubiquitination sites. *Nature structural & molecular biology*, 25(7), pp.631-640.
- Aoki, J.I., Muxel, S.M., Zampieri, R.A., Acuña, S.M., Fernandes, J.C.R., Vanderlinde, R.H., Sales, M.C.O.D.P. and Floeter-Winter, L.M., 2017. L-arginine availability and arginase activity: characterization of amino acid permease 3 in *Leishmania amazonensis*. *PLoS Neglected Tropical Diseases*, 11(10), p.e0006025.
- Arastu-Kapur, S., Anderl, J.L., Kraus, M., Parlati, F., Shenk, K.D., Lee, S.J., Muchamuel, T., Bennett, M.K., Driessen, C., Ball, A.J. and Kirk, C.J., 2011. Nonproteasomal targets of the proteasome inhibitors bortezomib and carfilzomib: a link to clinical adverse events. *Clinical Cancer Research*, 17(9), pp.2734-2743.
- Arendt, C.S. and Hochstrasser, M., 1997. Identification of the yeast 20S proteasome catalytic centers and subunit interactions required for active-site formation. *Proceedings of the National Academy of Sciences*, 94(14), pp.7156-7161.
- Arora, P., Narwal, M., Thakur, V., Mukhtar, O., Malhotra, P. and Mohammed, A., 2023. A *Plasmodium falciparum* ubiquitin-specific protease (Pf USP) is essential for parasite survival and its disruption enhances artemisinin efficacy. *Biochemical Journal*, 480(1), pp.25-39.
- Artavanis-Tsakonas, K., Misaghi, S., Comeaux, C.A., Catic, A., Spooner, E., Duraisingh, M.T. and Ploegh, H.L., 2006. Identification by functional proteomics of a deubiquitinating/deNeddylating enzyme in *Plasmodium falciparum*. *Molecular microbiology*, 61(5), pp.1187-1195.
- Artavanis-Tsakonas, K., Weihofen, W.A., Antos, J.M., Coleman, B.I., Comeaux, C.A., Duraisingh, M.T., Gaudet, R. and Ploegh, H.L., 2010. Characterization and structural studies of the *Plasmodium falciparum* ubiquitin and Nedd8 hydrolase UCHL3. *Journal of Biological Chemistry*, 285(9), pp.6857-6866.
- Avvakumov, G.V., Walker, J.R., Xue, S., Allali-Hassani, A., Asinas, A., Nair, U.B., Fang, X., Zuo, X., Wang, Y.X., Wilkinson, K.D. and Dhe-Paganon, S., 2012. Two ZnF-UBP domains in isopeptidase T (USP5). *Biochemistry*, 51(6), pp.1188-1198.
- Azevedo, C.S., Guido, B.C., Pereira, J.L., Nolasco, D.O., Corrêa, R., Magalhães, K.G., Motta, F.N., Santana, J.M., Grellier, P. and Bastos, I.M., 2017. Revealing a novel otubain-like enzyme from *Leishmania infantum* with deubiquitinating activity toward K48-linked substrate. *Frontiers in Chemistry*, 5, p.13.
- Babiano, R., Badis, G., Saveanu, C., Namane, A., Doyen, A., Díaz-Quintana, A., Jacquier, A., Fromont-Racine, M. and de La Cruz, J., 2013. Yeast ribosomal protein L7 and its homologue Rlp7 are simultaneously present at distinct sites on pre-60S ribosomal particles. *Nucleic Acids Research*, 41(20), pp.9461-9470.

- Balakirev, M.Y., Jaquinod, M., Haas, A.L. and Chroboczek, J., 2002. Deubiquitinating function of adenovirus proteinase. *Journal of virology*, 76(12), pp.6323-6331.
- Ballantine, J.A., Hassall, C.H., Jones, B.D. and Jones, G., 1967. The biosynthesis of phenols—XII.: Asperugin B, a metabolite of *Aspergillus rugulosus*. *Phytochemistry*, 6(8), pp.1157-1159.
- Bar, D.Z., Atkatsch, K., Tavarez, U., Erdos, M.R., Gruenbaum, Y. and Collins, F.S., 2018. Biotinylation by antibody recognition—a method for proximity labelling. *Nature methods*, 15(2), pp.127-133.
- Barak, E., Amin-Spector, S., Gerliak, E., Goyard, S., Holland, N. and Zilberstein, D., 2005. Differentiation of *Leishmania donovani* in host-free system: analysis of signal perception and response. *Molecular and biochemical parasitology*, 141(1), pp.99-108.
- Bardia, A., Parton, M., Kümmel, S., Estévez, L.G., Huang, C.S., Cortés, J., Ruiz-Borrego, M., Telli, M.L., Martin-Martorell, P., López, R. and Beck, J.T., 2018. Paclitaxel with inhibitor of apoptosis antagonist, LCL161, for localized triple-negative breast cancer, prospectively stratified by gene signature in a biomarker-driven neoadjuvant trial. *Journal of Clinical Oncology*, 36(31), pp.3126-3133.
- Barghout, S.H. and Schimmer, A.D., 2021. E1 enzymes as therapeutic targets in cancer. *Pharmacological reviews*, 73(1), pp.1-58.
- Bartholomeu, D.C., Teixeira, S.M.R. and Cruz, A.K., 2021. *Genomics and functional genomics in Leishmania and Trypanosoma cruzi: statuses, challenges and perspectives*. Memórias do Instituto Oswaldo Cruz, 116, p.e200634.
- Baudouin, H.C.M., Pfeiffer, L. and Ochsenreiter, T., 2020. A comparison of three approaches for the discovery of novel tripartite attachment complex proteins in *Trypanosoma brucei*. *PLoS neglected tropical diseases*, 14(9), p.e0008568.
- Bayona, J.C., Nakayasu, E.S., Laverriere, M., Aguilar, C., Sobreira, T.J., Choi, H., Nesvizhskii, A.I., Almeida, I.C., Cazzulo, J.J. and Alvarez, V.E., 2011. SUMOylation pathway in *Trypanosoma cruzi*: functional characterization and proteomic analysis of target proteins. *Molecular & Cellular Proteomics*, 10(12).
- Bea, A., Kröber-Boncardo, C., Sandhu, M., Brinker, C. and Clos, J., 2020. The *Leishmania donovani* SENP protease is required for SUMO processing but not for viability. *Genes*, 11(10), p.1198.
- Bello, A.I., Goswami, R., Brown, S.L., Costanzo, K., Shores, T., Allan, S., Odah, R. and Mohan, R.D., 2022. Deubiquitinases in neurodegeneration. *Cells*, 11(3), p.556.
- Beneke, T., Madden, R., Makin, L., Valli, J., Sunter, J. and Gluenz, E., 2017. A CRISPR Cas9 high-throughput genome editing toolkit for kinetoplastids. *Royal Society open science*, 4(5), p.170095.
- Benetatos, C.A., Mitsuuchi, Y., Burns, J.M., Neiman, E.M., Condon, S.M., Yu, G., Seipel, M.E., Kapoor, G.S., LaPorte, M.G., Rippin, S.R. and Deng, Y., 2014. Birinapant (TL32711), a bivalent SMAC mimetic, targets TRAF2-associated cIAPs, abrogates TNF-induced NF- κ B activation, and is active in patient-derived xenograft models. *Molecular cancer therapeutics*, 13(4), pp.867-879.
- Besche, H.C., Sha, Z., Kukushkin, N.V., Peth, A., Hock, E.M., Kim, W., Gygi, S., Gutierrez, J.A., Liao, H., Dick, L. and Goldberg, A.L., 2014. Autoubiquitination of the 26S proteasome on Rpn13 regulates breakdown of ubiquitin conjugates. *The EMBO journal*, 33(10), pp.1159-1176.
- Besteiro, S., Williams, R.A., Coombs, G.H. and Mottram, J.C., 2007. Protein turnover and differentiation in *Leishmania*. *International journal for parasitology*, 37(10), pp.1063-1075.

- Bharat, A. and Brown, E.D., 2014. Phenotypic investigations of the depletion of EngA in *Escherichia coli* are consistent with a role in ribosome biogenesis. *FEMS microbiology letters*, 353(1), pp.26-32.
- Bharti, H., Singal, A., Saini, M., Cheema, P.S., Raza, M., Kundu, S. and Nag, A., 2022. Repurposing the Pathogen Box compounds for identification of potent anti-malarials against blood stages of *Plasmodium falciparum* with PfUCL3 inhibitory activity. *Scientific Reports*, 12(1), p.918.
- Bhattacharya, A., Corbeil, A., do Monte-Neto, R.L. and Fernandez-Prada, C., 2020. Of drugs and trypanosomatids: new tools and knowledge to reduce bottlenecks in drug discovery. *Genes*, 11(7), p.722.
- Bickerton, G.R., Paolini, G.V., Besnard, J., Muresan, S. and Hopkins, A.L., 2012. Quantifying the chemical beauty of drugs. *Nature chemistry*, 4(2), pp.90-98.
- Billington, K., Halliday, C., Madden, R., Dyer, P., Barker, A.R., Moreira-Leite, F.F., Carrington, M., Vaughan, S., Hertz-Fowler, C., Dean, S. and Sunter, J.D., 2023. Genome-wide subcellular protein map for the flagellate parasite *Trypanosoma brucei*. *Nature microbiology*, 8(3), pp.533-547.
- Bingol, B., Tea, J.S., Phu, L., Reichelt, M., Bakalarski, C.E., Song, Q., Foreman, O., Kirkpatrick, D.S. and Sheng, M., 2014. The mitochondrial deubiquitinase USP30 opposes parkin-mediated mitophagy. *Nature*, 510(7505), pp.370-375.
- Blazejewski, S.M., Bennison, S.A., Ha, N.T., Liu, X., Smith, T.H., Dougherty, K.J. and Toyo-Oka, K., 2022. Rpsa signaling regulates cortical neuronal morphogenesis via its ligand, PEDF, and plasma membrane interaction partner, Itga6. *Cerebral Cortex*, 32(4), pp.770-795.
- Bogdan, C., 2020. Macrophages as host, effector and immunoregulatory cells in leishmaniasis: Impact of tissue micro-environment and metabolism. *Cytokine: X*, 2(4), p.100041.
- Borodovsky, A., Ovaa, H., Kolli, N., Gan-Erdene, T., Wilkinson, K.D., Ploegh, H.L. and Kessler, B.M., 2002. Chemistry-based functional proteomics reveals novel members of the deubiquitinating enzyme family. *Chemistry & biology*, 9(10), pp.1149-1159.
- Bose, P., Baron, N., Ben-Zvi, A. and Shapira, M., LeishIF3d is a non-canonical cap-binding protein specific for *Leishmania*. *Frontiers in Molecular Biosciences*, 10, p.356.
- Botelho, D., Wall, M.J., Vieira, D.B., Fitzsimmons, S., Liu, F. and Doucette, A., 2010. Top-down and bottom-up proteomics of SDS-containing solutions following mass-based separation. *Journal of proteome research*, 9(6), pp.2863-2870.
- Brahmachari, U., 1940. Gleanings from My Researches. Vol. I. Kala-Azar, its Chemotherapy. *Gleanings from My Researches. Vol. I. Kala-Azar, its Chemotherapy*.
- Branigan, E., Carlos Penedo, J. and Hay, R.T., 2020. Ubiquitin transfer by a RING E3 ligase occurs from a closed E2~ ubiquitin conformation. *Nature Communications*, 11(1), p.2846.
- Branon, T.C., Bosch, J.A., Sanchez, A.D., Udeshi, N.D., Svinkina, T., Carr, S.A., Feldman, J.L., Perrimon, N. and Ting, A.Y., 2018. Efficient proximity labelling in living cells and organisms with TurboID. *Nature biotechnology*, 36(9), pp.880-887.
- Braten, O., Livneh, I., Ziv, T., Admon, A., Kehat, I., Caspi, L.H., Gonen, H., Bercovich, B., Godzik, A., Jahandideh, S. and Jaroszewski, L., 2016. Numerous proteins with unique characteristics are degraded by the 26S proteasome following monoubiquitination. *Proceedings of the National Academy of Sciences*, 113(32), pp.E4639-E4647

- Brownell, J.E., Sintchak, M.D., Gavin, J.M., Liao, H., Bruzzese, F.J., Bump, N.J., Soucy, T.A., Milhollen, M.A., Yang, X., Burkhardt, A.L. and Ma, J., 2010. Substrate-assisted inhibition of ubiquitin-like protein-activating enzymes: the NEDD8 E1 inhibitor MLN4924 forms a NEDD8-AMP mimetic in situ. *Molecular cell*, 37(1), pp.102-111.
- Burza, S., Croft, S.L. and Boelaert, M., Leishmaniasis *Lancet*, 392 (10151)(2018). [View PDF](#) [View article](#) [View in Scopus](#), pp.951-970.
- Burge, R., 2020. The ubiquitination enzymes of *Leishmania mexicana* (Doctoral dissertation, University of York).
- Burge, R.J., Damianou, A., Wilkinson, A.J., Rodenko, B. and Mottram, J.C., 2020. Leishmania differentiation requires ubiquitin conjugation mediated by a UBC2-UEV1 E2 complex. *PLoS Pathogens*, 16(10), p.e1008784.
- Burge, R.J., Mottram, J.C. and Wilkinson, A.J., 2022. Ubiquitin and ubiquitin-like conjugation systems in trypanosomatids. *Current Opinion in Microbiology*, 70, p.102202.
- Busch, H., 1984. Ubiquitination of Proteins. In *Methods in Enzymology* (Vol. 106, pp. 238-262). Academic Press.
- Caba, C., Mohammadzadeh, A. and Tong, Y., 2022. On the study of deubiquitinases: Using the right tools for the job. *Biomolecules*, 12(5), p.703.
- Camacho, E., Rastrojo, A., Sanchiz, Á., González-De la Fuente, S., Aguado, B. and Requena, J.M., 2019. Leishmania mitochondrial genomes: maxicircle structure and heterogeneity of minicircles. *Genes*, 10(10), p.758.
- Cappadocia, L. and Lima, C.D., 2018. Ubiquitin-like protein conjugation: structures, chemistry, and mechanism. *Chemical reviews*, 118(3), pp.889-918.
- Carnielli, J.B., Monti-Rocha, R., Costa, D.L., Sesana, A.M., Pansini, L.N., Segatto, M., Mottram, J.C., Costa, C.H.N., Carvalho, S.F. and Dietze, R., 2019. Natural resistance of *Leishmania infantum* to miltefosine contributes to the low efficacy in the treatment of visceral leishmaniasis in Brazil. *The American journal of tropical medicine and hygiene*, 101(4), p.789.
- Cavalcanti, D.P. and de Souza, W., 2018. The kinetoplast of trypanosomatids: from early studies of electron microscopy to recent advances in atomic force microscopy. *Scanning*, 2018.
- Ceccarelli, D.F., Tang, X., Pelletier, B., Orlicky, S., Xie, W., Plantevin, V., Neculai, D., Chou, Y.C., Ogunjimi, A., Al-Hakim, A. and Varelas, X., 2011. An allosteric inhibitor of the human Cdc34 ubiquitin-conjugating enzyme. *Cell*, 145(7), pp.1075-1087.
- Celebi, G., Kesim, H., Ozer, E. and Kutlu, O., 2020. The effect of dysfunctional ubiquitin enzymes in the pathogenesis of most common diseases. *International journal of molecular sciences*, 21(17), p.6335.
- Celen, A.B. and Sahin, U., 2020. Sumoylation on its 25th anniversary: mechanisms, pathology, and emerging concepts. *The FEBS journal*, 287(15), pp.3110-3140.
- Chadchankar, J., Korboukh, V., Conway, L.C., Wobst, H.J., Walker, C.A., Doig, P., Jacobsen, S.J., Brandon, N.J., Moss, S.J. and Wang, Q., 2019. Inactive USP14 and inactive UCHL5 cause accumulation of distinct ubiquitinated proteins in mammalian cells. *Plos one*, 14(11), p.e0225145.

- Chandra, U., Yadav, A., Kumar, D. and Saha, S., 2017. Cell cycle stage-specific transcriptional activation of cyclins mediated by HAT2-dependent H4K10 acetylation of promoters in *Leishmania donovani*. *PLoS Pathogens*, 13(9), p.e1006615.
- Charlab, R., Tesh, R.B., Rowton, E.D. and Ribeiro, J.M., 1995. *Leishmania amazonensis*: sensitivity of different promastigote morphotypes to salivary gland homogenates of the sand fly *Lutzomyia longipalpis*. *Experimental parasitology*, 80(2), pp.167-175.
- Chen, J., Dexheimer, T.S., Ai, Y., Liang, Q., Villamil, M.A., Inglese, J., Maloney, D.J., Jadhav, A., Simeonov, A. and Zhuang, Z., 2011. Selective and cell-active inhibitors of the USP1/UAF1 deubiquitinase complex reverse cisplatin resistance in non-small cell lung cancer cells. *Chemistry & biology*, 18(11), pp.1390-1400.
- Chen, T., Zhou, T., He, B., Yu, H., Guo, X., Song, X. and Sha, J., 2014. mUbiSiDa: a comprehensive database for protein ubiquitination sites in mammals. *PLoS one*, 9(1), p.e85744.
- Chen, Z., Wang, Y., Song, Y., Song, S., He, Z., Feng, S., Li, W., Ding, Y., Zhang, J., Zhao, L. and Jiao, P., 2023. Duck MARCH8 Negatively Regulates the RLR Signaling Pathway through K29-Linked Polyubiquitination of MAVS. *The Journal of Immunology*, 210(6), pp.786-794.
- Chevalier, N., Rigden, D.J., Van Roy, J., Opperdoes, F.R. and Michels, P.A., 2000. *Trypanosoma brucei* contains a 2, 3-bisphosphoglycerate independent phosphoglycerate mutase. *European Journal of Biochemistry*, 267(5), pp.1464-1472.
- Choi, W.Y., Gemberling, M., Wang, J., Holdway, J.E., Shen, M.C., Karlstrom, R.O. and Poss, K.D., 2013. In vivo monitoring of cardiomyocyte proliferation to identify chemical modifiers of heart regeneration. *Development*, 140(3), pp.660-666.
- Clague, M.J., Urbé, S. and Komander, D., 2019. Breaking the chains: deubiquitylating enzyme specificity begets function. *Nature reviews Molecular cell biology*, 20(6), pp.338-352.
- Clayton, C., 2019. Regulation of gene expression in trypanosomatids: living with polycistronic transcription. *Open biology*, 9(6), p.190072.
- Cloutier, S., Laverdière, M., Chou, M.N., Boilard, N., Chow, C. and Papadopoulou, B., 2012. Translational control through eIF2 α phosphorylation during the *Leishmania* differentiation process. *PLoS One*, 7(5), p.e35085.
- Colland, F., Formstecher, E., Jacq, X., Reverdy, C., Planquette, C., Conrath, S., Trouplin, V., Bianchi, J., Aushev, V.N., Camonis, J. and Calabrese, A., 2009. Small-molecule inhibitor of USP7/HAUSP ubiquitin protease stabilizes and activates p53 in cells. *Molecular cancer therapeutics*, 8(8), pp.2286-2295.
- Conole, D., Mondal, M., Majmudar, J.D. and Tate, E.W., 2019. Recent developments in cell permeable deubiquitinating enzyme activity-based probes. *Frontiers in Chemistry*, 7, p.876.
- Corrales, R.M., Vaselek, S., Neish, R., Berry, L., Brunet, C.D., Crobu, L., Kuk, N., Mateos-Langerak, J., Robinson, D.R., Volf, P. and Mottram, J.C., 2021. The kinesin of the flagellum attachment zone in *Leishmania* is required for cell morphogenesis, cell division and virulence in the mammalian host. *PLoS Pathogens*, 17(6), p.e1009666.
- Correia, S.P., Chan, A.B., Vaughan, M., Zolboot, N., Perea, V., Huber, A.L., Kriebs, A., Moresco, J.J., Yates III, J.R. and Lamia, K.A., 2019. The circadian E3 ligase complex SCFFBXL3+ CRY targets TLK2. *Scientific reports*, 9(1), p.198.

- Coser, E.M., Ferreira, B.A., Branco, N., Yamashiro-Kanashiro, E.H., Lindoso, J.A.L. and Coelho, A.C., 2020. Activity of paromomycin against *Leishmania amazonensis*: Direct correlation between susceptibility in vitro and the treatment outcome in vivo. *International Journal for Parasitology: Drugs and Drug Resistance*, 14, pp.91-98.
- Creasy, D.M. and Cottrell, J.S., 2002. Error tolerant searching of uninterpreted tandem mass spectrometry data. *Proteomics*, 2(10), pp.1426-1434.
- Crowther, G.J., Booker, M.L., He, M., Li, T., Raverdy, S., Novelli, J.F., He, P., Dale, N.R., Fife, A.M., Barker Jr, R.H. and Kramer, M.L., 2014. Cofactor-independent phosphoglycerate mutase from nematodes has limited druggability, as revealed by two high-throughput screens. *PLoS Neglected Tropical Diseases*, 8(1), p.e2628.
- Crozier, T.W.M., 2016. Proteomic Analysis of Protein Complexes and Cell Cycle Regulation in *Trypanosoma Brucei* (Doctoral dissertation, University of Dundee).
- Cull, B., Prado Godinho, J.L., Fernandes Rodrigues, J.C., Frank, B., Schurigt, U., Williams, R.A., Coombs, G.H. and Mottram, J.C., 2014. Glycosome turnover in *Leishmania major* is mediated by autophagy. *Autophagy*, 10(12), pp.2143-2157.
- Currier, R.B., Cooper, A., Burrell-Saward, H., MacLeod, A. and Alford, S., 2018. Decoding the network of *Trypanosoma brucei* proteins that determines sensitivity to apolipoprotein-L1. *PLoS pathogens*, 14(1), p.e1006855.
- Dacher, M., Morales, M.A., Pescher, P., Leclercq, O., Rachidi, N., Prina, E., Cayla, M., Descoteaux, A. and Späth, G.F., 2014. Probing druggability and biological function of essential proteins in *Leishmania* combining facilitated null mutant and plasmid shuffle analyses. *Molecular microbiology*, 93(1), pp.146-166.
- Damasceno, J.D., Reis-Cunha, J., Crouch, K., Beraldi, D., Lapsley, C., Tosi, L.R., Bartholomeu, D. and McCulloch, R., 2020. Conditional knockout of RAD51-related genes in *Leishmania major* reveals a critical role for homologous recombination during genome replication. *PLoS genetics*, 16(7), p.e1008828.
- Dambacher, C.M., Worden, E.J., Herzik Jr, M.A., Martin, A. and Lander, G.C., 2016. Atomic structure of the 26S proteasome lid reveals the mechanism of deubiquitinase inhibition. *elife*, 5, p.e13027
- Damianou, A., Burge, R.J., Catta-Preta, C.M., Geoghegan, V., Nievas, Y.R., Newling, K., Brown, E., Burchmore, R., Rodenko, B. and Mottram, J.C., 2020. Essential roles for deubiquitination in *Leishmania* life cycle progression. *PLoS Pathogens*, 16(6), p.e1008455.
- Dang, L.C., Melandri, F.D. and Stein, R.L., 1998. Kinetic and mechanistic studies on the hydrolysis of ubiquitin C-terminal 7-amido-4-methylcoumarin by deubiquitinating enzymes. *Biochemistry*, 37(7), pp.1868-1879.
- das Chagas, B.D., Pereira, T.M., Cantanhêde, L.M., Da Silva, G.P., Boité, M.C., Pereira, L.D.O.R. and Cupolillo, E., 2022. Interspecies and intrastrain interplay among *Leishmania* spp. parasites. *Microorganisms*, 10(10), p.1883.
- de Almeida, R.F., Fernandes, M. and de Godoy, L.M.F., 2021. An updated map of *Trypanosoma cruzi* histone post-translational modifications. *Scientific Data*, 8(1), p.93.

- de Jong, A., Witting, K., Kooij, R., Flierman, D. and Ovaa, H., 2017. Release of enzymatically active deubiquitinating enzymes upon reversible capture by disulfide ubiquitin reagents. *Angewandte Chemie International Edition*, 56(42), pp.12967-12970.
- De Pablos, L.M., Ferreira, T.R., Dowle, A.A., Forrester, S., Parry, E., Newling, K. and Walrad, P.B., 2019. The mRNA-bound proteome of *Leishmania mexicana*: novel genetic insight into an ancient parasite. *Molecular & Cellular Proteomics*, 18(7), pp.1271-1284.
- De Pablos, L.M., Ferreira, T.R. and Walrad, P.B., 2016. Developmental differentiation in *Leishmania* lifecycle progression: post-transcriptional control conducts the orchestra. *Current opinion in microbiology*, 34, pp.82-89.
- de Poot, S.A., Tian, G. and Finley, D., 2017. Meddling with fate: the proteasomal deubiquitinating enzymes. *Journal of molecular biology*, 429(22), pp.3525-3545.
- Dhara, A., de Paula Baptista, R., Kissinger, J.C., Snow, E.C. and Sinai, A.P., 2017. Ablation of an ovarian tumor family deubiquitinase exposes the underlying regulation governing the plasticity of cell cycle progression in *Toxoplasma gondii*. *MBio*, 8(6), pp.10-1128.
- Dhara, A. and Sinai, A.P., 2016. A cell cycle-regulated *Toxoplasma* deubiquitinase, TgOTUD3A, targets polyubiquitin with specific lysine linkages. *Msphere*, 1(3), pp.10-1128.
- Dick, T.P., Nussbaum, A.K., Deeg, M., Heinemeyer, W., Groll, M., Schirle, M., Keilholz, W., Stevanovic, S., Wolf, D.H., Huber, R. and Rammensee, H.G., 1998. Contribution of proteasomal β -subunits to the cleavage of peptide substrates analysed with yeast mutants. *Journal of Biological Chemistry*, 273(40), pp.25637-25646.
- Dikic, I. and Schulman, B.A., 2023. An expanded lexicon for the ubiquitin code. *Nature Reviews Molecular Cell Biology*, 24(4), pp.273-287.
- Dikic, I., Wakatsuki, S. and Walters, K.J., 2009. Ubiquitin-binding domains—from structures to functions. *Nature reviews Molecular cell biology*, 10(10), pp.659-671.
- Dimova, N.V., Hathaway, N.A., Lee, B.H., Kirkpatrick, D.S., Berkowitz, M.L., Gygi, S.P., Finley, D. and King, R.W., 2012. APC/C-mediated multiple monoubiquitylation provides an alternative degradation signal for cyclin B1. *Nature cell biology*, 14(2), pp.168-176.
- Ding, Q., Zhang, Z., Liu, J.J., Jiang, N., Zhang, J., Ross, T.M., Chu, X.J., Bartkovitz, D., Podlaski, F., Janson, C. and Tovar, C., 2013. Discovery of RG7388, a potent and selective p53–MDM2 inhibitor in clinical development. *Journal of medicinal chemistry*, 56(14), pp.5979-5983.
- Dumetz, F., Cuypers, B., Imamura, H., Zander, D., D'Haenens, E., Maes, I., Domagalska, M.A., Clos, J., Dujardin, J.C. and De Muylder, G., 2018. Molecular preadaptation to antimony resistance in *Leishmania donovani* on the Indian subcontinent. *MSphere*, 3(2), pp.e00548-17.
- Duncan, S.M., Myburgh, E., Philippon, C., Brown, E., Meissner, M., Brewer, J. and Mottram, J.C., 2016. Conditional gene deletion with DiCre demonstrates an essential role for CRK3 in *Leishmania mexicana* cell cycle regulation. *Molecular microbiology*, 100(6), pp.931-944.
- Dupé, A., Dumas, C. and Papadopoulou, B., 2015. Differential subcellular localization of *Leishmania* Alba-domain proteins throughout the parasite development. *PLoS One*, 10(9), p.e0137243.
- Dutcher, J.D., 1968. The discovery and development of amphotericin B. *Diseases of the Chest*, 54, pp.296-298.

Ekkebus, R., van Kasteren, S.I., Kulathu, Y., Scholten, A., Berlin, I., Geurink, P.P., de Jong, A., Goerdayal, S., Neefjes, J., Heck, A.J. and Komander, D., 2013. On terminal alkynes that can react with active-site cysteine nucleophiles in proteases. *Journal of the American Chemical Society*, 135(8), pp.2867-2870.

Elu, N., Osinalde, N., Ramirez, J., Presa, N., Rodriguez, J.A., Prieto, G. and Mayor, U., 2022, January. Identification of substrates for human deubiquitinating enzymes (DUBs): an up-to-date review and a case study for neurodevelopmental disorders. In *Seminars in Cell & Developmental Biology*. Academic Press.

Engstler, M. and Beneke, T., 2023. Gene editing and scalable functional genomic screening in *Leishmania* species using the CRISPR/Cas9 cytosine base editor toolbox LeishBASEedit. *Elife*, 12, p.e85605.

Erker, Y., Neyret-Kahn, H., Seeler, J.S., Dejean, A., Atfi, A. and Levy, L., 2013. Arkadia, a novel SUMO-targeted ubiquitin ligase involved in PML degradation. *Molecular and cellular biology*, 33(11), pp.2163-2177.

Espinar-Marchena, F., Rodríguez-Galán, O., Fernández-Fernández, J., Linnemann, J. and de la Cruz, J., 2018. Ribosomal protein L14 contributes to the early assembly of 60S ribosomal subunits in *Saccharomyces cerevisiae*. *Nucleic acids research*, 46(9), pp.4715-4732.

Esposito, M., Akman, H.B., Giron, P., Ceregido, M.A., Schepers, R., Ramos Paez, L.C., La Monaca, E., De Greve, J., Coux, O., De Trez, C. and Lindon, C., 2020. USP13 controls the stability of Aurora B impacting progression through the cell cycle. *Oncogene*, 39(37), pp.6009-6023.

Fang, Z., Li, X., Yoshino, Y., Suzuki, M., Qi, H., Murooka, H., Katakai, R., Shirota, M., Pham, T.A.M., Matsuzawa, A. and Otsuka, K., 2023. Aurora A polyubiquitinates the BRCA1-interacting protein OLA1 to promote centrosome maturation. *Cell Reports*, 42(8).

Fernández, M.M., Malchiodi, E.L. and Algranati, I.D., 2011. Differential effects of paromomycin on ribosomes of *Leishmania mexicana* and mammalian cells. *Antimicrobial agents and chemotherapy*, 55(1), pp.86-93.

Fiebig, M., Kelly, S. and Gluenz, E., 2015. Comparative life cycle transcriptomics revises *Leishmania mexicana* genome annotation and links a chromosome duplication with parasitism of vertebrates. *PLoS pathogens*, 11(10), p.e1005186.

Fleischmann, J. and Campbell, D.A., 1994. Expression of the *Leishmania tarentolae* ubiquitin-encoding and mini-exon genes. *Gene*, 144(1), pp.45-51.

Flygare, J.A., Beresini, M., Budha, N., Chan, H., Chan, I.T., Cheeti, S., Cohen, F., Deshayes, K., Doerner, K., Eckhardt, S.G. and Elliott, L.O., 2012. Discovery of a potent small-molecule antagonist of inhibitor of apoptosis (IAP) proteins and clinical candidate for the treatment of cancer (GDC-0152). *Journal of medicinal chemistry*, 55(9), pp.4101-4113.

Foresti, O., Ruggiano, A., Hannibal-Bach, H.K., Ejsing, C.S. and Carvalho, P., 2013. Sterol homeostasis requires regulated degradation of squalene monooxygenase by the ubiquitin ligase Doa10/Teb4. *Elife*, 2, p.e00953.

Forestier, C.L., Machu, C., Loussert, C., Pescher, P. and Späth, G.F., 2011. Imaging host cell-*Leishmania* interaction dynamics implicates parasite motility, lysosome recruitment, and host cell wounding in the infection process. *Cell host & microbe*, 9(4), pp.319-330.

- Franco, J., Blackie, M.A., Toth, D., Smith, P.J., Capuano, J., Fastnacht, K. and Berkes, C., 2013. A structural comparative approach to identifying novel antimalarial inhibitors. *Computational Biology and Chemistry*, 45, pp.42-47.
- Frickel, E.M., Quesada, V., Muething, L., Gubbels, M.J., Spooner, E., Ploegh, H. and Artavanis-Tsakonas, K., 2007. Apicomplexan UCHL3 retains dual specificity for ubiquitin and Nedd8 throughout evolution. *Cellular microbiology*, 9(6), pp.1601-1610.
- Fukushima, T., Yoshihara, H., Furuta, H., Kamei, H., Hakuno, F., Luan, J., Duan, C., Saeki, Y., Tanaka, K., Iemura, S.I. and Natsume, T., 2015. Nedd4-induced monoubiquitination of IRS-2 enhances IGF signalling and mitogenic activity. *Nature communications*, 6(1), p.6780.
- Fulzele, A. and Bennett, E.J., 2018. Ubiquitin diGLY proteomics as an approach to identify and quantify the ubiquitin-modified proteome. *The Ubiquitin Proteasome System: Methods and Protocols*, pp.363-384.
- Gannavaram, S., Sharma, P., Duncan, R.C., Salotra, P. and Nakhasi, H.L., 2011. Mitochondrial associated ubiquitin fold modifier-1 mediated protein conjugation in *Leishmania donovani*. *PLoS one*, 6(1), p.e16156.
- Gannavaram, S., Connelly, P.S., Daniels, M.P., Duncan, R., Salotra, P. and Nakhasi, H.L., 2012. Deletion of mitochondrial associated ubiquitin fold modifier protein Ufm1 in *Leishmania donovani* results in loss of β -oxidation of fatty acids and blocks cell division in the amastigote stage. *Molecular microbiology*, 86(1), pp.187-198.
- Garloff, V., Krüger, T., Brakhage, A. and Rubio, I., 2023. Control of TurboID-dependent biotinylation intensity in proximity ligation screens. *Journal of Proteomics*, 279, p.104886.
- Gentzel, M., Pardo, M., Subramaniam, S., Stewart, A.F. and Choudhary, J.S., 2019. Proteomic navigation using proximity-labeling. *Methods*, 164, pp.67-72.
- Geoghegan, V., Carnielli, J.B., Jones, N.G., Saldivia, M., Antoniou, S., Hughes, C., Neish, R., Dowle, A. and Mottram, J.C., 2022. CLK1/CLK2-driven signalling at the *Leishmania* kinetochore is captured by spatially referenced proximity phosphoproteomics. *Communications biology*, 5(1), p.1305.
- Geoghegan, V., Mottram, J.C. and Jones, N.G., 2022. Tag thy neighbour: nanometre-scale insights into kinetoplastid parasites with proximity dependent biotinylation. *Frontiers in cellular and infection microbiology*, 12, p.549.
- George, D.E. and Tepe, J.J., 2021. Advances in proteasome enhancement by small molecules. *Biomolecules*, 11(12), p.1789.
- Gerald, N.J., Coppens, I. and Dwyer, D.M., 2007. Molecular dissection and expression of the Ldk39 kinesin in the human pathogen, *Leishmania donovani*. *Molecular microbiology*, 63(4), pp.962-979.
- Gheiratmand, L., Brasseur, A., Zhou, Q. and He, C.Y., 2013. Biochemical characterization of the bi-lobe reveals a continuous structural network linking the bi-lobe to other single-copied organelles in *Trypanosoma brucei*. *Journal of Biological Chemistry*, 288(5), pp.3489-3499.
- Gingras, A.C., Gstaiger, M., Raught, B. and Aebersold, R., 2007. Analysis of protein complexes using mass spectrometry. *Nature reviews Molecular cell biology*, 8(8), pp.645-654.
- Giraud, E., Lestinova, T., Derrick, T., Martin, O., Dillon, R.J., Volf, P., Müller, I., Bates, P.A. and Rogers, M.E., 2018. *Leishmania* proteophosphoglycans regurgitated from infected sand flies accelerate

dermal wound repair and exacerbate leishmaniasis via insulin-like growth factor 1-dependent signalling. *PLoS pathogens*, 14(1), p.e1006794.

Giri, S. and Shaha, C., 2019. Leishmania donovani parasite requires Atg8 protein for infectivity and survival under stress. *Cell Death & Disease*, 10(11), p.808.

Gómez-Arreaza, A., Acosta, H., Quiñones, W., Concepción, J.L., Michels, P.A. and Avilán, L., 2014. Extracellular functions of glycolytic enzymes of parasites: unpredicted use of ancient proteins. *Molecular and biochemical parasitology*, 193(2), pp.75-81.

Goos, C., Dejung, M., Wehman, A.M., M-Natus, E., Schmidt, J., Sunter, J., Engstler, M., Butter, F. and Kramer, S., 2019. Trypanosomes can initiate nuclear export co-transcriptionally. *Nucleic acids research*, 47(1), pp.266-282.

Gorka, M., Magnussen, H.M. and Kulathu, Y., 2022, December. Chemical biology tools to study Deubiquitinases and Ubl proteases. In *Seminars in Cell & Developmental Biology (Vol. 132, pp. 86-96)*. Academic Press.

Gostimskaya, I., 2022. CRISPR–Cas9: A History of Its Discovery and Ethical Considerations of Its Use in Genome Editing. *Biochemistry (Moscow)*, 87(8), pp.777-788.

Graeff, G.R., Steele, P.M., Peterson, C.L., Bennett, M.L. and Langer, P.J., 1993. Sequence of a Leishmania major gene encoding an ubiquitin fusion protein. *Gene*, 131(1), pp.155-156.

Grau-Bové, X., Sebé-Pedrós, A. and Ruiz-Trillo, I., 2015. The eukaryotic ancestor had a complex ubiquitin signaling system of archaeal origin. *Molecular biology and evolution*, 32(3), pp.726-739.

Gravel, N.H., Nelde, A., Bauer, J., Mühlenbruch, L., Schroeder, S., Neidert, M., Scheid, J., Lemke, S., Dubbelaar, M., Wacker, M. and Dengler, A., 2023. timsTOF mass spectrometry-based immunopeptidomics refines tumor antigen identification.

Grewal, J.S., Catta-Preta, C.M., Brown, E., Anand, J. and Mottram, J.C., 2019. Evaluation of clan CD C11 peptidase PNT1 and other Leishmania mexicana cysteine peptidases as potential drug targets. *Biochimie*, 166, pp.150-160.

Groll, M., Ditzel, L., Löwe, J., Stock, D., Bochtler, M., Bartunik, H.D. and Huber, R., 1997. Structure of 20S proteasome from yeast at 2.4 Å resolution. *Nature*, 386(6624), pp.463-471.

Grou, C.P., Pinto, M.P., Mendes, A.V., Domingues, P. and Azevedo, J.E., 2015. The de novo synthesis of ubiquitin: identification of deubiquitinases acting on ubiquitin precursors. *Scientific reports*, 5(1), p.12836.

Gubler, H., Clare, N., Galafassi, L., Geissler, U., Girod, M. and Herr, G., 2018. Helios: history and anatomy of a successful in-house enterprise high-throughput screening and profiling data analysis system. *SLAS DISCOVERY: Advancing the Science of Drug Discovery*, 23(5), pp.474-488.

Guerra, D.G., Vertommen, D., Fothergill-Gilmore, L.A., Opperdoes, F.R. and Michels, P.A., 2004. Characterization of the cofactor-independent phosphoglycerate mutase from Leishmania mexicana mexicana: Histidines that coordinate the two metal ions in the active site show different susceptibilities to irreversible chemical modification. *European journal of biochemistry*, 271(9), pp.1798-1810.

Gui, W., Paudel, P. and Zhuang, Z., 2020. Activity-Based Ubiquitin Probes for Investigation of Deubiquitinases. *Comprehensive Natural Products III*, p.589.

- Guo, N. and Peng, Z., 2013. MG132, a proteasome inhibitor, induces apoptosis in tumor cells. *Asia-Pacific Journal of Clinical Oncology*, 9(1), pp.6-11.
- Gupta, A.K., Das, S., Kamran, M., Ejazi, S.A. and Ali, N., 2022. The pathogenicity and virulence of Leishmania-interplay of virulence factors with host defences. *Virulence*, 13(1), pp.903-935.
- Gupta-Rossi, N., Ortica, S., Meas-Yedid, V., Heuss, S., Moretti, J., Olivo-Marin, J.C. and Israël, A., 2011. The adaptor-associated kinase 1, AAK1, is a positive regulator of the Notch pathway. *Journal of Biological Chemistry*, 286(21), pp.18720-18730.
- Guzzo, C.M., Berndsen, C.E., Zhu, J., Gupta, V., Datta, A., Greenberg, R.A., Wolberger, C. and Matunis, M.J., 2012. RNF4-dependent hybrid SUMO-ubiquitin chains are signals for RAP80 and thereby mediate the recruitment of BRCA1 to sites of DNA damage. *Science signaling*, 5(253), pp.ra88-ra88.
- Haanstra, J.R., González-Marcano, E.B., Gualdrón-López, M. and Michels, P.A., 2016. Biogenesis, maintenance and dynamics of glycosomes in trypanosomatid parasites. *Biochimica et Biophysica Acta (BBA)-Molecular Cell Research*, 1863(5), pp.1038-1048.
- Haas, A.L. and Rose, I.A., 1982. The mechanism of ubiquitin activating enzyme. A kinetic and equilibrium analysis. *Journal of Biological Chemistry*, 257(17), pp.10329-10337.
- Haglund, K., Sigismund, S., Polo, S., Szymkiewicz, I., Di Fiore, P.P. and Dikic, I., 2003. Multiple monoubiquitination of RTKs is sufficient for their endocytosis and degradation. *Nature cell biology*, 5(5), pp.461-466.
- Halbedl, S., Kratzer, M.C., Rahm, K., Crosta, N., Masters, K.S., Zippert, J., Bräse, S. and Gradl, D., 2013. Synthesis of novel inhibitors blocking Wnt signaling downstream of β -catenin. *FEBS letters*, 587(5), pp.522-527.
- Halcrow, E.F., Mazza, R., Diversi, A., Enright, A. and D'Avino, P.P., 2022. Midbody Proteins Display Distinct Dynamics during Cytokinesis. *Cells*, 11(21), p.3337.
- Halliday, C., Yanase, R., Catta-Preta, C.M.C., Moreira-Leite, F., Myskova, J., Pruzinova, K., Volf, P., Mottram, J.C. and Sunter, J.D., 2020. Role for the flagellum attachment zone in Leishmania anterior cell tip morphogenesis. *PLoS Pathogens*, 16(10), p.e1008494.
- Hamilton, Hazel Jean (2019) The Leish niche: the secretome of Leishmania and its role in parasite virulence. *PhD thesis*.
- Han, X., He, L., Xin, L., Shan, B. and Ma, B., 2011. PeaksPTM: mass spectrometry-based identification of peptides with unspecified modifications. *Journal of proteome research*, 10(7), pp.2930-2936.
- Hansen, F.M., Tanzer, M.C., Brüning, F., Bludau, I., Stafford, C., Schulman, B.A., Robles, M.S., Karayel, O. and Mann, M., 2021. Data-independent acquisition method for ubiquitinome analysis reveals regulation of circadian biology. *Nature Communications*, 12(1), p.254.
- Harakandi, C., Nininahazwe, L., Xu, H., Liu, B., He, C., Zheng, Y.C. and Zhang, H., 2021. Recent advances on the intervention sites targeting USP7-MDM2-p53 in cancer therapy. *Bioorganic Chemistry*, 116, p.105273.
- Harris, D.J., 2022. Breaking Ub with Leishmania mexicana: a ubiquitin activating enzyme as a novel therapeutic target for leishmaniasis (Doctoral dissertation, University of Glasgow).

- Hassiepen, U., Eidhoff, U., Meder, G., Bulber, J.F., Hein, A., Bodendorf, U., Lorthiois, E. and Martoglio, B., 2007. A sensitive fluorescence intensity assay for deubiquitinating proteases using ubiquitin-rhodamine110-glycine as substrate. *Analytical biochemistry*, 371(2), pp.201-207.
- Hendriks, I.A., Schimmel, J., Eifler, K., Olsen, J.V. and Vertegaal, A.C., 2015. Ubiquitin-specific protease 11 (USP11) deubiquitinates hybrid small ubiquitin-like modifier (SUMO)-ubiquitin chains to counteract RING finger protein 4 (RNF4). *Journal of Biological Chemistry*, 290(25), pp.15526-15537
- Henning, N.J., Boike, L., Spradlin, J.N., Ward, C.C., Liu, G., Zhang, E., Belcher, B.P., Brittain, S.M., Hesse, M.J., Dovala, D. and McGregor, L.M., 2022. Deubiquitinase-targeting chimeras for targeted protein stabilization. *Nature chemical biology*, 18(4), pp.412-421.
- Herfurth, M., Müller, F., Sjøgaard-Andersen, L. and Glatter, T., 2023. A miniTurbo-based proximity labeling protocol to identify conditional protein interactomes in vivo in *Myxococcus xanthus*. *STAR protocols*, 4(4), p.102657.
- Herndon, T.M., Deisseroth, A., Kaminskas, E., Kane, R.C., Koti, K.M., Rothmann, M.D., Habtemariam, B., Bullock, J., Bray, J.D., Hawes, J. and Palmby, T.R., 2013. US Food and Drug Administration approval: carfilzomib for the treatment of multiple myeloma. *Clinical cancer research*, 19(17), pp.4559-4563.
- Hideshima, T., Mitsiades, C., Akiyama, M., Hayashi, T., Chauhan, D., Richardson, P., Schlossman, R., Podar, K., Munshi, N.C., Mitsiades, N. and Anderson, K.C., 2003. Molecular mechanisms mediating antimyeloma activity of proteasome inhibitor PS-341. *Blood, The Journal of the American Society of Hematology*, 101(4), pp.1530-1534
- Hilton, N.A., Sladewski, T.E., Perry, J.A., Pataki, Z., Sinclair-Davis, A.N., Muniz, R.S., Tran, H.L., Wurster, J.I., Seo, J. and de Graffenried, C.L., 2018. Identification of TOEFAZ1-interacting proteins reveals key regulators of Trypanosoma brucei cytokinesis. *Molecular microbiology*, 109(3), pp.306-326.
- Hoare, C.A. and Wallace, F.G., 1966. Developmental stages of trypanosomatid flagellates: a new terminology. *Nature*, 212(5068), pp.1385-1386.
- Hochstrasser, M., 2000. Evolution and function of ubiquitin-like protein-conjugation systems. *Nature cell biology*, 2(8), pp.E153-E157.
- Hochstrasser, M., 2009. Origin and function of ubiquitin-like proteins. *Nature*, 458(7237), pp.422-429.
- Hodge, C.D., Edwards, R.A., Markin, C.J., McDonald, D., Pulvino, M., Huen, M.S., Zhao, J., Spyropoulos, L., Hendzel, M.J. and Glover, J.M., 2015. Covalent inhibition of Ubc13 affects ubiquitin signaling and reveals active site elements important for targeting. *ACS chemical biology*, 10(7), pp.1718-1728.
- Hodge, C.D., Spyropoulos, L. and Glover, J.M., 2016. Ubc13: the Lys63 ubiquitin chain building machine. *Oncotarget*, 7(39), p.64471.
- Hospenthal, M.K., Freund, S.M. and Komander, D., 2013. Assembly, analysis and architecture of atypical ubiquitin chains. *Nature structural & molecular biology*, 20(5), pp.555-565.
- Hotez, P.J., Bottazzi, M.E., Kaye, P.M., Lee, B.Y. and Puchner, K.P., 2023. Neglected tropical disease vaccines: hookworm, leishmaniasis, and schistosomiasis. *Vaccine*, 41(S2), pp.S176-S179.

- Hu, J., Huang, R., Liang, C., Wang, Y., Wang, M., Chen, Y., Wu, C., Zhang, J., Liu, Z., Zhao, Q. and Liu, Z., 2023. TRIM50 inhibits gastric cancer progression by regulating the ubiquitination and nuclear translocation of JUP. *Molecular Cancer Research*, pp.OF1-OF13.
- Hu, M., Li, P., Li, M., Li, W., Yao, T., Wu, J.W., Gu, W., Cohen, R.E. and Shi, Y., 2002. Crystal structure of a UBP-family deubiquitinating enzyme in isolation and in complex with ubiquitin aldehyde. *Cell*, 111(7), pp.1041-1054.
- Hu, M., Li, P., Song, L., Jeffrey, P.D., Chernova, T.A., Wilkinson, K.D., Cohen, R.E. and Shi, Y., 2005. Structure and mechanisms of the proteasome-associated deubiquitinating enzyme USP14. *The EMBO journal*, 24(21), pp.3747-3756.
- Huang, L., Kinnucan, E., Wang, G., Beaudenon, S., Howley, P.M., Huibregtse, J.M. and Pavletich, N.P., 1999. Structure of an E6AP-Ubch7 complex: insights into ubiquitination by the E2-E3 enzyme cascade. *Science*, 286(5443), pp.1321-1326.
- Huppelschoten, Y., 2022, December. State of the art in (semi-) synthesis of Ubiquitin-and Ubiquitin-like tools. In *Seminars in Cell & Developmental Biology* (Vol. 132, pp. 74-85). *Academic Press*.
- Hwang, J.T., Lee, A. and Kho, C., 2022. Ubiquitin and ubiquitin-like proteins in cancer, neurodegenerative disorders, and heart diseases. *International journal of molecular sciences*, 23(9), p.5053.
- Ikeda, F., 2023. Protein and non-protein targets of ubiquitin modification. *American Journal of Physiology-Cell Physiology*, 324(5), pp.C1053-C1060.
- Imhoff, R.D., Rosenthal, M.R., Ashraf, K., Bhanot, P., Ng, C.L. and Flaherty, D.P., 2023. Identification of covalent fragment inhibitors for Plasmodium falciparum UCHL3 with anti-malarial efficacy. *Bioorganic & Medicinal Chemistry Letters*, 94, p.129458.
- Inano, S., Sato, K., Katsuki, Y., Kobayashi, W., Tanaka, H., Nakajima, K., Nakada, S., Miyoshi, H., Knies, K., Takaori-Kondo, A. and Schindler, D., 2017. RFWD3-mediated ubiquitination promotes timely removal of both RPA and RAD51 from DNA damage sites to facilitate homologous recombination. *Molecular cell*, 66(5), pp.622-634.
- Iribarren, P.A., Berazategui, M.A., Bayona, J.C., Almeida, I.C., Cazzulo, J.J. and Alvarez, V.E., 2015. Different proteomic strategies to identify genuine small ubiquitin-like modifier targets and their modification sites in Trypanosoma brucei procyclic forms. *Cellular Microbiology*, 17(10), pp.1413-1422.
- Iyer, L.M., Koonin, E.V. and Aravind, L., 2004. Novel predicted peptidases with a potential role in the ubiquitin signaling pathway. *Cell Cycle*, 3(11), pp.1440-1450.
- Jaenicke, L.A., Brendebach, H., Selbach, M. and Hirsch, C., 2011. Yos9p assists in the degradation of certain nonglycosylated proteins from the endoplasmic reticulum. *Molecular Biology of the Cell*, 22(16), pp.2937-2945.
- Jamdhade, M.D., Pawar, H., Chavan, S., Sathe, G., Umasankar, P.K., Mahale, K.N., Dixit, T., Madugundu, A.K., Prasad, T.K., Gowda, H. and Pandey, A., 2015. Comprehensive proteomics analysis of glycosomes from Leishmania donovani. *OMICS: A Journal of Integrative Biology*, 19(3), pp.157-170.
- Janes, K.A., 2015. An analysis of critical factors for quantitative immunoblotting. *Science signaling*, 8(371), pp.rs2-rs2.

- Jiang, W., Li, X., Xu, H., Gu, X., Li, S., Zhu, L., Lu, J., Duan, X., Li, W. and Fang, M., 2023. UBL7 enhances antiviral innate immunity by promoting Lys27-linked polyubiquitination of MAVS. *Cell Reports*, 42(3).
- Jones, H.B., Heilig, R., Fischer, R., Kessler, B.M. and Pinto-Fernandez, A., 2021. ABPP-HT-high-throughput activity-based profiling of deubiquitylating enzyme inhibitors in a cellular context. *Frontiers in Chemistry*, 9, p.44.
- Jones, H.B., Heilig, R., Davis, S., Fischer, R., Kessler, B.M. and Pinto-Fernández, A., 2022. ABPP-HT*—Deep Meets Fast for Activity-Based Profiling of Deubiquitylating Enzymes Using Advanced DIA Mass Spectrometry Methods. *International Journal of Molecular Sciences*, 23(6), p.3263.
- Jones, N.G., Catta-Preta, C.M., Lima, A.P.C. and Mottram, J.C., 2018. Genetically validated drug targets in Leishmania: current knowledge and future prospects. *ACS infectious diseases*, 4(4), pp.467-477.
- Jones, N.G., Geoghegan, V., Moore, G., Carnielli, J.B., Newling, K., Calderón, F., Gabarró, R., Martín, J., Prinjha, R.K., Rioja, I. and Wilkinson, A.J., 2022. Bromodomain factor 5 is an essential regulator of transcription in Leishmania. *Nature Communications*, 13(1), p.4071.
- Jüdes, A., Bruch, A., Klassen, R., Helm, M. and Schaffrath, R., 2016. Sulfur transfer and activation by ubiquitin-like modifier system Uba4• Urm1 link protein urmylation and tRNA thiolation in yeast. *Microbial Cell*, 3(11), p.554.
- Jung, Y., Kim, H.D., Yang, H.W., Kim, H.J., Jang, C.Y. and Kim, J., 2017. Modulating cellular balance of Rps3 mono-ubiquitination by both Hel2 E3 ligase and Ubp3 deubiquitinase regulates protein quality control. *Experimental & molecular medicine*, 49(11), pp.e390-e390.
- Kaiser, M., Mäser, P., Tadoori, L.P., Ioset, J.R. and Brun, R., 2015. Antiprotozoal activity profiling of approved drugs: a starting point toward drug repositioning. *PLoS one*, 10(8), p.e0135556.
- Kanner, S.A., Shuja, Z., Choudhury, P., Jain, A. and Colecraft, H.M., 2020. Targeted deubiquitination rescues distinct trafficking-deficient ion channelopathies. *Nature methods*, 17(12), pp.1245-1253.
- Karamysheva, Z.N., Gutierrez Guarnizo, S.A. and Karamyshev, A.L., 2020. Regulation of translation in the protozoan parasite Leishmania. *International journal of molecular sciences*, 21(8), p.2981.
- Kargas, V., Castro-Hartmann, P., Escudero-Urquijo, N., Dent, K., Hilcenko, C., Sailer, C., Zisser, G., Marques-Carvalho, M.J., Pellegrino, S., Wawiorka, L. and Freund, S.M., 2019. Mechanism of completion of peptidyltransferase centre assembly in eukaryotes. *Elife*, 8, p.e44904.
- Karpiyevich, M., Adjalley, S., Mol, M., Ascher, D.B., Mason, B., van der Heden van Noort, G.J., Laman, H., Ovaa, H., Lee, M.C. and Artavanis-Tsakonas, K., 2019. Nedd8 hydrolysis by UCH proteases in Plasmodium parasites. *PLoS pathogens*, 15(10), p.e1008086.
- Kattenhorn, L.M., Korb, G.A., Kessler, B.M., Spooner, E. and Ploegh, H.L., 2005. A deubiquitinating enzyme encoded by HSV-1 belongs to a family of cysteine proteases that is conserved across the family *Herpesviridae*. *Molecular cell*, 19(4), pp.547-557.
- Kelsall, I.R., 2022. Non-lysine ubiquitylation: Doing things differently. *Frontiers in molecular biosciences*, 9, p.1008175.
- Kelsall, I.R., McCrory, E.H., Xu, Y., Scudamore, C.L., Nanda, S.K., Mancebo-Gamella, P., Wood, N.T., Knebel, A., Matthews, S.J. and Cohen, P., 2022. HOIL-1 ubiquitin ligase activity targets unbranched

glucosaccharides and is required to prevent polyglucosan accumulation. *The EMBO Journal*, 41(8), p.e109700.

Kido, K., Yamanaka, S., Nakano, S., Motani, K., Shinohara, S., Nozawa, A., Kosako, H., Ito, S. and Sawasaki, T., 2020. AirID, a novel proximity biotinylation enzyme, for analysis of protein–protein interactions. *Elife*, 9, p.e54983.

Kim, D.I., Jensen, S.C., Noble, K.A., Kc, B., Roux, K.H., Motamedchaboki, K. and Roux, K.J., 2016. An improved smaller biotin ligase for BioID proximity labeling. *Molecular biology of the cell*, 27(8), pp.1188-1196.

Kirchhoff, L.V., Kim, K.S., Engman, D.M. and Donelson, J.E., 1988. Ubiquitin genes in trypanosomatidae. *Journal of Biological Chemistry*, 263(25), pp.12698-12704.

Kisselev, A.F., Akopian, T.N. and Goldberg, A.L., 1998. Range of sizes of peptide products generated during degradation of different proteins by archaeal proteasomes. *Journal of Biological Chemistry*, 273(4), pp.1982-1989.

Kloehn, J., Saunders, E.C., O’Callaghan, S., Dagley, M.J. and McConville, M.J., 2015. Characterization of metabolically quiescent Leishmania parasites in murine lesions using heavy water labeling. *PLoS Pathogens*, 11(2), p.e1004683.

Koch, H., Raabe, M., Urlaub, H., Bindereif, A. and Preußner, C., 2016. The polyadenylation complex of Trypanosoma brucei: Characterization of the functional poly (A) polymerase. *RNA biology*, 13(2), pp.221-231.

Koegl, M., Hoppe, T., Schlenker, S., Ulrich, H.D., Mayer, T.U., and Jentsch, S. (1999). A novel ubiquitination factor, E4, is involved in multiubiquitin chain assembly. *Cell* 96, 635–644.

Kolli, B.K., Kostal, J., Zaborina, O., Chakrabarty, A.M. and Chang, K.P., 2008. Leishmania-released nucleoside diphosphate kinase prevents ATP-mediated cytolysis of macrophages. *Molecular and biochemical parasitology*, 158(2), pp.163-175.

Kolman, C.J., Toth, J. and Gonda, D.K., 1992. Identification of a portable determinant of cell cycle function within the carboxyl-terminal domain of the yeast CDC34 (UBC3) ubiquitin conjugating (E2) enzyme. *The EMBO journal*, 11(8), pp.3081-3090.

Komander, D. and Barford, D., 2008. Structure of the A20 OTU domain and mechanistic insights into deubiquitination. *Biochemical Journal*, 409(1), pp.77-85.

Kubitz, L., Bitsch, S., Zhao, X., Schmitt, K., Deweid, L., Roehrig, A., Barazzone, E.C., Valerius, O., Kolmar, H. and Béthune, J., 2022. Engineering of ultraID, a compact and hyperactive enzyme for proximity-dependent biotinylation in living cells. *Communications biology*, 5(1), p.657.

Kuhn, D.J., Chen, Q., Voorhees, P.M., Strader, J.S., Shenk, K.D., Sun, C.M., Demo, S.D., Bennett, M.K., Van Leeuwen, F.W., Chanan-Khan, A.A. and Orlowski, R.Z., 2007. Potent activity of carfilzomib, a novel, irreversible inhibitor of the ubiquitin-proteasome pathway, against preclinical models of multiple myeloma. *Blood, The Journal of the American Society of Hematology*, 110(9), pp.3281-3290.

Kumar, K., Singh, P.K., Rastogi, R. and Mukhopadhyay, A., 2016. Single GDP-dissociation Inhibitor Protein regulates endocytic and secretory pathways in Leishmania. *Scientific Reports*, 6(1), pp.1-10.

Kumar, P., Kumar, P., Mandal, D. and Velayutham, R., 2022. The emerging role of Deubiquitinases (DUBs) in parasites: A foresight review. *Frontiers in Cellular and Infection Microbiology*, p.1403.

- Kumari, S., Kumar, V., Tiwari, R.K., Ravidas, V., Pandey, K. and Kumar, A., 2022. -Amphotericin B: A drug of choice for Visceral Leishmaniasis. *Acta Tropica*, p.106661.
- Lacoursiere, R.E., Hadi, D. and Shaw, G.S., 2022. Acetylation, phosphorylation, ubiquitination (oh my!): Following post-translational modifications on the ubiquitin road. *Biomolecules*, 12(3), p.467.
- Laffitte, M.C.N., Leprohon, P., Hainse, M., Légaré, D., Masson, J.Y. and Ouellette, M., 2016. Chromosomal translocations in the parasite *Leishmania* by a MRE11/RAD50-independent microhomology-mediated end joining mechanism. *PLoS genetics*, 12(6), p.e1006117.
- Laffitte, M.C.N., Leprohon, P., Papadopoulou, B. and Ouellette, M., 2016. Plasticity of the *Leishmania* genome leading to gene copy number variations and drug resistance. *F1000Research*, 5.
- Lambourne, O.A., Bell, S., Wilhelm, L.P., Yarbrough, E.B., Holly, G.G., Russell, O.M., Alghamdi, A.M., Fdel, A.M., Varricchio, C., Lane, E.L. and Ganley, I.G., 2023. PINK1-dependent mitophagy inhibits elevated ubiquitin phosphorylation caused by mitochondrial damage. *Journal of Medicinal Chemistry*.
- Landfear, S.M., 2022. New Vistas in the Biology of the Flagellum—*Leishmania* Parasites. *Pathogens*, 11(4), p.447.
- Lange, S.M., Armstrong, L.A. and Kulathu, Y., 2022. Deubiquitinases: From mechanisms to their inhibition by small molecules. *Molecular cell*, 82(1), pp.15-29.
- Larochelle, M., Bergeron, D., Arcand, B. and Bachand, F., 2019. Proximity-dependent biotinylation mediated by TurboID to identify protein–protein interaction networks in yeast. *Journal of cell science*, 132(11), p.jcs232249.
- Laskay, T., Van Zandbergen, G. and Solbach, W., 2003. Neutrophil granulocytes—Trojan horses for *Leishmania major* and other intracellular microbes?. *Trends in microbiology*, 11(5), pp.210-214.
- Laskay, T., van Zandbergen, G. and Solbach, W., 2008. Neutrophil granulocytes as host cells and transport vehicles for intracellular pathogens: apoptosis as infection-promoting factor. *Immunobiology*, 213(3-4), pp.183-191.
- Lecona, E., Rodriguez-Acebes, S., Specks, J., Lopez-Contreras, A.J., Ruppen, I., Murga, M., Munoz, J., Mendez, J. and Fernandez-Capetillo, O., 2016. USP7 is a SUMO deubiquitinase essential for DNA replication. *Nature structural & molecular biology*, 23(4), pp.270-277.
- Lee, B.H., Lu, Y., Prado, M.A., Shi, Y., Tian, G., Sun, S., Elsasser, S., Gygi, S.P., King, R.W. and Finley, D., 2016. USP14 deubiquitinates proteasome-bound substrates that are ubiquitinated at multiple sites. *Nature*, 532(7599), pp.398-401.
- Lee, M.Y., Ajjappala, B.S., Kim, M.S., Oh, Y.K. and Baek, K.H., 2008. DUB-1, a fate determinant of dynein heavy chain in B-lymphocytes, is regulated by the ubiquitin–proteasome pathway. *Journal of cellular biochemistry*, 105(6), pp.1420-1429.
- Lee, S.D., Liu, H.Y., Graber, J.H., Heller-Trulli, D., Kaczmarek Michaels, K., Cerezo, J.F. and Moore, C.L., 2020. Regulation of the Ysh1 endonuclease of the mRNA cleavage/polyadenylation complex by ubiquitin-mediated degradation. *RNA biology*, 17(5), pp.689-702.
- Lei, X., Hu, X., Lu, Q., Fu, W., Sun, W., Ma, Q., Huang, D. and Xu, Q., 2023. Ubiquitin-conjugating enzymes as potential biomarkers and therapeutic targets for digestive system cancers. *Oncology Reports*, 49(3), pp.1-11.

Leimkühler, S., Wuebbens, M.M. and Rajagopalan, K.V., 2001. Characterization of Escherichia coli MoeB and its involvement in the activation of molybdopterin synthase for the biosynthesis of the molybdenum cofactor. *Journal of Biological Chemistry*, 276(37), pp.34695-34701.

Lepourcelet, M., Chen, Y.N.P., France, D.S., Wang, H., Crews, P., Petersen, F., Bruseo, C., Wood, A.W. and Shivdasani, R.A., 2004. Small-molecule antagonists of the oncogenic Tcf / β -catenin protein complex. *Cancer cell*, 5(1), pp.91-102.

Leto, D.E., Morgens, D.W., Zhang, L., Walczak, C.P., Elias, J.E., Bassik, M.C. and Kopito, R.R., 2019. Genome-wide CRISPR analysis identifies substrate-specific conjugation modules in ER-associated degradation. *Molecular cell*, 73(2), pp.377-389.

Li, C., Han, T., Li, Q., Zhang, M., Guo, R., Yang, Y., Lu, W., Li, Z., Peng, C., Wu, P. and Tian, X., 2021. MKRN3-mediated ubiquitination of Poly (A)-binding proteins modulates the stability and translation of GNRH1 mRNA in mammalian puberty. *Nucleic Acids Research*, 49(7), pp.3796-3813.

Liu, B., Jiang, S., Li, M., Xiong, X., Zhu, M., Li, D., Zhao, L., Qian, L., Zhai, L., Li, J. and Lu, H., 2018. Proteome-wide analysis of USP14 substrates revealed its role in hepatosteatosis via stabilization of FASN. *Nature Communications*, 9(1), p.4770.

Liu, H., Heller-Trulli, D. and Moore, C.L., 2022. Targeting the mRNA endonuclease CPSF73 inhibits breast cancer cell migration, invasion, and self-renewal. *Iscience*, 25(8), p.104804.

Liu, S., Lu, H., Zhao, Q., He, Y., Niu, J., Debnath, A.K., Wu, S. and Jiang, S., 2005. Theaflavin derivatives in black tea and catechin derivatives in green tea inhibit HIV-1 entry by targeting gp41. *Biochimica et Biophysica Acta (BBA)-General Subjects*, 1723(1-3), pp.270-281.

Liu, S., Luo, J., Zhen, X., Qiu, J., Ouyang, S. and Luo, Z.Q., 2020. Interplay between bacterial deubiquitinase and ubiquitin E3 ligase regulates ubiquitin dynamics on Legionella phagosomes. *Elife*, 9, p.e58114.

Liu, X.J., Xie, Q., Zhu, Y.F., Chen, C. and Ling, N., 2001. Identification of a nonpeptide ligand that releases bioactive insulin-like growth factor-I from its binding protein complex. *Journal of Biological Chemistry*, 276(35), pp.32419-32422.

Liu, Y., Lashuel, H.A., Choi, S., Xing, X., Case, A., Ni, J., Yeh, L.A., Cuny, G.D., Stein, R.L. and Lansbury, P.T., 2003. Discovery of inhibitors that elucidate the role of UCH-L1 activity in the H1299 lung cancer cell line. *Chemistry & biology*, 10(9), pp.837-846.

Lohraseb, I., McCarthy, P., Secker, G., Marchant, C., Wu, J., Ali, N., Kumar, S., Daly, R.J., Harvey, N.L., Kawabe, H. and Kleinfeld, O., 2022. Global ubiquitinome profiling identifies NEDD4 as a regulator of Profilin 1 and actin remodelling in neural crest cells. *Nature Communications*, 13(1), p.2018.

Lu, J., Ho, C.T., Ghai, G. and Chen, K.Y., 2000. Differential effects of theaflavin monogallates on cell growth, apoptosis, and Cox-2 gene expression in cancerous versus normal cells. *Cancer Research*, 60(22), pp.6465-6471.

Lu, Y., Lee, B.H., King, R.W., Finley, D. and Kirschner, M.W., 2015. Substrate degradation by the proteasome: a single-molecule kinetic analysis. *Science*, 348(6231), p.1250834.

Ludwig, K.R., Schroll, M.M. and Hummon, A.B., 2018. Comparison of in-solution, FASP, and S-trap based digestion methods for bottom-up proteomic studies. *Journal of proteome research*, 17(7), pp.2480-2490.

- Lustig, Y., Goldshmidt, H., Uliel, S. and Michaeli, S., 2005. The Trypanosoma brucei signal recognition particle lacks the Alu-domain-binding proteins: purification and functional analysis of its binding proteins by RNAi. *Journal of cell science*, 118(19), pp.4551-4562.
- Lv, Z., Yuan, L., Atkison, J.H., Aldana-Masangkay, G., Chen, Y. and Olsen, S.K., 2017. Domain alternation and active site remodelling are conserved structural features of ubiquitin E1. *Journal of Biological Chemistry*, 292(29), pp.12089-12099.
- Lystad, A.H. and Simonsen, A., 2019. Mechanisms and pathophysiological roles of the ATG8 conjugation machinery. *Cells*, 8(9), p.973.
- MacDonald, C., Winistorfer, S., Pope, R.M., Wright, M.E. and Piper, R.C., 2017. Enzyme reversal to explore the function of yeast E3 ubiquitin-ligases. *Traffic*, 18(7), pp.465-484.
- Magits, W. and Sablina, A.A., 2022. The regulation of the protein interaction network by monoubiquitination. *Current Opinion in Structural Biology*, 73, p.102333.
- Maga, J.A., Sherwin, T., Francis, S., Gull, K. and LeBowitz, J.H., 1999. Genetic dissection of the Leishmania paraflagellar rod, a unique flagellar cytoskeleton structure. *Journal of cell science*, 112(16), pp.2753-2763.
- Malberg, J.E., Platt, B., Rizzo, S.J.S., Ring, R.H., Lucki, I., Schechter, L.E. and Rosenzweig-Lipson, S., 2007. Increasing the levels of insulin-like growth factor-I by an IGF binding protein inhibitor produces anxiolytic and antidepressant-like effects. *Neuropsychopharmacology*, 32(11), pp.2360-2368.
- Malygin, A.A., Babaylova, E.S., Loktev, V.B. and Karpova, G.G., 2011. A region in the C-terminal domain of ribosomal protein SA required for binding of SA to the human 40S ribosomal subunit. *Biochimie*, 93(3), pp.612-617.
- Marchetti, M.A., Tschudi, C., Silva, E. and Ullu, E., 1998. Physical and transcriptional analysis of the Trypanosoma brucei genome reveals a typical eukaryotic arrangement with close interspersed RNA polymerase II and III-transcribed genes. *Nucleic acids research*, 26(15), pp.3591-3598.
- Martel, D., 2019. Functional characterisation of Leishmania casein Kinase 1.2 in the parasite and the mammalian host (*Doctoral dissertation, Université Paris Cité*).
- Martínez-Calvillo, S., Yan, S., Nguyen, D., Fox, M., Stuart, K. and Myler, P.J., 2003. Transcription of Leishmania major Friedlin chromosome 1 initiates in both directions within a single region. *Molecular cell*, 11(5), pp.1291-1299.
- Martín-Villanueva, S., Gutiérrez, G., Kressler, D. and de la Cruz, J., 2021. Ubiquitin and ubiquitin-like proteins and domains in ribosome production and function: chance or necessity? *International Journal of Molecular Sciences*, 22(9), p.4359.
- May, D.G., Scott, K.L., Campos, A.R. and Roux, K.J., 2020. Comparative application of BioID and TurboID for protein-proximity biotinylation. *Cells*, 9(5), p.1070.
- McConville, M.J., Turco, S.J., Ferguson, M.A. and Sacks, D.L., 1992. Developmental modification of lipophosphoglycan during the differentiation of Leishmania major promastigotes to an infectious stage. *The EMBO journal*, 11(10), pp.3593-3600.
- McCormick, L.E., Suarez, C., Herring, L.E., Cannon, K.S., Kovar, D.R., Brown, N.G. and Gupton, S.L., 2023. Multi-monoubiquitination controls VASP-mediated actin dynamics. *bioRxiv*, pp.2023-07.

- McCoy, C.J., Paupelin-Vaucelle, H., Gorilak, P., Beneke, T., Varga, V. and Gluenz, E., 2023. ULK4 and Fused/STK36 interact to mediate assembly of a motile flagellum. *Molecular Biology of the Cell*, 34(7), p.ar66.
- McCrary, E.H., Akimov, V., Cohen, P. and Blagoev, B., 2022. Identification of ester-linked ubiquitylation sites during TLR7 signalling increases the number of inter-ubiquitin linkages from 8 to 12. *Biochemical Journal*, 479(23), pp.2419-2431.
- McCullough, J., Row, P.E., Lorenzo, O., Doherty, M., Beynon, R., Clague, M.J. and Urbé, S., 2006. Activation of the endosome-associated ubiquitin isopeptidase AMSH by STAM, a component of the multivesicular body-sorting machinery. *Current Biology*, 16(2), pp.160-165.
- McKenna, S., Spyropoulos, L., Moraes, T., Pastushok, L., Ptak, C., Xiao, W. and Ellison, M.J., 2001. Noncovalent interaction between ubiquitin and the human DNA repair protein Mms2 is required for Ubc13-mediated polyubiquitination. *Journal of Biological Chemistry*, 276(43), pp.40120-40126.
- Meier, F., Beck, S., Grassl, N., Lubeck, M., Park, M.A., Raether, O. and Mann, M., 2015. Parallel accumulation–serial fragmentation (PASEF): multiplying sequencing speed and sensitivity by synchronized scans in a trapped ion mobility device. *Journal of proteome research*, 14(12), pp.5378-5387.
- Meier, F., Brunner, A.D., Koch, S., Koch, H., Lubeck, M., Krause, M., Goedecke, N., Decker, J., Kosinski, T., Park, M.A. and Bache, N., 2018. Online parallel accumulation–serial fragmentation (PASEF) with a novel trapped ion mobility mass spectrometer. *Molecular & Cellular Proteomics*, 17(12), pp.2534-2545.
- Meier, F., Brunner, A.D., Frank, M., Ha, A., Bludau, I., Voytik, E., Kaspar-Schoenefeld, S., Lubeck, M., Raether, O., Bache, N. and Aebersold, R., 2020. diaPASEF: parallel accumulation–serial fragmentation combined with data-independent acquisition. *Nature methods*, 17(12), pp.1229-1236.
- Meszka, I., Polanowska, J. and Xirodimas, D.P., 2022, December. Mixed in chains: NEDD8 polymers in the Protein Quality Control system. In *Seminars in Cell & Developmental Biology (Vol. 132, pp. 27-37)*. Academic Press.
- Mevisen, T.E., Hospenthal, M.K., Geurink, P.P., Elliott, P.R., Akutsu, M., Arnaudo, N., Ekkebus, R., Kulathu, Y., Wauer, T., El Oualid, F. and Freund, S.M., 2013. OTU deubiquitinases reveal mechanisms of linkage specificity and enable ubiquitin chain restriction analysis. *Cell*, 154(1), pp.169-184.
- Mevisen, T.E. and Komander, D., 2017. Mechanisms of deubiquitinase specificity and regulation. *Annual review of biochemistry*, 86, pp.159-192.
- Metzger, M.B., Hristova, V.A. and Weissman, A.M., 2012. HECT and RING finger families of E3 ubiquitin ligases at a glance. *Journal of cell science*, 125(3), pp.531-537.
- Meyer, C., Garzia, A., Morozov, P., Molina, H. and Tuschl, T., 2020. The G3BP1-Family-USP10 deubiquitinase complex rescues ubiquitinated 40S subunits of ribosomes stalled in translation from lysosomal degradation. *Molecular cell*, 77(6), pp.1193-1205.
- Molyneux, D.H., 2012. The 'Neglected Tropical Diseases': now a brand identity; responsibilities, context and promise. *Parasites & Vectors*, 5(1), pp.1-4.
- Moore, D.J., West, A.B., Dikeman, D.A., Dawson, V.L. and Dawson, T.M., 2008. Parkin mediates the degradation-independent ubiquitination of Hsp70. *Journal of neurochemistry*, 105(5), pp.1806-1819.

- Moore, E.M. and Lockwood, D.N., 2010. Treatment of visceral leishmaniasis. *Journal of global infectious diseases*, 2(2), p.151.
- Morell, M., Nguyen Duc, T., Willis, A.L., Syed, S., Lee, J., Deu, E., Deng, Y., Xiao, J., Turk, B.E., Jessen, J.R. and Weiss, S.J., 2013. Coupling protein engineering with probe design to inhibit and image matrix metalloproteinases with controlled specificity. *Journal of the American Chemical Society*, 135(24), pp.9139-9148.
- Morgan, M.T., Haj-Yahya, M., Ringel, A.E., Bandi, P., Brik, A. and Wolberger, C., 2016. Structural basis for histone H2B deubiquitination by the SAGA DUB module. *Science*, 351(6274), pp.725-728.
- Mulder, M.P., El Oualid, F., ter Beek, J. and Ovaa, H., 2014. A native chemical ligation handle that enables the synthesis of advanced activity-based probes: diubiquitin as a case study. *ChemBioChem*, 15(7), pp.946-949.
- Mullard, A., 2019. First targeted protein degrader hits the clinic. *Nature reviews. Drug discovery*.
- Murta, S.M., Vickers, T.J., Scott, D.A. and Beverley, S.M., 2009. Methylene tetrahydrofolate dehydrogenase/cyclohydrolase and the synthesis of 10-CHO-THF are essential in *Leishmania major*. *Molecular microbiology*, 71(6), pp.1386-1401.
- Nelson, J., McFerran, N.V., Pivato, G., Chambers, E., Doherty, C., Steele, D. and Timson, D.J., 2008. The 67 kDa laminin receptor: structure, function and role in disease. *Bioscience reports*, 28(1), pp.33-48.
- Ngoka, L., 2008. Sample prep for proteomics of breast cancer: proteomics and gene ontology reveal dramatic differences in protein solubilization preferences of radioimmunoprecipitation assay and urea lysis buffers. *Proteome science*, 6(1), pp.1-24.
- Nguyen, L., Plafker, K.S., Starnes, A., Cook, M., Klevit, R.E. and Plafker, S.M., 2014. The ubiquitin-conjugating enzyme, UbcM2, is restricted to monoubiquitylation by a two-fold mechanism that involves backside residues of E2 and Lys48 of ubiquitin. *Biochemistry*, 53(24), pp.4004-4014.
- Ohtake, F., Saeki, Y., Ishido, S., Kanno, J. and Tanaka, K., 2016. The K48-K63 branched ubiquitin chain regulates NF- κ B signaling. *Molecular cell*, 64(2), pp.251-266.
- Ohtake, F., Saeki, Y., Sakamoto, K., Ohtake, K., Nishikawa, H., Tsuchiya, H., Ohta, T., Tanaka, K. and Kanno, J., 2015. Ubiquitin acetylation inhibits polyubiquitin chain elongation. *EMBO reports*, 16(2), pp.192-201.
- Ohtake, F. and Tsuchiya, H., 2017. The emerging complexity of ubiquitin architecture. *The journal of biochemistry*, 161(2), pp.125-133.
- Oliinyk, D. and Meier, F., 2023. Ion mobility-resolved phosphoproteomics with dia-PASEF and short gradients. *Proteomics*, 23(7-8), p.2200032.
- Olsen, S.K. and Lima, C.D., 2013. Structure of a ubiquitin E1-E2 complex: insights to E1-E2 thioester transfer. *Molecular cell*, 49(5), pp.884-896.
- Omar, M.H., Lauer, S.M., Lau, H.T., Golkowski, M., Ong, S.E. and Scott, J.D., 2023. Proximity biotinylation to define the local environment of the protein kinase A catalytic subunit in adrenal cells. *STAR protocols*, 4(1), p.101992.

- Omondi, Z.N., Arserim, S.K., Töz, S. and Özbel, Y., 2022. Host–Parasite Interactions: Regulation of Leishmania Infection in Sand Fly. *Acta Parasitologica*, 67(2), pp.606-618.
- Opperdoes, F.R. and Borst, P., 1977. Localization of nine glycolytic enzymes in a microbody-like organelle in *Trypanosoma brucei*: the glycosome. *FEBS letters*, 80(2), pp.360-364.
- Opperdoes, F.R. and Michels, P.A.M., 1993. The glycosomes of the Kinetoplastida. *Biochimie*, 75(3-4), pp.231-234.
- Osman, M., Mistry, A., Keding, A., Gabe, R., Cook, E., Forrester, S., Wiggins, R., Di Marco, S., Colloca, S., Siani, L. and Cortese, R., 2017. A third generation vaccine for human visceral leishmaniasis and post kala azar dermal leishmaniasis: First-in-human trial of ChAd63-KH. *PloS neglected tropical diseases*, 11(5), p.e0005527.
- Otten, E.G., Werner, E., Crespillo-Casado, A., Boyle, K.B., Dharamdasani, V., Pathe, C., Santhanam, B. and Randow, F., 2021. Ubiquitylation of lipopolysaccharide by RNF213 during bacterial infection. *Nature*, 594(7861), pp.111-116.
- Paape, D., Barrios-Llerena, M.E., Le Bihan, T., Mackay, L. and Aebischer, T., 2010. Gel free analysis of the proteome of intracellular *Leishmania mexicana*. *Molecular and biochemical parasitology*, 169(2), pp.108-114.
- Padmanabhan, P.K., Ferreira, G.R., Zghidi-Abouzid, O., Oliveira, C., Dumas, C., Mariz, F.C. and Papadopoulou, B., 2021. Genetic depletion of the RNA helicase DDX3 leads to impaired elongation of translating ribosomes triggering co-translational quality control of newly synthesized polypeptides. *Nucleic Acids Research*, 49(16), pp.9459-9478.
- Paek, J., Kalocsay, M., Staus, D.P., Wingler, L., Pascolutti, R., Paulo, J.A., Gygi, S.P. and Kruse, A.C., 2017. Multidimensional tracking of GPCR signaling via peroxidase-catalyzed proximity labeling. *Cell*, 169(2), pp.338-349.
- Palić, S., Beijnen, J.H. and Dorlo, T.P., 2022. An update on the clinical pharmacology of miltefosine in the treatment of leishmaniasis. *International Journal of Antimicrobial Agents*, 59(1), p.106459.
- Panyain, N., Godinat, A., Lanyon-Hogg, T., Lachiondo-Ortega, S., Will, E.J., Soudy, C., Mondal, M., Mason, K., Elkhailifa, S., Smith, L.M. and Harrigan, J.A., 2020. Discovery of a potent and selective covalent inhibitor and activity-based probe for the deubiquitylating enzyme UCHL1, with antifibrotic activity. *Journal of the American Chemical Society*, 142(28), pp.12020-12026.
- Park, J., Shin, S.C., Jin, K.S., Lim, M.J., Kim, Y., Kim, E.E. and Song, E.J., 2023. USP35 dimer prevents its degradation by E3 ligase CHIP through auto-deubiquitinating activity. *Cellular and Molecular Life Sciences*, 80(4), p.112.
- Parsons, J.L., Khoronenkova, S.V., Dianova, I.I., Ternette, N., Kessler, B.M., Datta, P.K. and Dianov, G.L., 2012. Phosphorylation of PNKP by ATM prevents its proteasomal degradation and enhances resistance to oxidative stress. *Nucleic acids research*, 40(22), pp.11404-11415.
- Passos-Silva, D.G., Rajão, M.A., Nascimento de Aguiar, P.H., Vieira-da-Rocha, J.P., Machado, C.R. and Furtado, C., 2010. Overview of DNA Repair in *Trypanosoma cruzi*, *Trypanosoma brucei*, and *Leishmania major*. *Journal of nucleic acids*, 2010.

- Pearce, M.J., Mintseris, J., Ferreyra, J., Gygi, S.P. and Darwin, K.H., 2008. Ubiquitin-like protein involved in the proteasome pathway of Mycobacterium tuberculosis. *Science*, 322(5904), pp.1104-1107.
- Peng, Z., Liao, Z., Matsumoto, Y., Yang, A. and Tomkinson, A.E., 2016. Human DNA ligase I interacts with and is targeted for degradation by the DCAF7 specificity factor of the Cul4-DDB1 ubiquitin ligase complex. *Journal of Biological Chemistry*, 291(42), pp.21893-21902.
- Pérez Berrocal, D.A., Witting, K.F., Ovaa, H. and Mulder, M.P., 2020. Hybrid chains: a collaboration of ubiquitin and ubiquitin-like modifiers introducing cross-functionality to the ubiquitin code. *Frontiers in Chemistry*, 7, p.931.
- Perry, M.R., Prajapati, V.K., Menten, J., Raab, A., Feldmann, J., Chakraborti, D., Sundar, S., Fairlamb, A.H., Boelaert, M. and Picado, A., 2015. Arsenic exposure and outcomes of antimonial treatment in visceral leishmaniasis patients in Bihar, India: a retrospective cohort study. *PLoS neglected tropical diseases*, 9(3), p.e0003518.
- Peters, N.C., Egen, J.G., Secundino, N., Debrabant, A., Kimblin, N., Kamhawi, S., Lawyer, P., Fay, M.P., Germain, R.N. and Sacks, D., 2008. In vivo imaging reveals an essential role for neutrophils in leishmaniasis transmitted by sand flies. *Science*, 321(5891), pp.970-974.
- Petersen, A.L.D.O., Cull, B., Dias, B.R., Palma, L.C., Luz, Y.D.S., de Menezes, J.P., Mottram, J.C. and Veras, P.S., 2021. 17-AAG-induced activation of the autophagic pathway in Leishmania is associated with parasite death. *Microorganisms*, 9(5), p.1089.
- Peterson, B.G., Glaser, M.L., Rapoport, T.A. and Baldrige, R.D., 2019. Cycles of autoubiquitination and deubiquitination regulate the ERAD ubiquitin ligase Hrd1. *Elife*, 8, p.e50903.
- Petropolis, D.B., Rodrigues, J.C., Viana, N.B., Pontes, B., Pereira, C.F. and Silva-Filho, F.C., 2014. Leishmania amazonensis promastigotes in 3D Collagen I culture: an in vitro physiological environment for the study of extracellular matrix and host cell interactions. *PeerJ*, 2, p.e317.
- Pfeiffer, A., Luijsterburg, M.S., Acs, K., Wiegant, W.W., Helfricht, A., Herzog, L.K., Minoia, M., Böttcher, C., Salomons, F.A., van Attikum, H. and Dantuma, N.P., 2017. Ataxin-3 consolidates the MDC 1-dependent DNA double-strand break response by counteracting the SUMO-targeted ubiquitin ligase RNF 4. *The EMBO journal*, 36(8), pp.1066-1083.
- Piatnitskaia, S., Takahashi, M., Kitaura, H., Katsuragi, Y., Kakihana, T., Zhang, L., Kakita, A., Iwakura, Y., Nawa, H., Miura, T. and Ikeuchi, T., 2019. USP10 is a critical factor for Tau-positive stress granule formation in neuronal cells. *Scientific Reports*, 9(1), p.10591.
- Picchi, G.F., Zulkievicz, V., Krieger, M.A., Zanchin, N.T., Goldenberg, S. and De Godoy, L.M., 2017. Post-translational modifications of Trypanosoma cruzi canonical and variant histones. *Journal of proteome research*, 16(3), pp.1167-1179.
- Pimenta, P.F.P., Modi, G.B., Pereira, S.T., Shahabuddin, M. and Sacks, D.L., 1997. A novel role for the peritrophic matrix in protecting Leishmania from the hydrolytic activities of the sand fly midgut. *Parasitology*, 115(4), pp.359-369.
- Pinto-Fernández, A., Davis, S., Schofield, A.B., Scott, H.C., Zhang, P., Salah, E., Mathea, S., Charles, P.D., Damianou, A., Bond, G. and Fischer, R., 2019. Comprehensive landscape of active deubiquitinating enzymes profiled by advanced chemoproteomics. *Frontiers in chemistry*, 7, p.592.

- Polasky, D.A., Geiszler, D.J., Yu, F., Li, K., Teo, G.C. and Nesvizhskii, A.I., 2023. MSFragger-Labile: A Flexible Method to Improve Labile PTM Analysis in Proteomics. *Molecular & Cellular Proteomics*, 22(5).
- Ponte-Sucre, A., Gamarro, F., Dujardin, J.C., Barrett, M.P., López-Vélez, R., García-Hernández, R., Pountain, A.W., Mwenechanya, R. and Papadopoulou, B., 2017. Drug resistance and treatment failure in leishmaniasis: A 21st century challenge. *PLoS neglected tropical diseases*, 11(12), p.e0006052.
- Poulsen, S.L., Hansen, R.K., Wagner, S.A., van Cuijk, L., van Belle, G.J., Streicher, W., Wikström, M., Choudhary, C., Houtsmuller, A.B., Marteiijn, J.A. and Bekker-Jensen, S., 2013. RNF111/Arkadia is a SUMO-targeted ubiquitin ligase that facilitates the DNA damage response. *Journal of Cell Biology*, 201(6), pp.797-807.
- Pruneda, J.N. and Komander, D., 2019. Evaluating enzyme activities and structures of DUBs. *In Methods in enzymology (Vol. 618, pp. 321-341). Academic Press.*
- Purkait, B., Kumar, A., Nandi, N., Sardar, A.H., Das, S., Kumar, S., Pandey, K., Ravidas, V., Kumar, M., De, T. and Singh, D., 2012. Mechanism of amphotericin B resistance in clinical isolates of *Leishmania donovani*. *Antimicrobial agents and chemotherapy*, 56(2), pp.1031-1041.
- Pylypenko, O., Hammich, H., Yu, I.M. and Houdusse, A., 2018. Rab GTPases and their interacting protein partners: Structural insights into Rab functional diversity. *Small GTPases*, 9(1-2), pp.22-48.
- Pyrih, J., Rašková, V., Škodová-Sveráková, I., Pánek, T. and Lukeš, J., 2020. ZapE/Afg1 interacts with Oxa1 and its depletion causes a multifaceted phenotype. *Plos one*, 15(6), p.e0234918.
- Qin, C., Wang, Y.L., Zhou, J.Y., Shi, J., Zhao, W.W., Zhu, Y.X., Bai, S.M., Feng, L.L., Bie, S.Y., Zeng, B. and Zheng, J., 2023. RAP80 phase separation at DNA double-strand break promotes BRCA1 recruitment. *Nucleic Acids Research*, p.gkad686.
- Queiroz, L.Y., Kageyama, R. and Cimarosti, H.I., 2023. SUMOylation effects on neural stem cells self-renewal, differentiation, and survival. *Neuroscience Research*.
- Ramanathan, M., Majzoub, K., Rao, D.S., Neela, P.H., Zarnegar, B.J., Mondal, S., Roth, J.G., Gai, H., Kovalski, J.R., Siplashvili, Z. and Palmer, T.D., 2018. RNA–protein interaction detection in living cells. *Nature methods*, 15(3), pp.207-212.
- Ramazi, S. and Zahiri, J., 2021. Post-translational modifications in proteins: resources, tools and prediction methods. *Database*, 2021, p.baab012.
- Rashpa, R., Klages, N., Schvartz, D., Pasquarello, C. and Brochet, M., 2023. The Skp1-Cullin1-FBXO1 complex is a pleiotropic regulator required for the formation of gametes and motile forms in *Plasmodium berghei*. *Nature communications*, 14(1), p.1312.
- Rawlings, N.D., Waller, M., Barrett, A.J. and Bateman, A., 2014. MEROPS: the database of proteolytic enzymes, their substrates and inhibitors. *Nucleic acids research*, 42(D1), pp.D503-D509.
- Real, F., Mortara, R.A. and Rabinovitch, M., 2010. Fusion between *Leishmania amazonensis* and *Leishmania major* parasitophorous vacuoles: live imaging of coinfecting macrophages. *PLoS Neglected Tropical Diseases*, 4(12), p.e905.
- Reddy, B.U., Mullick, R., Kumar, A., Sudha, G., Srinivasan, N. and Das, S., 2014. Small molecule inhibitors of HCV replication from pomegranate. *Scientific reports*, 4(1), p.5411.

- Restrepo, C.M., Llanes, A., Cedeño, E.M., Chang, J.H., Álvarez, J., Ríos, M., Penagos, H., Suárez, J.A. and Lleonart, R., 2019. Environmental conditions may shape the patterns of genomic variations in *Leishmania panamensis*. *Genes*, *10*(11), p.838.
- Reverdy, C., Conrath, S., Lopez, R., Planquette, C., Atmanene, C., Collura, V., Harpon, J., Battaglia, V., Vivat, V., Sippl, W. and Colland, F., 2012. Discovery of specific inhibitors of human USP7/HAUSP deubiquitinating enzyme. *Chemistry & biology*, *19*(4), pp.467-477.
- Rhee, H.W., Zou, P., Udeshi, N.D., Martell, J.D., Mootha, V.K., Carr, S.A. and Ting, A.Y., 2013. Proteomic mapping of mitochondria in living cells via spatially restricted enzymatic tagging. *Science*, *339*(6125), pp.1328-1331.
- Ríos, J.L., Giner, R.M., Marín, M. and Recio, M.C., 2018. A pharmacological update of ellagic acid. *Planta medica*, *84*(15), pp.1068-1093.
- Ritorto, M.S., Ewan, R., Perez-Oliva, A.B., Knebel, A., Buhrlage, S.J., Wightman, M., Kelly, S.M., Wood, N.T., Virdee, S., Gray, N.S. and Morrice, N.A., 2014. Screening of DUB activity and specificity by MALDI-TOF mass spectrometry. *Nature communications*, *5*(1), p.4763.
- Robledo, S., Idol, R.A., Crimmins, D.L., Ladenson, J.H., Mason, P.J. and Bessler, M., 2008. The role of human ribosomal proteins in the maturation of rRNA and ribosome production. *Rna*, *14*(9), pp.1918-1929.
- Rodriguez Carvajal, A., Grishkovskaya, I., Gomez Diaz, C., Vogel, A., Sonn-Segev, A., Kushwah, M.S., Schodl, K., Deszcz, L., Orban-Nemeth, Z., Sakamoto, S. and Mechtler, K., 2021. The linear ubiquitin chain assembly complex (LUBAC) generates heterotypic ubiquitin chains. *Elife*, *10*, p.e60660.
- Rogers, M.B., Hilley, J.D., Dickens, N.J., Wilkes, J., Bates, P.A., Depledge, D.P., Harris, D., Her, Y., Herzyk, P., Imamura, H. and Otto, T.D., 2011. Chromosome and gene copy number variation allow major structural change between species and strains of *Leishmania*. *Genome research*, *21*(12), pp.2129-2142.
- Rogers, M.E. and Bates, P.A., 2007. *Leishmania* manipulation of sand fly feeding behaviour results in enhanced transmission. *PLoS pathogens*, *3*(6), p.e91.
- Rogers, M.E., Chance, M.L. and Bates, P.A., 2002. The role of promastigote secretory gel in the origin and transmission of the infective stage of *Leishmania mexicana* by the sandfly *Lutzomyia longipalpis*. *Parasitology*, *124*(5), pp.495-507.
- Rogers, M.E., Ilg, T., Nikolaev, A.V., Ferguson, M.A. and Bates, P.A., 2004. Transmission of cutaneous leishmaniasis by sand flies is enhanced by regurgitation of fPPG. *Nature*, *430*(6998), pp.463-467.
- Roux, K.J., Kim, D.I., Raida, M. and Burke, B., 2012. A promiscuous biotin ligase fusion protein identifies proximal and interacting proteins in mammalian cells. *The Journal of cell biology*, *196*(6), pp.801-810.
- Rowinsky, E.K., Paner, A., Berdeja, J.G., Paba-Prada, C., Venugopal, P., Porkka, K., Gullbo, J., Linder, S., Loskog, A., Richardson, P.G. and Landgren, O., 2020. Phase 1 study of the protein deubiquitinase inhibitor VLX1570 in patients with relapsed and/or refractory multiple myeloma. *Investigational new drugs*, *38*, pp.1448-1453.
- Rudolph, M.J., Wuebbens, M.M., Rajagopalan, K.V. and Schindelin, H., 2001. Crystal structure of molybdopterin synthase and its evolutionary relationship to ubiquitin activation. *Nature structural biology*, *8*(1), pp.42-46.

Rudzinska, M.A., D'ALESSANDRO, P.A. and Trager, W., 1964. The fine structure of *Leishmania donovani* and the role of the kinetoplast in the *Leishmania-leptomonad* transformation. *The Journal of Protozoology*, 11(2), pp.166-191.

Ruiz, E.J., Pinto-Fernandez, A., Turnbull, A.P., Lan, L., Charlton, T.M., Scott, H.C., Damianou, A., Vere, G., Riising, E.M., Da Costa, C. and Krajewski, W.W., 2021. USP28 deletion and small-molecule inhibition destabilizes c-MYC and elicits regression of squamous cell lung carcinoma. *Elife*, 10, p.e71596.

Ruschak, A.M., Religa, T.L., Breuer, S., Witt, S. and Kay, L.E., 2010. The proteasome antechamber maintains substrates in an unfolded state. *Nature*, 467(7317), pp.868-871.

Russell, C.N., Carter, J.L., Borgia, J.M., Bush, J., Calderón, F., Gabarró, R., Conway, S.J., Mottram, J.C., Wilkinson, A.J. and Jones, N.G., 2023. Bromodomain Factor 5 as a Target for Antileishmanial Drug Discovery. *ACS Infectious Diseases*.

Sahasrabudde, A.A., Nayak, R.C. and Gupta, C.M., 2009. Ancient *Leishmania coronin* (CRN12) is involved in microtubule remodelling during cytokinesis. *Journal of cell science*, 122(10), pp.1691-1699.

Sakamaki, J.I., Ode, K.L., Kurikawa, Y., Ueda, H.R., Yamamoto, H. and Mizushima, N., 2022. Ubiquitination of phosphatidylethanolamine in organellar membranes. *Molecular cell*, 82(19), pp.3677-3692.

Samavarchi-Tehrani, P., Samson, R. and Gingras, A.C., 2020. Proximity dependent biotinylation: key enzymes and adaptation to proteomics approaches. *Molecular & Cellular Proteomics*, 19(5), pp.757-773.

Sampson, C., Wang, Q., Otkur, W., Zhao, H., Lu, Y., Liu, X. and Piao, H.L., 2023. The roles of E3 ubiquitin ligases in cancer progression and targeted therapy. *Clinical and Translational Medicine*, 13(3), p.e1204.

Sanman, L.E. and Bogoy, M., 2014. Activity-based profiling of proteases. *Annual review of biochemistry*, 83, pp.249-273.

Santi, A.M.M. and Murta, S.M.F., 2022. Impact of genetic diversity and genome plasticity of *Leishmania* spp. in treatment and the search for novel chemotherapeutic targets. *Frontiers in Cellular and Infection Microbiology*, 12, p.9.

Santonico, E., 2020. Old and new concepts in ubiquitin and NEDD8 recognition. *Biomolecules*, 10(4), p.566.

Sap, K.A., Bezstarosti, K., Dekkers, D.H., Voets, O. and Demmers, J.A., 2017. Quantitative proteomics reveals extensive changes in the ubiquitinome after perturbation of the proteasome by targeted dsRNA-mediated subunit knockdown in *Drosophila*. *Journal of Proteome Research*, 16(8), pp.2848-2862.

Sasidharan, S. and Saudagar, P., 2021. Leishmaniasis: where are we and where are we heading?. *Parasitology research*, 120, pp.1541-1554.

Sato, T., Maekawa, S., Yasuda, S., Domeki, Y., Sueyoshi, K., Fujiwara, M., Fukao, Y., Goto, D.B. and Yamaguchi, J., 2011. Identification of 14-3-3 proteins as a target of ATL31 ubiquitin ligase, a regulator of the C/N response in *Arabidopsis*. *The Plant Journal*, 68(1), pp.137-146.

Sato, Y., 2022. Structural basis for the linkage specificity of ubiquitin-binding domain and deubiquitinase. *The Journal of Biochemistry*, 172(1), pp.1-7.

Sato, Y., Okatsu, K., Saeki, Y., Yamano, K., Matsuda, N., Kaiho, A., Yamagata, A., Goto-Ito, S., Ishikawa, M., Hashimoto, Y. and Tanaka, K., 2017. Structural basis for specific cleavage of Lys6-linked polyubiquitin chains by USP30. *Nature structural & molecular biology*, 24(11), pp.911-919.

Sauer, F., Klemm, T., Kollampally, R.B., Tessmer, I., Nair, R.K., Popov, N. and Kisker, C., 2019. Differential oligomerization of the deubiquitinases USP25 and USP28 regulates their activities. *Molecular cell*, 74(3), pp.421-435.

Saunders, E.C., Sernee, M.F., Ralton, J.E. and McConville, M.J., 2021. Metabolic stringent response in intracellular stages of Leishmania. *Current Opinion in Microbiology*, 63, pp.126-132.

Saveliev, S., Bratz, M., Zubarev, R., Szapacs, M., Budamgunta, H. and Urh, M., 2013. Trypsin/Lys-C protease mix for enhanced protein mass spectrometry analysis. *Nat Methods* 10, i-ii (2013).

Schlein, Y., Jacobson, R.L. and Messer, G., 1992. Leishmania infections damage the feeding mechanism of the sandfly vector and implement parasite transmission by bite. *Proceedings of the National Academy of Sciences*, 89(20), pp.9944-9948.

Schuffenhauer, A., Schneider, N., Hintermann, S., Auld, D., Blank, J., Cotesta, S., Engeloch, C., Fechner, N., Gaul, C., Giovannoni, J. and Jansen, J., 2020. Evolution of Novartis' small molecule screening deck design. *Journal of medicinal chemistry*, 63(23), pp.14425-14447.

Schulman, B.A. and Wade Harper, J., 2009. Ubiquitin-like protein activation by E1 enzymes: the apex for downstream signalling pathways. *Nature reviews Molecular cell biology*, 10(5), pp.319-331.

Schumacher, F.R., Wilson, G. and Day, C.L., 2013. The N-terminal extension of UBE2E ubiquitin-conjugating enzymes limits chain assembly. *Journal of molecular biology*, 425(22), pp.4099-4111.

Serafim, T.D., Coutinho-Abreu, I.V., Oliveira, F., Meneses, C., Kamhawi, S. and Valenzuela, J.G., 2018. Sequential blood meals promote Leishmania replication and reverse metacyclogenesis augmenting vector infectivity. *Nature microbiology*, 3(5), pp.548-555.

Sewduth, R.N., Baietti, M.F. and Sablina, A.A., 2020. Cracking the monoubiquitin code of genetic diseases. *International journal of molecular sciences*, 21(9), p.3036.

Shan, F., Mei, S., Zhang, J., Zhang, X., Xu, C., Liao, S. and Tu, X., 2019. A telomerase subunit homolog La protein from Trypanosoma brucei plays an essential role in ribosomal biogenesis. *The FEBS Journal*, 286(16), pp.3129-3147.

Sharma, R., Dill, B.D., Chourey, K., Shah, M., VerBerkmoes, N.C. and Hettich, R.L., 2012. Coupling a detergent lysis/cleanup methodology with intact protein fractionation for enhanced proteome characterization. *Journal of proteome research*, 11(12), pp.6008-6018.

Shevchenko, A., Tomas, H., Havli, J., Olsen, J.V. and Mann, M., 2006. In-gel digestion for mass spectrometric characterization of proteins and proteomes. *Nature protocols*, 1(6), pp.2856-2860.

Shrestha, R.K., Ronau, J.A., Davies, C.W., Guenette, R.G., Strieter, E.R., Paul, L.N. and Das, C., 2014. Insights into the mechanism of deubiquitination by JAMM deubiquitinases from cocystal structures of the enzyme with the substrate and product. *Biochemistry*, 53(19), pp.3199-3217.

Siah, M., Farzaei, M.H., Ashrafi-Kooshk, M.R., Adibi, H., Arab, S.S., Rashidi, M.R. and Khodarahmi, R., 2016. Inhibition of guinea pig aldehyde oxidase activity by different flavonoid compounds: An in vitro study. *Bioorganic chemistry*, 64, pp.74-84.

- Simicek, M., Lievens, S., Laga, M., Guzenko, D., Aushev, V.N., Kalev, P., Baietti, M.F., Strelkov, S.V., Gevaert, K., Tavernier, J. and Sablina, A.A., 2013. The deubiquitylase USP33 discriminates between RALB functions in autophagy and innate immune response. *Nature cell biology*, 15(10), pp.1220-1230.
- Sluimer, J. and Distel, B., 2018. Regulating the human HECT E3 ligases. *Cellular and molecular life sciences*, 75, pp.3121-3141.
- Snyder, N.A. and Silva, G.M., 2021. Deubiquitinating enzymes (DUBs): Regulation, homeostasis, and oxidative stress response. *Journal of Biological Chemistry*, 297(3).
- Soetens, O., De Craene, J.O. and André, B., 2001. Ubiquitin is required for sorting to the vacuole of the yeast general amino acid permease, Gap1. *Journal of Biological Chemistry*, 276(47), pp.43949-43957.
- Solleis, L., Ghorbal, M., MacPherson, C.R., Martins, R.M., Kuk, N., Crobu, L., Bastien, P., Scherf, A., Lopez-Rubio, J.J. and Sterkers, Y., 2015. First efficient CRISPR-Cas9-mediated genome editing in Leishmania parasites. *Cellular microbiology*, 17(10), pp.1405-1412.
- Song, J., Herrmann, J.M. and Becker, T., 2021. Quality control of the mitochondrial proteome. *Nature Reviews Molecular Cell Biology*, 22(1), pp.54-70.
- Soni, M. and Pratap, J.V., 2022. Development of novel anti-leishmanials: the case for structure-based approaches. *Pathogens*, 11(8), p.950.
- Soucy, T.A., Smith, P.G., Milhollen, M.A., Berger, A.J., Gavin, J.M., Adhikari, S., Brownell, J.E., Burke, K.E., Cardin, D.P., Critchley, S. and Cullis, C.A., 2009. An inhibitor of NEDD8-activating enzyme as a new approach to treat cancer. *Nature*, 458(7239), pp.732-736.
- Souza-Melo, N., Brito-Silva, N., Malvezzi, A.M., dos Santos, G.P., Alcântara, L.M., Alcantara, C.D.L., Cunha e Silva, N.L.D., Zoltner, M., Field, M.C. and Schenkman, S., 2023. Trypanosoma cruzi VDU deubiquitinase mediates surface protein trafficking and infectivity. *bioRxiv*, pp.2023-04.
- Spence, K., 2022. Investigating the role of the SNARE protein, Tlg2, in Leishmania mexicana (Doctoral dissertation, University of York).
- Steger, M., Demichev, V., Backman, M., Ohmayer, U., Ihmor, P., Müller, S., Ralser, M. and Daub, H., 2021. Time-resolved in vivo ubiquitinome profiling by DIA-MS reveals USP7 targets on a proteome-wide scale. *Nature communications*, 12(1), p.5399.
- Subbotin, R.I. and Chait, B.T., 2014. A Pipeline for Determining Protein-Protein Interactions and Proximities in the Cellular Milieu. *Molecular & Cellular Proteomics*, 13(11), pp.2824-2835.
- Sun, J., Movahed, N. and Zheng, H., 2020. LUNAPARK is an E3 ligase that mediates degradation of ROOT HAIR DEFECTIVE3 to maintain a tubular ER network in Arabidopsis. *Plant Cell*, 32(9), pp.2964-2978.
- Sundar, S., Chakravarty, J., Agarwal, D., Rai, M. and Murray, H.W., 2010. Single-dose liposomal amphotericin B for visceral leishmaniasis in India. *New England Journal of Medicine*, 362(6), pp.504-512.
- Sundar, S., Jha, T.K., Thakur, C.P., Sinha, P.K. and Bhattacharya, S.K., 2007. Injectable paromomycin for visceral leishmaniasis in India. *New England Journal of Medicine*, 356(25), pp.2571-2581.

Sundar, S., Makharia, A., More, D.K., Agrawal, G., Voss, A., Fischer, C., Bachmann, P. and Murray, H.W., 2000. Short-course of oral miltefosine for treatment of visceral leishmaniasis. *Clinical Infectious Diseases*, 31(4), pp.1110-1113.

Sunter, J. and Gull, K., 2017. Shape, form, function and Leishmania pathogenicity: from textbook descriptions to biological understanding. *Open biology*, 7(9), p.170165.

Sutherst, R.W., 2004. Global change and human vulnerability to vector-borne diseases. *Clinical microbiology reviews*, 17(1), pp.136-173.

Takehara, Y., Yashiroda, H., Matsuo, Y., Zhao, X., Kamigaki, A., Matsuzaki, T., Kosako, H., Inada, T. and Murata, S., 2021. The ubiquitination-deubiquitination cycle on the ribosomal protein eS7A is crucial for efficient translation. *Isience*, 24(3).

Tavana, O., Li, D., Dai, C., Lopez, G., Banerjee, D., Kon, N., Chen, C., Califano, A., Yamashiro, D.J., Sun, H. and Gu, W., 2016. HAUSP deubiquitinates and stabilizes N-Myc in neuroblastoma. *Nature medicine*, 22(10), pp.1180-1186.

Taylor, S.V., Kelleher, N.L., Kinsland, C., Chiu, H.J., Costello, C.A., Backstrom, A.D., McLafferty, F.W. and Begley, T.P., 1998. Thiamin biosynthesis in Escherichia coli: identification of ThiS thiocarboxylate as the immediate sulfur donor in the thiazole formation. *Journal of Biological Chemistry*, 273(26), pp.16555-16560.

Teixeira, D.E., Benchimol, M., Rodrigues, J.C., Crepaldi, P.H., Pimenta, P.F. and de Souza, W., 2013. The cell biology of Leishmania: how to teach using animations. *PLoS pathogens*, 9(10), p.e1003594.

Thomas, S., Green, A., Sturm, N.R., Campbell, D.A. and Myler, P.J., 2009. Histone acetylations mark origins of polycistronic transcription in Leishmania major. *BMC genomics*, 10(1), pp.1-15.

Tracz, M. and Bialek, W., 2021. Beyond K48 and K63: non-canonical protein ubiquitination. *Cellular & molecular biology letters*, 26(1), p.1.

TriTrypDB (2023) *Kinetoplastid Informatics Resources* (Accessed: 09 Oct 2023).

Tsukamoto, S., Takeuchi, T., Rotinsulu, H., Mangindaan, R.E., van Soest, R.W., Ukai, K., Kobayashi, H., Namikoshi, M., Ohta, T. and Yokosawa, H., 2008. Leucettamol A: a new inhibitor of Ubc13-Uev1A interaction isolated from a marine sponge, Leucetta aff. microrhaphis. *Bioorganic & Medicinal Chemistry Letters*, 18(24), pp.6319-6320.

Tunes, L.G., Morato, R.E., Garcia, A., Schmitz, V., Steindel, M., Corrêa-Junior, J.D., Dos Santos, H.F., Frezard, F., de Almeida, M.V., Silva, H. and Moretti, N.S., 2020. Preclinical gold complexes as oral drug candidates to treat leishmaniasis are potent trypanothione reductase inhibitors. *ACS Infectious Diseases*, 6(5), pp.1121-1139.

Turnbull, A.P., Ioannidis, S., Krajewski, W.W., Pinto-Fernandez, A., Heride, C., Martin, A.C., Tonkin, L.M., Townsend, E.C., Buker, S.M., Lancia, D.R. and Caravella, J.A., 2017. Molecular basis of USP7 inhibition by selective small-molecule inhibitors. *Nature*, 550(7677), pp.481-486.

Tyanova, S., Temu, T., Sinitcyn, P., Carlson, A., Hein, M.Y., Geiger, T., Mann, M. and Cox, J., 2016. The Perseus computational platform for comprehensive analysis of (prote) omics data. *Nature methods*, 13(9), pp.731-740.

Ushiyama, S., Umaoka, H., Kato, H., Suwa, Y., Morioka, H., Rotinsulu, H., Losung, F., Mangindaan, R.E., de Voogd, N.J., Yokosawa, H. and Tsukamoto, S., 2012. Manosterols A and B, sulfonated

sterol dimers inhibiting the Ubc13–Uev1A interaction, isolated from the marine sponge *Lissodendryx fibrosa*. *Journal of natural products*, 75(8), pp.1495-1499.

van der Wal, L., Bezstarosti, K. and Demmers, J.A., 2022. A ubiquitinome analysis to study the functional roles of the proteasome associated deubiquitinating enzymes USP14 and UCH37. *Journal of Proteomics*, 262, p.104592.

van Wijk, S.J. and Timmers, H.M., 2010. The family of ubiquitin-conjugating enzymes (E2s): deciding between life and death of proteins. *The FASEB Journal*, 24(4), pp.981-993.

Varca, A.C., Casalena, D., Chan, W.C., Hu, B., Magin, R.S., Roberts, R.M., Liu, X., Zhu, H., Seo, H.S., Dhe-Paganon, S. and Marto, J.A., 2021. Identification and validation of selective deubiquitinase inhibitors. *Cell Chemical Biology*, 28(12), pp.1758-1771.

Vassilev, L.T., Vu, B.T., Graves, B., Carvajal, D., Podlaski, F., Filipovic, Z., Kong, N., Kammlott, U., Lukacs, C., Klein, C. and Fotouhi, N., 2004. In vivo activation of the p53 pathway by small-molecule antagonists of MDM2. *Science*, 303(5659), pp.844-848.

Vélez -Ramírez, D. E., Shimogawa, M. M., Ray, S. S., Lopez, A., Rayatpisheh, S., Langousis, G., et al. (2021). APEX2 Proximity Proteomics Resolves Flagellum Subdomains and Identifies Flagellum Tip-Specific Proteins in *Trypanosoma Brucei*. *mSphere* 6, 1–19

Venticinque, L. and Meruelo, D., 2012. Comprehensive proteomic analysis of nonintegrin laminin receptor interacting proteins. *Journal of proteome research*, 11(10), pp.4863-4872.

Vijay-Kumar, S., Bugg, C.E. and Cook, W.J., 1987. Structure of ubiquitin refined at 1.8 Å resolution. *Journal of molecular biology*, 194(3), pp.531-544.

Vogl, A.M., Phu, L., Becerra, R., Giusti, S.A., Verschueren, E., Hinkle, T.B., Bordenave, M.D., Adrian, M., Heidersbach, A., Yankilevich, P. and Stefani, F.D., 2020. Global site-specific neddylation profiling reveals that NEDDylated cofilin regulates actin dynamics. *Nature Structural & Molecular Biology*, 27(2), pp.210-220.

Volf, P., Hajmova, M., Sadlova, J. and Votypka, J., 2004. Blocked stomodeal valve of the insect vector: similar mechanism of transmission in two trypanosomatid models. *International journal for parasitology*, 34(11), pp.1221-1227.

Vozandychova, V., Stojkova, P., Hercik, K., Rehulka, P. and Stulik, J., 2021. The ubiquitination system within bacterial host–pathogen interactions. *Microorganisms*, 9(3), p.638.

Wagner, S.A., Beli, P., Weinert, B.T., Nielsen, M.L., Cox, J., Mann, M. and Choudhary, C., 2011. A proteome-wide, quantitative survey of in vivo ubiquitylation sites reveals widespread regulatory roles. *Molecular & Cellular Proteomics*, 10(10).

Wang, C., Wan, X., Yu, T., Huang, Z., Shen, C., Qi, Q., Xiang, S., Chen, X., Arbely, E., Ling, Z.Q. and Liu, C.Y., 2020. Acetylation stabilizes phosphoglycerate dehydrogenase by disrupting the interaction of E3 ligase RNF5 to promote breast tumorigenesis. *Cell reports*, 32(6).

Wang, C., Xi, J., Begley, T.P. and Nicholson, L.K., 2001. Solution structure of ThiS and implications for the evolutionary roots of ubiquitin. *Nature structural biology*, 8(1), pp.47-51.

Wang, L., Delahunty, C., Fritz-Wolf, K., Rahlfs, S., Helena Prieto, J., Yates, J.R. and Becker, K., 2015. Characterization of the 26S proteasome network in *Plasmodium falciparum*. *Scientific Reports*, 5(1), p.17818.

- Wang, Y. and Dasso, M., 2009. SUMOylation and deSUMOylation at a glance. *Journal of cell science*, 122(23), pp.4249-4252.
- Wenzel, D.M., Lissounov, A., Brzovic, P.S. and Klevit, R.E., 2011. UBC7 reactivity profile reveals parkin and HHARI to be RING/HECT hybrids. *Nature*, 474(7349), pp.105-108.
- Wersmeyer-Wenk, B.E.A.T.E.E., ZÄHNER, H., KRONE, B. and ZEECK, A., 1981. Metabolic products of microorganisms. 207 Haloquinone, a new antibiotic active against halobacteria I. Isolation, characterization and biological properties. *The Journal of Antibiotics*, 34(12), pp.1531-1537.
- Wheeler, R.J., Gluenz, E. and Gull, K., 2015. Basal body multipotency and axonemal remodelling are two pathways to a 9+ 0 flagellum. *Nature communications*, 6(1), p.8964.
- Wheeler, R.J., Sunter, J.D. and Gull, K., 2016. Flagellar pocket restructuring through the Leishmania life cycle involves a discrete flagellum attachment zone. *Journal of cell science*, 129(4), pp.854-867.
- Wiborg, O., Pedersen, M.S., Wind, A., Berglund, L.E., Marcker, K.A. and Vuust, J., 1985. The human ubiquitin multigene family: some genes contain multiple directly repeated ubiquitin coding sequences. *The EMBO journal*, 4(3), pp.755-759.
- Wilde, M.L., Ruparel, U., Klemm, T., Lee, V.V., Calleja, D.J., Komander, D. and Tonkin, C.J., 2023. Characterisation of the OTU domain deubiquitinase complement of Toxoplasma gondii. *Life Science Alliance*, 6(6).
- Wilkinson, K.D., 1997. Regulation of ubiquitin-dependent processes by deubiquitinating enzymes. *The FASEB Journal*, 11(14), pp.1245-1256.
- Williams, R.A., Smith, T.K., Cull, B., Mottram, J.C. and Coombs, G.H., 2012. ATG5 is essential for ATG8-dependent autophagy and mitochondrial homeostasis in Leishmania major. *PLoS pathogens*, 8(5), p.e1002695.
- Wiwanitkit, V., 2012. Interest in paromomycin for the treatment of visceral leishmaniasis (kala-azar). Therapeutics and clinical risk management, pp.323-328.
- Won, M.M., Baublis, A. and Burleigh, B.A., 2023. Proximity-dependent biotinylation and identification of flagellar proteins in Trypanosoma cruzi. *Msphere*, pp.e00088-23.
- World Health Organization- Leishmaniasis. Available at: <https://www.who.int/data/gho/data/themes/topics/gho-ntd-leishmaniasis> (Accessed: 14 August 2023).
- Wu, P.Y., Hanlon, M., Eddins, M., Tsui, C., Rogers, R.S., Jensen, J.P., Matunis, M.J., Weissman, A.M., Wolberger, C.P. and Pickart, C.M., 2003. A conserved catalytic residue in the ubiquitin-conjugating enzyme family. *The EMBO journal*, 22(19), pp.5241-5250.
- Wu, Y.Y., Li, W., Xu, Y., Jin, E.H. and Tu, Y.Y., 2011. Evaluation of the antioxidant effects of four main theaflavin derivatives through chemiluminescence and DNA damage analyses. *Journal of Zhejiang University Science B*, 12, pp.744-751.
- Wyllie, S., Brand, S., Thomas, M., De Rycker, M., Chung, C.W., Pena, I., Bingham, R.P., Bueren-Calabuig, J.A., Cantizani, J., Cebrian, D. and Craggs, P.D., 2019. Preclinical candidate for the treatment of visceral leishmaniasis that acts through proteasome inhibition. *Proceedings of the National Academy of Sciences*, 116(19), pp.9318-9323.

- Xia, J., Yang, Y., Chen, X., Song, K., Ma, G., Yang, Y., Yao, C. and Du, A., 2024. An apicoplast-localized deubiquitinase contributes to the cell growth and apicoplast homeostasis of *Toxoplasma gondii*. *Veterinary Research*, 55(1), pp.1-15.
- Xu, G.W., Ali, M., Wood, T.E., Wong, D., Maclean, N., Wang, X., Gronda, M., Skrtic, M., Li, X., Hurren, R. and Mao, X., 2010. The ubiquitin-activating enzyme E1 as a therapeutic target for the treatment of leukemia and multiple myeloma. *Blood, The Journal of the American Society of Hematology*, 115(11), pp.2251-2259.
- Xue, Q., Tang, D., Chen, X. and Liu, J., 2023. Targeting deubiquitinases for cancer therapy. *Clinical and Translational Discovery*, 3(5), p.e242.
- Xu, R., Lin, L., Jiao, Z., Liang, R., Guo, Y., Zhang, Y., Shang, X., Wang, Y., Wang, X., Yao, L. and Liu, S., 2024. Deaggregation of mutant *Plasmodium yoelii* de-ubiquitinase UBP1 alters MDR1 localization to confer multidrug resistance. *Nature Communications*, 15(1), p.1774.
- Xu, S., Hu, S., Zhu, L. and Wang, W., 2021. Haloquinone chloroimides as toxic disinfection by products identified in drinking water. *Environmental Science & Technology*, 55(24), pp.16347-16357.
- Xu, S.L., Shrestha, R., Karunadasa, S.S. and Xie, P.Q., 2023. Proximity labelling in plants. *Annual Review of Plant Biology*, 74, pp.285-312.
- Yagoubat, A., Crobu, L., Berry, L., Kuk, N., Lefebvre, M., Sarrazin, A., Bastien, P. and Sterkers, Y., 2020. Universal highly efficient conditional knockout system in *Leishmania*, with a focus on untranscribed region preservation. *Cellular microbiology*, 22(5), p.e13159.
- Yamada, D., Kawabe, K., Tosa, I., Tsukamoto, S., Nakazato, R., Kou, M., Fujikawa, K., Nakamura, S., Ono, M., Oohashi, T. and Kaneko, M., 2019. Inhibition of the glutamine transporter SNAT1 confers neuroprotection in mice by modulating the mTOR-autophagy system. *Communications Biology*, 2(1), p.346.
- Yan, W., Zhong, Y., Hu, X., Xu, T., Zhang, Y., Kales, S., Qu, Y., Talley, D.C., Baljinnyam, B., LeClair, C.A. and Simeonov, A., 2023. Auranofin targets UBA1 and enhances UBA1 activity by facilitating ubiquitin trans-thioesterification to E2 ubiquitin-conjugating enzymes. *Nature Communications*, 14(1), p.4798.
- Yang, F., Xing, Y., Li, Y., Chen, X., Jiang, J., Ai, Z. and Wei, Y., 2018. Monoubiquitination of cancer stem cell marker CD133 at lysine 848 regulates its secretion and promotes cell migration. *Molecular and Cellular Biology*, 38(15), pp.e00024-18.
- Yang, Q., Zhao, J., Chen, D. and Wang, Y., 2021. E3 ubiquitin ligases: styles, structures and functions. *Molecular Biomedicine*, 2, pp.1-17.
- Yan, H., Kong, X., Zhang, T., Xiao, H., Feng, X., Tu, H. and Feng, J., 2020. Prevalence of *Plasmodium falciparum* Kelch 13 (PfK13) and ubiquitin-specific protease 1 (pfubp1) gene polymorphisms in returning travelers from Africa reported in Eastern China. *Antimicrobial Agents and Chemotherapy*, 64(11), pp.10-1128.
- Yang, Y., Kitagaki, J., Dai, R.M., Tsai, Y.C., Lorick, K.L., Ludwig, R.L., Pierre, S.A., Jensen, J.P., Davydov, I.V., Oberoi, P. and Li, C.C.H., 2007. Inhibitors of ubiquitin-activating enzyme (E1), a new class of potential cancer therapeutics. *Cancer research*, 67(19), pp.9472-9481.
- Ye, Y., Akutsu, M., Reyes-Turcu, F., Enchev, R.I., Wilkinson, K.D. and Komander, D., 2011. Polyubiquitin binding and cross-reactivity in the USP domain deubiquitinase USP21. *EMBO reports*, 12(4), pp.350-357.

- Yee, K., Martinelli, G., Vey, N., Dickinson, M.J., Seiter, K., Assouline, S., Drummond, M., Yoon, S.S., Kasner, M., Lee, J.H. and Kelly, K.R., 2014. Phase 1/1b study of RG7388, a potent MDM2 antagonist, in acute myelogenous leukemia (AML) patients (Pts). *Blood*, 124(21), p.116.
- Yilmaz, I.C., Dunuroglu, E., Ayanoglu, I.C., Ipekoglu, E.M., Yildirim, M., Girginkardesler, N., Ozbel, Y., Toz, S., Ozbilgin, A., Aykut, G. and Gursel, I., 2022. Leishmania kinetoplast DNA contributes to parasite burden in infected macrophages: Critical role of the cGAS-STING-TBK1 signaling pathway in macrophage parasitemia. *Frontiers in Immunology*, 13, p.1007070.
- Yousuf, M., Shamsi, A., Khan, P., Shahbaaz, M., AlAjmi, M.F., Hussain, A., Hassan, G.M., Islam, A., Rizwanul Haque, Q.M. and Hassan, M.I., 2020. Ellagic acid controls cell proliferation and induces apoptosis in breast cancer cells via inhibition of cyclin-dependent kinase 6. *International journal of molecular sciences*, 21(10), p.3526.
- Yuan, W.C., Lee, Y.R., Lin, S.Y., Chang, L.Y., Tan, Y.P., Hung, C.C., Kuo, J.C., Liu, C.H., Lin, M.Y., Xu, M. and Chen, Z.J., 2014. K33-linked polyubiquitination of coronin 7 by Cul3-KLHL20 ubiquitin E3 ligase regulates protein trafficking. *Molecular cell*, 54(4), pp.586-600.
- Zhang, J.H., Chung, T.D. and Oldenburg, K.R., 1999. A simple statistical parameter for use in evaluation and validation of high throughput screening assays. *Journal of biomolecular screening*, 4(2), pp.67-73.
- Zhang, N., Chen, R., Young, N., Wishart, D., Winter, P., Weiner, J.H. and Li, L., 2007. Comparison of SDS- and methanol-assisted protein solubilization and digestion methods for Escherichia coli membrane proteome analysis by 2-D LC-MS/MS. *Proteomics*, 7(4), pp.484-493.
- Zhang, N., Jiang, N., Zhang, K., Zheng, L., Zhang, D., Sang, X., Feng, Y., Chen, R., Yang, N., Wang, X. and Cheng, Z., 2020. Landscapes of protein posttranslational modifications of African Trypanosoma parasites. *Iscience*, 23(5), p.101074.
- Zhang, P.F., Huang, Y.L., Fu, Q., He, W.T., Xiao, K. and Zhang, M., 2021. Integrated analysis of phosphoproteome and ubiquitylome in epididymal sperm of buffalo (Bubalus bubalis). *Molecular Reproduction and Development*, 88(1), pp.15-33.
- Zhang, W.W., Karmakar, S., Gannavaram, S., Dey, R., Lypaczewski, P., Ismail, N., Siddiqui, A., Simonyan, V., Oliveira, F., Coutinho-Abreu, I.V. and DeSouza-Vieira, T., 2020. A second generation leishmanization vaccine with a markerless attenuated Leishmania major strain using CRISPR gene editing. *Nature Communications*, 11(1), p.3461.
- Zhang, W.W., Lypaczewski, P. and Matlashewski, G., 2017. Optimized CRISPR-Cas9 genome editing for Leishmania and its use to target a multigene family, induce chromosomal translocation, and study DNA break repair mechanisms. *MSphere*, 2(1), pp.10-1128.
- Zhang, W.W. and Matlashewski, G., 2015. CRISPR-Cas9-mediated genome editing in Leishmania donovani. *MBio*, 6(4), pp.10-1128.
- Zhang, Y.H., Zhou, C.J., Zhou, Z.R., Song, A.X. and Hu, H.Y., 2011. Domain analysis reveals that a deubiquitinating enzyme USP13 performs non-activating catalysis for Lys63-linked polyubiquitin. *PloS one*, 6(12), p.e29362.
- Zhao, C., Chen, X., Yang, C., Zang, D., Lan, X., Liao, S., Zhang, P., Wu, J., Li, X., Liu, N. and Liao, Y., 2017. Repurposing an antidandruff agent to treating cancer: zinc pyrithione inhibits tumor growth via targeting proteasome-associated deubiquitinases. *Oncotarget*, 8(8), p.13942.

- Zhao, X., Fiske, B., Kawakami, A., Li, J. and Fisher, D.E., 2011. Regulation of MITF stability by the USP13 deubiquitinase. *Nature communications*, 2(1), p.414.
- Zhao, Y., Qin, F., Boyd, J.M., Anichina, J. and Li, X.F., 2010. Characterization and determination of chloro- and bromo-benzoquinones as new chlorination disinfection byproducts in drinking water. *Analytical Chemistry*, 82(11), pp.4599-4605.
- Zheng, N. and Shabek, N., 2017. Ubiquitin ligases: structure, function, and regulation. *Annual review of biochemistry*, 86, pp.129-157.
- Zhu, H., Zhang, T., Wang, F., Yang, J. and Ding, J., 2019. Structural insights into the activation of USP46 by WDR48 and WDR20. *Cell Discovery*, 5(1), p.34.
- Zoltner, M., Leung, K.F., Alford, S., Horn, D. and Field, M.C., 2015. Modulation of the surface proteome through multiple ubiquitylation pathways in African trypanosomes. *PLoS pathogens*, 11(10), p.e1005236.
- Zou, Q., Liu, M., Liu, K., Zhang, Y., North, B.J. and Wang, B., 2023. E3 ubiquitin ligases in cancer stem cells: key regulators of cancer hallmarks and novel therapeutic opportunities. *Cellular Oncology*, pp.1-26.
- Zhou, Y. and Zou, P., 2020. The evolving capabilities of enzyme-mediated proximity labelling. *Current Opinion in Chemical Biology*, 60, pp.30-38